Ferric iron in $CaTiO_3$ perovskite as an oxygen barometer for kimberlitic magmas: Experimental Calibration and Applications

By

Anthony John Bellis
B.Sc., McGill University, 2002

A Thesis Submitted in Partial Fulfillment of the
Requirements for the Degree of

MASTER OF SCIENCE

In the School of Earth and Ocean Sciences

Supervisor: Dr. Dante Canil

ABSTRACT

An oxygen barometer to estimate fO_2 during the crystallization of kimberlites is developed using the Fe content of perovskite (Pv), a common groundmass phase in these rocks. With increasing fO_2, more Fe exists in the kimberlitic liquid as Fe^{3+}, and thus partitions into Pv, which accepts only Fe^{3+} into its crystal structure. Experiments to study the partitioning of Fe^{3+} between Pv and kimberlite liquid were conducted on simple and complex anhydrous kimberlite bulk compositions at 100 kPa over a range temperatures (1130 - 1300°C) and of fO_2's from NNO+4 to NNO-5 (NNO, nickel-nickel oxide buffer) and at Nb and REE levels of 0 to 1.5 wt% and 1500 ppm respectively. For Nb-free experiments, the Fe_2O_3 content of Pv increases with fO_2 according to the relation (at 2σ):

$$Fe_2O_{3\ Pv}\ (wt\%) = 0.25\ (0.04)\ \Delta NNO + 1.83(0.06)$$

For experiments doped with Nb, two universal equations for the relationship between the Fe and Nb in Pv, and fO_2 were defined. Based on a slope intercept fitting method (SIM) we obtain:

$$\text{Log Fe } (0.04)=0.058(0.004)*\Delta NNO + 0.26(0.02)*\text{Log Nb} - 0.91(0.03)$$

Based on a multiple linear regression method (MLR):

$$\text{Fe } (0.031)= 0.004(0)*\Delta NNO + 0.50(0.021)*\text{Nb} + 0.030(0.001)$$

with uncertainties at 2σ, and Nb and Fe as cation units per 3 oxygens in both equations. Over the range of conditions of our experiments, these relationships show no temperature (T) dependence and are not affected by the bulk Fe content of the kimberlite starting material. The Fe_2O_3 content of Pv from natural kimberlites compiled from the literature corresponds to fO_2 conditions of NNO-5 to NNO+1. Data on zoned Pv from a single

kimberlite, the Phoenix pipe, suggests that cores record lower fO_2 than rims, NNO–1 in cores compared to NNO+1.5 in rims.

Within the Somerset Island cluster, Pv from six pipes display an average relative fO_2 of NNO-4 to NNO+1. Within individual kimberlite pipes, however, the fO_2 range recorded by Pv narrows to NNO-2.6 +/- 0.6 within the Nikos1 pipe, and NNO +/- 2 within the Zulu pipe. Within the Lac de Gras cluster, Pv from five pipes display an average relative fO_2 of NNO-2.5 to NNO+6. However, within a single kimberlite, the Grizzly pipe, the fO_2 range recorded by Pv narrows to NNO+/- 1. The range in fO_2 recorded by Pv may result from the diversity and complexity of processes that ensue during the emplacement of kimberlite magma (crystallization, assimilation and degassing), a detailed record of which is revealed by a comprehensive study of perovskite parageneses in these complex rocks.

TABLE OF CONTENTS

LIST OF TABLES

LIST OF FIGURES

ACKNOWLEDGMENTS

I wish to thank first and foremost Dante Canil for his patience and wisdom. I have enjoyed my time at UVic and you are a major reason for that. I also wish to thank M. Raudsepp and J. Spence for assistance with EMP and ICP-MS analysis, respectively, and J. MacKenzie and L. Coogan for helpful discussions. I especially thank R. Eccles for sharing his perovskite data from the Phoenix kimberlite. This research was supported by an NSERC of Canada Discovery Grant to D.C.

1.

INTRODUCTION

1.1 MOTIVATION

Kimberlites are unique and complex rocks that, despite decades of study, remain poorly understood. Given that kimberlites are one of the main host rocks for diamonds, information regarding their intensive variables (i.e. T, fO_2) could prove valuable not only in determining the likely presence and quality of diamonds in a pipe, but also in determining the conditions at depth in their deep mantle source region. One of the major complicating factors in kimberlite study is that primitive kimberlite magma is seldom preserved as kimberlites completely crystallize during emplacement. The composition of primary kimberlite magma is enigmatic, as kimberlites sampled at the surface represent a mixture of minerals formed during crystallization (phenocrysts) and xenoliths/xenocrysts derived from the mantle and crust. Furthermore, as a kimberlite eruption has never been witnessed, the precise mode of kimberlite emplacement remains unknown.

1.2 KIMBERLITES

Kimberlites are a group of volatile-rich (CO_2), ultramafic, alkaline igneous rocks (Mitchell, 1986). Their texture is typically inequigranular with phenocrysts and macrocrysts (and in some instances megacrysts), set in a fine-grained matrix (Clement *et al.*, 1984). The phenocrysts are mostly primary olivine and phlogopite. The mega/macrocryst (mantle xenocrysts) assemblage typically consists of anhedral crystals of olivine with lesser amounts of magnesian ilmenite, Cr-poor titanian pyrope, diopside (commonly subcalcic), phlogopite, enstatite, Ti-poor chromite and garnet (Mitchell, 1997). The matrix is typically fine-grained and contains a second generation of primary minerals: monticellite, phlogopite, serpentine, calcite, perovskite, spinel (magnesian ulvospinel-Mg-chromite-ulvospinel-magnetite solid solutions) and apatite (Mitchell,

1997). Both mantle and crustal xenoliths are commonly present and diamonds are rare constituents.

Kimberlite magma is heterogeneous and its constituents include mantle-derived solids (xenoliths, xenocrysts and diamonds), silicate melt (from which phenocryst and groundmass minerals crystallize) and volatiles (mainly H_2O and CO_2). The study of kimberlite magma is complicated through contamination by crustal material, segregation and degassing of volatiles and alteration by deuteric fluid of magma during emplacement.

1.3 TEXTURAL CLASSIFICATION

Considerable textural variation exists in kimberlites and is associated with different emplacement and reworking processes. Three main facies were defined by Mitchell (1986) (Figure 1.1). Crater facies kimberlites occur close to the paleosurface and are composed of extrusive volcaniclastic kimberlite (VK) rock types such as lavas, epiclastic and pyroclastic rocks and resedimented volcaniclastic kimberlite (RVK) with further subdivisions made according to sedimentological and volcanological terms (Mitchell, 1986). While most kimberlites bodies probably hosted crater facies rocks as a result of their emplacement mechanism, this zone is commonly obscured by post-emplacement erosion (Haggerty, 1994). Diatreme facies kimberlites consist of intrusive volcaniclastic kimberlite (VK) rock types such as tuffaceous kimberlite (TK) and tuffaceous kimberlite breccia (TKB). Diatreme facies rocks commonly reside steep-sided, inverted cone-shaped pipes, but may or may not be present. Hypabyssal facies kimberlites are only ever exposed by deep erosion and are composed solely of intrusive magmatic kimberlite (MK) rock types. The hypabyssal environment is structurally controlled and consists of dykes and blows, sills and root zone intrusions (pipes) and in some cases represents the lowermost portion of the volcanic pipe system.

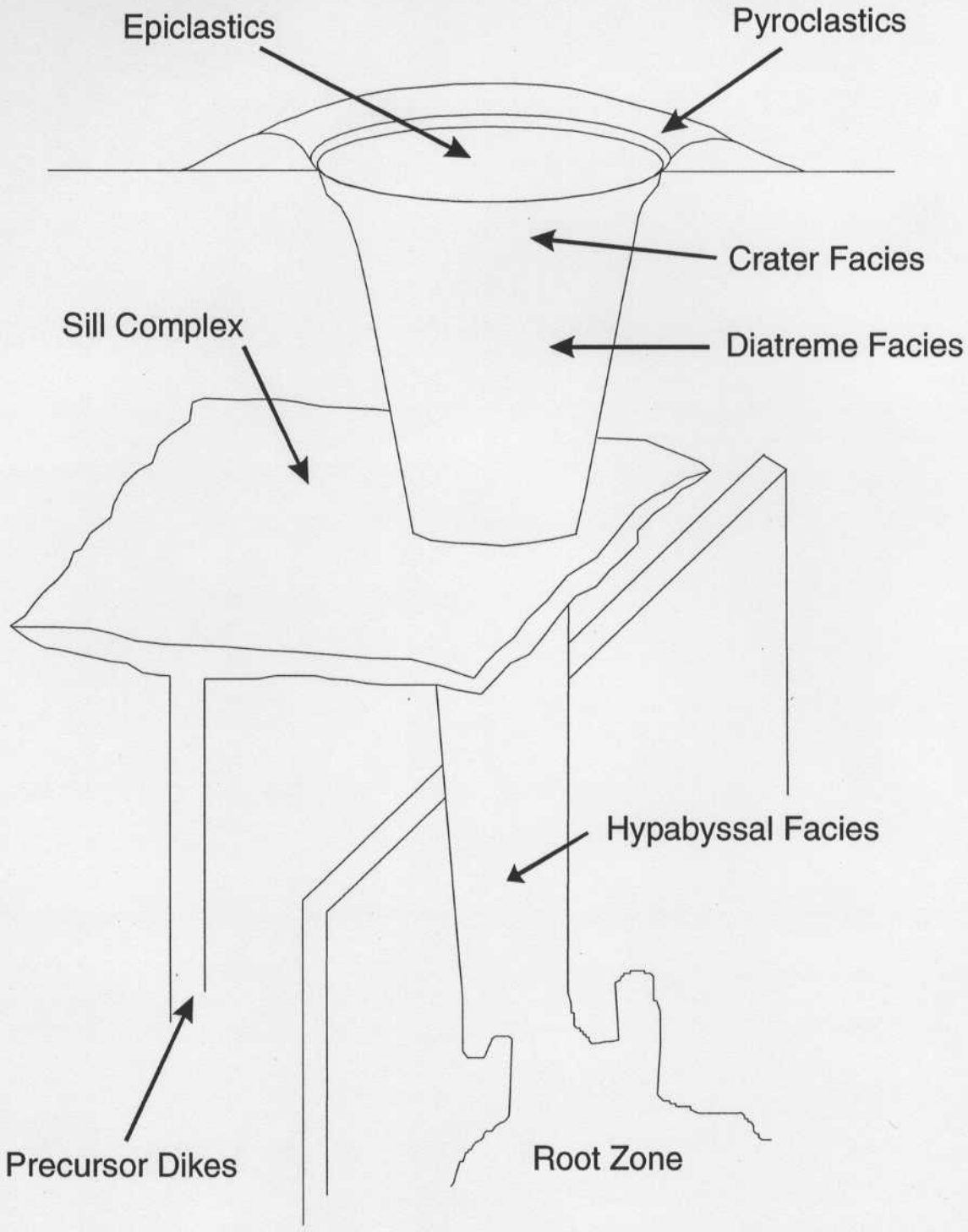

Figure 1.1: Model of an idealized kimberlite magmatic system prior to surficial erosional processes (adapted from Mitchell, 1986).

1.4 KIMBERLITE ORIGINS AND EMPLACEMENT

The origins of kimberlite have been investigated since the rock type was first defined (Wagner, 1914). LeRoex *et al.* (2003), suggest that partial melting of asthenospheric mantle generates volatile and incompatible enriched melt at depth. Intrusion of this melt into the depleted lower lithosphere results in metasomatisation of the lithosphere. Re-melting of the metasomatised lithosphere generates kimberlite magma, which incorporates ultramafic mantle material prior to emplacement (LeRoex et al., 2003). While the depth of partial melting is a matter of debate (Ringwood *et al.*, 1992; Edgar & Charbonneau, 1993; Haggerty, 1994), it is widely accepted that kimberlites form by small degrees (<1%) of partial melting of carbonated garnet lherzolite mineral assemblages (Ringwood *et al.*, 1992).

Most known kimberlites are younger than 600 Ma, though this may reflect the preservation potential of these bodies (Haggerty, 1994). Haggerty (1994) recognized seven distinct episodes of worldwide kimberlite magmatism: (1) a mid-Cretaceous spike at 80-120 Ma prominent throughout Africa, North America, Brazil and Siberia, (2) a spike at 200 Ma in Africa, North America, Brazil and Siberia, (3) 320-360- Ma in Siberia, (4) 360-400 Ma in North America and Siberia, (5) 460 Ma in China, Eastern Europe, Siberia, Canada and Zimbabwe, (6) 1.1-1.2 Ga in all localities cited as well as in India, Canada, Australia and West Africa and the oldest (7) a 1.6-1.7 Ga spike in South Africa and Venezuala.

One of the main questions still unanswered concerning kimberlites is whether the intensive variables (i.e. T, fO_2) they record reflect the formation mantle conditions at depths or the conditions inherited during transport and emplacement.

2.

EXPERIMENTAL CALIBRATION OF THE FERRIC IRON IN $CaTiO_3$ PEROVSKITE OXYGEN BAROMETER

2.1 INTRODUCTION

Iron exists in terrestrial magmas as Fe^{2+} and Fe^{3+}, the ratio of which depends on oxygen fugacity (fO_2). Kennedy (1948) first recognized the utility of Fe^{3+}/Fe^{2+} as a record of fO_2 in magmas, and as a general petrogenetic indicator. Fudali (1965) further documented how Fe^{3+}/Fe^{2+} increases with acidity in rocks from the Cascades and emphasized how fO_2 is one of the most important parameters in controlling differentiation, by dictating how iron partitions into the liquidus minerals or coexisting liquid.

Fe^{3+}/Fe^{2+} in melts is governed by the redox reaction:

$$Fe^{2+}O + 1/4O_2 = Fe^{3+}O_{1.5} \qquad (1)$$

for which empirical expressions relating Fe^{3+}/Fe^{2+}, temperature (T), fO_2 and composition of silicate liquids have been established by experimental studies (Kress & Carmichael, 1988; Sack *et al.*, 1980; Thornber *et al.*, 1980). This expression permits fO_2 to be measured along the entire liquid line of descent of glassy magmas and has been used to examine how fO_2 influences the speciation of volatile elements, or is a reflection of their source region or degassing history (Carmichael, 1991; Haggerty, 1994).

Kimberlites composition and intensive variables (e.g. T, fO_2) reveal the conditions that occur in their mantle source region, or during their ascent to the surface, where they commonly carry diamond or precipitate carbonate. The stability and dissolution of

carbon-bearing minerals in kimberlite magmas are directly influenced by the fO_2 of the magma during its ascent. As the only primary source of diamonds, the fO_2 of kimberlites may thereby determine the likely presence or quality of diamonds in this magma, as well as its degassing history.

Unfortunately, kimberlites never preserve glass and so empirical expressions noted above relating Fe^{3+}/Fe^{2+} of glass, T, fO_2 and composition cannot be applied. Previous work on the fO_2 of kimberlite has been limited by the lack of fresh material (LeRoex *et al.*, 2003; Mitchell, 1986). The discovery of fresh kimberlites in the Lac de Gras region (Pell, 1995) affords some constraints on their fO_2. For example, Fedortchouk and Canil (2004) examined liquidus spinel included in fresh olivine phenocrysts and showed that kimberlites co-precipitate these minerals between 1030°C and 1170°C at a maximum fO_2 from ΔNNO –3.0 to -2.2, but that the certainty of fO_2 values varies with the activity of SiO_2 (a_{SiO2}) of the magma, which is only broadly constrained (Mitchell, 1973; 1986).

To address this issue, I develop an empirical oxygen barometer for kimberlites based on the partitioning of Fe between silicate liquid and perovskite ($CaTiO_3$), an accessory mineral common in the groundmass of kimberlites. Perovskite is orthorhombic in symmetry, though the term pseudocubic is often to describe its structure. The presence of large ions, such as calcium and some rare earth metals distorts the TiO_6 octahedrons that constitute the framework of the mineral, resulting in an orthorhombic symmetry. With increasing fO_2, more Fe exists in the kimberlitic liquid as Fe^{3+}, and thus partitions more easily into perovskite, which has been shown by Mössbauer spectroscopy to accept only Fe^{3+} into its crystal structure (Muir *et al.*, 1984)

Some kimberlite perovskites, especially rim compositions, can have high amounts of Nb_2O_5 and REE oxides (up to 15 wt%), and select rim compositions show correlations between Fe^{3+} and these cations (Figure 2.1). This suggests coupled substitutions at high concentrations of Nb and/or REE oxides in perovskites, potentially complicating a simple empirical oxybarometer derived from Fe^{3+} alone. In a compilation of literature data (n=131), 85% of the kimberlite perovskites contain less than 1 wt% Nb_2O_5, and 95% contain less than 5 wt% REE oxides, none of which show any relationship between Fe^{3+} and REE or Nb at these concentrations (Figure 2.1). Nonetheless, to be certain, and to make this study most applicable to natural kimberlites with variable compositions, I also specifically investigated the effects of REE's and Nb on the partition of Fe^{3+} into perovskite.

Using experimental data the effects of composition, T and fO_2 on the partitioning of Fe between perovskite and kimberlite liquid is examined. In part II of this study I apply the experimental results from Part I in order to provide estimates of fO_2 during the crystallization of perovskite in some well-characterized natural kimberlites.

2.2 METHODS

2.2.1 Starting Materials

The first experimental challenge was to establish starting compositions that are representative of the wide compositional variation in kimberlites (Figure 2.2). The abundance of xenolithic components in kimberlites makes identification of a primitive or primary magma difficult. Examples of compositions that approximate primary magma are described at the Mayeng (Apter *et al.*, 1984), Benfontein (Mitchell, 1997), Koidu (Taylor *et al.*, 1994), and Aries kimberlites (Edwards *et al.*, 1992).

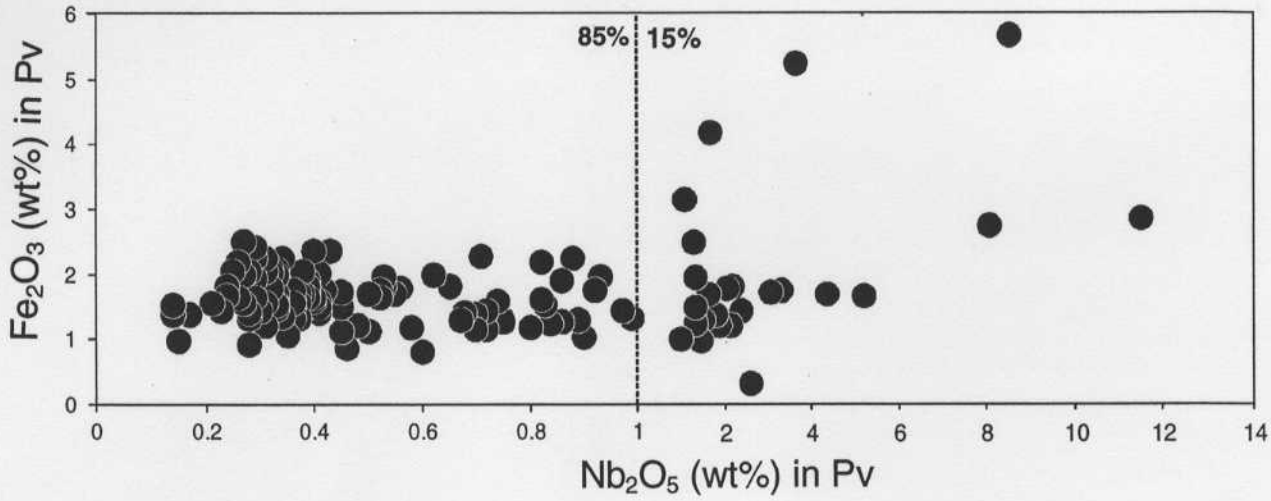

Figure 2.1: Plot of Nb_2O_5 (wt%) content versus Fe_2O_3 (wt%) content of natural perovskites. Data from the literature (n=131) show that 85% of perovskites have Nb contents less than 1wt% and 15% of perovskites have Nb content greater than 1wt% (Mitchell and Fritz, 1973; Clarke and Mitchell, 1975; Mitchell, 1878; Mitchell,1986; Chakhmouradian and Mitchell, 2000; Eccles et al.,2004).

Edgar et al. (1988) and Shee (1986) argue that the scarcity of xenoliths and xenocrysts, the low SiO_2 content and the fine-grained nature of the aphanitic kimberlite at Wesselton, South Africa indicate that it is a primitive magma composition. Price et al. (2000) contend that the aphanitic margins of thin, hypabyssal kimberlite dykes from the Jericho kimberlite are primary liquids, based on the lack of macrocrysts, the fine-grained and homogeneous nature of the groundmass and the bulk composition. Thus, the starting compositions for these experiments were based on the Wesselton and Jericho compositions, which are richer in Ca and poorer in Mg than most kimberlites (Figure 2.2). The presence of xenoliths generally results in a drop in Ca and an increase in Mg, therefore the scarcity of xenoliths may account for the high Ca and low Mg content of the base compositions. The Jericho composition has a higher CaO and lower MgO and TiO_2 content relative to that of Wesselton.

Kimberlites contain between 5 and 20 wt% H_2O and/or CO_2 (see Figure 2.2 for references). Because the primary objective of this work is to study the effect of fO_2 and T on the partitioning of Fe between perovskite and kimberlite liquid, all experiments were conducted at 100 kPa in a gas-mixing furnace where fO_2 is controlled precisely. Under experimental conditions H_2O and/or CO_2 cannot be maintained in solution, and as a result, these volatiles were excluded from the starting compositions. The Wesselton and Jericho kimberlite analyses were re-calculated on a volatile-free basis and synthetic kimberlite starting compositions were then constructed from these modified base compositions. The lack of H_2O will increase crystallization T relative to the natural hydrous case, but as shown later, this does not affect the anhydrous phase assemblages.

Kimberlites have high MgO contents in part due to accumulation of mantle olivine xenocrysts, estimated to be on the order of ~60 mol% in some of the Lac de Gras kimberlites (Fedortchouk & Canil, 2004). In order to increase the amount of liquid present in the experiments, the xenolithic olivine component was removed from the synthetic starting compositions and thereby the amount of olivine in run products was reduced. Subtratction of 60% and 50% mantle olivine component (Fo_{90}) from the Wesselton and Jericho base compositions respectively, reduced their MgO concentrations, and therefore crystallization T, and enhanced the quantity of melt present (Figure 2.2). The $CaCO_3$ component in the Jericho composition was reduced by the removal of all CaO assigned to its CO_2 content, because as noted above, the experiments were by design without CO_2.

The resultant kimberlite starting compositions (Table 2.1) were synthesized from reagent grade oxides SiO_2, TiO_2, Al_2O_3, Fe_2O_3, MnO, MgO, $CaCO_3$, Na_2CO_3, K_2CO_3 and P_2O_5 according to the normalized anhydrous compositions of the Wesselton and Jericho kimberlites (WD2, JD). In addition, simpler analogs (WC1, WC2, WC3, JC and JC2) were created by mixing fewer component oxides (SiO_2, TiO_2, Fe_2O_3, MgO and $CaCO_3$). Kimberlites also contain high concentrations of rare earth elements (REE), Sr and Nb, which are known to substitute up to 10 mol% as $CeFeO_3$, $CeNbO_3$, $Th_{0.5}TiO_3$, $SrTiO_3$ and $NaNbO_3$ components in perovskite (Carmichael, 1967; Chakhmouoradian & Mitchell, 2000; Mitchell, 1972; Nickel & McAdam, 1963; Smith, 1970). Two of the simpler system compositions (WC2 and WC4) were doped with 300ppm Ce and a 'cocktail' of 1000ppm of each of Ce, La, Sr, Nb, respectively - concentrations similar to those found in natural kimberlites (Chakhmouoradian & Mitchell, 2000; Eccles *et al.*, 2004). The

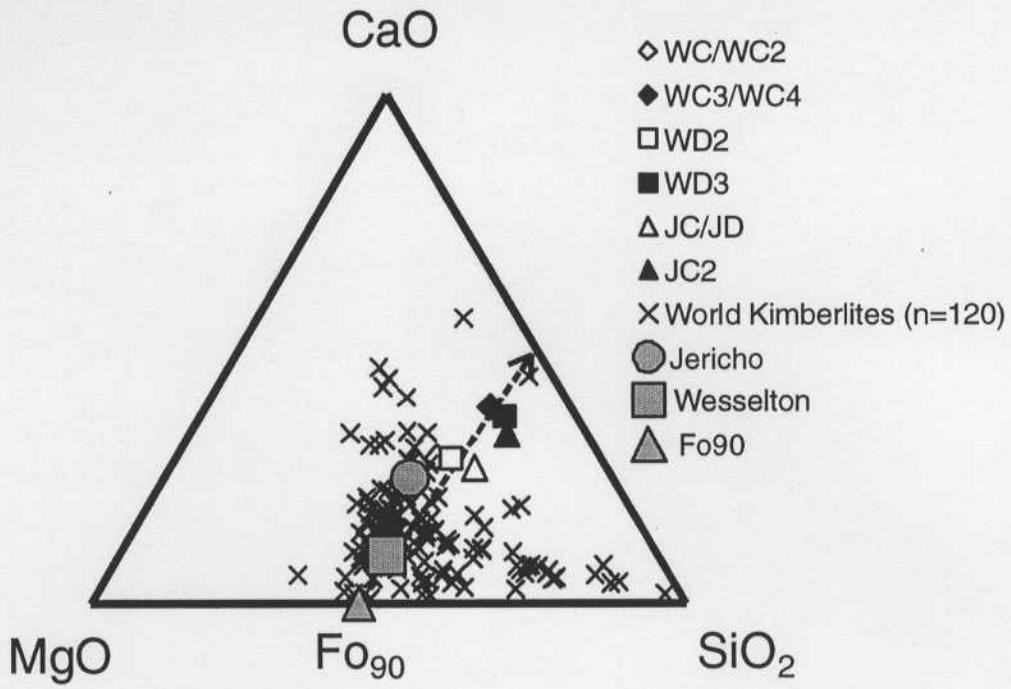

Figure 2.2: Ternary plot of starting materials (wt%) for experiments compared to world kimberlites (re-calculated volatile-free). Dashed line shows the starting compositions along on an olivine (Fo_{90}) control line toward the Jericho and Wesselton base compositions.(Price *et al.*, 2000), (Kopylova *et al.*, 1998), (Shee, 1986), (Berg & Carlson, 1998), (Clement, 1982), (Smith *et al.*, 1985), (Illupin & Lutz, 1971), (Berg & Carlson, 1998), (Smith *et al.*, 1979), (Zhang & Liu, 1983), (Gurney & Switzer, 1973), (Apter *et al.*, 1984), (Dawson & Hawthorne, 1973), (Robinson, 1975), (Skinner & Scott, 1979), (Dawson, 1972), (Scott Smith *et al.*, 1984), (Scott, 1979), (Dawson, 1967), (Muramatsu, 1983), (Illupin & Lutz, 1971), (Illupin *et al.*, 1974), (Eccles *et al.*, 2004), (LeRoex *et al.*, 2003), (Schmidberger & Francis, 2001).

latter trace elements were added to the oxide mixtures as standard element solutions and dried before grinding and decarbonation. Finally, two subsets of the simple system composition (WC5) were doped with 0.5 wt% and 1.5 wt% reagent grade Nb_2O_5, respectively, in order to examine the effects of Nb on Fe partitioning.

To further enhance the amount of liquid present in experiments at low T (1130°C), the approach of Toplis et al. (1995), was followed and a second set of kimberlite analogs (WC3, WC4, WD3 and JC2) was synthesized based on the composition of the residual glass compositions forming after ~85% crystallization in the first set of analogs (WC1, WD2, JC2). The use of these 'lower T' analogs allowed for easier phase description and identification along the entire liquid line of descent of the synthetic kimberlites from above the liquidus to as much as ~98% crystallization.

Reagent grade oxides and carbonates were dried at 700°C for 24 hours and then weighed and mixed with a mortar and pestle. P_2O_5 is hydroscopic and was therefore weighed and added shortly before mixing. Each mixture was ground under acetone in an agate mortar, decarbonated in a Pt crucible in a box furnace for ~24 hours at 950°C, and then fused for 24 hours at 1525°C in a box furnace and poured onto a metal plate. The quenched glass was then crushed and ground under acetone in an agate mortar to a grain size of less than 100 μm. Starting glass compositions were analyzed by EMP for major and minor elements and by LAM for trace elements (Table 2.1). Methods will be discussed below.

2.2.2 Experiments

Experiments were performed in a Deltech DT-31 vertical tube furnace over a range of fO_2 from four units above the NNO buffer to five log units below this buffer at T

Table 2.1: Starting compositions for experiments (wt%), * represents total Fe as Fe_2O_3.

Oxide	WC1	WC2	WC3	WC4	WC5(0.5)	WC5(2)	WC5(5)	WD2	WD3	JC2
SiO_2	34.2	33.4	31.5	31.7	32.3	32.8	32.7	32.7	34.3	38.2
TiO_2	7.8	7.7	11.9	12.0	11.1	7.9	7.8	6.6	7.3	7.7
Al_2O_3	0.3	0.5	0.2	0.2	0.2	0.2	0.2	7.6	11.0	0.3
Fe_2O_3*	13.4	12.9	20.0	19.6	21.0	14.7	14.5	11.3	11.5	18.6
MnO	0.0	0.0	0.0	0.0	0.0	0.0	0.0	0.3	0.3	0.0
MgO	21.3	21.3	8.8	8.8	9.3	20.9	20.6	17.8	8.0	9.5
CaO	22.2	22.4	25.4	25.4	25.4	21.9	21.9	20.0	24.3	23.5
Na_2O	0.0	0.0	0.0	0.0	0.0	0.0	0.0	0.1	0.1	0.0
K_2O	0.0	0.0	0.0	0.0	0.0	0.0	0.0	2.7	0.9	0.1
P_2O_5	0.3	0.1	0.1	0.2	0.1	0.1	0.1	0.1	0.3	0.1
Nb_2O_5	0.00	0.00	0.00	0.00	0.12	0.60	1.45	0.00	0.00	0.00
Sr(ppm)	72	72	84	1470	-	-	-	73	84	93
La(ppm)	4.0	4.6	4.3	1545	-	-	-	4.2	4.3	35.0
Ce(ppm)	3.9	282	3.7	1051	-	-	-	3.7	3.9	4.4
Total	99.5	98.3	98.1	97.8	99.4	98.5	97.8	99.1	97.9	98.0

of 1130 to 1300°C (Table 2.2). For each experiment, sample powders were diluted into a slurry with acetone, then loaded onto loops of 0.15mm-diameter Pt wire and after drying, were sintered using a torch. Iron-loss to Pt loops was avoided by running each experiment in duplicate, with pre-saturation of the Pt loop under the desired T and fO_2 conditions for a minimum of 24 hours. When pre-saturation was complete, the glass bead was dissolved in HF and a new slurry was sintered to the Fe pre-saturated Pt loop and run at identical T-fO_2 conditions for the final experiment. Temperature was measured with a Pt-$Pt_{90}Rh_{10}$ thermocouple calibrated at the melting point of gold. Uncertainty in the measurement of Temperature was 5 degrees celsius. Oxygen fugacity was controlled by CO-CO_2 gas mixing and measured in each experiment with a solid zirconia electrolyte cell. Fluctuations in the EMF were less than ±5mV during each experiment, which corresponds to ±0.05 log fO_2 units. Run durations varied from 24 hours at 1400°C to 72 hours at 1130°C.

For each experiment, the samples were introduced to the vertical tube furnace and the desired fO_2 was achieved after approximately five minutes, once all air was purged from the tube by the CO-CO_2 gas mixture. For reversal experiments, samples were introduced to the furnace at a lower fO_2 for approximately five minutes and then raised to a higher fO_2. Ideally, samples should have been left to equilibrate at the lower fO_2 for 24 hours before being raised to a higher fO_2. In some experiments, samples were either introduced to the furnace above the run T and cooled slowly (10°C/hour) or samples were introduced to the furnace at the run T, heated rapidly and held their for 10 minutes, then cooled slowly (10°C/hour) to the run T, in order to grow larger perovskite crystals (Table 2.2). Results from all heating paths are consistent. At the end of each experiment,

Table 2.2: Experimental run conditions and phase assemblages

Run #		T(°C)	Duration(h)	log fO2	ΔNNO*	Pv	L	Olv	Mo	Me	Geh	Px	Ulv
DT301	WC1	1300	27	-2.6	4.1	X	X	X					
DT312	WC1	1275	24	-8.8	-2.1	X	X	X		X			
DT313	WC1	1295	24	-8.6	-2.1	X	X	X		X			
DT316	WC1	1275	24	-7.4	-0.7	X	X	X		X			
DT317	WC1	1275	24	-6.9	-0.1	X	X	X	X	X			
DT336	WC1	1250	24	-7.2	-0.2	X	X	X		X			
DT339[T]	WC1	1255	24	-7.7	-0.7	X	X	X	X	X			
DT342[T]	WC1	1255	48	-7.8	-0.8	X	X	X	X	X			
DT343[T]	WC1	1255	96	-7.7	-0.7	X	X	X		X			
DT346	WC1	1250	24	-9.1	-2.1	X	X	X		X			
DT347	WC1	1255	24	-10.2	-3.2	X	X	X	X	X			
DT350	WC1	1255	24	-11.0	-4.1	X	X	X		X			
DT351	WC1	1255	26	-10.5	-3.5	X	X	X	X	X			
DT353	WC1	1250	24	-8.5	-1.5	X	X	X	X	X			
DT382	WC1	1255	29	-9.9	-3.0	X	X	X	X				
DT384	WC1	1255	25	-8.6	-1.6	X	X	X	X				
DT389	WC1	1255	24	-10.5	-3.5	X	X	X	X				
DT384	WC2	1255	25	-8.6	-1.6	X	X	X	X				
DT389	WC2	1255	24	-10.5	-3.5	X	X	X	X				
DT444	WC3	1180	87	-9.8	-2.0	X	X	X		X			
DT468**	WC3	1130	70	-13.2	-4.8	X	X		X			X	X
DT463**	WC3	1130	70	-12.0	-3.6	X	X			X		X	X
DT460**[R]	WC3	1130	68	-11.1	-2.7	X	X		X	X		X	X
DT451**	WC3	1130	70	-10.5	-2.1	X	X			X		X	X
DT468**	WC4	1130	70	-13.2	-4.8	X	X		X	X		X	
DT463**	WC4	1130	70	-12.0	-3.6	X	X		X	X		X	X
DT460**[R]	WC4	1130	68	-11.1	-2.7	X	X		X	X		X	X
DT468**	WD3	1130	70	-13.2	-4.8	X	X			X		X	X
DT463**	WD3	1130	70	-12.0	-3.6	X	X			X		X	
DT460**[R]	WD3	1130	68	-11.1	-2.7	X	X			X	X	X	X
DT451**	WD3	1130	70	-10.5	-2.1	X	X			X	X	X	
DT468**	JC2	1130	70	-13.2	-4.8	X	X					X	X
DT463**	JC2	1130	70	-12.0	-3.6	X	X			X		X	X
DT460**[R]	JC2	1130	68	-11.1	-2.7	X	X			X		X	X
DT451**	JC2	1130	70	-10.5	-2.1	X	X			X		X	X
DT503[#]	WC5(.5)	1240	27	-10.1	-3.0	X	X						
DT503[#]	WC5(2)	1240	27	-10.1	-3.0	X	X						
DT504[#]	WC5(2)	1240	38	-8.8	-1.6	X	X	X	X				
DT507[#]	WC5(2)	1240	25	-8.0	-1.0	X	X	X	X				
DT510[#]	WC5(2)	1240	24	-3.6	3.5	X	X	X	X				
DT511[#]	WC5(2)	1230	46	-6.6	0.6	X	X						
DT503[#]	WC5(5)	1240	27	-10.1	-3.0	X	X	X	X				
DT504[#]	WC5(5)	1240	38	-8.8	-1.6	X	X	X	X				
DT507[#]	WC5(5)	1240	25	-8.0	-1.0	X	X	X	X				
DT510[#]	WC5(5)	1240	24	-3.6	3.5	X	X	X	X				
DT511[#]	WC5(5)	1230	46	-6.6	0.6	X	X						

All experiments at 100kPa

[#]T-log fO2 relation for this buffer given in Frost (1991)

**Experiment slowly cooled at 10°C/h from 1180°C to final temperature

[#]Experiment rapidly heated to 1270°C for 5 min. then slowly cooled at 10°C/h to final temperature

[T]Time Series experiments (24 hours,48hours,96hours)

[R] Reversal experiments

Pv=Perovskite, L=Liquid, Olv=Olivine, Mo=Monticellite, Me=Melilite, Geh=Gehlenite, Px=Pyroxene, Ulv=Ulvospinel

samples were removed from the furnace and quenched to a glass within seconds in a stream of air. Run products were crushed, mounted in oil and examined under transparent light. The remaining chips were mounted in epoxy, and polished.

2.2.3 Analytical Methods

Coexisting phases were qualitatively examined by backscatter SEM (Hitachi S-3500N Scanning Electron Microscope) at the University of Victoria using a 15kV, 20nA primary beam. Back-scattered electron (BSE) images of run products were acquired with a Philips XL30 electron microscope at the University of British Columbia (Figure 2.3). Electron microprobe analyses of run products were carried out with a CAMECA SX50 electron microprobe at the University of British Columbia. Major and minor elements were determined at 15.0 kV acceleration voltage and a beam current of 20.1 nA with a 1μm beam. Analytical conditions were 20 s counting time on peaks and background for all major elements except for Fe, Ce and La (60 s), Sr (120 s) and Nb (160 s). Natural and synthetic standards were used for calibration. Standards were albite (Na), olivine (Mg, Si), orthoclase (Al, K), apatite (P), diopside (Ca), rutile (Ti), synthetic rhodonite (Mn) and fayalite (Fe). Drake standard glasses (3.5wt% REE) were used for Ce, La, Sr and Nb in glass and perovskite phases. Between five and twenty analysis points were measured for phases in each run product and were averaged (Table 2.3). Data reduction was done with the "PAP" $\varphi(\rho Z)$ method (Pouchou & Pichoir, 1985).

LA-ICP-MS analyses were carried out at the University of Victoria, using a VG Elemental PQ II S+ ICP-MS and a Merchantek solid-state, frequency quadrupled Nd:YAG UV laser ablation system in a He atmosphere. Trace elements in homogeneous starting glasses were determined using a laser spot size of 50μm at a frequency of 10Hz

with an energy of ~1.8mJ. ^{43}Ca was used as the internal standard for NIST 613 and starting glasses. Each block of analyses consisted of measuring the NIST glass twice followed by less than 10 unknowns then re-measuring the NIST glass twice again. Data was recorded as time resolved spectra collected over 90 seconds with 30 seconds allotted to collecting backgrounds. The individual measurements were normalized and reduced to concentrations using PlasmaLab©. Accuracy and precision on standard glasses are better than 10% (Canil *et al.*, 2003; Chen *et al.*, 2000).

2.3. RESULTS

2.3.1 Phase Equilibria

Phase proportions were calculated by mass balance of compositional data for all phases with the bulk composition. All experiments produced a mass balance with low residuals for all elements and phases totaling to within 2% of the bulk composition. Glass is present in all experiments. Olivine (<200μm) saturates in the higher MgO starting materials (WC1, WC2, WD2), followed by monticellite (<200μm), perovskite (10-50μm) and melilite group minerals (melilite, åkermanite, gehlenite) (10-50μm) depending on the presence of Al in the starting material (Figure 2.3). Pyroxene (<200μm), ulvöspinel (10-50μm) and kirschteinite (<200μm) appear in lower T (low MgO) compositions (WC3, WC4, WC5, WD3, JC2).

The details of phase equilibria and composition in all starting compositions are complex and part of a larger study, and for the sake of brevity are included only as an appendix to this study. Only compositions that are saturated in perovskite are reported in this study (Table 2.3-2.5). Detailed investigation of the two simple system compositions (WC, JC) over a large T interval (1130-1295°C) produced varying amounts of perovskite

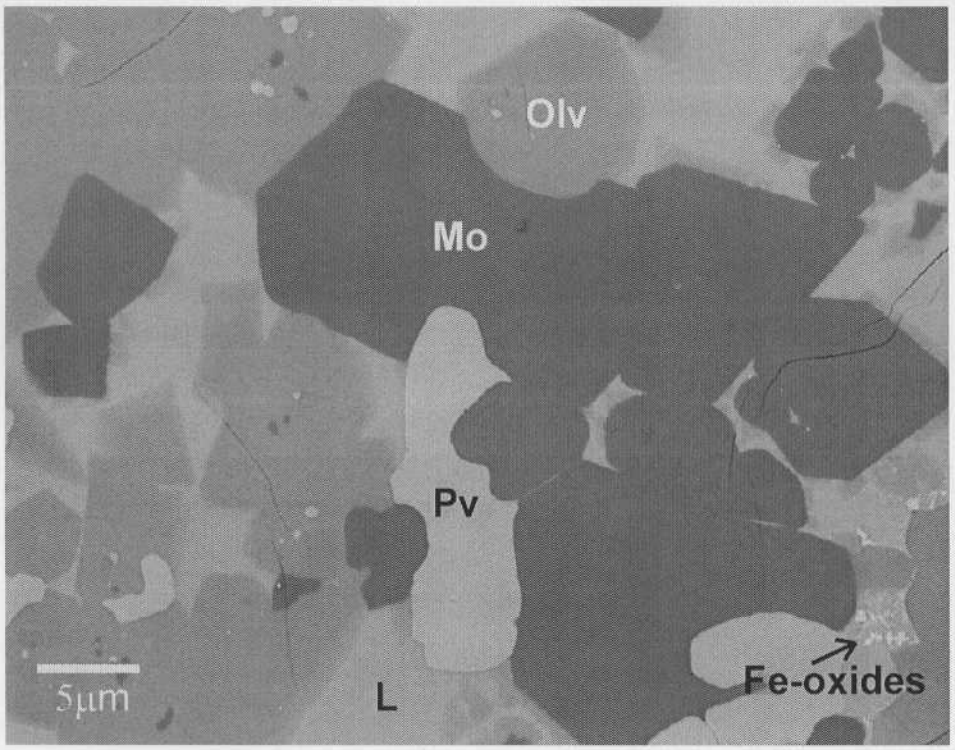

Figure 2.3: Back-scattered electron (BSE) image of some characteristic run products. The image was acquired with a Philips XL30 electron microscope at the University of British Columbia. Pv= Perovskite, Olv = Olivine, Mo = Monticellite, L = Liquid. Monticellite show quench textures of consisting of olivine. Fe-oxides were too small to be examined by EMP.

Table 2.3: Average compositions of Perovskite (wt%) with STDEV (1σ) and Run conditions

Run		DNNO	T(oC)	n	SiO_2	+/-	Al_2O_3	+/-	CaO	+/-	MgO	+/-	Na_2O	+/-	K_2O	+/-	FeO*	+/-	MnO	+/-	TiO_2	+/-	P_2O_5	+/-	Nb_2O_5	+/-	Ce_2O_3	+/-	SrO	+/-	La_2O_3	+/-	Total
DT301	WC1	4.1	1300	10	1.39	0.61	0.81	0.18	40.5	0.40	0.51	0.31	0.02	0.00	0.01	0.00	2.82	0.25	0.07	0.04	52.6	0.93	0.22	0.12									98.99
DT317	WC1	-0.1	1275	6	0.04	0.02	0.03	0.02	41.1	0.28	0.08	0.01	0.01	0.00	0.01	0.01	1.61	0.27	0.01	0.01	57.7	0.34	0.03	0.03									100.57
DT336	WC1	-0.2	1250	10	0.13	0.16	0.02	0.01	40.1	0.25	0.08	0.04	0.01	0.01	0.00	0.01	1.76	0.11	0.01	0.02	56.8	0.26	0.01	0.01									98.90
DT316	WC1	-0.7	1275	5	0.02	0.01	0.06	0.01	40.3	0.22	0.08	0.01	0.02	0.01	0.01	0.01	1.50	0.02	0.02	0.03	57.0	0.22	0.06	0.01									99.03
DT339	WC1	-0.7	1255	10	0.14	0.15	0.04	0.02	40.3	0.41	0.09	0.04	0.01	0.01	0.00	0.01	1.48	0.08	0.01	0.02	57.0	0.26	0.03	0.03									99.03
DT343	WC1	-0.7	1255	10	0.09	0.08	0.05	0.01	40.3	0.33	0.07	0.02	0.01	0.01	0.01	0.01	1.34	0.14	0.00	0.00	57.0	0.21	0.04	0.03									98.90
DT342	WC1	-0.8	1255	10	0.12	0.10	0.04	0.02	40.1	0.34	0.13	0.14	0.01	0.01	0.01	0.01	1.47	0.27	0.01	0.01	56.8	0.32	0.02	0.03									98.69
DT353	WC1	-1.5	1250	10	0.16	0.11	0.05	0.01	40.3	0.25	0.07	0.02	0.02	0.01	0.01	0.01	1.42	0.27	0.01	0.01	56.7	0.49	0.03	0.03									98.73
DT384	WC1	-1.6	1255	10	0.12	0.13	0.06	0.01	40.7	0.21	0.08	0.02	0.00	0.01	0.00	0.00	1.18	0.08	0.00	0.00	57.7	0.31	0.03	0.03									99.86
DT346	WC1	-2.1	1250	10	0.13	0.10	0.06	0.01	40.2	0.18	0.08	0.02	0.02	0.02	0.01	0.01	1.14	0.12	0.00	0.01	57.2	0.26	0.03	0.02									98.93
DT312	WC1	-2.1	1275	5	0.09	0.05	0.05	0.03	40.9	0.25	0.10	0.03	0.01	0.01	0.01	0.01	1.12	0.24	0.02	0.02	58.2	0.28	0.02	0.03									100.52
DT313	WC1	-2.1	1295	6	0.14	0.23	0.05	0.01	40.9	0.28	0.14	0.06	0.01	0.01	0.00	0.01	1.03	0.13	0.02	0.02	58.1	0.31	0.04	0.04									100.43
DT382	WC1	-2.9	1255	10	0.36	0.60	0.07	0.01	40.6	0.29	0.11	0.14	0.01	0.01	0.01	0.01	1.21	0.33	0.01	0.02	57.5	0.74	0.04	0.04									99.89
DT347	WC1	-3.2	1255	10	0.05	0.02	0.07	0.02	40.7	0.22	0.08	0.01	0.01	0.01	0.00	0.00	0.90	0.09	0.00	0.01	57.4	0.35	0.02	0.02									99.18
DT351	WC1	-3.5	1255	10	0.13	0.09	0.06	0.02	40.5	0.40	0.09	0.02	0.01	0.01	0.00	0.00	0.98	0.31	0.01	0.02	57.3	0.50	0.03	0.03									99.11
DT389	WC1	-3.5	1255	10	0.15	0.31	0.08	0.02	40.6	0.27	0.07	0.02	0.01	0.01	0.00	0.00	1.08	0.25	0.01	0.01	57.7	0.36	0.03	0.03									99.69
DT350	WC1	-4.1	1255	10	0.09	0.11	0.09	0.01	40.4	0.33	0.08	0.02	0.01	0.02	0.01	0.01	0.83	0.08	0.01	0.02	57.9	0.18	0.05	0.03									99.46
DT384	WC2	-1.6	1255	15	0.20	0.39	0.12	0.02	40.4	0.29	0.10	0.10	0.01	0.01	0.00	0.01	1.26	0.21	0.01	0.01	57.2	0.51	0.03	0.03			0.33	0.05					99.74
DT389	WC2	-3.5	1255	15	0.06	0.06	0.13	0.02	40.4	0.14	0.08	0.02	0.01	0.01	0.00	0.01	0.95	0.15	0.01	0.02	57.6	0.31	0.03	0.02			0.32	0.02					99.59
DT444	WC3	-2.0	1180	10	0.05	0.02	0.03	0.01	40.7	0.24	0.04	0.01	0.01	0.01	0.01	0.01	1.12	0.09	0.01	0.01	57.2	0.36	0.03	0.02									99.13
DT451	WC3	-2.1	1130	10	0.13	0.21	0.04	0.02	40.4	0.24	0.05	0.04	0.01	0.01	0.01	0.01	1.30	0.19	0.00	0.01	56.6	0.36	0.05	0.05									98.61
DT460	WC3	-2.7	1130	10	0.07	0.02	0.03	0.01	40.3	0.19	0.04	0.02	0.02	0.01	0.01	0.01	1.04	0.07	0.01	0.01	57.4	0.37	0.05	0.03									99.01
DT463	WC3	-3.6	1130	10	0.09	0.08	0.04	0.02	40.6	0.11	0.04	0.02	0.01	0.01	0.01	0.01	1.21	0.15	0.02	0.01	56.5	0.52	0.05	0.01									98.54
DT468	WC3	-4.8	1130	10	0.05	0.01	0.04	0.02	40.4	0.29	0.04	0.02	0.02	0.02	0.01	0.01	1.12	0.05	0.01	0.01	57.0	0.37	0.04	0.04									98.66
DT460	WC4	-2.7	1130	10	0.17	0.21	0.05	0.02	39.6	0.22	0.07	0.03	0.01	0.01	0.00	0.01	1.11	0.09	0.02	0.02	56.8	0.34	0.04	0.03	0.35	0.05	0.48	0.08	0.09	0.02	0.47	0.06	99.25
DT463	WC4	-3.6	1130	10	0.04	0.03	0.06	0.02	39.6	0.25	0.04	0.01	0.01	0.01	0.01	0.01	1.37	0.13	0.01	0.02	56.3	0.41	0.06	0.05	0.38	0.06	0.46	0.08	0.17	0.06	0.43	0.05	98.90
DT468	WC4	-4.8	1130	10	0.03	0.02	0.07	0.04	39.7	0.21	0.05	0.01	0.02	0.01	0.01	0.01	1.13	0.16	0.01	0.02	56.4	0.35	0.04	0.02	0.42	0.06	0.41	0.04	0.17	0.09	0.38	0.05	98.82
DT387	WD2	-2.0	1180	20	0.92	1.33	0.70	0.39	40.2	0.62	0.24	0.28	0.01	0.01	0.06	0.04	1.11	0.35	0.05	0.03	56.3	1.81	0.03	0.03									99.64
DT376	WD2	-2.3	1180	15	0.30	0.47	0.54	0.13	40.6	0.22	0.10	0.09	0.02	0.02	0.04	0.02	0.94	0.12	0.04	0.03	57.3	0.67	0.04	0.02									99.90
DT451	WD3	-2.1	1130	10	0.12	0.07	0.44	0.03	40.4	0.05	0.03	0.01	0.01	0.01	0.02	0.02	1.21	0.49	0.06	0.03	56.0	0.55	0.02	0.03									98.26
DT460	WD3	-2.7	1130	10	0.06	0.02	0.51	0.08	40.7	0.24	0.04	0.01	0.02	0.02	0.01	0.01	0.67	0.22	0.04	0.02	56.7	0.32	0.04	0.04									98.78
DT463	WD3	-3.6	1130	10	0.05	0.03	0.42	0.03	40.7	0.31	0.03	0.01	0.02	0.02	0.01	0.01	0.76	0.09	0.05	0.03	56.4	0.22	0.05	0.03									98.50
DT468	WD3	-4.8	1130	10	0.06	0.02	0.56	0.06	40.9	0.15	0.05	0.01	0.02	0.01	0.02	0.01	0.54	0.13	0.02	0.02	56.7	0.35	0.03	0.03									98.81
DT451	JC2	-2.1	1130	10	0.04	0.01	0.04	0.02	40.5	0.23	0.03	0.01	0.01	0.01	0.01	0.01	1.19	0.06	0.01	0.01	56.9	0.39	0.03	0.03									98.80
DT460	JC2	-2.7	1130	10	0.05	0.03	0.04	0.01	40.3	0.24	0.04	0.01	0.01	0.01	0.01	0.01	0.92	0.14	0.01	0.02	57.7	0.27	0.05	0.03									99.14
DT463	JC2	-3.6	1130	10	0.06	0.02	0.04	0.01	40.6	0.32	0.04	0.01	0.02	0.02	0.00	0.01	1.15	0.10	0.02	0.02	56.7	0.32	0.02	0.02									98.73
DT468	JC2	-4.8	1130	10	0.03	0.01	0.04	0.01	40.6	0.28	0.03	0.01	0.02	0.02	0.01	0.00	1.15	0.14	0.01	0.01	56.8	0.26	0.02	0.03									98.77
DT503	WC5(.5)	-3.0	1240	10	0.02	0.01	0.00	0.00	39.6	0.26	0.08	0.02	0.01	0.01	0.01	0.01	1.11	0.09	0.02	0.03	56.5	0.35			0.42	0.04							97.81
DT510	WC5(2)	3.5	1240	10	0.05	0.03	0.00	0.00	40.0	0.19	0.09	0.02	0.02	0.02	0.00	0.00	3.36	0.17	0.02	0.02	51.9	0.22			4.15	0.12							99.66
DT511	WC5(2)	0.6	1230	10	0.18	0.35	0.00	0.00	39.8	0.57	0.15	0.25	0.02	0.02	0.01	0.00	2.77	0.19	0.01	0.02	52.7	0.55			3.76	0.12							99.41
DT507	WC5(2)	-1.0	1240	10	0.11	0.11	0.00	0.00	39.9	0.17	0.10	0.03	0.00	0.01	0.00	0.00	2.63	0.15	0.01	0.01	52.8	0.31			3.45	0.10							98.99
DT504	WC5(2)	-1.5	1240	10	0.70	1.67	0.00	0.01	39.5	0.84	0.24	0.36	0.01	0.01	0.01	0.01	2.70	1.12	0.01	0.02	52.5	2.33			3.27	0.18							99.03
DT503	WC5(2)	-3.0	1240	10	0.04	0.01	0.00	0.00	40.0	0.24	0.15	0.01	0.01	0.01	0.00	0.01	1.70	0.11	0.01	0.01	53.9	0.42			3.24	0.23							99.01
DT510	WC5(5)	3.5	1240	10	0.35	0.69	0.00	0.00	39.3	0.35	0.21	0.18	0.01	0.01	0.00	0.00	5.08	0.19	0.01	0.01	46.8	0.81			7.83	0.17							99.53
DT511	WC5(5)	0.6	1230	10	0.03	0.02	0.00	0.00	39.6	0.25	0.14	0.02	0.02	0.02	0.01	0.01	4.22	0.28	0.01	0.02	48.8	0.44			7.35	0.20							100.12
DT507	WC5(5)	-1.0	1240	10	0.04	0.01	0.00	0.00	39.6	0.16	0.18	0.02	0.01	0.01	0.00	0.01	3.78	0.34	0.00	0.00	49.1	0.61			6.70	0.22							99.44
DT504	WC5(5)	-1.5	1240	10	0.07	0.07	0.00	0.00	39.1	0.27	0.22	0.04	0.01	0.01	0.01	0.01	3.49	0.45	0.01	0.02	48.9	0.80			7.27	0.49							99.01
DT503	WC5(5)	-3.0	1240	10	0.53	1.40	0.00	0.01	39.1	0.73	0.35	0.31	0.01	0.01	0.01	0.01	3.20	0.88	0.01	0.02	49.6	1.90			6.42	0.53							99.23

and up to ~75% melt. Experiments below 1130°C were not attempted, as the small amount of melt present would have precluded high-quality glass analyses. The solidus was not determined as part of this study. In addition to the phases listed in Table 2.2, Fe-oxides were observed in run products but were too small to be analyzed quantitatively by EMP (Figure 2.3).

The experimental conditions for all compositions that saturated in perovskite are shown in Figure 2.4. The WC composition saturates in perovskite at 1295°C, followed by the WD composition at 1180°C, whereas the JC composition does not saturate until 1130°C. Perovskite is subhedral to anhedral and ranges in size depending on cooling history from 10-50μm. No zoning was encountered in perovskites from experimental runs (Figure 2.3). Modal abundances of perovskite range from 4 to 16%, depending on T and bulk compositions.

2.3.2 Perovskite and Liquid Compositions

With changing fO_2, perovskites show variance in their Fe content as well as in Nb, Sr and REE in strongly doped compositions (Table 2.3, Table 2.4). At fO_2 conditions that apply to most natural magmas (i.e. above NNO-3.5) there is a large change in $Fe^{3+}/\Sigma Fe$ of the liquid saturated in perovskite with changing fO_2, whereas below NNO-3.5, there is little change in this ratio (Figure 2.5). For this reason, less variability in the Fe_2O_3 content of perovskite is expected at conditions below NNO-3.5. Compositions that saturate in perovskite were investigated at variable fO_2 and constant T (Figure 2.6 and 2.7) and at constant fO_2 and variable T (Figure 2.8). A positive correlation was found between fO_2 and the Fe_2O_3 content of perovskites in the Wesselton-based compositions (WC, WC2 – Figure 2.8a) and T variations of ~200°C have no observable effect on the Fe_2O_3 content

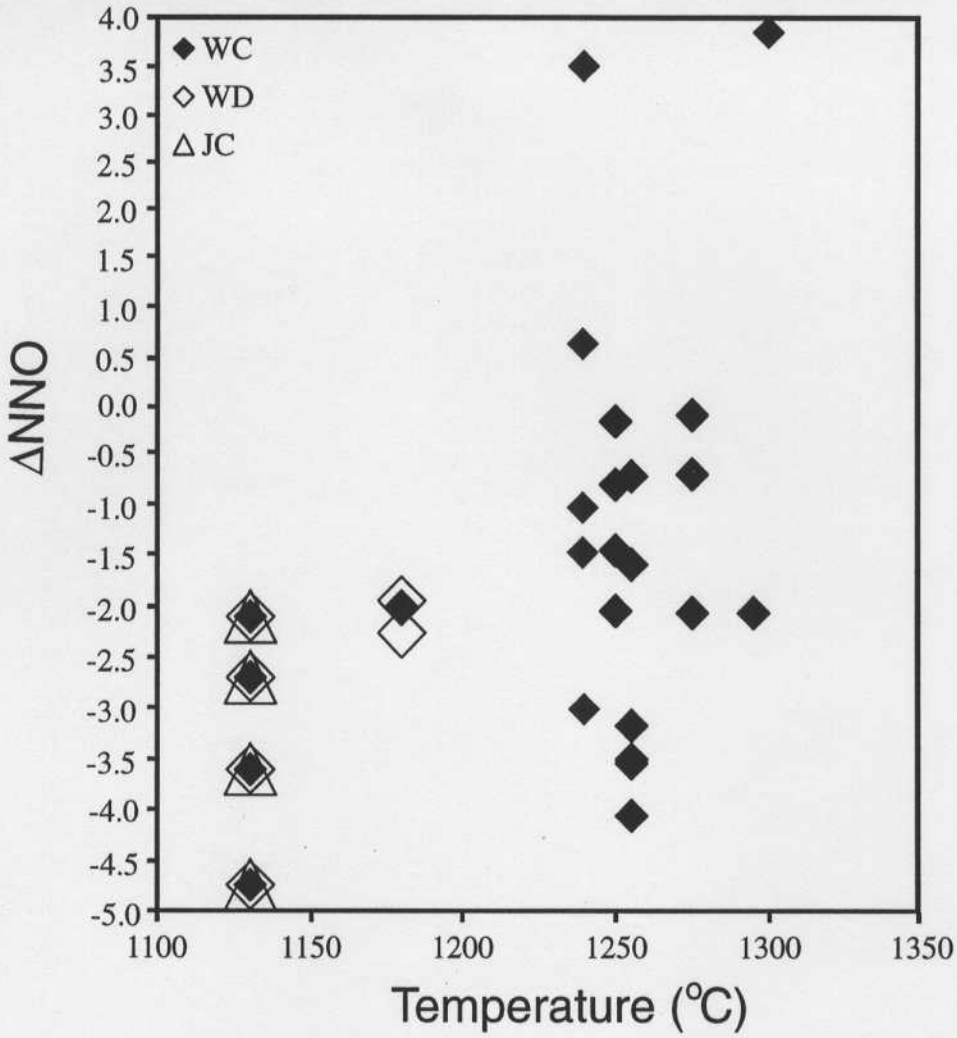

Figure 2.4: Liquidus conditions (T, fO_2) for experimental perovskites. fO_2 is reported relative to the NNO buffer from Frost (1991).

Table 2.4: Cation abundance based on 3 atoms of oxygen for Perovskite and Run conditions

Sample		ΔNNO	T(°C)	n	Na+	Ca2+	Sr2+	La3+	Ce3+	ΣA	Ti4+	Al3+	Fe3+	Nb5+	ΣB
DT301	WC1	4.1	1300	10	0.001	1.001	0.000	0.000	0.000	1.00	0.923	0.023	0.045	0.000	0.99
DT317	WC1	-0.1	1275	5	0.000	0.991	0.000	0.000	0.000	0.99	0.978	0.001	0.030	0.000	1.01
DT336	WC1	-0.2	1250	10	0.000	0.984	0.000	0.000	0.000	0.98	0.977	0.001	0.034	0.000	1.01
DT316	WC1	-0.7	1275	5	0.001	0.987	0.000	0.000	0.000	0.99	0.980	0.002	0.029	0.000	1.01
DT339	WC1	-0.7	1255	10	0.000	0.986	0.000	0.000	0.000	0.99	0.979	0.001	0.028	0.000	1.01
DT343	WC1	-0.7	1255	10	0.001	0.989	0.000	0.000	0.000	0.99	0.981	0.001	0.026	0.000	1.01
DT342	WC1	-0.8	1255	10	0.001	0.986	0.000	0.000	0.000	0.99	0.979	0.001	0.028	0.000	1.01
DT353	WC1	-1.5	1250	10	0.001	0.989	0.000	0.000	0.000	0.99	0.978	0.001	0.027	0.000	1.01
DT384	WC1	-1.6	1255	10	0.000	0.987	0.000	0.000	0.000	0.99	0.984	0.002	0.022	0.000	1.01
DT346	WC1	-2.1	1250	10	0.001	0.986	0.000	0.000	0.000	0.99	0.984	0.002	0.022	0.000	1.01
DT312	WC1	-2.1	1275	5	0.000	0.987	0.000	0.000	0.000	0.99	0.985	0.001	0.021	0.000	1.01
DT313	WC1	-2.1	1295	5	0.000	0.987	0.000	0.000	0.000	0.99	0.984	0.001	0.019	0.000	1.00
DT382	WC1	-2.9	1255	10	0.000	0.985	0.000	0.000	0.000	0.98	0.978	0.002	0.023	0.000	1.00
DT347	WC1	-3.2	1255	10	0.000	0.994	0.000	0.000	0.000	0.99	0.985	0.002	0.017	0.000	1.00
DT351	WC1	-3.5	1255	10	0.000	0.991	0.000	0.000	0.000	0.99	0.984	0.002	0.019	0.000	1.00
DT389	WC1	-3.5	1255	10	0.000	0.987	0.000	0.000	0.000	0.99	0.984	0.002	0.020	0.000	1.01
DT350	WC1	-4.1	1255	10	0.001	0.983	0.000	0.000	0.000	0.98	0.990	0.002	0.016	0.000	1.01
DT384	WC2	-1.6	1255	10	0.001	0.984	0.000	0.000	0.003	0.99	0.978	0.003	0.024	0.000	1.01
DT389	WC2	-3.5	1255	10	0.000	0.984	0.000	0.000	0.003	0.99	0.986	0.003	0.018	0.000	1.01
DT444	WC3	-2.0	1180	10	0.000	0.996	0.000	0.000	0.000	1.00	0.983	0.001	0.021	0.000	1.00
DT451	WC3	-2.1	1130	10	0.000	0.993	0.000	0.000	0.000	0.99	0.979	0.001	0.025	0.000	1.00
DT460	WC3	-2.7	1130	10	0.001	0.988	0.000	0.000	0.000	0.99	0.987	0.001	0.020	0.000	1.01
DT463	WC3	-3.6	1130	10	0.000	0.999	0.000	0.000	0.000	1.00	0.978	0.001	0.023	0.000	1.00
DT468	WC3	-4.8	1130	10	0.001	0.993	0.000	0.000	0.000	0.99	0.984	0.001	0.021	0.000	1.01
DT460	WC4	-2.7	1130	10	0.001	0.973	0.001	0.004	0.004	0.98	0.979	0.001	0.021	0.004	1.01
DT463	WC4	-3.6	1130	10	0.000	0.978	0.002	0.004	0.004	0.99	0.975	0.002	0.026	0.004	1.01
DT468	WC4	-4.8	1130	10	0.001	0.980	0.002	0.003	0.003	0.99	0.978	0.002	0.022	0.004	1.01
DT451	WD3	-2.1	1130	10	0.000	0.997	0.000	0.000	0.000	1.00	0.970	0.012	0.023	0.000	1.01
DT460	WD3	-2.7	1130	10	0.001	0.998	0.000	0.000	0.000	1.00	0.977	0.014	0.013	0.000	1.00
DT463	WD3	-3.6	1130	10	0.001	1.002	0.000	0.000	0.000	1.00	0.976	0.011	0.015	0.000	1.00
DT468	WD3	-4.8	1130	10	0.001	1.002	0.000	0.000	0.000	1.00	0.976	0.015	0.010	0.000	1.00
DT451	JC2	-2.1	1130	10	0.001	0.995	0.000	0.000	0.000	1.00	0.982	0.001	0.023	0.000	1.01
DT460	JC2	-2.7	1130	10	0.000	0.986	0.000	0.000	0.000	0.99	0.990	0.001	0.018	0.000	1.01
DT463	JC2	-3.6	1130	10	0.001	0.999	0.000	0.000	0.000	1.00	0.980	0.001	0.022	0.000	1.00
DT468	JC2	-4.8	1130	10	0.001	0.998	0.000	0.000	0.000	1.00	0.981	0.001	0.022	0.000	1.00
DT503	WC5(.5)	-3.0	1240	10	0.001	0.984	0.000	0.000	0.000	0.98	0.986	0.000	0.019	0.004	1.01
DT510	WC5(2)	3.5	1240	10	0.001	0.992	0.000	0.000	0.000	0.99	0.903	0.000	0.058	0.043	1.00
DT511	WC5(2)	0.6	1230	10	0.001	0.985	0.000	0.000	0.000	0.99	0.915	0.000	0.048	0.039	1.00
DT507	WC5(2)	-1.0	1240	10	0.000	0.991	0.000	0.000	0.000	0.99	0.921	0.000	0.046	0.036	1.00
DT504	WC5(2)	-1.6	1240	10	0.000	0.986	0.000	0.000	0.000	0.99	0.926	0.000	0.041	0.034	1.00
DT503	WC5(2)	-3.0	1240	10	0.000	0.990	0.000	0.000	0.000	0.99	0.937	0.000	0.030	0.034	1.00
DT511	WC5(5)	3.5	1240	10	0.001	0.985	0.000	0.000	0.000	0.99	0.852	0.000	0.074	0.077	1.00
DT510	WC5(5)	0.6	1230	10	0.001	0.986	0.000	0.000	0.000	0.99	0.824	0.000	0.090	0.083	1.00
DT504	WC5(5)	-1.0	1240	10	0.000	0.980	0.000	0.000	0.000	0.98	0.864	0.000	0.059	0.077	1.00
DT507	WC5(5)	-1.6	1240	10	0.000	0.991	0.000	0.000	0.000	0.99	0.862	0.000	0.066	0.071	1.00
DT503	WC5(5)	-3.0	1240	10	0.001	0.980	0.000	0.000	0.000	0.98	0.883	0.000	0.050	0.066	1.00

Table 2.5: Average composition of Liquid (wt%) in equilibrium with Perovskite with STDEV (1σ) and Run conditions

(Kress and Carmichael, 1988)

Run		ΔNNO	T(oC)	n	SiO2	+/-	TiO_2	+/-	Al_2O_3	+/-	Fe_2O_3*	+/-	MnO	+/-	MgO	+/-	CaO	+/-	Na_2O	+/-	K_2O	+/-	P_2O_5	+/-	SrO	+/-	Nb_2O_5	+/-	La_2O_3	+/-	Ce_2O_3	+/-	Total	$Fe^{3+}/\Sigma Fe$	FeO	Fe_2O_3
DT301	WC1	4.1	1300	10	28.7	0.32	6.6	0.29	5.68	0.16	6.6	0.39	0.30	0.04	12.6	0.13	34.2	1.05	0.02	0.02	0.02	0.02	4.01	0.10									98.75	0.91	0.6	6.0
DT317	WC1	-0.1	1275	5	32.8	0.29	11.3	0.27	0.45	0.01	15.0	0.16	0.01	0.02	11.7	0.34	27.6	0.25	0.01	0.01	0.00	0.00	0.14	0.04									99.04	0.47	10.0	8.9
DT336	WC1	-0.2	1250	10	30.6	0.58	12.0	1.30	0.66	0.07	21.0	0.76	0.01	0.02	8.5	1.25	25.3	0.96	0.02	0.02	0.02	0.01	0.20	0.06									98.37	0.48	10.2	9.3
DT316	WC1	-0.7	1275	5	32.2	1.75	11.9	1.79	0.59	0.04	16.7	1.53	0.01	0.02	10.7	0.70	25.8	1.36	0.01	0.01	0.01	0.01	0.20	0.07									98.17	0.40	10.0	8.8
DT339	WC1	-0.7	1255	10	31.9	0.37	12.0	0.85	0.65	0.07	19.0	1.07	0.02	0.02	9.2	1.21	25.5	0.74	0.02	0.01	0.03	0.01	0.21	0.07									98.39	0.40	11.1	7.4
DT343	WC1	-0.7	1255	10	31.9	0.13	11.3	0.15	0.66	0.04	18.3	1.44	0.00	0.00	10.4	0.37	25.3	1.55	0.03	0.01	0.02	0.01	0.26	0.05									98.14	0.40	11.6	7.7
DT342	WC1	-0.8	1255	10	32.1	0.42	11.4	0.77	0.64	0.03	18.9	0.59	0.02	0.03	9.5	0.90	25.6	0.57	0.03	0.01	0.03	0.01	0.26	0.05									98.36	0.39	10.7	8.7
DT353	WC1	-1.5	1250	10	31.8	0.95	12.1	1.72	0.72	0.11	18.5	0.62	0.01	0.01	9.2	1.17	25.7	0.79	0.02	0.02	0.02	0.01	0.25	0.07									98.36	0.31	10.2	4.6
DT384	WC1	-1.6	1255	10	31.3	1.14	13.1	1.83	0.85	0.12	19.5	0.87	0.01	0.01	8.0	1.46	25.0	0.56	0.01	0.01	0.01	0.01	0.18	0.04									98.07	0.29	12.6	5.1
DT346	WC1	-2.1	1250	10	32.5	0.25	11.8	0.84	0.75	0.05	18.7	0.63	0.01	0.01	9.2	1.08	25.3	0.69	0.04	0.01	0.02	0.01	0.22	0.05									98.59	0.24	14.4	4.6
DT312	WC1	-2.1	1275	5	33.5	0.71	12.5	0.92	0.69	0.05	14.8	0.18	0.01	0.01	10.0	1.15	27.2	0.42	0.02	0.01	0.01	0.01	0.20	0.04									98.97	0.23	14.0	4.3
DT313	WC1	-2.1	1295	5	35.1	0.16	12.2	0.17	0.57	0.01	11.3	0.37	0.01	0.01	11.8	0.42	28.1	0.36	0.02	0.00	0.01	0.01	0.16	0.05									99.29	0.24	14.1	4.6
DT382	WC1	-2.9	1255	10	32.3	0.43	12.5	1.10	0.98	0.14	19.7	0.90	0.01	0.01	7.9	1.23	24.8	0.75	0.01	0.00	0.01	0.01	0.29	0.06									98.50	0.17	16.4	3.3
DT347	WC1	-3.2	1255	10	32.8	0.89	11.8	1.09	0.75	0.07	17.4	0.86	0.01	0.02	9.7	1.14	25.6	0.60	0.01	0.01	0.00	0.01	0.23	0.05									98.32	0.15	12.8	2.2
DT351	WC1	-3.5	1255	10	33.0	0.34	12.9	1.14	0.82	0.08	17.6	0.90	0.01	0.02	8.4	1.27	25.4	0.84	0.01	0.01	0.01	0.01	0.22	0.07									98.39	0.13	9.9	1.5
DT389	WC1	-3.5	1255	10	32.5	0.29	13.1	1.02	1.02	0.11	19.3	0.81	0.01	0.01	7.3	1.00	24.9	0.88	0.01	0.01	0.01	0.01	0.25	0.04									98.45	0.13	15.4	2.3
DT350	WC1	-4.1	1255	10	33.0	0.60	13.3	1.40	0.94	0.11	17.7	1.01	0.01	0.01	7.7	1.33	25.4	0.84	0.02	0.02	0.01	0.01	0.35	0.04									98.42	0.10	18.9	2.1
DT384	WC2	-1.6	1255	10	32.6	0.23	11.2	0.18	1.44	0.04	18.1	0.87	0.01	0.01	9.5	0.14	25.5	0.87	0.02	0.01	0.02	0.01	0.14	0.04							0.03	0.05	100.98	0.29	12.9	5.3
DT389	WC2	-3.5	1255	10	32.8	0.29	12.2	1.09	1.69	0.19	17.7	0.38	0.01	0.02	8.0	0.99	25.7	0.36	0.01	0.01	0.01	0.01	0.14	0.03							0.01	0.01	101.72	0.13	15.4	2.3
DT444	WC3	-2.0	1180	10	32.6	0.20	12.2	0.14	0.35	0.02	24.2	0.13	0.01	0.02	6.7	0.08	22.8	0.16	0.01	0.01	0.01	0.01	0.16	0.05									99.13	0.28	17.5	6.7
DT451	WC3	-2.1	1130	10	30.5	0.62	9.2	0.35	0.76	0.03	26.3	0.91	0.01	0.02	4.2	0.41	24.0	0.63	0.03	0.02	0.06	0.03	3.45	0.47									98.53	0.29	20.8	8.5
DT460	WC3	-2.7	1130	10	30.5	0.60	8.9	0.83	0.77	0.10	25.9	1.65	0.01	0.02	3.9	0.33	23.7	0.95	0.02	0.01	0.21	0.06	4.40	0.76									98.28	0.23	21.6	6.4
DT463	WC3	-3.6	1130	10	32.6	2.61	6.4	4.82	0.67	0.58	28.0	2.43	0.02	0.02	7.2	4.35	23.2	2.54	0.02	0.02	0.04	0.04	0.55	0.48									98.72	0.15	21.9	4.0
DT468	WC3	-4.8	1130	10	30.6	0.38	11.0	0.73	1.18	0.09	29.4	0.62	0.00	0.00	3.6	0.28	21.2	0.27	0.03	0.02	0.04	0.02	0.57	0.05									97.71	0.09	24.0	2.3
DT460	WC4	-2.7	1130	10	30.8	0.53	8.2	0.52	0.80	0.08	26.3	0.68	0.01	0.01	4.5	0.23	23.7	0.66	0.02	0.02	0.05	0.02	3.35	0.19	0.07	0.03	0.35	0.04	0.27	0.05	0.19	0.06	98.52	0.23	22.8	6.7
DT463	WC4	-3.6	1130	10	31.4	0.15	10.3	0.22	0.91	0.04	29.5	0.48	0.01	0.01	4.0	0.22	21.3	0.28	0.02	0.01	0.02	0.01	0.85	0.06	0.14	0.02	0.09	0.01	0.06	0.04	0.04	0.03	98.74	0.15	16.7	3.1
DT468	WC4	-4.8	1130	10	31.5	0.16	10.2	0.21	1.05	0.04	28.8	0.32	0.01	0.01	4.2	0.18	21.3	0.25	0.02	0.01	0.01	0.01	1.03	0.06	0.17	0.01	0.10	0.02	0.08	0.04	0.04	0.04	98.54	0.09	24.0	2.3
DT451	WD3	-2.1	1130	10	32.5	0.28	6.6	0.07	8.79	0.09	19.6	0.26	0.76	0.04	4.6	0.05	23.8	0.18	0.06	0.02	0.47	0.05	0.77	0.04									97.96	0.29	14.2	5.8
DT460	WD3	-2.7	1130	10	32.8	0.24	6.5	0.10	8.99	0.08	19.9	0.26	0.66	0.04	4.4	0.07	23.5	0.14	0.07	0.01	0.65	0.04	0.65	0.06									98.17	0.23	15.3	4.5
DT463	WD3	-3.6	1130	10	31.5	0.24	6.4	0.08	9.01	0.06	20.1	0.15	0.68	0.05	4.6	0.06	23.1	0.19	0.07	0.02	0.64	0.05	0.65	0.05									96.74	0.15	16.6	3.0
DT468	WD3	-4.8	1130	10	31.9	0.22	6.5	0.12	9.51	0.25	19.6	0.61	0.66	0.04	4.9	0.10	23.9	0.29	0.04	0.02	0.18	0.21	0.70	0.25									97.90	0.09	26.3	2.5
DT451	JC2	-2.1	1130	10	31.7	0.25	10.2	0.24	0.81	0.02	28.7	0.72	0.01	0.01	3.5	0.18	22.6	0.53	0.02	0.02	0.02	0.01	0.87	0.06									98.42	0.29	21.3	8.7
DT460	JC2	-2.7	1130	10	31.9	0.52	9.7	0.55	0.90	0.05	27.2	1.59	0.01	0.02	2.8	0.37	24.2	1.20	0.03	0.01	0.07	0.02	1.45	0.14									98.31	0.23	21.0	6.2
DT463	JC2	-3.6	1130	10	30.8	0.23	10.2	0.14	0.85	0.02	30.1	0.34	0.01	0.02	3.5	0.12	22.0	0.22	0.03	0.01	0.02	0.01	0.63	0.05									98.12	0.15	24.3	4.4
DT468	JC2	-4.8	1130	10	31.0	0.55	10.6	0.39	0.79	0.05	29.9	0.70	0.01	0.02	3.5	0.52	22.1	0.52	0.02	0.01	0.01	0.01	0.47	0.05									98.38	0.09	17.9	1.7
DT503	WC5(.5)	-3.0	1240	10	33.4	0.17	10.9	0.18	0.19	0.02	19.8	0.11	0.01	0.02	9.5	0.07	25.4	0.28	0.01	0.01	0.01	0.01					0.13	0.02					99.26	0.17	24.9	5.1
DT510	WC5(2)	3.5	1240	10	31.9	0.36	11.6	0.19	0.32	0.03	16.4	0.16	0.01	0.01	10.3	0.52	26.6	0.32	0.02	0.02	0.01	0.01	0.08	0.01			0.89	0.05					98.17	0.89	1.8	14.4
DT511	WC5(2)	0.6	1230	10	30.3	0.30	11.1	1.16	0.77	0.07	25.8	0.57	0.00	0.01	7.4	1.03	23.9	0.44	0.01	0.01	0.00	0.01	0.18	0.02			0.97	0.12					100.28	0.60	10.3	15.2
DT507	WC5(2)	-1.0	1240	10	30.3	0.78	13.4	1.45	0.97	0.12	25.1	0.70	0.01	0.02	5.2	1.06	24.1	0.52	0.01	0.01	0.01	0.01					1.23	0.14					100.33	0.39	15.4	9.7
DT504	WC5(2)	-1.6	1240	10	31.3		11.0		0.74		22.0		0.01		8.2		24.9		0.01		0.00						1.03							0.29	15.6	6.4
DT503	WC5(2)	-3.0	1240	10	31.0	2.28	13.3	2.15	1.03	0.13	22.9	2.95	0.02	0.02	6.3	1.39	23.7	2.12	0.01	0.01	0.01	0.01					1.46	0.26					99.73	0.17	19.0	3.9
DT511	WC5(5)	3.5	1240	10	31.5	0.23	10.7	0.07	0.30	0.03	16.2	0.14	0.01	0.02	10.7	0.30	26.4	0.26	0.02	0.01	0.01	0.01	0.08	0.01			2.14	0.04					98.12	0.89	1.8	14.4
DT510	WC5(5)	0.6	1230	10	30.5	0.21	10.2	0.46	0.67	0.04	23.5	1.04	0.01	0.01	8.0	0.52	24.6	0.82	0.02	0.01	0.00	0.00	0.14	0.01			2.42	0.08					99.96	0.60	9.5	14.0
DT504	WC5(5)	-1.0	1240	10	30.5	0.54	11.8	0.72	0.70	0.04	23.1	0.82	0.01	0.01	6.2	0.61	24.7	0.76	0.01	0.01	0.00	0.00					2.88	0.18					99.88	0.39	14.1	9.0
DT507	WC5(5)	-1.6	1240	10	31.0		10.3		0.69		21.6		0.01		8.2		24.5		0.01		0.01						2.72							0.29	15.3	6.3
DT503	WC5(5)	-3.0	1240	10	31.4	1.18	11.9	1.37	0.77	0.08	19.9	1.96	0.00	0.01	7.4	0.98	24.8	1.72	0.01	0.01	0.01	0.01					3.35	0.56					99.54	0.17	16.5	3.4

of perovskites in any starting composition (Figure 2.8a). The bulk Fe content of the starting material also does not affect the amount of Fe partitioned into Pv at a given fO_2 (Figure 2.9). Increasing amounts of Nb in the starting material result in an increase in the amount of Fe in perovskite at any particular fO_2 condition, though the effect of fO_2 on Fe in Pv (slope) remains similar for a given level of Nb in the starting material (Figure 2.10).

2.3.3 Equilibrium and Reversals

Time series experiments conducted on the WC compositions (Figure 2.11) demonstrate no change in perovskite composition over run times varying from 24 to 96 hours, suggesting that equilibrium was attained in 24 hours and that no Fe loss to the platinum loop occurred.

Reversals of the Fe content of perovskite were attempted at 1130°C. Perovskites from reversal experiments that approached run conditions from lower fO_2 (i.e. reducing conditions), are shown by arrows in Figure 2.6b. In the case of WD3, perovskite has a Fe^{3+} content that plots low relative to other experiments on the WD3 composition. It appears that the Fe^{3+} content of perovskite in this experiment did not change when the fO_2 was increased to the final run conditions (Figure 2.6b). In the case of WC3 and JC2 compositions, however, the reversal experiment was successful, with the Fe^{3+} content of perovskite at the lower fO_2 conditions adjusting to the higher fO_2 (Figure 2.6b). Experiments run with different thermal histories, starting either at the run T, or cooling to the run T slowly, produced similar results, though crystals were much larger with slow cooling.

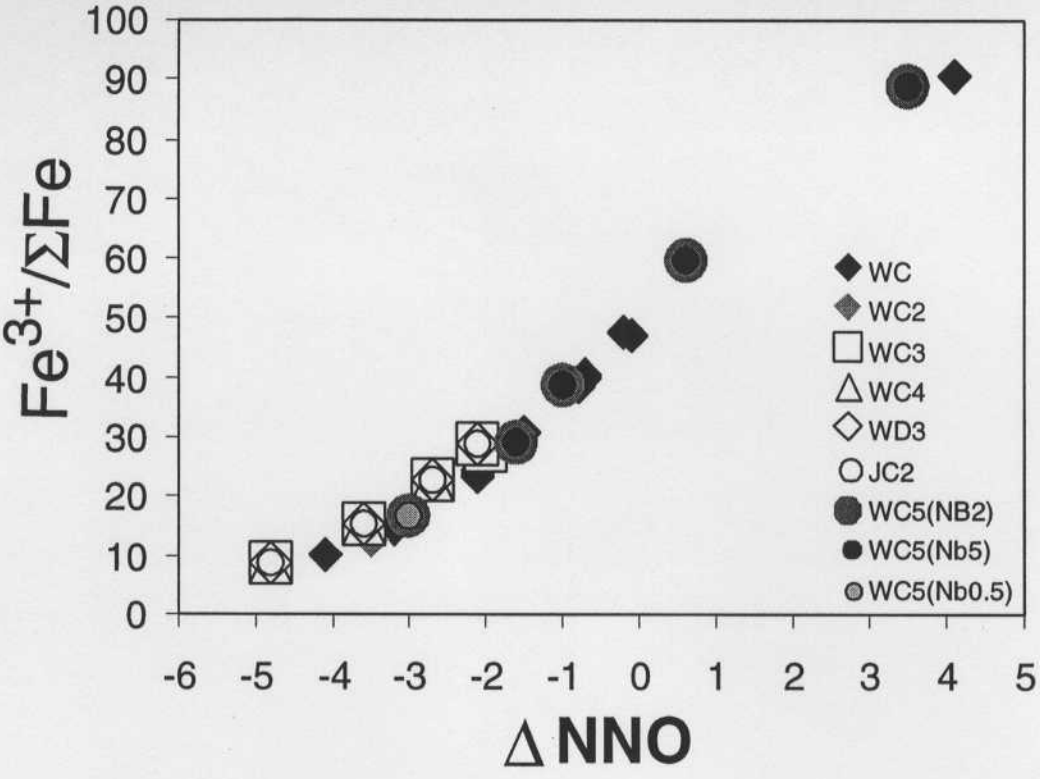

Figure 2.5: Iron oxidation as a function of oxygen fugacity for coexisting liquids compositions calculated at T-fO_2 of the experiments using the method of Kress and Carmichael (1988).

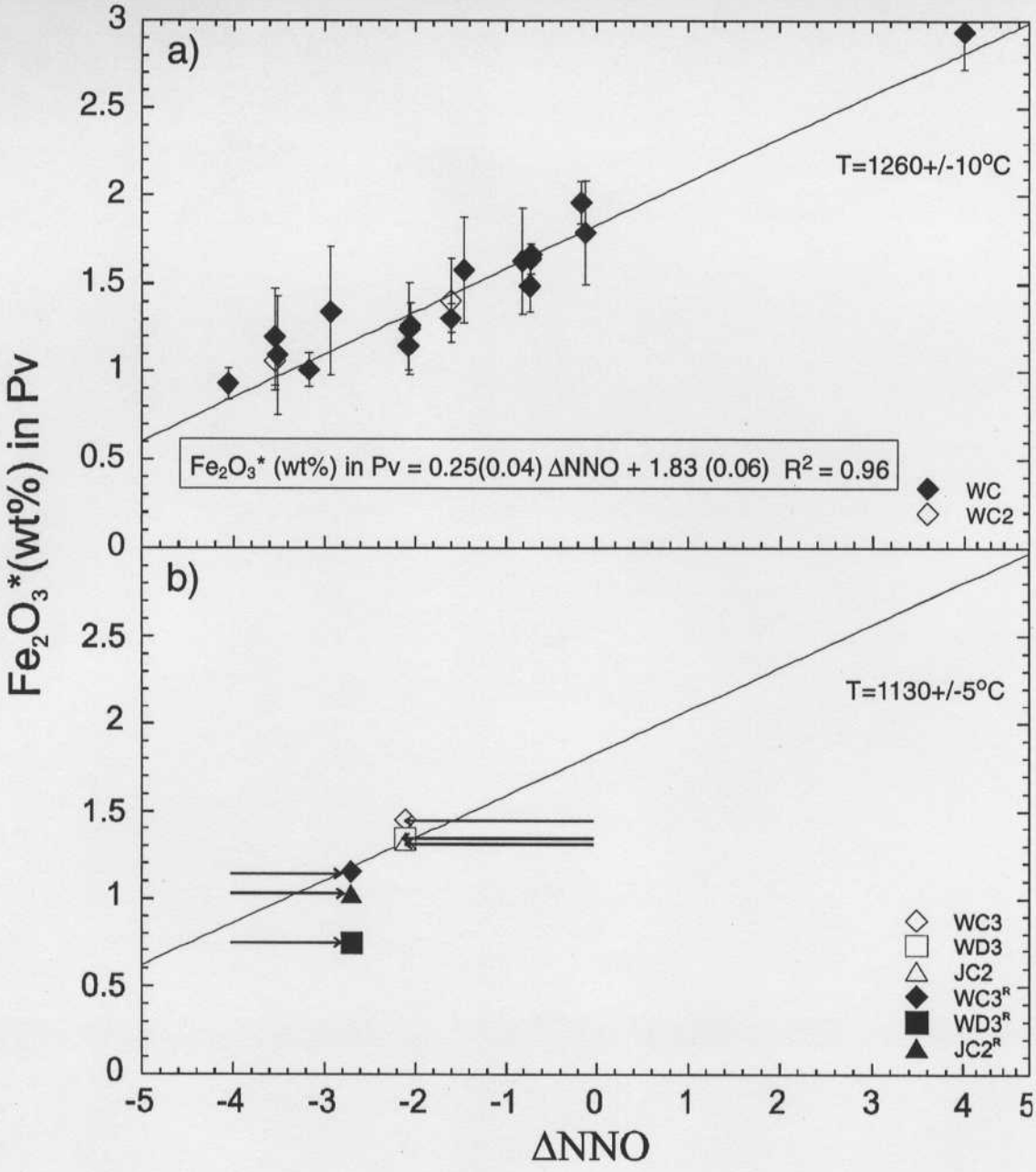

Figure 2.6: a) Weighted least square regression of Fe_2O_3* (wt%) in perovskites from simple Wesselton compositions (WC and WC2) versus ΔNNO. Error bars are ± 1σ. b) Fe_2O_3* (wt%) in perovskites from normal and reversal experiments at T=1130°C. Arrows depict the reversal path taken before equilibrium was reached.

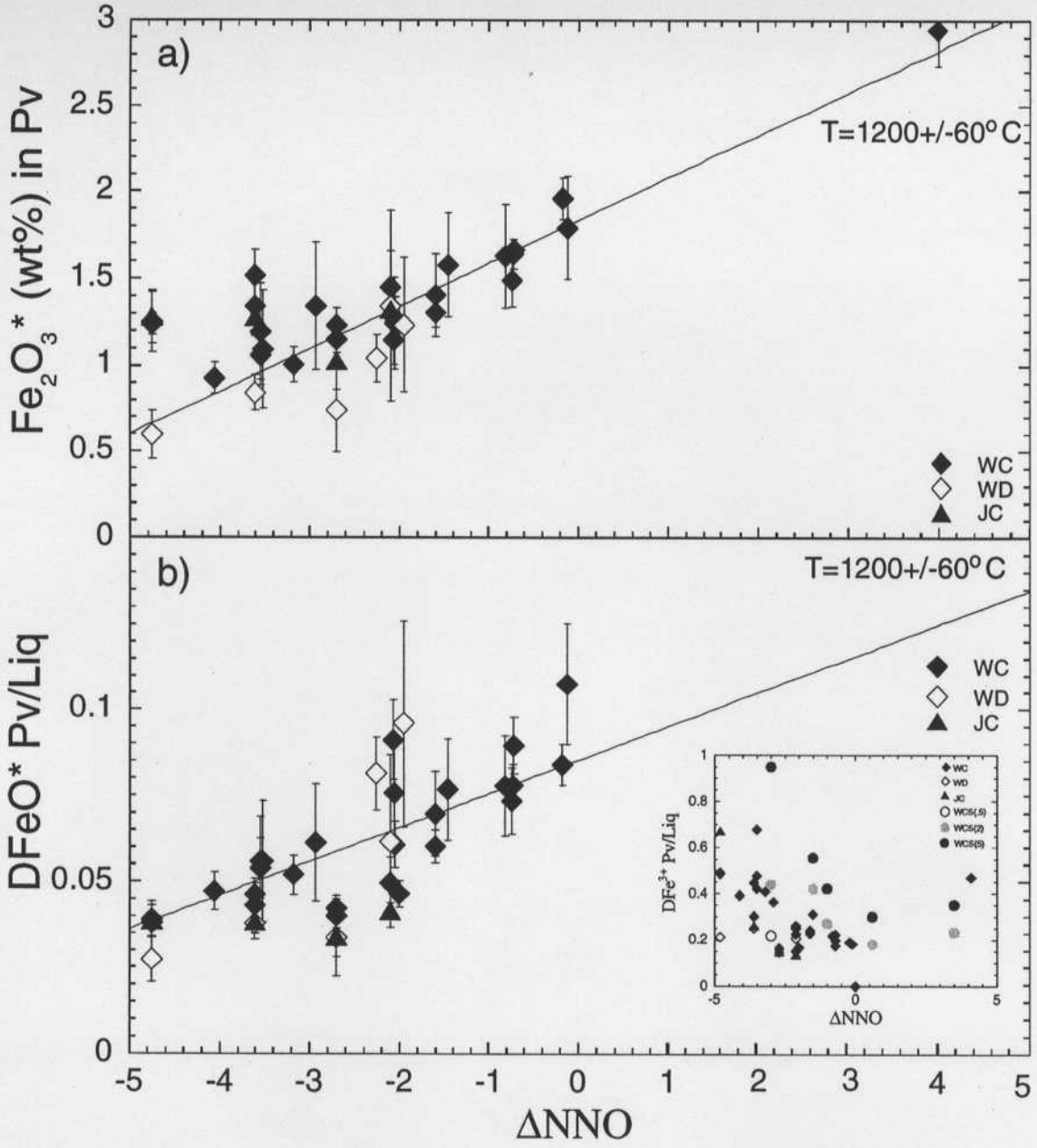

Figure 2.7: a) Fe_2O_3* (wt%) in perovskites from all compositions versus ΔNNO. b) DFeO* Pv/Liq from all compositions versus ΔNNO. Solid line is weighted least square regression of data based on WC data. Error bars are ± 1σ.

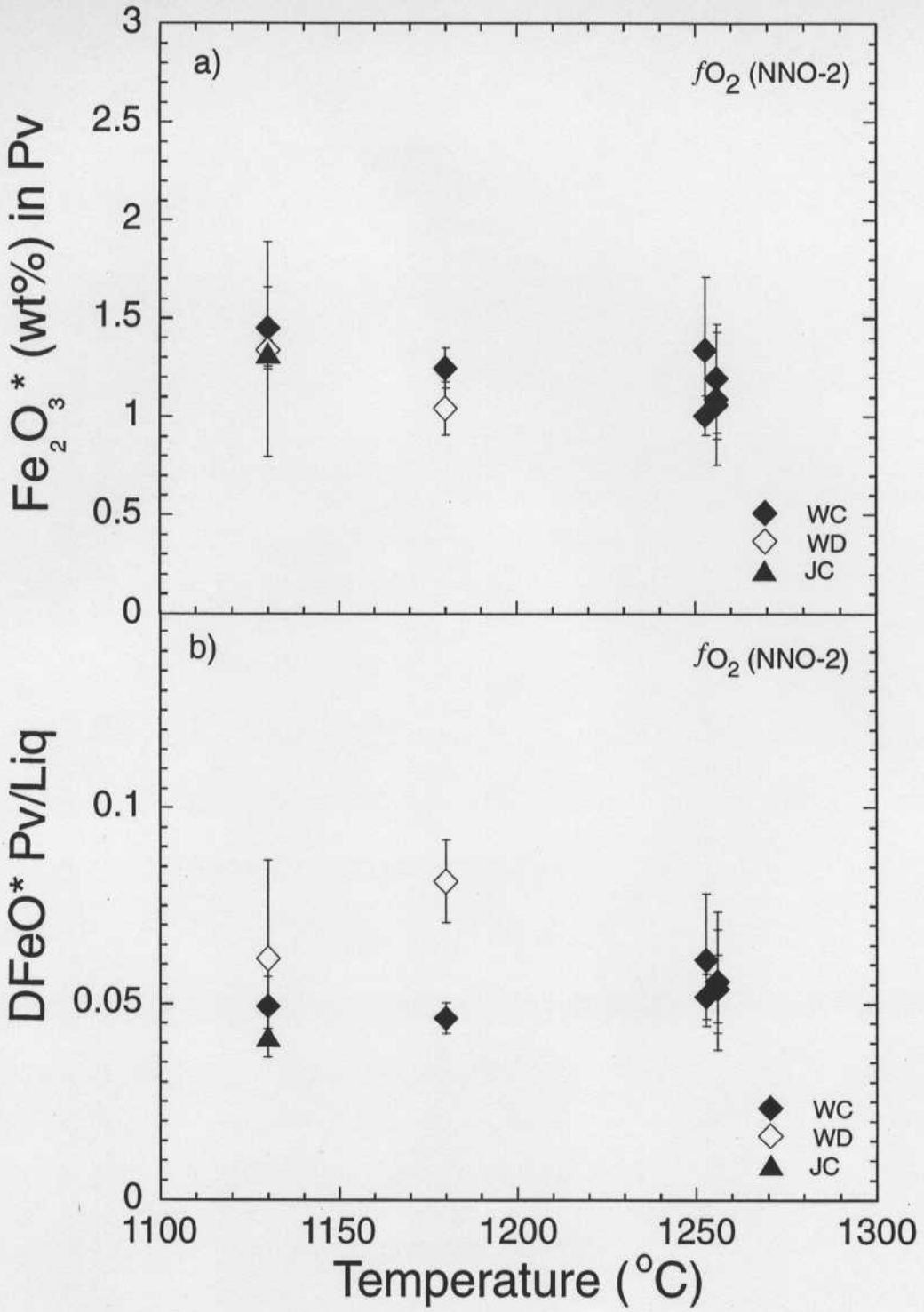

Figure 2.8: a) Fe_2O_3* (wt%) in perovskite versus T at constant fO_2 (NNO-2) in all compositions. b) DFeO* Pv/Liq versus T at constant fO_2 (NNO-2) in all compositions.

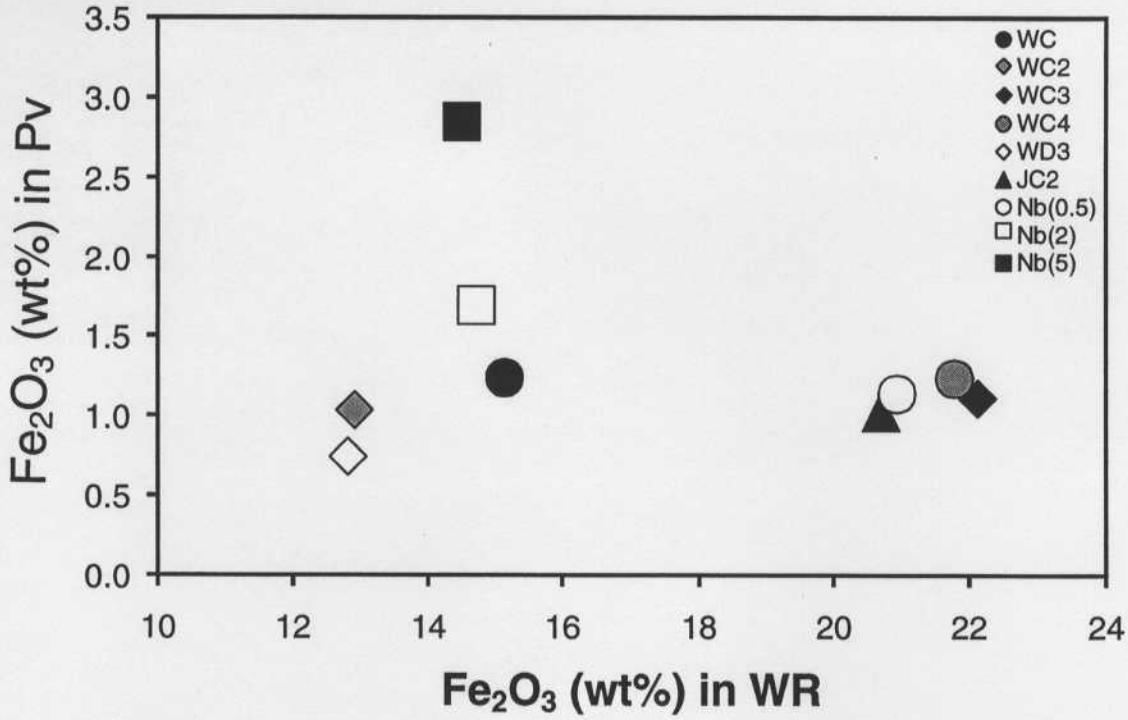

Figure 2.9: Plot showing the lack of correlation of Fe_2O_3* (wt%) in Pv with Fe content of bulk rock kimberlite in experiments (T=constant, fO_2=constant).

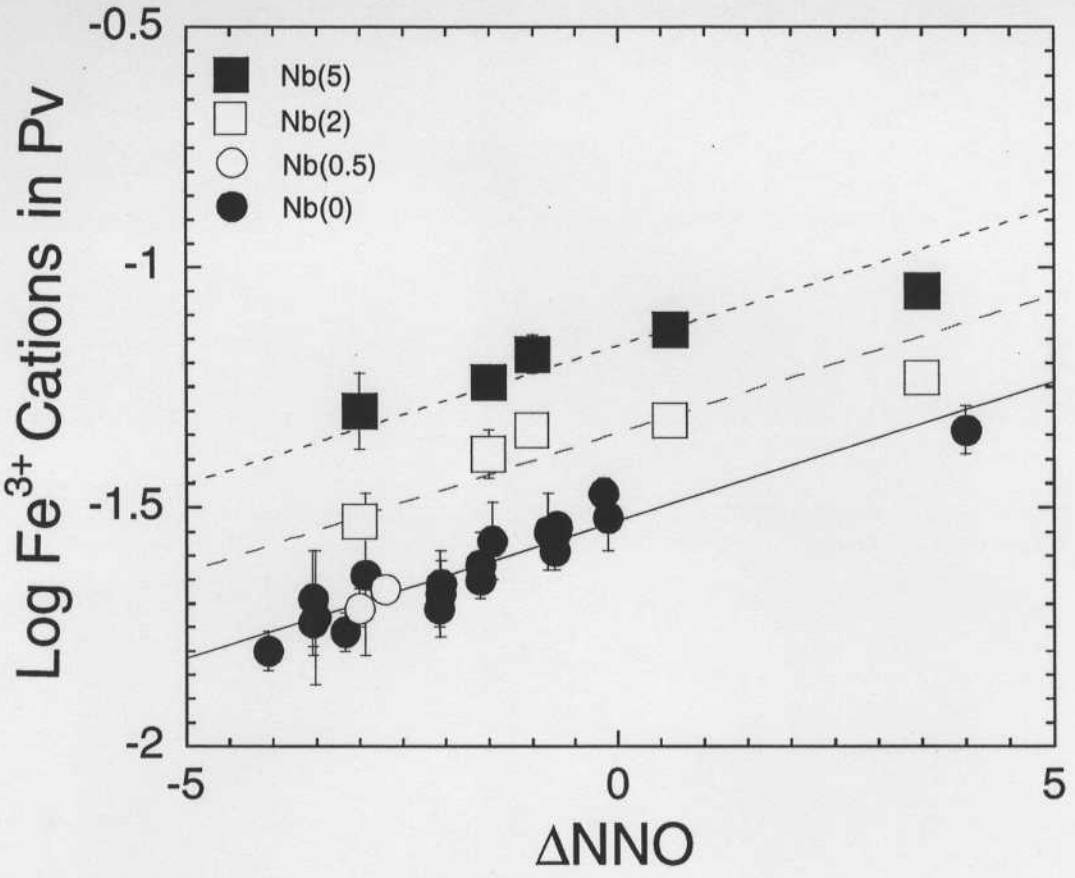

Figure 2.10: Log Fe^{3+} cations in perovskites from all compositions versus ΔNNO. Solid line is based on weighted least square regression of undoped Nb experiments. Dashed lines are constant slope fit to Nb doped data. Error bars are ± 1σ.

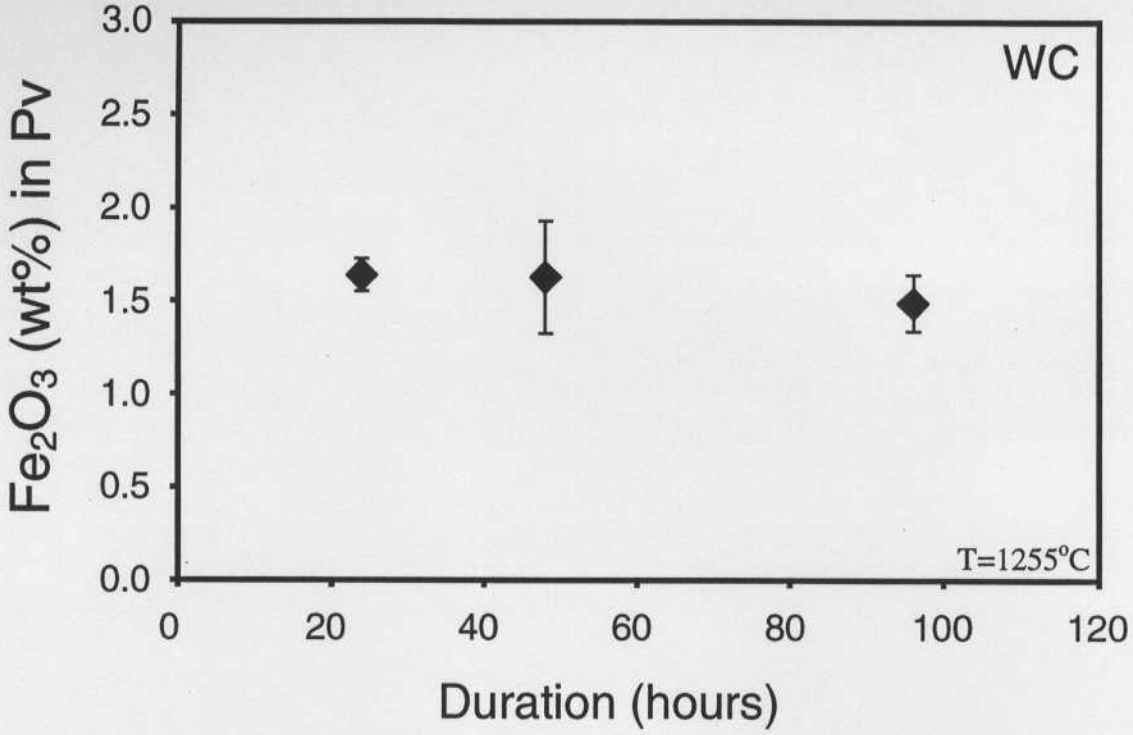

Figure 2.11: Results of time series experiments on WC composition show constant $Fe_2O_3^*$ (wt%) in perovskite with increasing duration, suggesting equilibrium was reached in 24h.

2.4. DISCUSSION

2.4.1. Perovskite saturation

With the possible exception of ulvöspinel, fO_2 is not a strong variable in controlling phase appearance in the experiments. The appearance of perovskite is controlled primarily by T and liquid composition. Compositions must have sufficient Ti and the appropriate a_{SiO2} in order for perovskite to crystallize. The T of perovskite appearance is controlled by the Ti-content of the liquid. For example, WC with 7.8 wt% TiO_2 saturates in perovskite at 1295°C, followed by WD with 6.1 wt% TiO_2 at 1180°C and finally JC with 2.2 wt% TiO_2 at 1130°C (Figure 2.4). The initial bulk Fe content of the starting materials varies from 13.4 wt% Fe_2O_3 in WC to 10.4 wt% Fe_2O_3 in WD (Table 2.3) and has no observable influence on the saturation T of perovskite. Increase in the saturation T of perovskite with increased Nb-content of the liquid was also observed.

2.4.2. Substitution mechanism for Fe^{3+} in perovskite

The correlation of Ti and Fe^{3+} cations in perovskite from undoped starting compositions suggests that the latter substitutes on the octahedral B site (ABO_3) (Figure 2.12b-inset). The substitution of Fe^{3+} for Ti^{4+} in perovskite, however, requires a coupled substitution for charge balance (e.g. $Ca^{2+}Ti^{4+}$ <==> $Me^{3+}Fe^{3+}$, where Me is a metal cation). Unlike in natural perovskites, no correlation was found between Fe^{3+} and Ce^{3+} and La^{3+}. Furthermore, the latter cations are in too low a concentration in the perovskites from the experiments (when compared to natural kimberlites) to satisfy the coupled substitution.

Data for natural perovskites (Figure 2.1) show that Fe and Nb may couple in order to substitute for Ti. A plot of Nb and Fe cations plotted against Ti cations for all

experiments doped with Nb shows a linear 1:1 correlation across a range of fO_2 from NNO-3 to NNO+3.5 (Figure 2.12a). For these starting compositions, Nb, Fe and Ti are the only cations that occupy the octahedral site in the experimental perovskites, and correlations amongst these cations provide further evidence for the coupled substitution of Fe and Nb for Ti (Figure 2.12b and 2.12c). Figure 2.12b and 2.12c show that Fe and Nb substitute for Ti in equal amounts, and each has a 1:1 substitution ratio. Both Fe and Nb account for all Ti substitutions (up to 20%), within error (Figure 2.12a).

Therefore, for Nb-doped experiments the following substitution reaction maintains charge balance:

$$2\,Ti^{4+} \rightarrow Fe^{3+} + Nb^{5+} \qquad (2)$$

at the octahedral site of experimental perovskites over fO_2 conditions ranging from NNO-3 to NNO+3.5.

It has been suggested that oxygen vacancies in the perovskite structure increase with Fe concentration (McCammon *et al.*, 2000). The results from this study show that Fe concentration increases with fO_2. Since more Fe has been found to substitute for Ti with increasing fO_2 (Figure 2.11), more oxygen vacancies must exist in the perovskite structure with increasing fO_2 (i.e. increasing Fe concentration). To further examine how the coupled substitution of Fe and Nb is affected by fO_2, Figure 2.13 shows Fe and Nb cations plotted against Ti cations for a range of fO_2, with Fe cations serving as a proxy for fO_2, and a limited range of Nb-doping (approximately 1.5wt%).

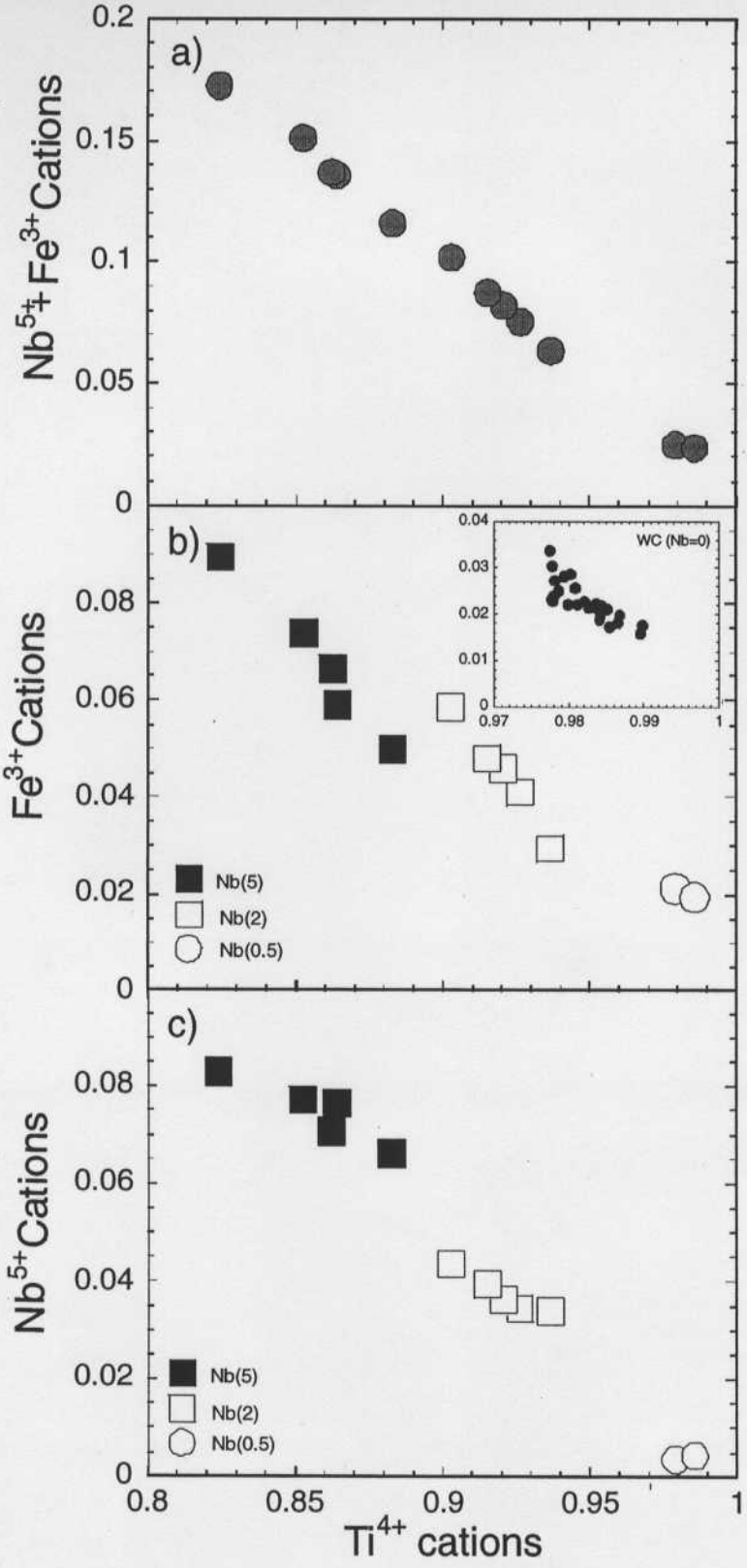

Figure 2.12:

a) Sum of Nb and Fe cations plotted against Ti cations for all experiments at constant fO_2.

b) Plot of Fe cations versus Ti cations for all Nb doped experiments and (inset) covariation of Fe^{3+} for Ti^{4+} in experiments from the WC composition (Nb=0) suggesting substitution of Fe^{3+} on the octahedral site (B) in experimental perovskites (ABO3).

c) Nb cations versus Ti cations for several Nb doping levels.

At high fO_2, Fe substitutes for Ti slightly above the 1:1 substitution ratio defined in Figure 2.12b. At high fO_2 conditions, the presence of more oxygen vacancies (represented by $\square^+$) allows Fe to substitute for Ti according to:

$$Ti^{4+} \rightarrow Fe^{3+} + \square^+ \qquad (3)$$

Conversely, at low fO_2, the lack of oxygen vacancies reduces the amount of Fe substituting for Ti by oxygen vacancy substitution and hence reduces the amount of Fe available to couple with Nb, thereby reducing the amount of Nb in experimental perovskites.

2.4.3. Effect of Temperature and Volatiles

The liquidus temperatures of perovskites in these experiments are higher than those of natural kimberlites, which are deduced to be between 700 and 850°C (Mitchell, 1986). The higher liquidus T found in these experiments is attributed to the lack of volatiles in the starting materials. The liquidus T of perovksite in a Wesselton kimberlite containing 6.20 wt% H_2O and 4.77wt% CO_2 at pressures of 1.0 - 4.0 GPa (Edgar *et al.*, 1988) was extrapolated to 100 KPa to provide an estimate of the perovskite liquidus in volatile-bearing kimberlite at the pressure of these experiments (Figure 2.14). The extrapolated liquidus T is only ~100°C lower than that for the equivalent anhydrous Wesselton compositions in this study. This difference is attributed to the effect of H_2O, which suppresses crystallization T. The presence or absence of H_2O, however, does not affect anhydrous phase assemblages. Over the crystallization interval examined, the identical phase assemblage (Ol+Mo+Px+Pv+L) in volatile-free Wesselton kimberlite (WC, WD) was observed as was observed by Edgar et al. (1988) in the same kimberlite in the presence of H_2O and CO_2.

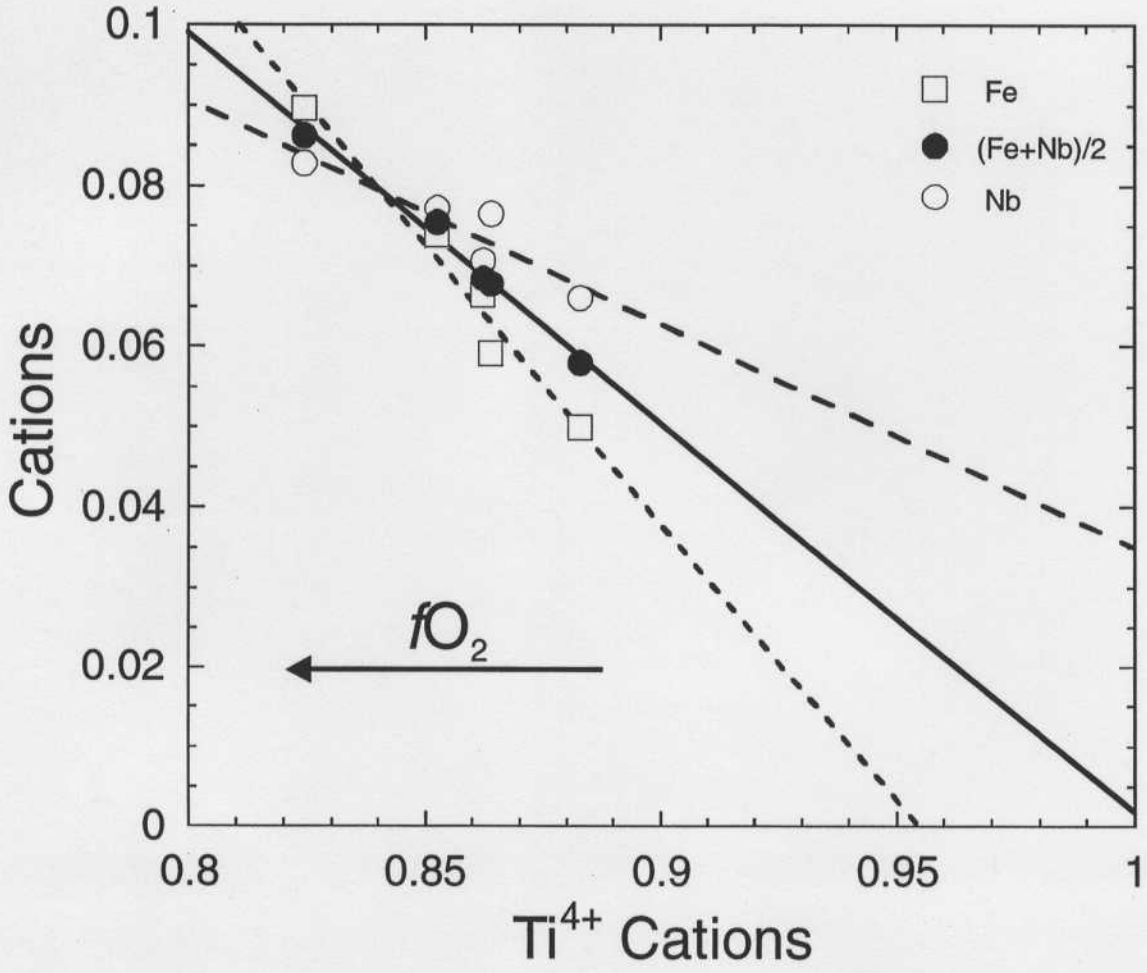

Figure 2.13: Fe and Nb cations plotted against Ti cations for a range of fO_2 (Fe cations act as a proxy for fO_2) and a limited range of Nb-dopings (approximately 1.5wt%).

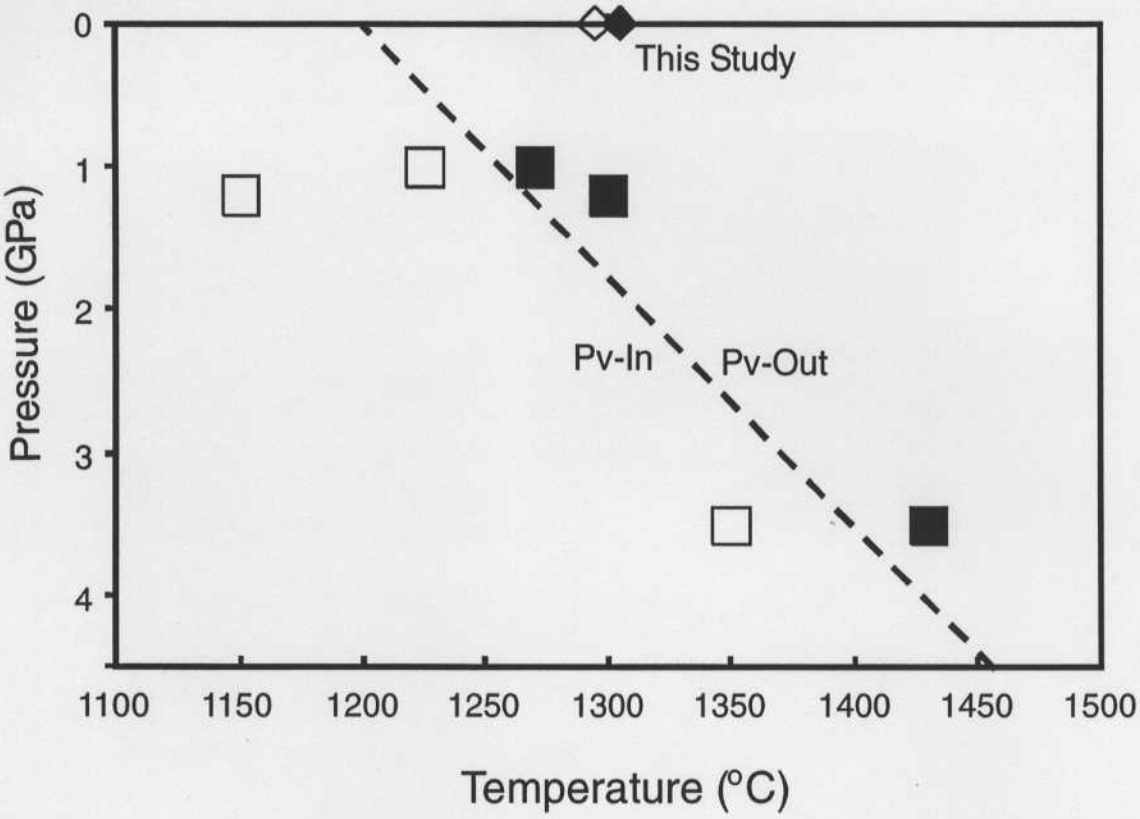

Figure 2.14: Liquidus temperatures for perovksites (open=Pv in, solid=Pv out) in experiments conducted by Edgar et al. (1988) between 1 and 4 GPa on Wesselton kimberlite with 6.20wt% H_2O and 4.77wt% CO_2 (squares) compared to that for perovskites in the equivalent volatile-free Wesselton kimberlite starting compositions from this study (diamonds).

The partitioning of total iron between perovskite and liquid, expressed as D_{FeO^*} Pv/Liq shows only a slight T dependence, with a barely discernible variation over ~200°C (Figure 2.8b). The change in D_{FeO^*} Pv/Liq, however, is mainly attributed to T-dependent changes in the Fe^{3+} content of the liquid (Kress & Carmichael, 1988), rather than in the Fe_2O_3 content of the perovskite, which remains constant over a significant T range (Figure 2.8a). Thus, in these experiments, T has no observable effect on the amount of Fe which substitutes into perovskite (Figure 2.8a).

2.4.4. Effect of fO_2

For a given bulk composition, fO_2 is by far the largest and most significant of all variables for the Fe_2O_3 content of perovskite. For all bulk compositions (WC, WD, JC) the Fe^{3+} content of perovskite (expressed as wt% Fe_2O_3) was found to show a strong correlation with fO_2 over a range of T from 1100°C to 1300°C. At fO_2 conditions below NNO-3.5, perovskites from WC and JC show nearly constant Fe_2O_3 (Figure 2.7a) suggesting this relation may break down. Recall, that at these low fO_2 conditions, however, the $Fe^{3+}/\Sigma Fe$ in the liquid coexisting with perovskite shows little variation (Figure 2.5), and therefore the Fe_2O_3 content of the perovskites essentially becomes constant regardless of fO_2. Nonetheless, the Fe_2O_3 in perovskites from the WD composition continue to decrease below NNO-3.5 (Figure 2.7a).

The reason for the difference in behaviour between different starting compositions may be due to the presence of Fe-gehlenite [$Ca_2(Fe^{3+})_2SiO_7$] on the liquidus of the WD composition. Gehlenite accepts only Fe^{3+} (Deer *et al.*, 1992) and at low fO_2 conditions, increases the competition for the decreasing amount of Fe^{3+} available in the coexisting liquid. Hence, the Fe_2O_3 of perovskite from this composition continues to decrease below

NNO-3.5. On the other hand, åkermanite [$Ca_2(Mg^{2+},Fe^{2+})Si_2O_7$] is on the liquidus of both the WC and JC compositions, but preferentially accepts Fe^{2+} over Fe^{3+} (McConnell, 1999; Seifert *et al.*, 1987) and so has little or no effect on the Fe^{3+} available to perovskite. Hence, the Fe_2O_3 content of perovskite from these compositions remains constant as their source of Fe^{3+} in the coexisting liquid becomes essentially constant below NNO-3.5. Note that the bulk partition of total iron between perovskite and liquid (D_{FeO^*} Pv/Liq) shows a strong correlation with fO_2 over a range of T from 1100°C to 1300°C for all compositions (Figure 2.7b). Unlike the Fe_2O_3 content of perovskite, D_{FeO^*} Pv/Liq continues to decrease in all compositions below NNO-3.5. In a thermodynamic sense, the exchange of Fe between perovskite and liquid (embodied in D) is not affected by what other minerals are present. Therefore, DFeO* Pv/Liq continues to decrease, even when the $Fe^{3+}/\Sigma Fe$ in the liquid coexisting with perovskite is low, regardless of what other minerals appear on the liquidus (Figure 2.7b).

2.5. CALIBRATION OF AN OXYGEN BAROMETER

Weighted least squares regression of data from perovskites that crystallized in the Nb-free WC composition (n=16) between 1130°C to 1300°C over a range of fO_2 from NNO-4 to NNO+4 (Figure 2.6a) gives the relationship (referred to as BC05) (at 2σ):

$$Fe_2O_3^* \text{ in Pv (wt\%)} = 0.25\ (0.04)\ fO_2 + 1.83\ (0.06) \qquad (4)$$

Perovskites from compositions WD and JC were excluded from this regression because they only precipitated at 1130°C, and were restricted to low fO_2, where low $Fe^{3+}/\Sigma Fe$ in the liquid coexisting with perovskite resulted in a constant Fe-content of the perovskites (Figure 2.7a). At $fO_2 \geq \Delta$NNO-3.5, equation (4) reproduces 75% of all experimental data from all Nb-free starting compositions in this study (n=31) to within 0.5 log fO_2 units and

85% of all data to within 0.7 log fO_2 units. These are conservative estimates of the uncertainty in equation (4) as an oxygen barometer. The slope value of 0.25 in equation (4) is expected because the oxidation of Fe^{2+} to Fe^{3+} (equation 1) has an equilibrium constant:

$$K = (aFe^{3+}) / (aFe^{2+})(fO_2{}^{¼}) \quad (5)$$

which scales to the power of ¼ (or 0.25) of the fO_2.

At a given fO_2, Nb levels affect the Fe content of perovskite (Figure 2.10). Two independent fitting methods were used to describe the role of Nb on Fe partitioning as a function of fO_2 in perovskite. For the "slope-intercept method" (SIM), Fe cations (Table 2.4) were fitted with a constant slope of 0.25 based on the Nb-free experiments (i.e. equation 4, Figure 2.10). The intercepts from this fit for each individual Nb doping level were then plotted against log Nb cations of the perovskite, and fitted to a linear equation. The resulting linear equation was then substituted as the second term on the right-hand side of equation (4) (i.e. the intercept in the Nb-free experiments), to give the SIM oxygen barometer (at 2σ):

$$\text{Log Fe } (0.04)=0.058(0.004)*\Delta\text{NNO}+0.26(0.02)*\text{LogNb}-0.91(0.03) \quad (6)$$

The multiple linear regression (MLR) method was used to simultaneously describe the relationship of Fe, Nb and fO_2 (Table 2.4) in all experimental data, defining an oxygen barometer (at 2σ):

$$\text{Fe } (0.031)= 0.004(0)*\Delta\text{NNO} + 0.50(0.021)*\text{Nb} + 0.030(0.001) \quad (7)$$

In both (6) and (7), Nb and Fe are in cation units per oxygens.

While both SIM and MLR fits are significant, at high fO_2 the SIM method (equation 6) has a tendency to underestimate the observed fO_2 (Figure 2.15a). On the

other hand, the MLR fit (equation 7) reproduces data well over the entire range of fO_2 (Figure 2.15b). The confidence levels with which each fitting method can be applied are remarkably similar. Both the SIM and MLR methods can reproduce 80% of the dataset to within 1 log fO_2 unit. Divergence of calculated from observed values at high fO_2 is attributed to a deviation from linearity of the relationship between Fe^{3+} cations and ΔNNO at extremely high fO_2 (Figure 2.10). Such high fO_2's (near air) are probably never realized during emplacement of any terrestrial magma (Carmichael, 1991). Due to the range of fO_2 and Nb contents over which the MLR method (equation 7) agrees with observed data it is recommended as the best oxybarometer. Because the majority of world kimberlite perovskites do not contain more that 1wt% Nb_2O_5 (Figure 2.1), the simple, Nb-free oxygen barometer (equation 4) could also be suitable in many cases.

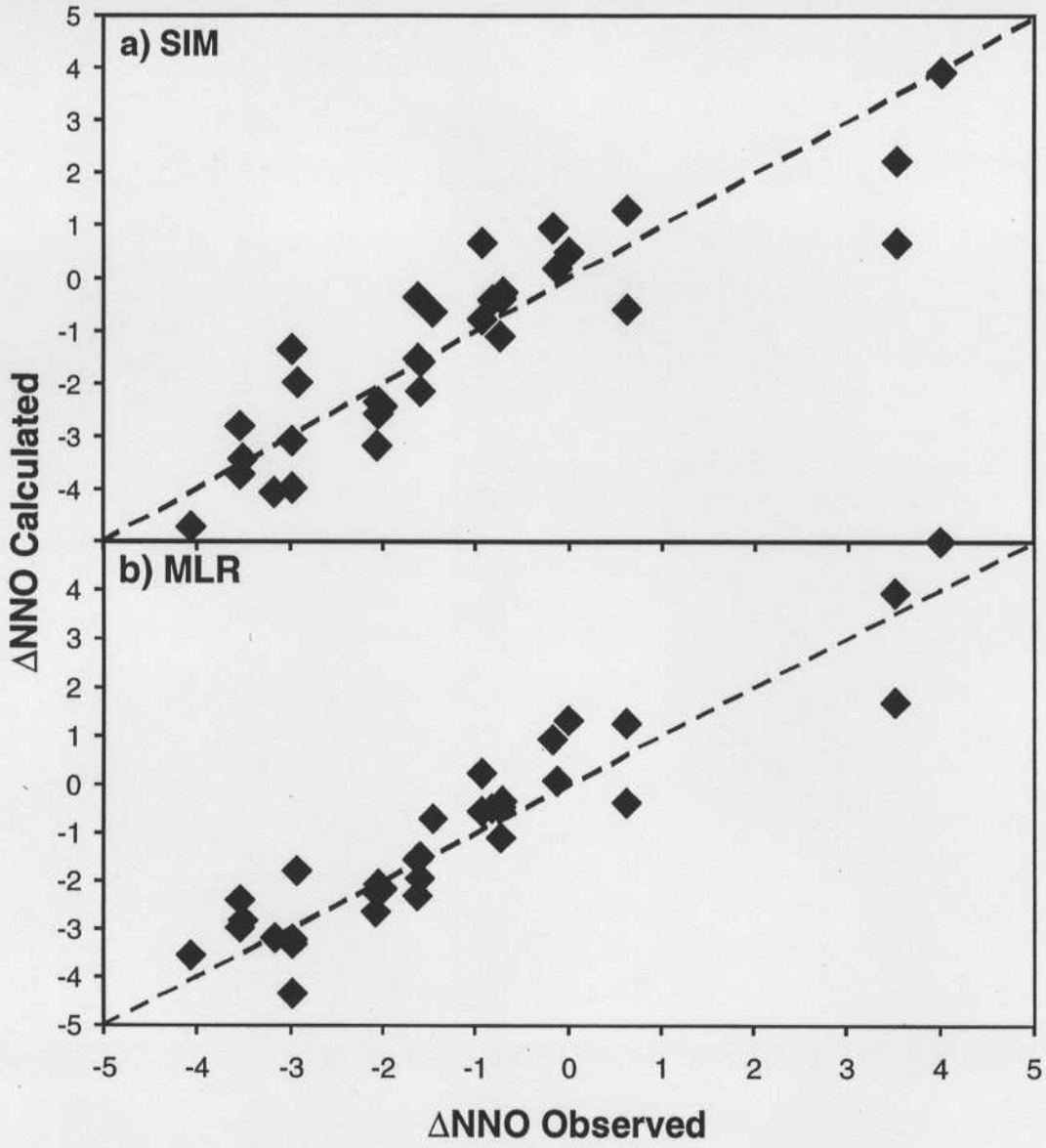

Figure 2.15: Results of calculated fO_2 based on a) the slope intercept method (SIM) and b) the multiple linear regression method (MLR) versus observed fO_2 with a 1:1 dashed line for reference.

3.

APPLICATION OF THE FERRIC IRON IN $CaTiO_3$ PEROVSKITE OXYGEN BAROMETER

3.1 INTRODUCTION

Kimberlites are a rare and unique magma type and one of the few known primary host rocks for diamond. The oxygen fugacity (fO_2) and temperature (T) of kimberlites may reflect their deep mantle source regions and may be corrosive of the diamonds that they carry. Due to their textural complexity and because no kimberlite eruption has ever been witnessed, their ascent paths and emplacement remain poorly understood.

Olivine and chromite are early phases in the paragenetic sequence of kimberlite magma crystallization (Mitchell, 1986). Fedortchouk and Canil (2004) have shown, in fresh kimberlites from Lac de Gras, olivine phenocrysts formed between 1030°C and 1170°C at a maximum fO_2 from three log units below to 2.2 log units below the nickel-nickel oxide (NNO) buffer. It is possible, if not likely, however, that the fO_2 of kimberlites changes during their crystallization and emplacement, possibly as a result of degassing of the volatile rich melts (Haggerty, 1973; Mitchell, 1975). To characterize the fO_2 evolution of kimberlites requires methods to determine the fO_2 of kimberlites along their entire liquid line of decent, not just during initial olivine precipitation.

Haggerty (1973) has suggested that variations in fO_2 are controlled by variations in CO/CO_2 and H_2/H_2O ratios in late stage melts. The role of volatiles (H_2O, CO_2) in changing fO_2 has been addressed during the ascent of magma (Sato, 1978; Brey *et al.*, 1991; Carmichael, 1991; Brey & Ryabchikov, 1994). The influence of gas-forming

elements (H, C) on fO_2 is important for understanding the speciation of redox sensitive elements, such as Fe, during their formation or emplacement. Sato (1978) suggested that the electrons necessary to reduce H^+ ions to H_2 are likely supplied by Fe^{2+} ions, which are oxidized to Fe^{3+} according to:

$$2H^+ + 2Fe^{2+} \leftrightarrow H_2 + 2Fe^{3+} \quad (8)$$

Thus, if H^+ ions are degassed as H_2, then the magma is oxidized. However, when H_2 molecules combine with O^{2-} ions to form H_2O, subsequent degassing would result in reduction of the magma according to:

$$H_2 + \tfrac{1}{2}O_2 \leftrightarrow H_2O \quad (9)$$

Sato (1978) also suggested that elemental C may combine with O^{2-} ions to form CO_2 and CO, and subsequent degassing would result in reduction of the magma according to:

$$C + O_2 \leftrightarrow CO_2 \quad (10a)$$

$$C + \tfrac{1}{2}O_2 \leftrightarrow CO \quad (10b)$$

The stability and dissolution of carbon-bearing minerals in kimberlite magmas are directly influenced by variations in fO_2 of the magma during its ascent and emplacement. The fO_2 may thereby determine the likely presence or quality of diamonds in this magma.

The purpose of this paper is to apply the experimentally calibrated oxygen barometers from Part I of this study to determine the redox state of natural kimberlites. A literature compilation is used to examine the global variation in fO_2 recorded by perovskite in kimberlites. Literature data on a single northern Alberta pipe (Eccles *et al.*, 2004), and new data gathered in a detailed study of different perovskite parageneses from eleven well-characterized kimberlite pipes, for which information on age, diamond

populations and diamond quality are available, are used to determine fO_2 variation within and between provinces, as well as within a given cluster and between eruptive phases of a single pipe. Information on the redox state of kimberlites is compared to all other mantle-derived magma types as well as to the redox state of the cratonic mantle, through which kimberlites must ascend. This information is then used to further unravel in rich detail the fO_2 recorded during degassing (H_2O, CO_2) and crystallization of this complex magma type during kimberlite formation and emplacement.

3.2 SAMPLES

3.2.1. Global dataset

Kimberlites are generally found to intrude the oldest (>1.7 Ga), most tectonically stable, and thickest (~200 km) regions of the continental lithosphere (Haggerty, 1994). Kimberlite occurences are distributed worldwide, but are generally associated with Archean or Proterozoic cratons throughout Africa, North America, South America, Siberia, Eastern Europe, China, India and Australia. A compilation of global kimberlite whole rock and perovskite analyses was assembled from the literature (see Figure 2.2 for references). The paragenesis of the perovskites and information on kimberlite type are not commonly reported, although this data is important in intepreting the fO_2 of kimberlites during emplacement.

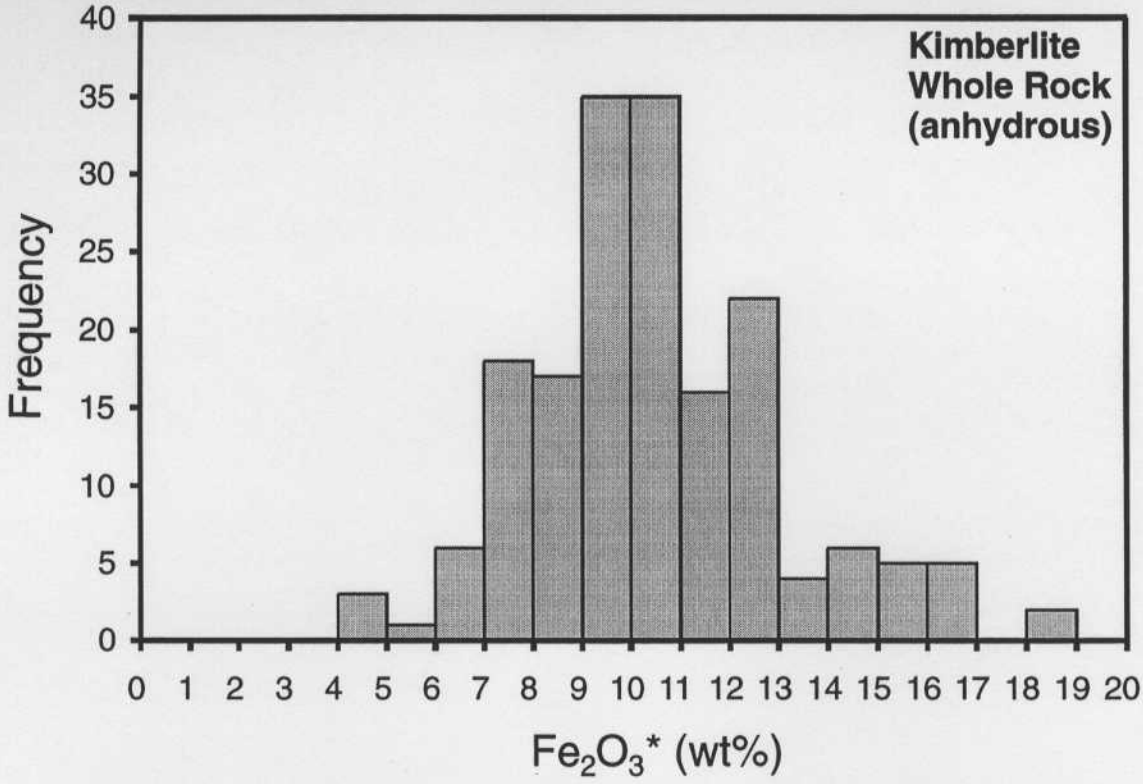

Figure 3.1: Histogram of bulk Fe (with all Fe expressed as Fe_2O_3 in wt%) in global kimberlites from the literature (re-calculated volatile-free) (see Figure 2.2 for references).

Heaman et al. (2004) identified five kimberlite domains within North America containing 540 kimberlites: (1) a Mesoproterozoic kimberlite province in Ontario, (2) an Eocambrian/Cambrian Labrador Sea Province in northern Quebec and Labrador, (3) an Eastern Jurassic province, (4) a central Cretaceous corridor and (5) a western mixed domain. In this study, the fO_2 recorded by perovksite from three of these kimberlite domains in North America will be studied in detail; the Phoenix Pipe of Northern Alberta (domain 3), the Lac de Gras kimberlite field of the Northwest Territories (domain 4) and the Somerset Island kimberlite field from Nunavut (domain 3).

3.2.2. Phoenix kimberlite

A detailed description of the geological setting of the northern Alberta kimberlite province was recently provided by Eccles et al. (2004). The abundance of literature data on both zoned and unzoned perovskites from the Phoenix pipe make it a suitable location to evaluate the variation of fO_2 within a single pipe. The Phoenix kimberlite is located in the Birch Mountains kimberlite field of northern Alberta. Basement rocks in the area belong to the Talston magmatic arc domain (1.78-1.98 Ga) and are overlain by ~500m of Phanerozoic sedimentary rocks deposited in the Western Canada Sedimentary Basin. The northern Alberta kimberlite province is dominated by Pyroclastic kimberlites (PK) followed by resedimented volcaniclastic kimberlite (RVK) (Eccles *et al.*, 2004). Several types of lapilli containing perovskite are found in the PK rocks, which may reflect multiple eruption episodes that have subsequently mixed during emplacement.

Rb-Sr phlogopite and U-Pb perovskite ages of 70.9 Ma and 70.3 Ma, respectively, are interpreted as yielding the crystallization and emplacement age of the Phoenix kimberlite pipe (Aravanis, 1999). More recently, Eccles et al (2003) determined a

crystallization age of 77.6+/-1.1 Ma based on U-Pb analysis of perovskite. The different ages may reflect separate eruption events in the same pipe.

3.2.3. Somerset Island

Somerset Island is located on the northern margin of the North American continent and is believed to overlie an Archean mantle root based on late-Archean Re depletion ages from peridotite xenoliths hosted in kimberlites (Irvine *et al.*, 1999). Kimberlites intrude middle Proterozoic to early Paleozoic sediments that overlie the crystalline Precambrian basement of the Boothia uplift (Stewart, 1987). Mitchell and Meyer (1980), have shown that the Somerset Island kimberlites are mainly brecciated diatremes and hypabyssal root zones with rare magmatic kimberlite. Schmidberger and Francis (1999), describe one of the Nikos kimberlites (Nikos 3) as non-brecciated with a magmatic texture. The Somerset Island kimberlites range in emplacement ages from 88-105 Ma based on U-Pb dating of perovskite (Heaman, 1989; Smith *et al.*, 1989), and belong to the central Cretaceous kimberlite corridor (Heaman et al., 2004).

Perovskite from the Somerset Island kimberlites (Table 3.2) occurs mainly as discrete, compositionally unzoned crystals commonly mantled by Fe-Ti oxides. Application of the oxybarometers is limited to unzoned perovskites from six different pipes within the Somerset Island kimberlite field (Table 3.1).

Batty Complex

The Batty Complex kimberlite is a dark green hypabyssal kimberlite. Perovskites are 20-100 μm, subhedral to euhedral and unzoned (Figure 3.2a).

Elwin Bay

The Elwin Bay kimberlite is transitory between hypabyssal and tuffistic kimberlite, containing altered olivines and pelletal lapilli. Perosvkites are 50-100 μm, euhedral and unzoned (Figure 3.2b).

Zulu

Zulu (currently referred to as 'Freighttrain') is a brown, highly altered tuffistic kimberlite with altered olivine and pelletal lapilli. There are at least two generations of perovskite: one zoned with 30-35 μm, subhedral to euhedral, cores mantled by 10-15 μm rims (Figure 3.2c), and a second set of 20-50 μm, subhedral to euhedral, unzoned crystals.

K4

The K4 kimberlite is a dark green hypabyssal kimberlite. Perovskites are 30-80 μm, sub to euhedral and resorbed (Figure 3.2d). Some crystals display mottled compositional zoning.

Nikos 1

JP1 is a tuffistic kimberlite breccia, containing 20-100 μm, subhedral perovskites with thin rims (<1μm) of Fe-Ti oxide. Perovskite also occurs as mantles on Fe-Ti oxides which mantle perovskite. The inverse texture also occurs with Fe-Ti oxides mantling Perovskite all of which are mantled by Fe-Ti oxides.

JP1-101D is a dark green hypabyssal kimberlite, containing two separate generations of perovskite. A set of 50 μm, anhedral, perovskite cores with thick rims of Fe-Ti oxide are most abundant (Figure 3.2e). A set of 20-40 μm, subhedral to euhedral, resorbed perovskites is also recognized (Figure 3.2f).

Table 3.1: Kimberlite locality, age, geology, relative fO_2 estimates (1σ) and perovskite description.

Locality	Age (Ma)	Kimberlite Geology	Pv Type	Perovskite Description	n	Matrix Minerals Carb	Ap	Mnt	Phl	Chr	Ti-Mt	Pyr	ΔNNO BC05	SIM	MLR
Lac de Gras															
Panda	53.0+/-3.8	Volcaniclastic Kimberlite, resedimented VK with minor primary VK	II	10-30μm, euhedral, cubic, compositional zoning	14	X	X			X	X		3.3 (0.8)	-1.5 (0.7)	-2.5 (0.8)
Grizzly	51.1+/-7.1	Hypabyssal Kimberlite, macrocrystic, heterolithic	II	unzoned,10-30μm, subhedral to euhedral, cubic grains	7	X	X	X	X	X	X		4.1 (0.6)	-0.1 (0.6)	0.5 (1.0)
			III	unzoned,10-30μm, subhedral to euhedral, cubic grains											
			I	Core 1: 5μm, subhedral to euhedral, cubic grains	1								-3.8	-2.9	-3.4
			III	Rim 1: 5-7μm, subhedral to euhedral, cubic grains											
			II	Core 2: 25 μm, subhedral to euhedral, cubic grains											
			III	Rim 2: 5 μm, subhedral to euhedral, cubic grains											
			II	Core 3: 10 μm, subhedral to euhedral, cubic grains											
			III	Rim 3: 10-15μm, subhedral to euhedral, cubic grains											
Misery		Volcaniclastic Kimberlite, associated dykes of macrocrystic HK	II	10-20μm, sub to euhedral, cubic, compositionally zoned	9	X	X		X	X	X		6.5 (0.4)	2.5 (0.3)	5.7 (0.6)
			III	10-20μm, sub to euhedral, cubic, compositionally zoned											
Aaron	45.2+/-1.3														
hypabyssal		Hypabyssal Kimberlite	II	50-100μm, anhedral to subhedral, unzoned	4	X	X	X	X	X	X		6.6 (1.0)	1.7 (0.7)	3.6 (1.6)
volcaniclastic		Pelletal Volcaniclastic	II	10 μm, unzoned, corroded, euhedral, cubic	12	X			X	X		X	6.0 (0.8)	1.4 (0.6)	3.1 (1.2)
Torrie	late Cretaceous-early Paleocene	Volcaniclastic Kimberlite Tuff and Tuff Breccia. Macrocrystic, heterolithic, organic-bearing.	II	small central zone of cubic, zoned crystal	1	X	X		X	X	X	X	5.3	2.2	4.7
			II	30-50 μm, compositionally zoned with Olv and Chr inclusions	3								3.3 (1.6)	0.7 (1.0)	1.9 (1.9)
Somerset Island															
BND	100	Hypabyssal Kimberlite		20-100μm, unzoned, sub to euhedral, corroded margins	15	X			X	X	X		-4.4 (0.5)	-5.0 (0.4)	-4.1 (0.3)
K4		Hypabyssal Kimberlite		30-80 μm, sub to euhedral, corroded margins	9	X			X	X			-0.8 (0.7)	-2.2 (0.7)	-2.0 (0.6)
Zulu		Tuffistic Kimberlite olivine altered, pelletal lapilli		20-50 μm, unzoned, subhedral to euhedral, corroded margins with reaction rims and Olv inclusions	5	X	X			X	X		2.3 (1.0)	-0.4 (0.6)	0.2 (0.7)
				Cores: 30-35 μm sub to euhedral with cubic cores	3								3.0 (2.0)	0.3 (0.4)	1.0 (0.7)
				Rims : 10-15 μm euhedral mantles on cubic cores									2.5 (1.0)	-1.0 (0.9)	-0.8 (1.3)
Elwin Bay	105	Hypabyssal and Tuffistic Kimberlite, olivines altered, pelletal lapilli		50-100μm, subhedral, rims of Fe-Ti oxides, corroded margins	10	X			X	X	X		-1.1 (0.8)	-2.3 (0.6)	-2.2 (0.6)
Nikos Main	100														
JP1		Tuffistic Kimberlite Breccia, xenoliths not reacted out		20-100μm, sub to euhedral, with thin rim of Fe-Ti oxide (<1μm)	8	X	X	X	X	X	X		-2.3 (0.7)	-3.3 (0.6)	-3.0 (0.5)
				Pv cores (<1μm) mantled by Fe-Ti oxides with Pv rims (<2μm)											
				Pv cores (<2μm) mantled by Fe-Ti oxides (60μm)											
JP1-101D		Hypabyssal Kimberlite		20-40 μm, sub to euhedral, resorbed	4	X			X	X	X		-0.1 (1.2)	-3.5 (1.3)	-3.3 (1.4)
				Cores : 50μm, anhedral with thick rims of Fe-Ti oxide	5								-1.2 (1.3)	-2.2 (1.3)	-2.0 (1.1)
				Rims : Fe-Ti oxide rims											
Nikos 3	100														
JP3		Hypabyssal Kimberlite		50μm, euhedral, unzoned	8	X			X	X			-1.5 (0.7)	-4.1 (0.4)	-3.6 (0.3)

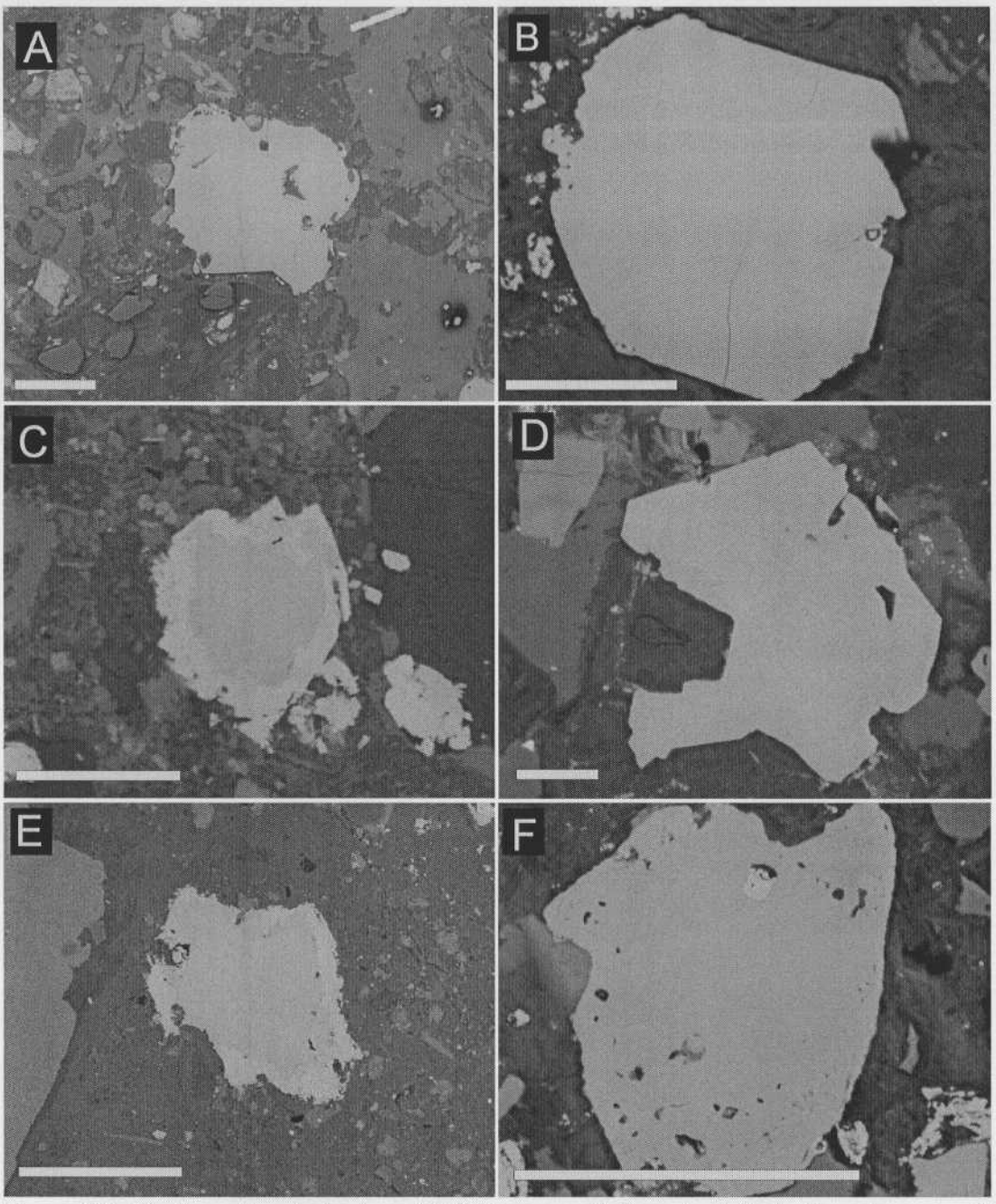

Figure 3.2: Back-scattered electron (BSE) Images of characteristic textures in perovskites from Somerset Island kimberlites. Scale bar is 50 μm for all images. (A) Unzoned, subhedral perovskite, Batty Complex. (B) Unzoned, euhedral perovskite, Elwin Bay. (C) Zoned, subhedral perovskite with Fe-Ti oxide rim, Zulu. (D) Resorbed, euhedral perovskite, K4. (E) Zoned, anhedral perovskite with thick Fe-Ti oxide rim, Nikos1. (F) Resorbed, subhedral perovskite, Nikos1.

Table 3.2: Representative Compositions of Perovskite from Somerset Island Kimberlites

Wt. %	1	2	3	4	5	6	7	8
Na_2O	0.39	0.32	0.38	0.53	0.62	0.41	0.46	0.65
CaO	37.53	37.37	36.66	34.23	35.75	37.42	36.51	33.24
SrO	0.13	0.16	0.14	0.22	0.10	0.10	0.10	0.08
La_2O_3	0.61	0.79	0.96	1.42	1.00	0.63	0.66	1.19
Ce_2O_3	1.47	1.84	2.26	3.68	2.62	1.48	1.76	3.36
Pr_2O_3	0.13	0.20	0.29	0.41	0.28	0.16	0.28	0.35
Nd_2O_3	0.55	0.72	0.90	1.28	1.14	0.63	0.76	1.43
ThO_2	0.13	0.32	0.23	0.78	0.40	0.16	0.30	1.16
TiO_2	55.71	53.83	53.72	50.40	52.98	55.00	54.96	51.30
Al_2O_3	0.00	0.12	0.15	0.07	0.00	0.01	0.00	0.07
Fe_2O_3	0.94	1.44	1.50	2.30	1.35	1.23	1.45	1.61
$Nb2O_5$	0.58	0.82	0.88	2.12	1.62	0.70	0.73	2.32
Ta_2O_5	0.03	0.05	0.05	0.17	0.11	0.06	0.06	0.23
Total	98.34	98.11	98.29	97.80	98.16	98.13	98.20	97.23
Na	0.018	0.015	0.017	0.025	0.029	0.019	0.021	0.031
Ca	0.943	0.950	0.933	0.897	0.918	0.945	0.924	0.872
Sr	0.002	0.002	0.002	0.003	0.001	0.001	0.001	0.001
La	0.005	0.007	0.008	0.013	0.009	0.006	0.006	0.011
Ce	0.013	0.016	0.020	0.033	0.023	0.013	0.015	0.030
Pr	0.001	0.002	0.003	0.004	0.002	0.001	0.002	0.003
Nd	0.005	0.006	0.008	0.011	0.010	0.005	0.006	0.013
Th	0.001	0.002	0.001	0.004	0.002	0.001	0.002	0.007
ΣA	0.987	1.000	0.992	0.990	0.995	0.990	0.978	0.967
Ti	0.983	0.961	0.960	0.927	0.955	0.975	0.977	0.946
Al	0.000	0.003	0.004	0.002	0.000	0.000	0.000	0.002
Fe	0.017	0.026	0.027	0.042	0.024	0.022	0.026	0.030
Nb	0.006	0.009	0.009	0.024	0.018	0.007	0.008	0.026
Ta	0.000	0.000	0.000	0.001	0.001	0.000	0.000	0.002
ΣB	1.006	0.999	1.001	0.996	0.998	1.005	1.011	1.004

1. discrete unzoned crystal in groundmass, Beatty Complex; 2. unzoned slightly resorbed crystal in groundmass, Elwin Bay; 3. discrete weakly zoned crystal in groundmass, K4 pipe; 4. discrete unzoned crystal in groundmass, Zulu (Freighttrain); 5. discrete unzoned crystal in groundmass, JP3 (Nikos); 6. discrete unzoned crystal with rim of Fe-Ti oxides, JP1 (Nikos); 7. Pv core mantled by Fe-Ti oxides, JP101D (Nikos); 8. discrete unzoned crystal in groundmass, resorbed, JP101D (Nikos).

Nikos 3

JP3 is a dark green hypabyssal kimberlite, containing 50 μm discrete, euhedral perovskites that are unzoned, some of which are resorbed. A second generation of perovskites occur as 30 μm mantles on anhedral Fe-Ti-Mg cores.

3.2.4. Lac de Gras

The Lac de Gras field is located in the central part of the Archean Slave Structural province. Kimberlites from the Lac de Gras area intrude a granite-greenstone terrane (Bleeker & Davis, 1999). Bedrock geology comprises greywacke-mudstone turbidites and granitoid intrusives. Phanerozoic sedimentary rocks are not preserved in the Lac de Gras area, but must have been present during kimberlite intrusion, as evidenced by late-Cretaceous to early-Tertiary shale xenoliths within the kimberlite pipes (Nassichuk & McIntyre, 1995).

The Lac de Gras kimberlites range in ages from 45-75 Ma based mainly on Rb-Sr dating of phlogopite (Creaser *et al.*, 2003), with a large proportion (19 out of 47) of Eocene age (45.2-53.3 Ma). Creaser et al. (2003), determined four distinct episodes of Eocene kimberlite magmatism in the Lac de Gras field: (1) Mark Array (47.8+/-0.3 Ma), (2) Panda Array (53.2 +/- 0.3 Ma), (3) A154 Array (55.3+/-0.3 Ma) and (4) Cobra Array (59.0+/-0.7 Ma). Eocene kimberlite pipes appear to be the only ones of economic significance (Heaman *et al.*, 2004).

Nowicki et al. (2004), provide a detailed description of the Lac de Gras area geology. The abundance of previous work on the Lac de Gras kimberlites, as well as the wealth of information on diamond populations and diamond quality (Fedortchouk *et al.*, 2005), makes them an ideal suite for the application of the oxybarometers developed in

this study. In order to evaluate their ability to produce reliable fO_2 estimates, oxybarometer estimates from this study are compared to estimates determined by Ol-Sp oxybarometry (Fedortchouk *et al.*, 2005), as well as to diamond quality data.

Perovskites from the Lac de Gras kimberlites are varied and complex. Chakhmouradian and Mitchell (2001), distinguished four types of perovskite (Table 3.3) based on composition and texture. Type I perovksites are REE-Nb-Al poor with mantles of relatively high Sr and K. The majority of the perovskite crystals are classified as type II, have elevated Al, Fe, Nb and LREE, and are found as discrete crystals as well as rims on ilmenite. Type III are notably enriched in Na, Sr, Nb and LREE and are found as rims on type I and II perovskites. The evolutionary trend from type I through type II to type III perovskite is charcterized by an increase in incompatible Nb (Chakhmouradian and Mitchell, 2001). Type III are believed to result from the re-equilibration of type I and II perovskites at near-solidus conditions. Therefore, the oxybarometers experimentally calibrated in Part I are applied only to type I and II perovskites in five different Lac de Gras kimberlite pipes (Table 3.1).

Torrie

The Torrie kimberlite is composed of organic-bearing kimberlite tuff and tuff breccia. Perovskites occur as discrete, compositionally zoned grains (Figure 3.3a).

Aaron

The Aaron pipe consists of a grey, hypabyssal kimberlite, with little or no alteration (sample AN2) as well as a friable, green pelletal volcaniclastic kimberlite, with serpentine alteration and abundant wall-rock xenoliths (samples AN4 and AN5).

Perovskites from the hypabyssal kimberlite are 50-100 μm, angular and in some instances resorbed. Perovskites from the volcaniclastic kimberlite are 20-100 μm and euhedral with compositional zoning (Figure 3.3f).

Grizzly

The Grizzly kimberlite is a dark green, hypabyssal kimberlite, containing three generations of perovskite. A generation of subhedral to euhedral cores with relatively low Nb content (types I), are overgrown with Type III rims (elevated Nb) (Figure 3.3c). Compositionally zoned perovskites are 10-30 μm, subhedral to euhedral, and are typically low in Nb (type II) (Figure 3.3d). Unzoned perovskites elevated in Nb (type III) were also recognized.

Misery

The Misery kimberlite is volcaniclastic, containing two generations of perovskite similar in habit: one relatively low Nb, 10-20 μm, subhedral, and unzoned generation and a second generation with more elevated Nb (Figure 3.3b). The Misery kimberlite is also associated with dykes of macrocrystic hypabyssal kimberlite.

Panda

The Panda kimberlite is mainly a resedimented volcaniclastic kimberlite, containing 10-30 μm, unzoned, euhedral, perovskites (Figure 3.3e).

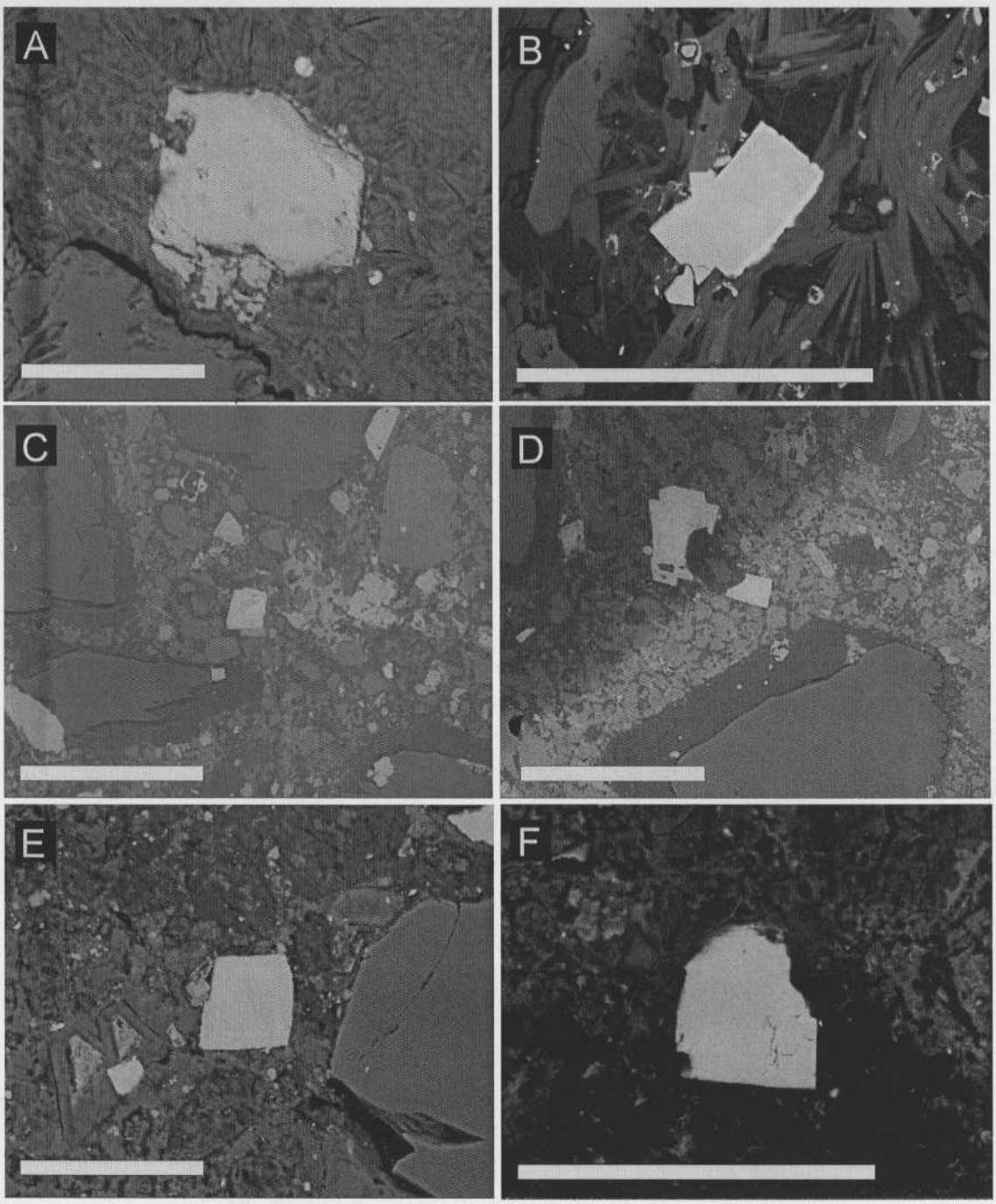

Figure 3.3: Back-scattered electron (BSE) images of characteristic textures in perovskites from Lac de Gras kimberlites. Scale bar is 50 μm for all images. (A) Unzoned, euhedral perovskite, Torrie. (B) Unzoned, euhedral perovskite, Misery. (C) Zoned, subhedral perovskite cores (type I) with rims of elevated Nb perovskite (type III), Grizzly. (D) Unzoned, euhedral perovskite (type II), Grizzly. (E) Unzoned, euhedral perovskite, Panda. (F) Unzoned, subhedral perovskite, Aaron.

Table 3.3: Representative Compositions of Perovskite from Lac de Gras Kimberlites

Wt.%	1	2	3	4	5	6	7	8	9	10	11	12	13	14	15
Type	I	III	II	III	II	III	III	II	II	III	II	II	II	II	II
Na_2O	0.57	0.73	0.20	1.26	0.19	1.01	0.87	0.62	0.56	1.35	0.71	0.37	0.52	0.39	0.47
CaO	38.63	31.22	34.28	32.06	34.56	28.34	31.97	32.79	32.96	30.85	32.18	35.00	33.10	33.72	33.42
SrO	0.49	0.09	0.16	0.11	0.17	0.13	0.11	0.10	0.17	0.13	0.10	0.15	0.08	0.12	0.10
La_2O_3	0.11	1.43	1.67	1.06	1.80	1.41	1.72	1.65	1.78	1.45	1.70	1.64	1.63	1.62	1.68
Ce_2O_3	0.02	3.53	4.38	3.21	4.15	3.64	4.21	4.32	4.57	4.39	4.47	3.42	4.05	3.95	4.04
Pr_2O_3	0.00	0.49	0.52	0.37	0.56	0.41	0.63	0.46	0.48	0.46	0.46	0.32	0.44	0.43	0.45
Nd_2O_3	0.03	1.23	1.32	1.03	1.21	1.09	1.19	1.31	1.39	1.25	1.34	1.08	1.31	1.28	1.31
ThO_2	0.00	0.95	1.29	1.35	0.63	0.60	0.84	2.14	1.58	2.02	2.18	0.42	2.11	1.02	1.33
TiO_2	56.62	35.31	46.75	39.05	46.70	35.06	36.35	47.61	46.97	44.49	46.89	50.42	46.27	45.74	45.73
Al_2O_3	0.00	0.86	0.52	0.02	0.54	0.75	0.27	0.22	0.14	0.00	0.20	0.52	0.45	0.44	0.44
Fe_2O_3	1.03	6.94	4.23	4.36	4.18	13.85	5.58	2.76	3.77	3.32	2.47	2.73	3.46	3.85	3.58
$Nb2O_5$	0.28	11.14	2.89	13.27	2.94	13.37	13.64	3.47	3.17	7.43	4.67	1.74	3.79	4.91	4.66
Ta_2O_5	0.00	0.76	0.47	0.57	0.26	0.26	0.39	0.70	0.49	0.73	0.76	0.10	0.82	0.50	0.61
Total	98.02	94.87	98.69	97.86	98.07	100.20	98.17	98.34	98.29	98.15	98.28	98.21	98.09	98.09	97.92
Na	0.026	0.037	0.010	0.062	0.009	0.049	0.043	0.030	0.027	0.066	0.034	0.017	0.025	0.019	0.023
Ca	0.960	0.879	0.906	0.869	0.915	0.756	0.876	0.873	0.878	0.831	0.860	0.908	0.884	0.896	0.892
Sr	0.007	0.001	0.002	0.002	0.002	0.002	0.002	0.001	0.002	0.002	0.001	0.002	0.001	0.002	0.001
La	0.001	0.014	0.015	0.010	0.016	0.013	0.016	0.015	0.016	0.013	0.016	0.015	0.015	0.015	0.015
Ce	0.000	0.034	0.040	0.030	0.038	0.033	0.039	0.039	0.042	0.040	0.041	0.030	0.037	0.036	0.037
Pr	0.000	0.005	0.005	0.003	0.005	0.004	0.006	0.004	0.004	0.004	0.004	0.003	0.004	0.004	0.004
Nd	0.000	0.012	0.012	0.009	0.011	0.010	0.011	0.012	0.012	0.011	0.012	0.009	0.012	0.011	0.012
Th	0.000	0.006	0.007	0.008	0.004	0.003	0.005	0.012	0.009	0.012	0.012	0.002	0.012	0.006	0.008
ΣA	0.993	0.988	0.997	0.992	1.000	0.870	0.998	0.987	0.991	0.980	0.981	0.987	0.990	0.988	0.992
Ti	0.988	0.698	0.868	0.743	0.868	0.656	0.699	0.890	0.879	0.841	0.880	0.918	0.868	0.853	0.857
Al	0.000	0.027	0.015	0.001	0.016	0.022	0.008	0.006	0.004	0.000	0.006	0.015	0.013	0.013	0.013
Fe	0.018	0.137	0.079	0.083	0.078	0.259	0.107	0.052	0.071	0.063	0.046	0.050	0.065	0.072	0.067
Nb	0.003	0.132	0.032	0.152	0.033	0.150	0.158	0.039	0.036	0.084	0.053	0.019	0.043	0.055	0.053
Ta	0.000	0.005	0.003	0.004	0.002	0.002	0.003	0.005	0.003	0.005	0.005	0.001	0.006	0.003	0.004
ΣB	1.009	1.000	0.997	0.982	0.996	1.090	0.974	0.992	0.992	0.994	0.991	1.003	0.995	0.996	0.994

3.2.5. Analytical Methods

Back-scattered electron (BSE) images of samples were acquired with a Philips XL30 electron microscope at the University of British Columbia. Electron microprobe analyses of samples were carried out with a CAMECA SX50 electron microprobe at the University of British Columbia. Major and minor elements were determined at 15.0 kV acceleration voltage and a beam current of 20.1 nA with a 1μm beam. Analytical conditions were 20 s counting time on peaks for all major elements except for Fe, Ce and La (60 s), Sr (120 s) and Nb (160 s). Natural and synthetic standards were used for calibration. Standards were albite (Na), olivine (Mg, Si), orthoclase (Al, K), apatite (P), diopside (Ca), rutile(Ti), synthetic rhodonite (Mn) and fayalite (Fe). Drake standard glasses (3.5wt% REE) were used to probe for Ce, La, Sr and Nb in glass and perovskite phases. Data reduction was done with the "PAP" $\varphi(\rho Z)$ method (Pouchou & Pichoir, 1985). Representative compositions of perovskite from Somerset Island (Table 3.2) and Lac de Gras (Table 3.3) show close to ideal stoichiometry.

Based on a detailed study of perovskite textures and compositions, the perovskite parageneses in each pipe was determined (Table 3.1). Between one and three generations of perovskite were recognized in all pipes. Estimates of fO_2 for each generation was based on analysis of between one and fifteen perovskites with standard deviations (at 1σ) shown in Table 3.1.

MLR and SIM 'Ferric iron in perovskite' oxybarometers are considered superior to the Nb-free oxygen barometer (BC05-equation 4) because they were calibrated on more complex Nb + REE bearing perovskites (See Part I of this study). Both MLR and SIM methods are tested in select examples below; however, only MLR is reported (and

represented in figures) for the purpose of comparison, as it best reproduces experimental data over the entire range of fO_2, while the SIM method has a tendency to underestimate the experimental fO_2.

3.3. RESULTS

3.3.1. Global dataset

A compilation of the bulk rock Fe-content for world kimberlites recalculated volatile-free (with total Fe expressed as wt% Fe_2O_3*) shows an average value of 9-11 wt% Fe_2O_3 (Figure 3.1). Experimental data (this study) show that fO_2, and not bulk Fe content of kimberlite, is the determining factor for variation in the Fe_2O_3 content of perovskites, which is also shown by data for perovksites in well-characterized natural kimberlites (Figure 3.4). The Fe_2O_3 content of perovskite from natural kimberlites compiled from the literature varies from 1 to 2wt%, which corresponds to fO_2 conditions of NNO-5 to NNO+1 (Figure 3.5) when calculated using the MLR oxybarometer.

3.3.2. Phoenix Pipe

To scrutinize the range of fO_2 recorded by different growth histories in natural perovskites, data from a single kimberlite, the Phoenix pipe, for which mineral chemical data for both cores and rims is available, will be examined (Eccles *et al.*, 2004).
Data from the Phoenix pipe allows us to apply the MLR oxygen barometers in a general way, and to comment on the range of possible fO_2 found in a single kimberlite pipe.

Perovskite cores in the crater facies of the Phoenix pipe display an average Fe_2O_3 content (Figure 3.6a) consistently lower than the rims (Figure 3.6b), corresponding to differences in relative fO_2 of NNO–2 to NNO-0 in the cores (Figure 3.6c) compared to NNO+1 to NNO+2 in the rims (Figure 3.6d). As noted above (Figure 3.4), this difference

cannot be attributed to changing FeO with crystallization and differentiation in kimberlites, and is most simply interpreted as increasing fO_2 associated with cooling and differentiation during emplacement.

3.3.3. Somerset Island

Within the Somerset Island cluster, perovskites from six pipes display an average Fe_2O_3 content of 1 to 2.5wt% (Table 3.2), corresponding to a relative fO_2 of NNO-5 to NNO-0 using SIM or NNO-4 to NNO+1 using MLR (Figure 3.7). Note that the two oxybarometric methods produce the same result within error except at very high fO_2, which is the same conclusion reached in Part I of this study. Within the Nikos1 pipe, perovskites with Fe-Ti oxide rims record a relative fO_2 of NNO-2.0 using MLR, while resorbed perovskites record a relative fO_2 of NNO-3.3 (Table 3.1, Figure 3.9). Within the Zulu pipe, perovskite cores record a relative fO_2 of NNO+0.5 to NNO+1.8, whereas, rims record a relative fO_2 of NNO+0.6 to NNO-1.9. Unzoned perovskites record a relative fO_2 of NNO+1.1 to NNO-0.9 (Table 3.1, Figure 3.9).

3.3.4. Lac de Gras

Within the Lac de Gras cluster perovskites from five pipes display an average Fe_2O_3 content of 2.5 to 4 wt% (Table 3.3), corresponding to a relative fO_2 of NNO-1.5 to NNO+2.5 using (SIM) or NNO-2.5 to NNO+6 using (MLR) (Figure 3.8). Within the Grizzly pipe, type I perovskites record an Fe_2O_3 content of 1.0 wt%, corresponding to a relative fO_2 of NNO-3.4. Type II perovskites display a range of Fe_2O_3 contents from 2.5 to 3.0wt% corresponding to a relative fO_2 of NNO-1 to NNO+1. Type III perovskites record high Fe and Nb content corresponding to elevated relative fO_2 (Figure 3.9).

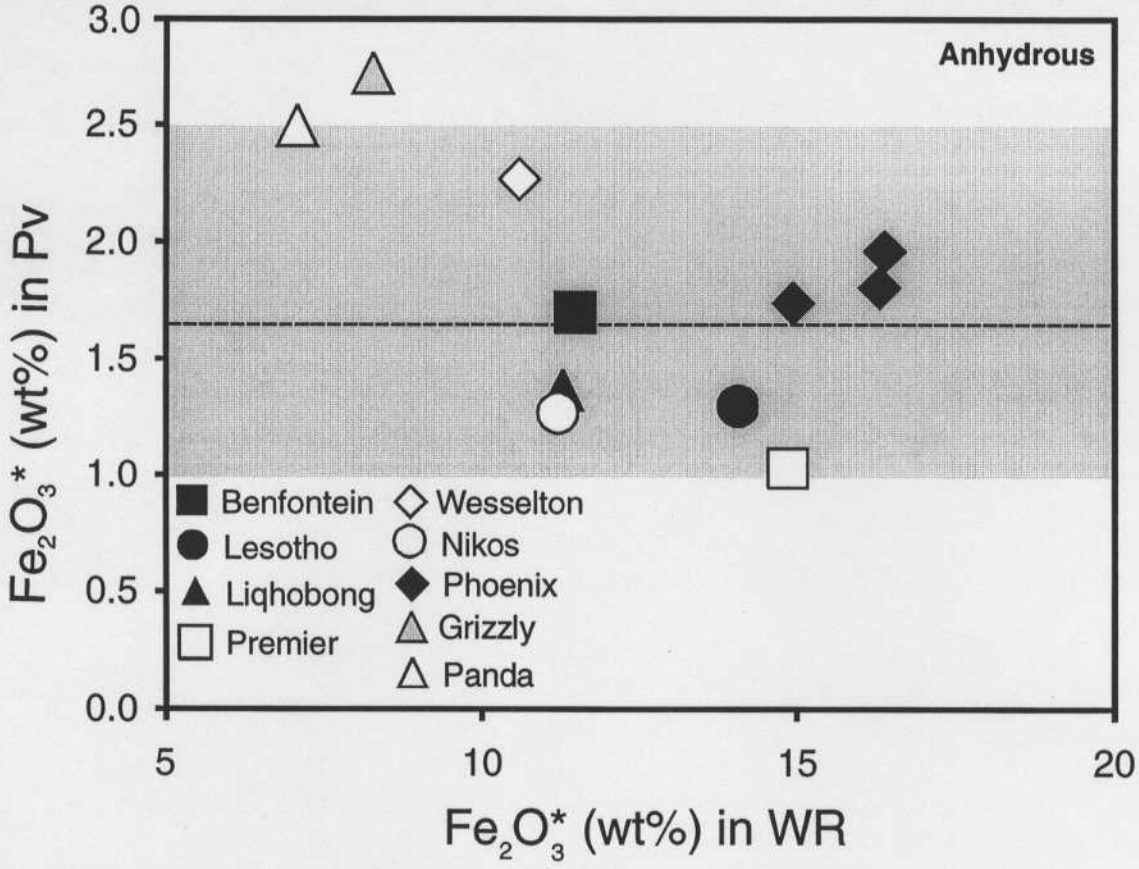

Figure 3.4: Bulk Fe in global kimberlites (re-calculated volatile-free) versus Fe content in Perovskite (with all Fe expressed as $Fe_2O_3^*$ in wt%) for some well-characterized kimberlites as well as kimberlites examined in this study. Shaded area represents range in Fe content for kimberlite perovskites and dashed line represents the average Fe content in kimberlite perovskites. (Clement, 1982), (Gurney & Switzer, 1973), (Robinson, 1975), (Eccles *et al.*, 2004), (Dawson & Hawthorne, 1973), (Schmidberger & Francis, 2001).

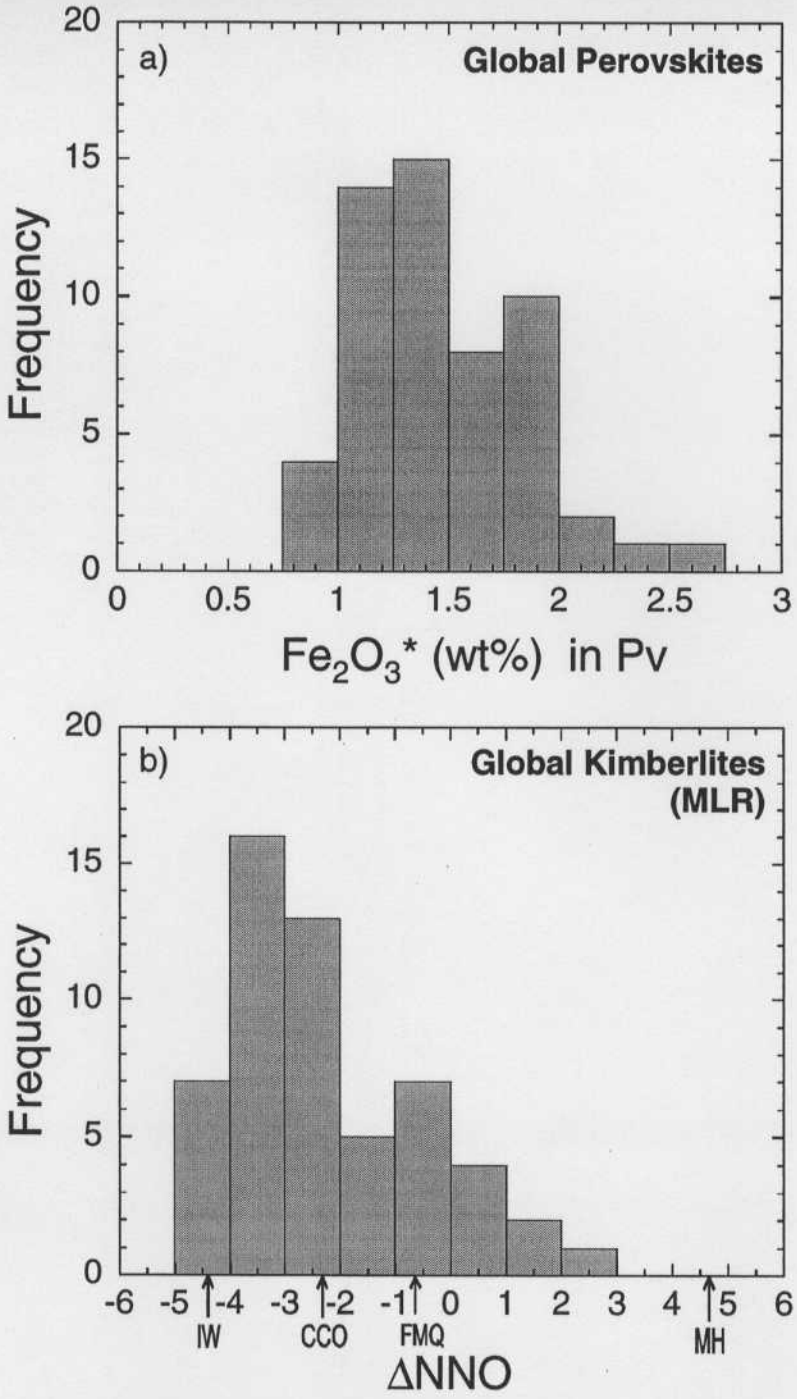

Figure 3.5: a) Fe_2O_3* (wt%) of natural perovskites [(Eccles *et al.*, 2004), (Chakhmouoradian & Mitchell, 2000), (Mitchell, 1986)] and b) corresponding ΔNNO calculated from data in (a) using the MLR perovskite oxygen barometer. Buffers are shown at 0.2 GPa and 1200°C for reference (Frost, 1991)

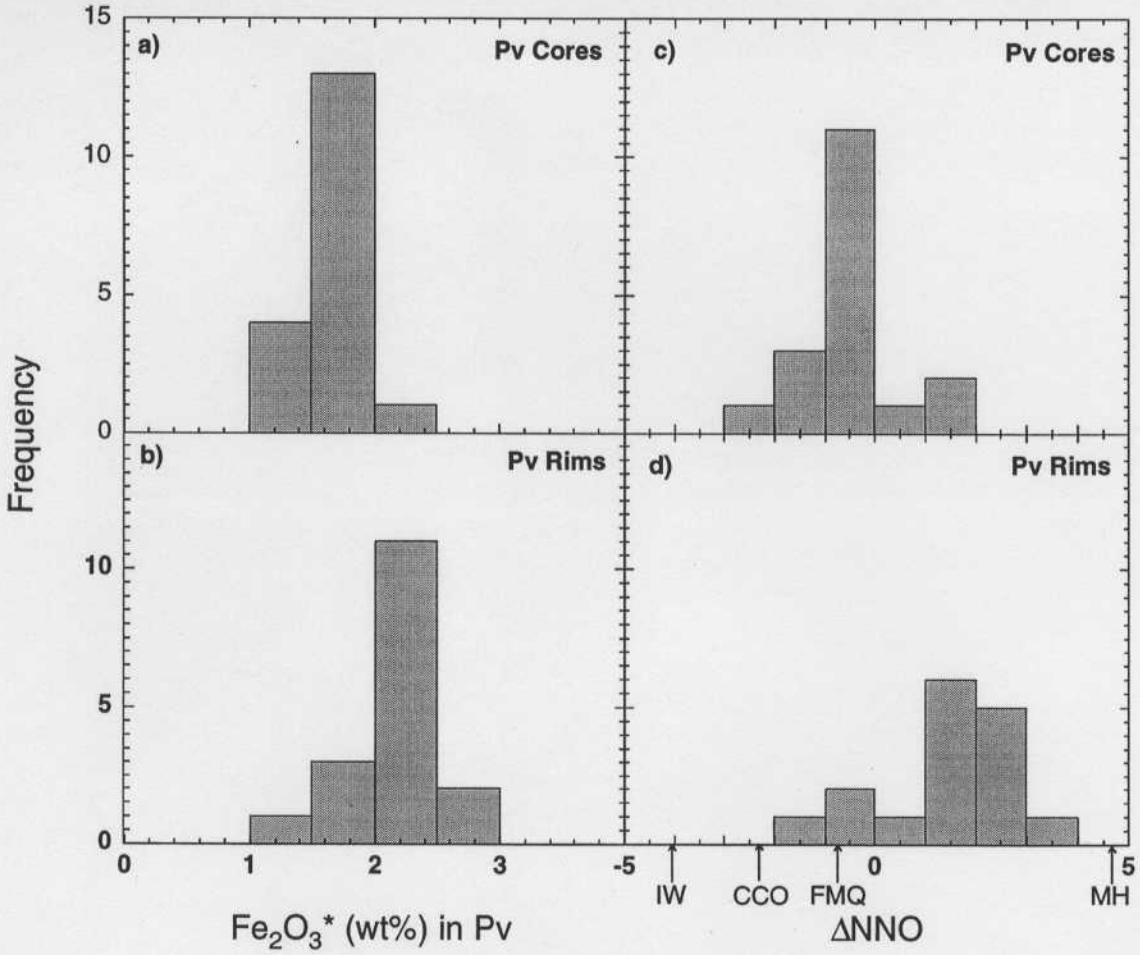

Figure 3.6: a) Fe_2O_3* (wt%) of perovskite cores (n=22) and b) Fe_2O_3* (wt%) of perovskite rims (n=22) from the Phoenix kimberlite in northern Alberta, Canada (Eccles *et al.*, 2004). c) ΔNNO calculated from data in (a) using the MLR perovskite oxygen barometer. d) ΔNNO calculated from data in (b) using the MLR perovskite oxygen barometer. Buffers are shown at 0.2 GPa and 1200°C for reference (Frost, 1991)

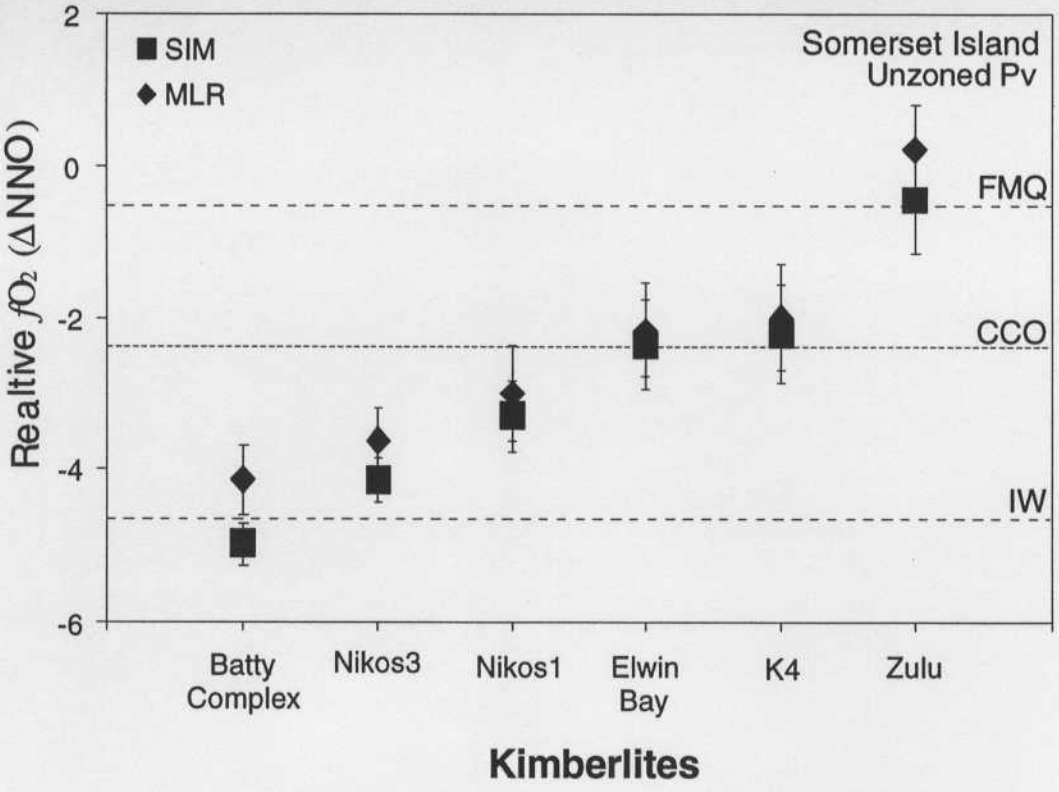

Figure 3.7: Relative fO_2 of kimberlites from Somerset Island calculated using SIM (squares) and MLR (diamonds) perovskite oxygen barometers. Error bars are ± 1σ. Buffers are shown at 0.2 GPa and 1200°C for reference (Frost, 1991).

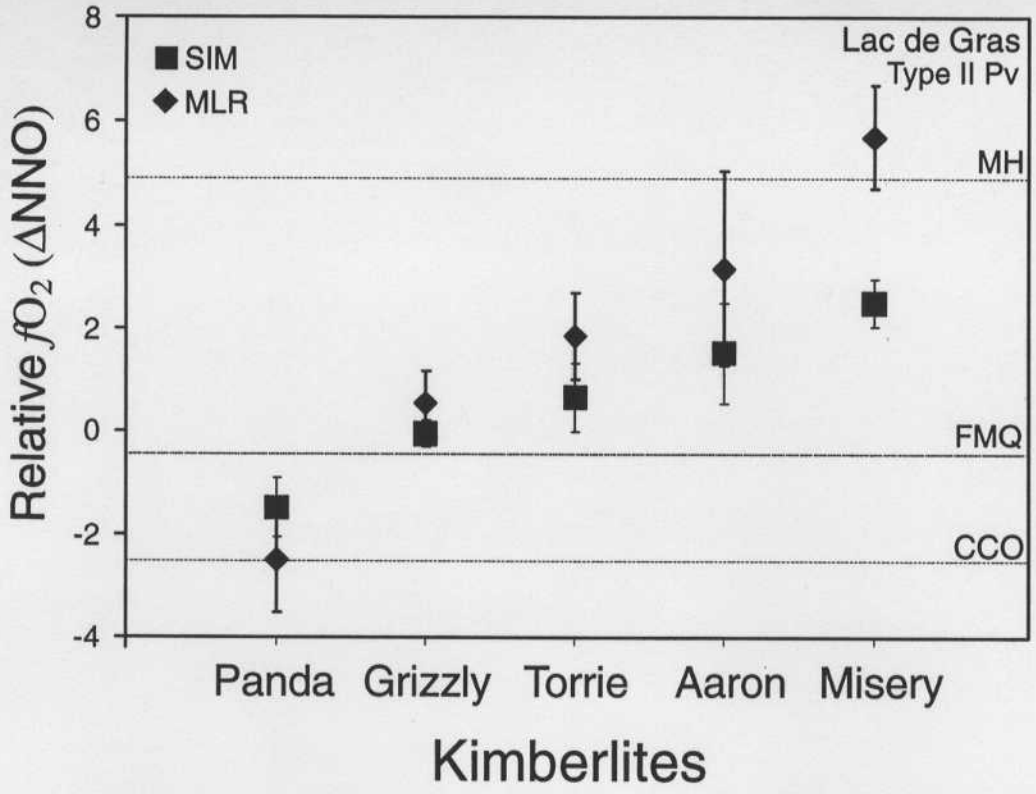

Figure 3.8: Relative fO_2 of kimberlites from Lac de Gras calculated using SIM (squares) and MLR (diamonds) perovskite oxygen barometer. Error bars are ± 1σ. Buffers are shown at 0.2 GPa and 1200°C for reference (Frost, 1991).

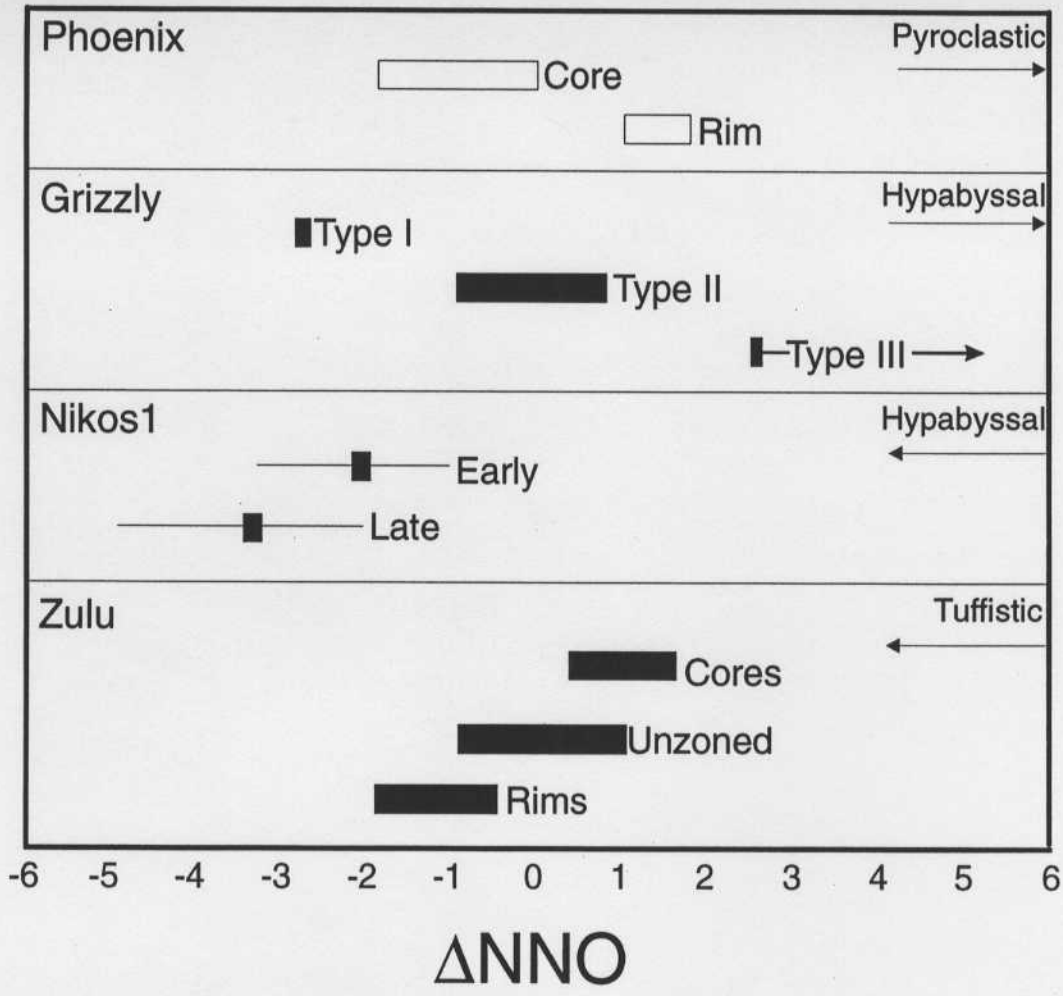

Figure 3.9: Relative fO_2 (reported relative to NNO buffer) of Phoenix, Grizzly, Nikos1 and Zulu pipes calculated using MLR perovskite oxygen barometer. Solid bars (data from this study) and open bars (data from Eccles et al, 2004) demonstrate the range in relative fO_2. Error bars (Nikos1) are $\pm 1\sigma$. Arrows indicate temporal evolution.

3.4. DISCUSSION

3.4.1. Global range of fO_2 in kimberlites

Global kimberlites display a range of fO_2 conditions from NNO-5 to NNO+1 (Figure 3.10), based on application of the SIM and MLR oxybarometers. The relative oxygen fugacity of MORB ranges from NNO-3 to NNO-1 (Christie *et al.*, 1986), and that of Kilauea lavas range from NNO-1.5 to NNO-0.5 (Carmichael & Ghiorso, 1986). The basalts, basaltic–andesites and andesites from western Mexico show a range in relative fO_2 from NNO-0.5 to NNO+2.5, while the lamprophyric and related alkaline lavas from the same region show a relative fO_2 from NNO+3 to NNO+5 (Carmichael, 1991). Relative oxygen fugacity recorded by samples of cratonic mantle lithosphere ranges from NNO-6 to NNO-0.5 (Woodland & Koch, 2003), (McCammon & Kopylova, 2004).

Global kimberlites display a range of fO_2 conditions that is wider than that of any other magma type. In experiments, Gudfinnson and Presnall (2005), have shown that primitive kimberlite magma with up to 15 wt% CO_2 can be produced by less than 1% melting of a CO_2-bearing peridotite. Analyses of primitive kimberlite melts that are believed to approximate primary kimberlite magma (ie. Jericho, Canada and Wesselton, South Africa) contain between 10 and 17 wt% 'primary' CO_2 (Price *et al.*, 2000). During emplacement, kimberlites could elevate their CO_2 content (up to 20 wt%) and their H_2O content (up to 12wt%) by crystallization of anhydrous minerals as suggested by bulk rock analyses (Appendix I - Kimberlite database). Variability in volatile content and degassing histories in kimberlites during their emplacement could explain the wide range of fO_2 conditions recorded by this magma type.

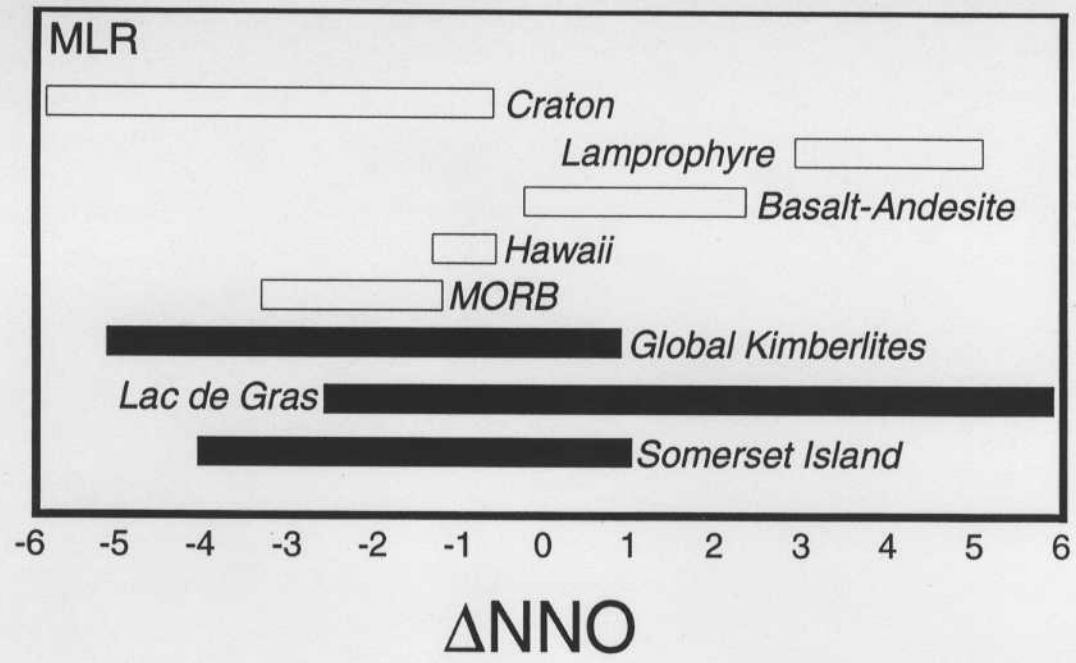

Figure 3.10: Relative fO_2 (reported relative to the NNO buffer) of samples of cratonic mantle lithosphere (Woodland and Koch, 2003 ; McCammon , 2004), lamprophyres (Luhr *et al.*, 1989; Carmichael *et al.*, 1996), basalts, basaltic–andesites and andesites from western Mexico (Hasenaka & Carmichael, 1987), MORB (Christie *et al.*, 1986), Kilauea lavas (Carmichael & Ghiorso, 1986) and global kimberlites (see Figure 2.2 for references), based on application of the MLR perovskite oxygen barometer.

The effect of H_2 degassing on kimberlites by the mechanism described by Sato (1978) is to oxidize the magma (equation 8). On the other hand, degassing of H_2O from the magma involves combining H_2 with O^{2-} ions to form H_2O, reducing the magma (equation 9). Similarly, the combination of elemental carbon from the magma with O^{2-} ions to form CO_2 and CO gases that are subsequently degassed should result in reduction of the magma (equation 10a and b) (Sato, 1978). Mitchell (1975), used calculations in the system C-H-O-S to show that at the typical T and P range of kimberlite emplacement, H_2O is the dominant fluid phase and at low pressures (i.e. late stages of crystallization) there is a fluid phase of H_2O and CO_2. The presence of H_2O and CO_2 phases is supported by the late stage serpentinization, the hydration of primary minerals and the formation of late stage carbonates recognized in most kimberlites (Mitchell, 1975).

The effect of volatiles on the fO_2 recorded by perovskites can be examined in a limited number of well-characterised kimberlites for which perovskite analysis and volatile contents are known. The fO_2 recorded by perovskite using MLR, increases with increasing H_2O and decreasing CO_2 in the whole rock (Figure 3.11). Whether these H_2O contents are primary is dubious; H_2O content of the whole rock may simply reflect the serpentinization of olivine and concomitant hydration of other anhydrous minerals during emplacement. Therefore, higher amounts of H_2O preserved in the WR (now as hydrous minerals) suggest minimal H_2O was lost by degassing and hence the magma is less reduced by the mechanism in equation (9). Lower amounts of H_2O preserved in the whole rock could indicate the magma has undergone extensive degassing of H_2O and thereby reduced according to equation (9) (Figure 3.11a).

Nonetheless, we would not necessarily expect a correlation for the latter process with the fO_2 recorded by perovskite. Furthermore, serpentinization is a reducing process, and if H_2O were introduced to kimberlites during this process, we would expect to see the opposite trend in Figure 3.11a. Therefore, higher amounts of H_2O preserved in the whole rock (now as hydrous minerals) suggest minimal loss of H_2O by degassing. Hence reducing the magma by loss of H_2O (equation 9) is not thought to have been an important process. Lower amounts of H_2O preserved in the whole rock could indicate the magma has undergone extensive degassing of H_2O and thereby reduced according to equation (9) (Figure 3.11a).

We consider the CO_2 content in the whole rock to reflect a CO_2 component bound in carbonate that physically separates as isolated interstitial pools or segregations from the (silicate) magma during the late-stages of emplacement and crystallization in kimberlite (Clarke & Mitchell, 1975; Clement, 1975; Clement & Skinner, 1979). Dawson and Hawthorne (1973) recognized that carbonate segregations in the Benfontein sill had migrated from their region of formation and intruded other partially consolidated layers of the sill. This observation suggests that the parent material from which the late-stage CO_2 component separates need not be completely solidified prior to the formation of carbonate segregations, which would account for their globular shape. Spinel, perovskite, monticellite, and other earlier crystallizing phases, however, are notably absent from the carbonate segregations (Mitchell, 1986), suggesting that the parental kimberlitic magma is at least partially crystalline prior to carbonate segregation. Similar globular segregations are observed at DuToitspan and Finsch kimberlites.

Higher amounts of CO_2 preserved in the whole rock analyses (Figure 3.11b) are interpreted as larger amount of trapped carbonate segregation. As these segregations are, by

definition, extracted from the conjugate (silicate) kimberlite magma, they indicate that the silicate fraction of the kimberlite magma (which eventually crystallizes perovskite) has undergone extensive carbon loss as CO_2 and thereby could be reduced by this process (equation 3a) (Figure 3.11b). Therefore, the observation that fO_2 estimates decrease with increasing H_2O, and also with the loss of CO_2 (by carbonate segregation), is in agreement with the mechanism described by Sato (1978), showing loss of these volatiles by either degassing (H_2O) or by partitioning into the carbonate fraction (CO_2) results in reduction of the residual silicate magma.

3.4.2. fO_2 variability within a pipe

The wide range of fO_2 recorded by perovskites from the Phoenix kimberlite (Figure 3.6c,d and Figure 3.9) is attributed to the fact that these perovskites crystallized during different emplacement episodes or from distinct magma batches. Indeed, the Eccles et al. (2004) samples derive from several different lapilli found within the crater facies environment, which Eccles et al. consider to have resulted from multiple eruption episodes. Such mixing of different generations of phenocrysts is common in kimberlite (Mitchell, 1986). As a result, perovskites from these pyroclastic samples are likely to have recorded varied and separate eruption events in the development of the Phoenix pipe. As exemplified by the Phoenix samples, natural kimberlites experience multiple stages of crystallization under changing conditions that ensue during cooling and degassing. These changes are likely encoded in the zonation observed in natural perovskites and other minerals in kimberlite (Chakhmouoradian & Mitchell, 2000). The cores of the Phoenix pipe perovskites record more reduced conditions relative to the rims

(Figure 3.9), suggesting that this kimberlite magma underwent oxidation during emplacement.

Within the Nikos1 pipe from the Somerset Island area, different fO_2 estimates were recorded by texturally distinct perovskites within a single phase of intrusion. For example, in the hypabyssal sample JP1-101D, two separate generations of perovskite were identified. A set of perovskite cores with rims of Fe-Ti oxides are most abundant, while resorbed grains also occur. Considering that as crystallization proceeds, incompatible Nb should increase in the melt, perovskites that crystallize during the later stages of crystallization should be elevated in Nb. The set of resorbed, unzoned perovskites has the highest Nb content and no rims. This coupled with their resorbed texture is interpreted as evidence that they appeared during the latest stage of magma crystallization. Conversely, the perovskites with rims of Fe-Ti oxides are low in Nb and are classified as 'early' in Figure 3.12. Their composition is different from that in equilibrium with magma in the latest stages of crystallization therefore, Fe-Ti oxides, rather than perovskite, formed as mantles on these perovskites.

Variation in texture and rim size within a single phase suggests that fO_2 does not remain constant during the emplacement process. In fact, within a single phase of the Nikos1 pipe, perovskites record a continuous variation in relative fO_2 from early, Fe-Ti oxide-mantled perovskites (NNO–2.0), to late-stage, highly resorbed, unzoned perovskites (NNO –3.0) (Table 3.1, Figure 3.9), suggesting that an overall decrease in fO_2 occurred during emplacement. Unlike the Phoenix pipe, which consists of a mixture of lapilli from separate eruption events mixed within a crater environment, the Nikos1 kimberlite is hypabyssal and was emplaced during a single event. Thus, there appears to

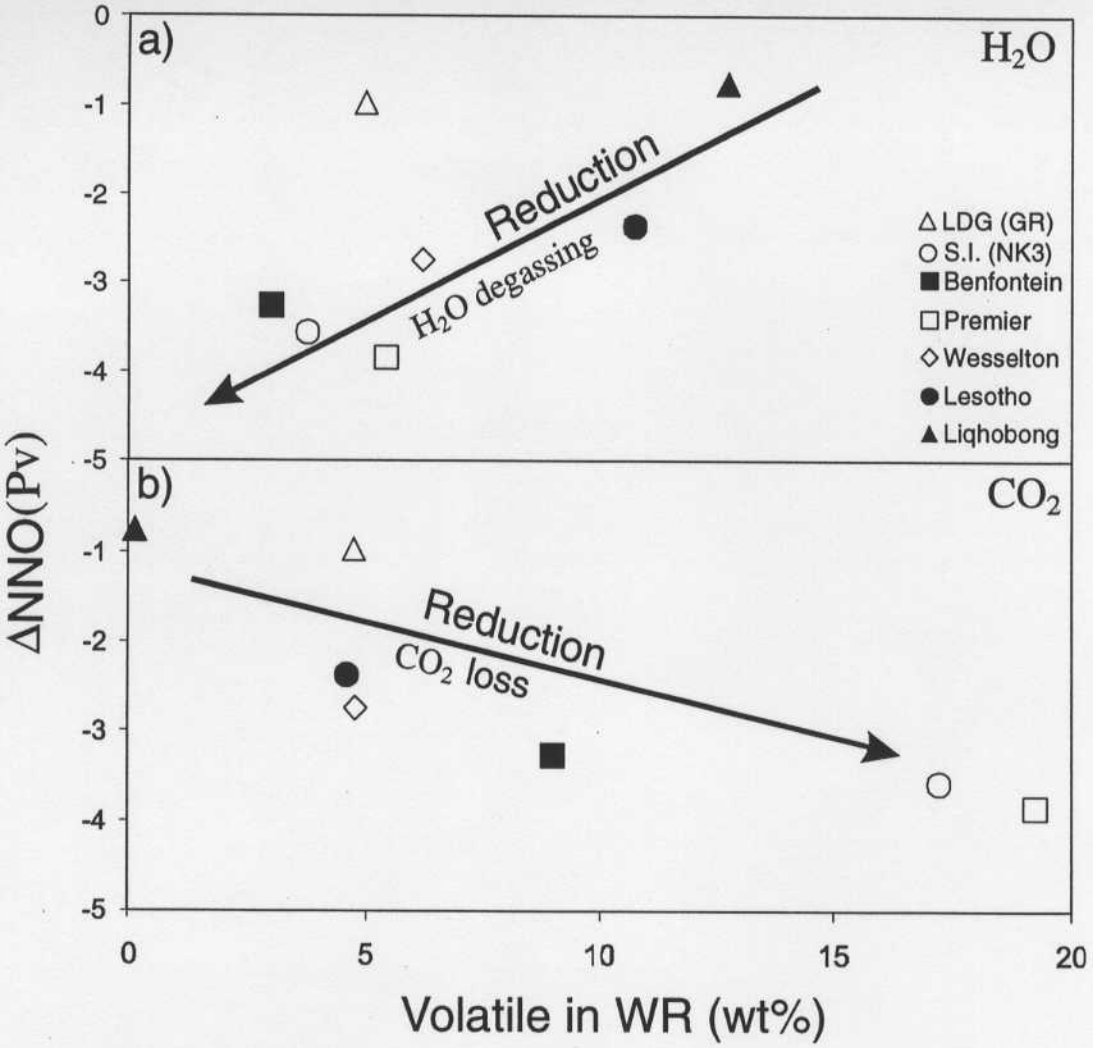

Figure 3.11: a) bulk rock H_2O content (wt%) and b) bulk rock CO_2 content (wt%) of some well-characterized kimberlites versus relative fO_2 (based on MLR perovskite oxygen barometer). Arrows depict trend of reduction. (see Figure 2.2 for references).

be no relationship between the value, or trend in fO_2 as recorded by perovskite and the texture of the kimberlite.

Discrete zoned and unzoned perovskites from the Zulu pipe define a trend of reduction during emplacement. Although Zulu is a tuffisitic kimberlite, examination of the cores and rims of a single perovskite crystal minimizes the possibility of 'mixing' separate eruptive events. As shown in Figure 3.9, perovskite cores record relative fO_2 conditions from NNO+0.5 to NNO+1.9, while rims record NNO-2 to NNO+0.5 suggesting reduction during emplacement. Unzoned perovskites from this pipe record intermediate fO_2 conditions from NNO-1.0 to NNO+1.0.

The Panda pipe from the Lac de Gras cluster contains unzoned type II perovskites. Using the MLR oxygen barometer, an average relative fO_2 for the Panda pipe of NNO-2.5 ±0.8 is estimated. Fedortchouk and Canil (2005), estimated a relative fO_2 of NNO-2.9 ± 0.2 for this same pipe using Ol-Sp oxygen barometry. Both methods give comparable estimates, but the Ol-Sp oxybarometer apparently gives better precision.

In general, fO_2's recorded by perovksite are higher relative to those recorded by Ol-Sp but this is not unexpected as these two minerals appear at different stages in the crystallization of the kimberlite magma. The resolution of the oxybarometers developed in this study may have the advantage that discrete stages in the evolution of the magma may be recorded by the different generations of perovskite.

Within the Grizzly pipe from the Lac de Gras cluster, all three compositional varieties of perovskite (Type I, II and III) are recognized. As shown in Figure 3.9, an evolutionary trend exists from Nb-poor, reduced type I perovskites (NNO-3.4), to intermediate type II perovskites (NNO-1 to NNO+1) to Nb-rich, highly oxidized type III

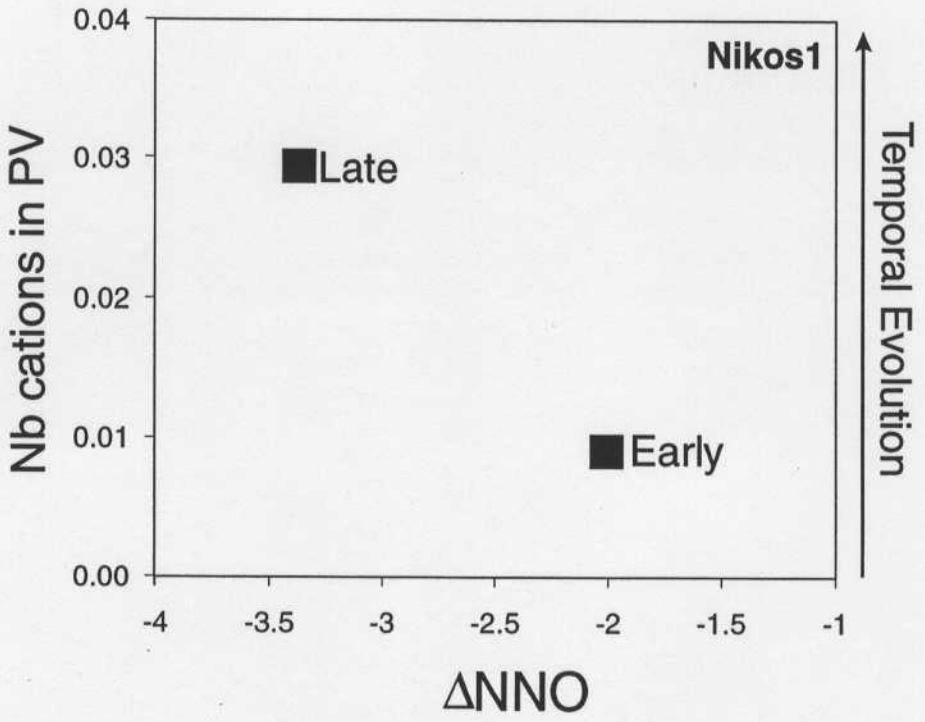

Figure 3.12: Nb cations in two generations of perovskite from the Nikos1 pipe (Somerset Island) versus relative fO_2 calculated based on the MLR perovskite oxygen barometer. Temporal evolution is inferred by an increase in incompatible Nb content in the perovskite.

perovskites, suggesting oxidation of the kimberlite magma during emplacement, similar to that observed in the Phoenix pipe. In the Grizzly pipe, Ol-Sp oxybarometer records relative fO_2 estimates from NNO–3.1 to NNO-2.5 (Fedortchouk *et al.*, 2005), within the range of fO_2 estimates defined by type I perovskite and type II perovskites based on oxybarometers from this study.

3.4.3. Kimberlite fO_2 and diamonds

The stability and dissolution of carbon-bearing minerals in kimberlite magmas are directly influenced by the fO_2 of the magma during its ascent according to:

$$C + O_2 \leftrightarrow CO_2 \qquad (10a)$$

This suggests that with increasing fO_2, diamond in the kimberlite magma should be oxidized to CO_2. Furthermore, if a kimberlite magma resides at too high an fO_2 for too long during its ascent, it is possible that all diamonds may be resorbed and the kimberlite would prove barren.

Previous work on diamond populations in select kimberlites from the Lac de Gras area (Fedortchouk *et al.*, 2005), make it possible to relate the fO_2 estimates determined in this study to diamond grade and quality. While diamond grade is mostly a result of the quantity of diamond sampled in the mantle by an ascending kimberlite magma, estimates of kimberlite fO_2 may have utility in predicting the quality of diamonds. The degree of resorption for diamonds in pipes from the Lac de Gras area is shown in Figure 3.13 (Fedourtchouk and Canil, 2005). The kimberlite pipes with the highest fO_2 (i.e. Misery) have the highest proportion of highly resorbed diamonds (~67%), while pipes with lower estimated fO_2 (i.e. Panda and Grizzly) have lower proportions of highly resorbed diamonds (14% at Panda and 50% at Grizzly). Kimberlite pipes with the lowest estimated

fO_2 (i.e. Panda) have higher proportions of lesser resorbed diamonds (~54%), while pipes with higher estimated fO_2 (i.e. Grizzly and Misery) have lower proportions of lesser resorbed diamonds (20% at Grizzly and 10% at Misery). These results suggest that oxygen fugacity affects the quality of diamonds preserved in the magma, likely according to equation (10a). Furthermore, these results indicate that the oxybarometers developed in this study accurately reflect the conditions that diamonds experience during kimberlite ascent and emplacement.

3.4.4. Kimberlite fO_2 within a province

In the Nikos pipe, early perovskite (characterized by low Nb) record higher fO_2 than late Pv (characterized by high Nb), suggesting that fO_2 decreases during crystallization (Figure 3.9). The Zulu pipe also records decreasing fO_2 from core to rim (Figure 3.9). This evolutionary trend from oxidized early/core perovskites to reduced late/rim perovskites suggests that reduction may dominate during emplacement of the Somerset Island kimberlites. Conversely, in the Grizzly pipe, perovskites record increasing fO_2 from type I through type II to type III perovskites (Figure 3.9). This evolutionary trend is similar to that recognized in the Phoenix pipe from N. Alberta suggesting that oxidation may dominate during emplacement of the Lac de Gras kimberlites. The wide range of fO_2 conditions recorded in each province reflects the range of emplacement and degassing histories experienced by the individual pipes that make up a given cluster.

3.4.5. fO_2 between provinces

Perovskites from the Somerset Island field record fO_2 conditions from NNO-4 to NNO+1, while perovskites from the Lac de Gras kimberlites record fO_2 from NNO-2.5 to

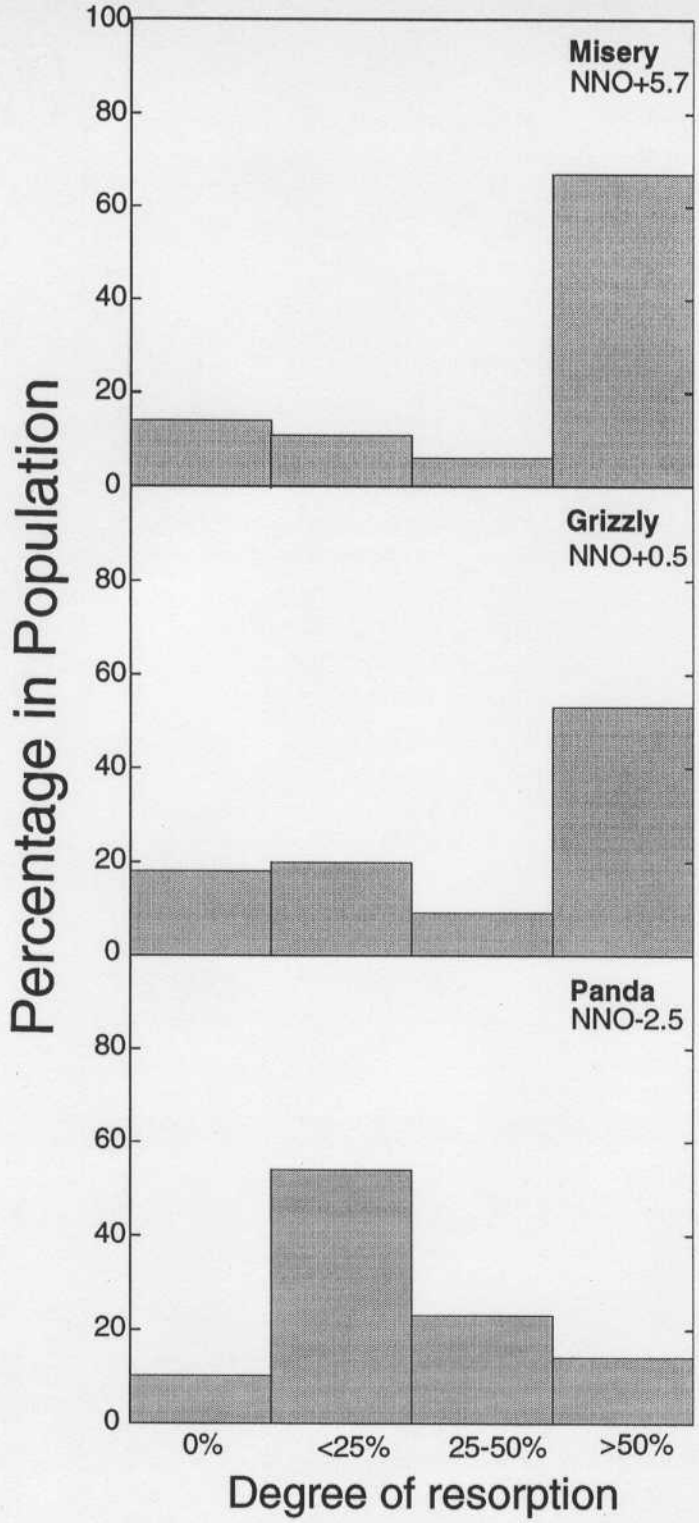

Figure 3.13: The degree of resorption for diamonds (%) in pipes from the Lac de Gras area versus percentage in the population (Fedortchouk *et al.*, 2005).

NNO+6.0 (Figure 3.10). While overlap does exist, the Somerset Island field is in general more reduced relative to the Lac de Gras field. Beyond this difference, these two provinces appear to experience very different emplacement histories. The Somerset Island perovskites (i.e. Nikos1 and Zulu) record reduction of magma during emplacement, likely due to loss of H_2O and/or CO_2 from the melt during the late stages of emplacement (Figure 3.11). The Lac de Gras perovskites record extremely oxidized conditions during emplacement. While the dominance of H_2 loss over H_2O/CO_2 loss during the late stages of emplacement may be responsible for these high fO_2's (Figure 3.14c), we explore other possibilities shown schematically in Figure 3.14.

It is possible that the fO_2 recorded in kimberlite magmas is a reflection of their source region (Carmichael, 1991), as has been surmised for many other mantle-derived magmas (Figure 14a). It is a well-known trend that more oxidized magmas tend to be more hydrous (Carmichael, 1991), and this also appears to be true for kimberlites (Figure 3.11), if their H_2O contents are to be deemed primary.

The Mascota minette lavas of Western Mexico also record exceptionally high fO_2, some not unlike those of the kimberlites from this study. To explain these high fO_2, Carmichael et al. (1996), suggested partial melting of phlogopite (as veins) in a lherzolite source. Phlogopite has a high Fe^{3+}/Fe^{2+} and high Mg#, and during partial melting in veins would contribute a low volume but oxidized magma with a high Mg#. As partial melting of a phlogopite veined lherzolite proceeds, liquids produced will have increasing Mg# as the proportion of phlogopite increases in the partial melt (Carmichael *et al.*, 1996). The case for the Mascota minette lavas is convincing because major and trace data for that rock series lie along trends leading to phlogopite. No such trend, however, is evident for fresh Lac de Gras samples or any other kimberlite rock series. It appears that for kimberlites, the presence of

phlogopite in the source region does not provide a method to produce the high fO_2's recorded by their perovskites in the Lac de Gras region or elsewhere.

Large amounts of crystallization may serve to change the fO_2 of magmas that originate from a similar source region. As shown schematically in Figure 3.14b, olivine and monticellite are two minerals that crystallize early in kimberlite magma, and preferentially take in Fe^{2+}, causing an increase in the $Fe^{3+}/\Sigma Fe$ ratio of the residual melt. Our experimental data from Part I show that up to 30% crystallization of olivine and monticellite in the magma has already occurred at the onset of perovskite saturation. Perovskites in some kimberlites, therefore, could record a high $Fe^{3+}/\Sigma Fe$ ratio present in the melt, simply due to their later appearance on the liquidus. Kimberlite magmas that underwent more profound olivine and monticellite crystallization, perhaps by H_2O loss, may have more Fe^{3+} to partition into perovskite upon saturation in that mineral.

Taking all of these different modes of fO_2 differentiation into account, we suggest that two separate mechanisms affect the fO_2 of kimberlite magma. So far, we see that differences in the source region, rooted in differences in composition (i.e. phlogopite content) of the mantle source and or variations in dissolved H_2O content do not explain the range of fO_2 recorded in this magma type. Differentiation of fO_2 during emplacement of kimberlites due to crystallization and volatile loss serves to best explain the wide range of fO_2 recorded within a single kimberlite pipe, or a single kimberlite province. More robust constraints on the primary H_2O and CO_2 content of kimberlites and further study on the effects of hydrogen speciation on the $Fe^{3+}/\Sigma Fe$ ratio of kimberlite melts, as is recognized in silicic melts (Baker & Rutherford, 1996; Gaillard *et al.*, 2001), is needed to elucidate the pathway of this unique and enigmatic rock type.

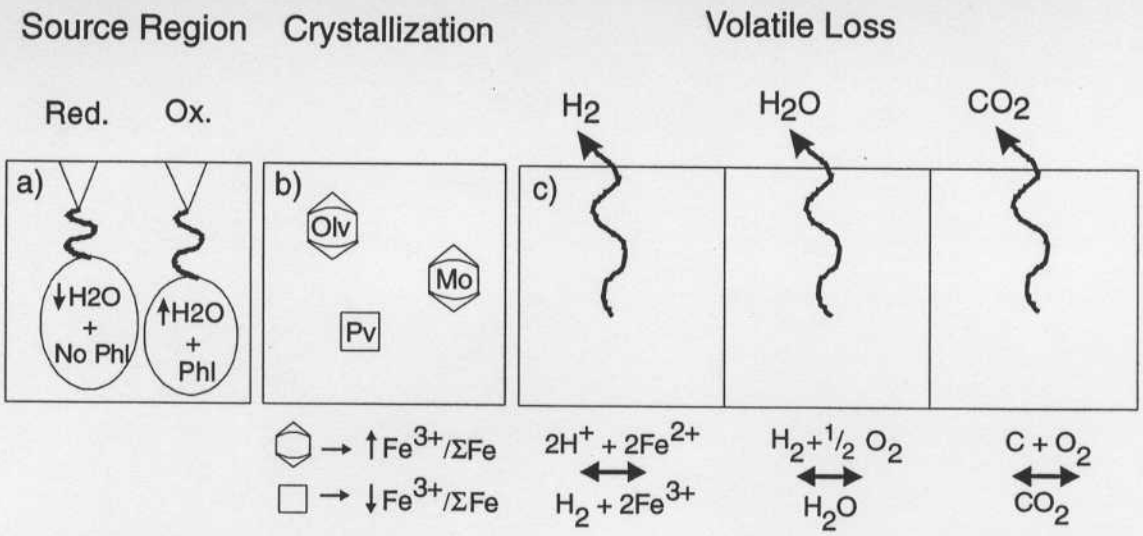

Figure 3.14: Schematic diagram showing: a) Oxidized magmas tend to be more hydrous (Carmichael, 1991), while partial melting of phlogopite (high Fe^{3+}/Fe^{2+}) veins in a lherzolite source would serve to oxidize magma (Carmichael *et al.*, 1996). b) Effect of olivine and monticellite crystallization on the $Fe^{3+}/\Sigma Fe$ ratio of the residual melt and Fe^{3+} content of perovksite. c) Effects of degassing or volatile loss on the $Fe^{3+}/\Sigma Fe$ ratio and fO_2 of the residual melt.

4.

SUMMARY

4.1 EXPERIMENTAL CONCLUSIONS

The appearance of perovskite in kimberlite magma is controlled primarily by T and the Ti-content, Nb-content and a_{SiO2} of the liquid. For a given bulk composition, fO_2 is by far the largest and most significant of all variables in controlling the Fe_2O_3 content of perovskite, while T has no observable effect.

In Nb-free experiments, Fe is found to substitute for Ti with increasing fO_2 by coupling with oxygen vacancies. In Nb-doped experiments the correlation of Ti, Fe and Nb cations shows that these cations occupy the octahedral B site in the experimental perovskites (ABO_3). Furthermore, Fe and Nb substitute for Ti in equal amounts and account for all Ti substitutions. Therefore, I conclude that for compositions containing Nb, Fe and Nb couple in substitution for Ti, over fO_2 conditions ranging from NNO-3.5 to NNO+3.5.

4.2 APPLICATIONS

4.2.1. Degassing of Volatiles

Global kimberlites display a range of fO_2 conditions that is wider than that of any other magma type. However, the fO_2 recorded by perovskite increases with increasing H_2O and decreasing CO_2 in the whole rock. As kimberlites are highly variable in volatile content and may contain up to 20wt% CO_2 and up to 12wt% H_2O, the variability in volatile degassing history during emplacement could explain the wide range of fO_2 conditions recorded by this magma type (Figure 4.1).

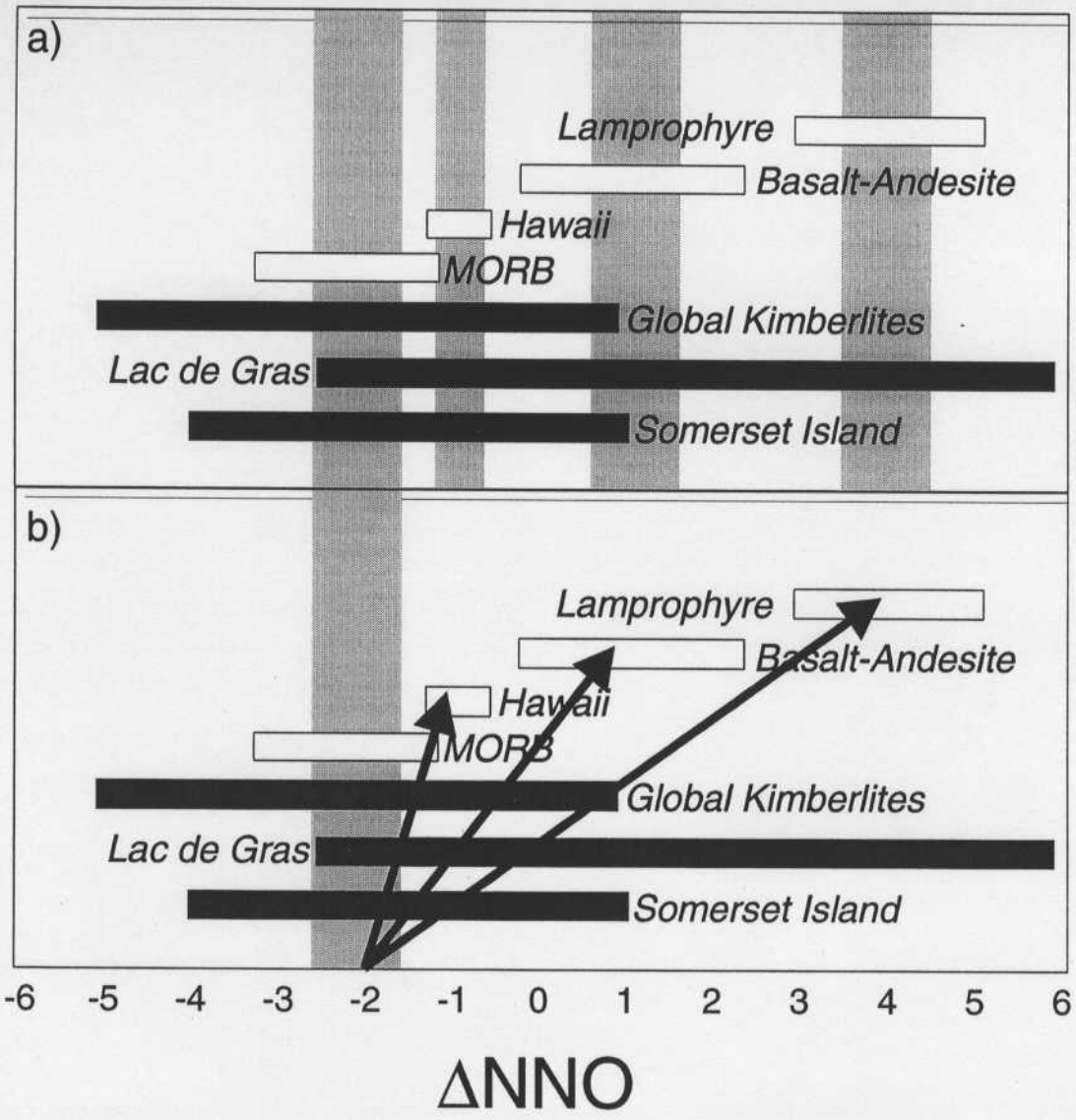

Figure 4.1: Relative fO_2 of different rock types (Luhr *et al.*, 1989; Carmichael *et al.*, 1996; Hasenaka & Carmichael, 1987; Christie *et al.*, 1986; Carmichael & Ghiorso, 1986) and global kimberlites (see Figure 2.2 for references), based on application of the MLR perovskite oxygen barometer. a) Shaded areas represent fO_2 conditions for individual source regions in a heterogeneous mantle. b) Shaded area represents fO_2 conditions for a theoretical common source region with arrows depicting independent evolutionary fO_2 paths based on individual differentiation processes.

By examining global kimberlites, it was discovered that higher amounts of H_2O preserved in the WR as hydrous minerals (suggesting minimal degassing of H_2O) correlate with oxidized magmas. While higher amounts of CO_2 preserved in the whole rock as carbonates (suggesting elevated degassing of CO_2) correlate with reduced magmas. While the effect of degassing CO_2 and H_2O would be to reduce the magma, degassing of H_2 would oxidize the magma. Hence, it is important to consider the speciation of volatile elements during degassing in order to completely characterize the emplacement process.

4.2.2. Kimberlite textures

Kimberlites experience multiple stages of crystallization under changing conditions that ensue during cooling and degassing. Kimbelite texture must be considered when applying the 'Ferric iron in perovskite oxygen barometer'. Perovskites from volcaniclastic kimberlites record a mixture of emplacement episodes or magma batches, but by examining the cores and rims of single perovskite crystals the risk of mixing separate eruptive events can be minimized. Perovskites from hypabyssal kimberlites record the evolution of fO_2 during emplacement of a single magma phase.

4.2.3. Comparisons with other oxygen barometers

In general, the fO_2 recorded by perovksite is higher than the fO_2 recorded by Ol-Sp oxygen barometers. As olivine crystallizes earlier than perovskite (Mitchell, 1986), these two minerals may record different stages in the crystallization history of the kimberlite magma. The oxybarometers developed in this study have the added advantage that different generations of perovskite may record discrete stages in the evolution of the magma.

4.2.4. Applications as a Diamond quality indicator

By examining kimberlites for which diamond quality data is known, results suggest that oxygen fugacity affects the quality of diamonds preserved in the magma. Thus, by determining the fO_2 of an un-characterized kimberlite pipe using the 'Ferric iron in perovskite oxygen barometer', general information on the quality of potential diamonds contained within the pipe may be attained. As results show, kimberlites that experience high fO_2 conditions during emplacement have the highest proportion of highly resorbed diamonds. While, kimberlites that experience low fO_2 conditions during emplacement have lower proportions of highly resorbed diamonds.

4.2.5. Emplacement mechanisms between kimberlite provinces

By using the 'Ferric iron in perovskite oxygen barometer', the contrasting nature of emplacement mechanisms for the Somerset Island and Lac de Gras kimberlites has been revealed. In general, Somerset Island kimberlites become increasingly reduced during emplacement, while the Phoenix kimberlite and the Lac de Gras kimberlites appear to be oxidized during emplacement. This suggests that while magma source regions may vary in fO_2, due to the heterogeneous nature of the mantle (Figure 4.1a), differentiation during emplacement due to variations in volatile degassing and speciation of degassed elements are responsible for the wide range of fO_2 recorded across magma types, within a kimberlite province and even within a single kimberlite pipe (Figure 4.1b).

REFERENCES

Apter, D. B., Harper, F. J., Wyatt, B. A. & Scott Smith, B. H., 1984. The geology of the Mayeng kimberlite sill complex, South Africa. In: *The International Kimberlite Conference*, pp. 43-57.

Aravanis, T., 1999. Legend property assessment report, Birch Mountains area, Alberta. In: *20000003.*, pp. 23.

Berg, G. W., 1998. Geochemical relations which reflect the history of kimberlites from the type area of Kimberley, South Africa. In: *Extended Abstracts, 7th International Kimberlite Conference.*, pp. 76-78, Cape Town: Cape Town University.

Berg, G. W. & Carlson, J. A., 1998. The Leslie kimberlite pipe of Lac de Gras, Northwest Territories, Canada: evidence of near surface hypabyssal emplacement. In: *Extended Abstracts, 7th International Kimberlite Conference.*, pp. 81-83, Cape Town: University of Cape Town.

Bleeker, W. & Davis, W. J., 1999. The 1991-1996 NATMAP Slave Province Project: Introduction. *Can. J. Earth Sci*, **36**, 1033-1042.

Brey, G. P., Kogarko, L. N. & Ryabchikov, I. D., 1991. Carbon dioxide in kimberlitic melts. *N. Jb. Miner. Mh.*, **4**, 159-168.

Brey, G. P. & Ryabchikov, I. D., 1994. Carbon dioxide in strongly silica undersaturated melts and origin of kimberlite magmas. *N. Jb. Miner. Mh.*, **10**, 449-463.

Carmichael, I. S. E., 1967. The Iron-Titanium Oxides of Salic Volcanic Rocks and their Associated Ferromagnesian Silicates. *Contributions to Mineralogy and Petrology*, **14**, 36-64.

Carmichael, I. S. E., 1991. The redox states of basic and silicic magmas: a reflection of their source regions? *Contributions to Mineralogy and Petrology*, **106**, 129-141.

Carmichael, I. S. E. & Ghiorso, M. S., 1986. Oxidation-reduction relations in basic magma: a case for homogeneous equilibria. *Earth and Planetary Science Letters*, **78**, 200-210.

Carmichael, I. S. E., Lange, R. A. & Luhr, J. F., 1996. Quaternary minettes and associated volcanic rocks of Mascota, western Mexico: a consequence of plate extension above a subduction modifies mantle wedge. *Contributions to Minerlaogy and Petrology*, **124**, 302-333.

Chakhmouoradian, A. R. & Mitchell, R. H., 2000. Occurence, alteration patterns and compositional variation of perovskite in kimberlites. *The Canadian Mineralogist*, **38**, 975-994.

Chakhmouradian, A. R. & Mitchell, R. H., 2001. Three compositional varieties of perovskite from kimberlites of the Lac de Gras field (Northwest Territories, Canada). *Mineralogical Magazine*, **65**(1), 133-148.

Christie, D. M., Carmichael, I. S. E. & Langmuir, C. H., 1986. Oxidation states of mid-ocean ridge basalt glasses. *Earth and Planetary Science Letters*, **79**, 397-411.

Clement, C. R., 1982. A comparative geological study of some major kimberlite pipes in the Northern Cape and Orange Free State. *Unpub. Ph.D. Thesis Thesis, University of Cape Town, Cape Town.*

Clement, C. R., Skinner, E. M. W. & Scott Smith, B. H., 1984. Kimberlite redefined. *Journal of Geology*, **92**, 223-228.

Creaser, R. A., Grutter, H., Carlson, J. & Crawford, B., 2003. Macrocrystal phlogopite Rb-Sr dates for the Ekati property kimberlites, Slave Province, Canada: evidence for multiple intrusive episodes in the Paleocene and Eocene. *Lithos*, **76**, 399-414.

Dawson, J. B., 1967. Geochemistry and origin of kimberlite. In: *Ultramafic and related Rocks* (ed Wyllie, P. J.), pp. 241-251, John Wiley and Sons., New York.

Dawson, J. B., 1972. Kimberlites and their relationship to the upper mantle. *The Royal Society of London. Philosophical Transactions. Series A.*, **271**, 297-311.

Dawson, J. B. & Hawthorne, J. B., 1973. Magmatic sedimentation and carbonatitic differentiation in kimberlite sills at Benfontein, South Africa. *Journal of the Geological Society of London*, **129**, 61-85.

Deer, W. A., Howie, R. A. & Zussman, J., 1992. *An introduction to the rock-forming minerals*. Prentice Hall, Essex, England.

Eccles, D. R., Heaman, L. M., Luth, R. W. & Creaser, R. A., 2003. Petrogenetic considerations for the late Cretaceous northern Alberta kimberlite province. In: *Proceedings of the 8th International Kimberlite Conference*, pp. 62, Victoria, BC.

Eccles, D. R., Heaman, L. M., Luth, R. W. & Creaser, R. A., 2004. Petrogenesis of the late Cretaceous northern Alberta kimberlite province. *Lithos*, **76**, 435-459.

Edgar, A. D., Arima, M., Baldwin, D. K., Bell, D. R., Shee, S. R., Skinner, E. M. W. & Walker, E. C., 1988. High pressure - high temperature melting experiments on a SiO2-poor, CaO-rich aphanitic kimberlite from the Wesselton mine, Kimberley, South Africa. *American Mineralogist*, **73**, 524-533.

Edgar, A. D. & Charbonneau, H. E., 1993. Melting experiments on a SiO2-poor, CaO-rich aphanitic kimberlite from 5-10 GPa and their bearing on sources of kimberlite magmas. *American Mineralogist*, **78**, 132-142.

Edwards, D., Rock, N. M. S., Taylor, W. R., Griffin, B. J. & Ramsay, R. R., 1992. Mineralogy and petrology of the Aries diamondiferous kimberlite pipe, Central Kimberley Block, Western Australia. *Journal of Petrology*, **33**, 1157-1191.

Fedortchouk, Y. & Canil, D., 2004. Intensive variables in kimberlite magmas, Lac de Gras, Canada, and implications for diamond survival. *Journal of Petrology*, **45**, 1725-1745.

Fedortchouk, Y., Canil, D. & Carlson, J. A., 2005. Dissolution forms in Lac de Gras diamonds and their relationship to the temperature and redox state of kimberlite magma. *Contributions to Mineralogy and Petrology*, 150, 54-69.

Frost, B. R., 1991. Introduction to oxygen fugacity and its petrologic significance. In: *Oxide Minerals: petrologic and magnetic significance* (ed Lindsley, D. H.), pp. 1-10, Mineralogical Society of America, Washington, D.C.

Fudali, R. F., 1965. Oxygen fugacities of basaltic and andesitic magmas. *Geochimica Cosmochimica Acta*, **29**, 1063-75.

Gudfinnson, G. H. & Presnall, D. C., 2005. Continuous Gradations among Primary Carbonatitic, Kimberlitic, Melilitic, Basaltic, Picritic and Komatiitic Melts in Equilibrium with Garnet Lherzolite at 3-8 GPa. *Journal of Petrology*, **46**(8), 1646-1659.

Gurney, J. J. & Ebrahim, S., 1973. Chemical composition of Lesotho kimberlites. *Lesotho Kimberlites*, 280-294.

Gurney, J. J. & Switzer, G. S., 1973. The discovery of garnets closely related to diamonds in the Finsch pipe, South Africa. *Contributions to Mineralogy and Petrology*, **39**, 103-116.

Haggerty, S. E., 1973. *Spinels of unique composition associated with ilmenite reactions in the Liqhobong kimberlite pipe, Lesotho*. Cape and Transvaal Printers Ltd., Cape Town.

Haggerty, S. E., 1994. Superkimberlites: A geodynamic diamond window to the Earth's core. *Earth and Planetary Science Letters*, **122**, 57-69.

Hasenaka, T. & Carmichael, I. S. E., 1987. The cinder cones of Michoacan-Guanajuato, Central Mexico: petrology and chemistry. *Journal of Petrology*, **28**, 241-269.

Heaman, L. H., 1989. The nature of the subcontinental mantle from Sr-Nd-Pb isotope studies on kimberlite perovskite. *Earth and Planetary Science Letters*, **92**, 323-334.

Heaman, L. M., Kjarsgaard, B. A. & Creaser, R. A., 2004. The temporal evolution of North Amercan kimberlites. *Lithos*, **76**, 377-397.

Illupin, I. P. & Lutz, B. G., 1971. The chemical composition of kimberlite and questions on the origin of kimberlite magmas. *Sovietskaya Geologiya*, **6**, 61-73.

Illupin, I. P., Sobolev, S. F., Zolotarev, B. P. & Lebedev-Zinovyev, A. A., 1974. Geochemical specialization of kimberlites from various parts of Yakutia. *Geochemistry International*, **11**, 357-370.

Irvine, G. J., Kopylova, M. G., Carlson, R. W., Pearson, D. G., Shirey, S. B. & Kjarsgaard, B. A., 1999. Age of the lithosphere mantle beneath and around the Slave craton: a rhenium-osmium isotopic study of peridotite xenoliths from the

Jericho and Somerset Island kimberlites. In: *Ninth Annual V.M. Goldschmidt Conference.*, pp. 134-135, Houston: Lunar and Planetary Institute.

Kennedy, G. C., 1948. Equilibrium between volatiles and iron oxides in igneous rocks. *American Journal of Science*, 529-548.

Kopylova, M. G., Russell, J. K. & Cookenboo, H., 1998. Petrography and chemistry of the Jericho kimberlite (Slave Craton, Northern Canada). In: *Extended Abstracts, 7th International Kimberlite Conference.*, pp. 449-451, Cape Town, University of Cape Town.

Kress, V. C. & Carmichael, I. S. E., 1988. Stoichiometry of the iron-oxidation reaction in silicate melts. *American Mineralogist*, **73**, 1267-1274.

LeRoex, A. P., Bell, D. R. & Davis, P., 2003. Petrogenesis of Group I kimberlites from Kimberley, South Africa: Evidence fromm bulk-rock geochemistry. *Journal of Petrology*, **44**(12), 2261-2286.

Luhr, J. F., Allan, J. F., Carmichael, I. S. E., Nelson, S. A. & Hasenaka, T., 1989. Primitive calc-alkaline and alkaline rock types from the Western Mexican volcanic belt. *Journal of Geophysical Research*, **94**, 4515-4530.

McCammon, C. & Kopylova, M. G., 2004. A redox profile of the Slave mantle and oxygen fugacity control in the cratonic mantle. *Contributions to Mineralogy and Petrology*, **148**, 55-68.

McConnell, J. D. C., 1999. The analysis of incommensurate structures in terms of full space group theory, and the application of the method to melilite. *Z. Kristallographie*, **214**, 457-464.

Mitchell, R. H., 1972. Composition of perovskite in kimberlite. *American Mineralogist*, **57**, 1748-1753.

Mitchell, R. H., 1973. Composition of olvine, silica activity and oxygen fugacity in kimberlite. *Lithos*, **6**, 65-81.

Mitchell, R. H., 1975. Theoretical aspects of gaseous and isotopic equilibria in the system C-H-O-S with application to kimberlite. *Physics and Chemistry of the Earth*, **9**, 903-915.

Mitchell, R. H., 1986. *Kimberlites: Mineralogy, Geochemistry, and Petrology*. Plenum.

Mitchell, R. H., 1997. *Kimberlites, Orangeites, Lamproites, Melilitites, and Minettes: a Petrological Atlas*. Almaz Press, Thunder Bay, Ontario.

Mitchell, R. H. & Meyer, H. O. A., 1980. Mineralogy of micaceous kimberlite from the Jos dyke, Somerset Island. *Candian Mineralogist*, **18**, 241-250.

Muir, I. J., Metson, J. B. & Bancroft, G. M., 1984. ^{57}Mossbauer spectra of perovskite and titanite. *Canadian Mineralogist*, **22**, 689-694.

Muramatsu, Y., 1983. Geochemical investigations of kimberlites from the Kimberley area, South Africa. *Geochemical Journal*, **17**, 71-86.

Nassichuk, W. W. & McIntyre, D. J., 1995. Cretaceous and Tertiary fossils discovered in kimberlites at Lac de Gras in the Slave Province, Northwest Territories. In: *Interior Plains and Arctic Canada - Plaines interieures et region arctique du Canada*, pp. 109-114, Geological Survey of Canada, Ottawa, ON, Canada.

Nickel, E. H. & McAdam, R. C., 1963. Niobium perovskite from Oka, Quebec: A new classification for minerals from the perovskite group. *Canadian Mineralogist*, **7**, 683-697.

Nowicki, T., Crawford, B., Dyck, D., Carlson, J., McElroy, R., Oshust, P. & Helmstaedt, H., 2004. The geology of kimberlite pipes of the Ekati property, Northwest Terrirtories, Canada. *Lithos*, **76**, 1-27.

Pell, J. A., 1995. Kimberlites in the Slave structural province, Northwest Territories: A preliminary review. *EGS 1995-12, NWT Geological Mapping Division, DIAND.*

Pouchou, J. L. & Pichoir, F., 1985. PAP $\phi(\rho Z)$ procedure for improved quantitative microanalysis. *Microbeam Analysis*, 104-106.

Price, S. E., Russell, J. K. & Kopylova, M. G., 2000. Primitive magma from the Jericho pipe, N.W.T., Canada: Constraints on primary kimberlite melt chemistry. *Journal of Petrology*, **41**(6), 789-808.

Ringwood, A. E., Kesson, S. E., Hibberson, W. O. & Ware, N., 1992. Origin of kimberlites and related magmas. *Earth and Planetary Science Letters*, **113**, 521-538.

Robinson, D. N., 1975. Magnetite-serpentine-calcite dikes at Premier Mine and aspects of their relationship to kimberlite and to carbonatite of alkalic carbonatite complexes. *Physics and Chemistry of the Earth*, **9**, 61-70.

Sack, R. O., Carmichael, I. S. E., Rivers, M. & Ghiorso, M. S., 1980. Ferric-Ferrous equilibria in natural silicate liquids at 1 bar. *Contributions to Mineralogy and Petrology*, **75**, 369-376.

Sato, M., 1978. Oxygen Fugacity of Basaltic Magmas and the Role of Gas-Forming Elements. *Geophysical Research Letters*, **5**(6), 447-449.

Schmidberger, S. S. & Francis, D., 1999. Nature of the mantle roots beneath the North American craton: mantle xenolith evidence from Somerset Island kimberlites. *Lithos*, **48**, 195-216.

Schmidberger, S. S. & Francis, D., 2001. Constraints on the trace element composition of the Archean mantle root beneath Somerset Island, Arctic Canada. *Journal of Petrology*, **42**, 1095-1117.

Scott, B. H., 1979. Petrogenesis of kimberlites and associated potassic lamprophyres from Central West Greenland. In: *Second International Kimberlite Conference.*, pp. 190-205.

Scott Smith, B. H., Danchin, R. V., Harris, J. W. & Stracke, K. J., 1984. Kimberlites near Orroroo, South Australia. In: *Third International Kimberlite Conference*, pp. 121-142.

Seifert, F., Czank, M., Simons, B. & Schmahl, W., 1987. A commensurate-incommensurate phase transition in iron-bearing akermanites. *Physics and Chemistry of Minerals*, **14**, 26-35.

Shee, S. R., 1986. The petrogenesis of the Wesselton mine kimberlites, Kimberley, South Africa. *Unpub. Ph.D. thesis Thesis, University of Cape Town.*

Skinner, E. M. W. & Scott, B. H., 1979. Petrography, mineralogy and geochemistry of kimberlites and associated lamprophyre dykes near Swartruggens, Western Transvaal, R.S.A. In: *Kimberlite Symposium II (Extended Abstracts*, Cambridge.

Smith, A. L., 1970. Sphene, perovskite and co-existing Fe-Ti oxide minerals. *American Mineralogist*, **55**, 264-269.

Smith, C. B., Allsopp, H. L., Garvie, O. G., Kramers, J. D., Jackson, P. F. S. & Clement, C. R., 1989. Note on the U-Pb perovskite method for dating kimberlites:examples from Wesselton and DeBeers mines, South Africa and Somerset Island, Canada. *Chemical Geology (Isotope Geos.)*, **79**, 137-145.

Smith, C. B., Gurney, J. J., Skinner, E. M. W., Clement, C. R. & Ebrahim, N., 1985. Geochemical character of southern African kimberlites: a new approach based upon isotopic constraints. *Transactions of the Geological Society of South Africa*, **88**, 267-280.

Smith, C. B., McCallum, M. E., Coopersmith, H. G. & Eggler, D. H., 1979. Petrochemistry and structure of kimberlites in the Front Range and Laramie Range, Colorado Wyoming. In: *Second International Kimberlite Conference*, pp. 186-189.

Stewart, W. D., 1987. Late Proterozoic to early tertiary stratigraphy of Somerset Island and northern Boothia Peninsula, District of Franklin., pp. 78, Geological Survey of Canada Papers.

Taylor, W. R., Tompkins, L. A. & Haggerty, S. E., 1994. Comparative geochemistry of West African kimberlites: evidence for a micaceous kimberlite endmember of sublithospheric origin. *Geochimica et Cosmochimica Acta*, **58**, 4017-4037.

Thornber, C. R., Roeder, P. L. & Foster, J. R., 1980. The effect of composition on the ferric-ferrous ratio in basaltic liquids at atmospherc pressure. *Geochimica et Cosmochimica Acta*, **44**, 525-532.

Toplis, M. J. & Carrol, M. R., 1995. An experimental study of the influence of oxygen fugacity on Fe-ti oxide stability, phase relations, and mineral-melt equilibria in ferro-baslatic systems. *Journal of Petrology*, **36**(5), 1137-1170.

Wagner, P. A., 1914. *The Diamond Fields of South Africa.* Transvaal Leader, Johannesburg.

Woodland, A. B. & Koch, M., 2003. Variation in Oxygen Fugacity with depth in the upper mantle beneath the Kaapvaal craton, Southern Africa. *Earth and Planetary Science Letters*, **214**, 295-310.

Zhang, R. & Liu, B., 1983. Kimberlites from North China. *Geochemical Journal*, **17**, 209-221.

Appendix I. Database of global literature kimberlite occurrences and their wt % compositions

Reference	Location	SiO2	TiO2	Al2O3	Fe2O3	FeO	MnO	MgO	CaO	Na2O	K2O	P2O5	CO2	H2O+	Total	LOI	C.I.	Fe_2O_3*
Price et al.,2000	Jericho,CA(JD51)	20.8	0.9	1.8	6.5	0.6	0.2	16.7	25.5	0.1	0.2	0.9	18.8	6.3	99.07	25.5		7.1
Price et al.,2000	Jericho,CA(JD69-1)	24.2	0.5	1.1	2.2	3.6	0.2	19.7	22.3	0.1	0.3	0.7	16.9	7.1	98.89	24.0		6.2
Price et al.,2000	Jericho,CA(JD69-2)	27.0	0.5	1.3	2.2	3.5	0.1	22.4	19.4	0.2	0.4	0.6	14.0	7.9	99.45	22.0		6.0
Price et al.,2000	Jericho,CA(JD69-3)	29.1	0.5	1.4	2.1	3.8	0.1	23.7	16.7	0.1	0.5	0.6	13.0	7.2	98.63	20.4		6.3
Price et al.,2000	Jericho,CA(JD82-1)	28.8	0.6	1.4	5.3	1.5	0.2	23.3	16.9	0.1	0.4	0.7	12.4	7.2	98.64	20.4		6.9
Price et al.,2000	Jericho,CA(JD82-2)	28.1	0.7	1.6	2.7	4.2	0.2	23.1	16.7	0.2	0.5	0.8	12.1	7.7	98.45	20.1		7.3
Price et al.,2000	Jericho,CA(JD82-3)	30.3	0.8	1.8	3.0	4.6	0.2	25.1	13.3	0.2	0.4	0.8	9.8	8.6	98.79	18.5		8.1
Price et al.,2000	Jericho,CA(LGS07-1)	34.0	0.8	2.1	2.2	5.4	0.2	35.3	7.1	0.2	0.4	0.7	4.8	5.9	99.04	10.4		8.1
Price et al.,2000	Jericho,CA(LGS07-2)	32.9	1.1	2.1	2.6	5.2	0.2	34.4	7.5	0.2	0.3	0.8	4.9	6.6	98.66	11.4		8.3
Price et al.,2000	Jericho,CA(LGS07-3)	31.9	1.2	2.3	2.8	5.2	0.2	34.0	8.7	0.2	0.3	1.0	5.8	5.6	98.95	11.2		8.5
Koploya et al.,1998	Jericho,CA (n=10)	30.5	1.0	2.0	2.9	4.9	0.2	32.9	9.5	0.1	0.1	0.5	7.0	7.3	98.92	14.1		8.4
Koploya et al.,1998	Jericho,CA(Ph.1(n=18)	33.0	1.0	1.8	2.5	5.5	0.2	36.1	6.8	0.1	0.2	0.4	4.8	6.2	98.54	10.9		8.6
Koploya et al.,1998	Jericho,CA(Ph. 2(n=10	35.3	0.8	2.8	2.7	4.4	0.1	30.6	6.6	0.2	0.6	0.3	4.4	9.7	98.35	14.4		7.5
Koploya et al.,1998	Jericho,CA(Ph. 3(n=9))	33.6	0.8	1.9	2.7	4.7	0.1	34.8	6.6	0.1	0.2	0.2	5.0	7.9	98.67	12.9		7.9
Shee,1986	Wesselton,SA	25.6	3.4	3.3		10.3	0.2	27.2	15.3	0.3	0.7	1.8	4.8	6.2	99.05			11.4
Berg et al.,1998	Leslie,CA	31.7	0.7	1.2	9.2		0.2	40.9	8.1	0.0	0.4	0.3			99.45	5.6		9.2
Berg,1998	Dutoitspan,SA	31.7	1.6	1.9	8.8		0.2	36.2	8.0	0.4	0.7	0.8			101.24	9.9		8.8
Smith et al.,1985	Group 1A, SA(n=10)	32.1	2.0	2.6	9.2		0.2	28.5	8.2	0.2	1.1	1.1	4.3	8.6	98.10			9.2
Clement,1982	Kimberley,AU(n=30)	30.0	1.8	2.6	9.4		0.2	29.4	10.9	0.3	1.2	1.6	5.4	7.3	100.10			9.4
Smith et al.,1985	Group 1B,SA(n=7)	25.7	3.0	3.1	12.7		0.2	23.8	14.1	0.2	0.6	1.1	8.6	7.2	100.30			12.7
Illupin et al.,1971	Siberia,RU(n=623)	27.6	1.6	3.2	8.4		0.1	24.3	14.1	0.2	0.8	0.5	10.8	7.9	99.50			8.4
Clement,1982	DeBeers,SA	30.0	1.7	2.0	5.2	3.3	0.2	32.5	10.9	0.2	0.7	1.9			99.30	10.7		8.9
Clement,1982	Wesselton,SA	32.0	2.3	2.7	5.6	3.2	0.2	32.4	6.7	0.1	1.1	1.5			99.36	11.5		9.2
Clement,1982	Dutoitspan,SA	34.4	0.7	1.0	4.1	3.6	0.1	38.6	7.0	0.2	0.8	1.7			99.65	7.4		8.1
Smith et al.,1985a	Jagersfontein	37.5	0.4	2.3	3.9	3.4	0.1	34.4	2.1	0.0	0.7	0.2			98.88	13.9		7.7
Spriggs,1988	Berseba Reserve#2	33.9	1.8	3.9	10.5		0.2	30.7	8.6	0.2	0.9	0.8			100.31	8.9		10.5
Spriggs,1988	Anis Kubub	33.9	1.5	4.3	8.3		0.2	21.9	14.6	1.0	2.9	1.4			99.51	9.6		8.3
Pell,1995	Slave ,CA(1)	32.8	0.5	2.0	8.3		0.2	34.6	7.8	0.2	0.4	0.7			97.51	10.0		8.3
Pell,1995	Slave ,CA(2)	33.0	0.4	1.1	8.4		0.2	40.4	7.3	0.2	0.2	0.6			97.99	6.3		8.4
Pell,1995	Slave ,CA(3)	33.3	0.4	1.2	8.5		0.2	40.2	6.9	0.2	0.2	0.6			98.66	7.1		8.5
Pell,1995	Slave ,CA(4)	40.0	0.3	3.5	6.0		0.1	24.2	3.9	0.3	0.6	0.2			98.62	19.7		6.0
Pell,1995	Slave ,CA(5)	40.6	0.4	5.4	5.7		0.2	18.3	10.2	0.5	1.6	0.5			100.15	16.8		5.7
Pell,1995	Slave ,CA(6)	42.4	0.3	5.2	6.7		0.1	26.9	2.9	0.3	0.8	0.2			99.89	14.1		6.7

Reference	Location	SiO2	TiO2	Al2O3	Fe2O3	FeO	MnO	MgO	CaO	Na2O	K2O	P2O5	CO2	H2O+	Total	LOI	C.I.	Fe_2O_3*
Pell,1995	Slave ,CA(7)	39.8	0.2	3.0	6.6		0.1	30.2	3.4	0.1	0.9	0.2			99.70	15.2		6.6
Pell,1995	Slave ,CA(8)	40.7	0.2	3.4	6.9		0.1	32.0	3.1	0.1	0.5	0.2			98.52	11.3		6.9
Pell,1995	Slave ,CA(9)	39.4	0.4	7.4	9.1		0.1	22.9	2.0	0.1	1.2	0.2			98.28	15.5		9.1
Pell,1995	Slave ,CA(10)	37.6	0.3	2.5	7.5		0.2	28.8	5.8	0.1	2.1	0.1			99.01	14.1		7.5
Pell,1995	Slave ,CA(11)	42.5	0.9	5.6	7.1		0.1	22.2	6.2	0.3	2.7	0.3			98.61	10.7		7.1
Pell,1995	Slave ,CA(12)	34.2	0.5	3.5	8.0		0.2	25.5	8.8	0.2	0.3	0.8			96.64	14.8		8.0
Pell,1995	Slave ,CA(13)	46.1	0.4	8.6	6.0		0.1	16.8	7.0	0.8	2.9	0.3			98.78	9.8		6.0
Pell,1995	Slave ,CA(14)	36.9	1.8	3.2	10.1		0.1	29.2	1.2	0.4	0.6	0.4			98.77	14.9		10.1
Pell,1995	Slave ,CA(15)	23.7	1.0	4.1	7.8		0.1	28.3	7.2	0.1	0.7	0.8			91.00	17.1		7.8
Berg & Carlson	Leslie (LDC-07 220)	31.7	0.7	1.2	9.2		0.2	40.9	8.1	0.0	0.4	0.3		0.7	98.24	5.6		9.2
Berg & Carlson	Leslie(LDC-09 140)	32.7	0.5	1.5	8.7		0.2	39.5	8.4	0.0	0.3	0.4		0.4	98.44	6.3		8.7
Berg & Carlson	du Toitspan(KDT 25)	31.7	1.6	1.9	8.8		0.2	36.2	8.0	0.4	0.7	0.8		0.7	100.05	9.9		8.8
Berg & Carlson	Leslie(LDC-03 427)	43.0	0.2	2.4	7.4		0.1	34.3	4.3	2.6	3.2	0.3		0.4	99.87	2.1		7.4
Berg & Carlson	Bultfontein(KBULT 28)	39.3	0.6	6.0	7.7		0.1	26.3	4.6	1.6	1.5	0.5		5.2	95.36	7.2		7.7
Fresq et al.,1975	Premier Mine	45.6	1.7	4.8	8.8		0.1	22.7	6.4	0.8	1.3	0.3	0.2	7.2	99.78			8.8
Fresq et al.,1975	Ebenhaezer West	34.9	0.8	6.6	5.1		0.1	10.9	15.9	0.4	2.1	0.3	11.8	10.6	99.45			5.1
Gurney et al.,1973	Lemphane	38.1	2.1	7.0	9.6	1.5	0.2	16.9	6.5	0.1	0.3	0.5	1.7	15.1	99.65			11.3
Gurney et al.,1973	Liqhobong	38.7	1.1	7.2	6.4	2.9	0.1	23.4	5.9	0.1	0.3	0.3	0.1	12.7	99.27			9.7
Smith et al.,1979	Sloan, USA	30.4	0.9	1.9	4.0	2.0	0.1	25.9	14.8	0.0	0.3	0.4	8.9	10.2	99.95			6.2
Smith et al.,1979	Sloan, USA	33.8	1.4	2.3	7.8	1.6	0.2	32.1	5.4	0.1	0.3	0.7	3.2	10.9	100.10			9.6
Zhang & Liu,1983	Shandong,China	32.1	0.8	0.9	5.5	3.2	0.2	38.5	5.7	0.1	0.2	0.4		9.4	90.52	3.1		9.0
Gurney et al.,1973	Lesotho(Dike 202)	32.5	1.4	2.1	5.1	3.8	0.2	31.4	7.6	0.1	1.6	0.5	4.5	8.0	98.91			9.3
Gurney et al.,1973	Lesotho(Pipe 200)	30.4	3.0	3.1	5.1	6.3	0.2	25.1	9.7	0.1	2.2	1.2	5.3	6.9	98.60			12.1
Apter et al.,1984	Mayeng	29.2	4.7	2.0	11.9		0.9	31.1	7.5	0.1	0.9	0.7			98.85	9.9		11.9
Dawson et al.,1973	Benfontein	28.6	1.1	2.0	4.0	5.4	0.1	34.0	11.9	0.2	0.1	0.3	9.0	3.0	99.68			10.0
Dawson et al.,1973	Benfontein	25.2	1.9	2.9	3.7	6.7	0.2	29.7	13.6	0.0	0.2	2.2	12.8	1.2	100.23			11.2
Robinson,1975	Premier	16.9	0.9	0.8	7.0	3.5	0.2	16.6	26.4		0.0	1.4	19.2	5.4	98.39			10.9
Skinner et al.,1979	Swattruggens	38.9	1.7	4.0	8.6		0.2	19.9	7.1	0.3	4.7	1.3			97.93	11.4		8.6
Dawson,1972	New Elands	36.1	1.5	4.4	6.8	2.7	0.2	22.8	8.3	0.3	5.0	1.5	3.8	6.2	99.56			9.8
Scott Smith et al.,19	Orroroo	31.0	1.3	3.1	8.9		0.2	24.0	11.4	0.1	1.6	0.6			98.41	16.3		8.9
Scott,1979	Holtsteinborg	32.4	3.9	3.8	4.2	9.5	0.2	26.6	8.0	0.3	2.1	0.3	5.9	3.2	100.26			14.7
Scott,1979	Holtsteinborg	26.5	1.8	0.6	6.7	6.5	0.2	32.8	9.6	0.1	0.1	0.7	10.6	5.6	101.77			13.9
Scott,1979	Holtsteinborg	16.4	1.9	1.3	3.5	5.5	0.2	17.2	24.8	1.0	0.1	1.8	23.4	3.2	100.28			9.5

Reference	Location	SiO2	TiO2	Al2O3	Fe2O3	FeO	MnO	MgO	CaO	Na2O	K2O	P2O5	CO2	H2O+	Total	LOI	C.I.	Fe_2O_3*
Dawson, 1967		35.2	2.3	4.4		9.8	0.1	27.9	7.6	0.3	1.0	0.7	3.3	7.4	100.03			10.9
Dawson, 1967		31.1	2.0	4.9		10.5	0.1	23.9	10.6	0.3	2.1	0.7	7.1	5.9	99.24			11.7
Gurney et al.,1973	Lesotho	33.2	2.0	4.5	6.8	3.4	0.2	22.8	9.4	0.2	0.8	0.7	4.6	10.7	99.23			10.6
Gurney et al.,1973	South Africa	36.4	1.0	5.1		7.7	0.2	17.4	11.2	0.4	1.5	0.6			81.64			8.6
Muramatsu,1983	South Africa	34.0	1.5	3.4	4.6	3.8	0.2	25.4	9.5	0.5	1.6	1.1	5.1	8.3	99.01			8.8
Scott,1979	Holsteinborg	30.2	3.4	2.5	3.9	8.7	0.2	27.5	9.7	0.3	1.8	0.5	7.4	3.7	99.91			13.6
Zhang and Liu,1983	Shandong/Liaoning	30.0	1.5	2.5	6.0	3.0	0.2	28.6	10.1	0.2	0.5	0.7			83.33			9.3
Ilupin and Lutts,1971	Siberian Kimberlites	27.6	1.7	3.2	5.4	2.8	0.1	24.3	14.1	0.2	0.8	0.6	10.8	8.1	99.86			8.5
Ilupin et al.,1974	Alakit, Siberia	27.0	1.5	2.5	5.5	1.7	0.1	25.5	13.6	0.1	0.3	0.5	11.1	10.2	99.73			7.4
Ilupin et al.,1974	Malaya Botuoba	25.5	1.2	3.0	3.9	2.4	0.1	17.0	21.4	0.2	0.5	0.6	16.2	7.6	99.48			6.6
Ilupin et al.,1974	Chomurdakh	26.6	1.9	3.1	5.6	3.0	0.1	25.5	13.5	0.1	0.8	0.8	10.9	7.9	99.73			8.9
Ilupin et al.,1974	Luchankan	32.2	2.8	4.4	6.0	4.0	0.2	22.5	10.9	0.3	1.7	0.7	6.4	7.8	99.70			10.4
Eccles et al., 2004	Alberta, Canada	36.9	0.0	0.2	3.5		0.1	27.6	1.0	0.1	0.3	0.1			99.71	30	1.3	3.5
Eccles et al., 2004	Alberta, Canada	31.7	0.1	0.6	7.9		0.1	42.8	4.0	0.1	0.1	0.3			99.54	12	0.8	7.9
Eccles et al., 2004	Alberta, Canada	28.5	0.1	0.6	5.9		0.1	38.8	1.6	0.0	0.1	0.3			99.54	24	0.7	5.9
Eccles et al., 2004	Alberta, Canada	29.6	1.2	2.0	8.9		0.2	33.8	6.6	0.1	0.3	0.2			99.54	17	0.9	8.9
Eccles et al., 2004	Alberta, Canada	29.7	0.9	2.8	8.9		0.2	32.3	7.5	0.0	0.2	0.5			99.17	16	1.0	8.9
Eccles et al., 2004	Alberta, Canada	22.3	1.2	3.5	9.1		0.2	18.0	15.5	0.4	0.5	0.6			99.25	28	1.4	9.1
Eccles et al., 2004	Alberta, Canada	12.7	1.4	3.0	7.6		0.2	14.0	23.1	0.2	0.2	0.7			99.29	36	1.1	7.6
Eccles et al., 2004	Alberta, Canada	34.8	0.8	1.4	9.5		0.1	40.9	1.5	0.0	0.2	0.2			99.54	10	0.9	9.5
Eccles et al., 2004	Alberta, Canada	32.9	0.5	2.1	9.0		0.1	36.9	3.6	0.1	0.2	0.3			99.49	14	0.9	9.0
Eccles et al., 2004	Alberta, Canada	31.9	0.6	2.0	7.8		0.1	34.8	5.4	0.0	0.3	0.4			99.28	16	1.0	7.8
Eccles et al., 2004	Alberta, Canada	33.5	0.6	1.6	8.4		0.1	37.2	3.6	0.1	0.2	0.4			99.45	14	0.9	8.4
Eccles et al., 2004	Alberta, Canada	28.9	0.8	1.6	7.7		0.1	29.1	11.8	0.1	0.2	0.5			99.27	19	1.0	7.7
Eccles et al., 2004	Alberta, Canada	41.4	0.5	5.9	5.7		0.1	19.8	7.1	0.1	1.5	0.5			99.51	17	2.1	5.7
Eccles et al., 2004	Alberta, Canada	29.9	0.9	1.9	8.2		0.2	33.5	8.2	0.1	0.5	0.9			99.00	15	0.9	8.2
Eccles et al., 2004	Alberta, Canada	28.1	0.5	2.7	8.3		0.1	31.5	6.1	0.1	0.4	0.4			99.47	21	1.0	8.3
Eccles et al., 2004	Alberta, Canada	29.5	0.5	2.5	8.6		0.1	35.4	6.0	0.1	0.2	0.4			99.30	16	0.9	8.6
Eccles et al., 2004	Alberta, Canada	70.1	0.6	11.5	4.3		0.0	1.9	1.4	1.0	1.9	0.2			99.30	6.3	14.3	4.3
Eccles et al., 2004	Alberta, Canada	25.6	1.0	3.4	6.6		0.1	19.7	19.8	0.4	2.5	0.6			99.35	20	1.2	6.6
Eccles et al., 2004	Alberta, Canada	28.4	1.4	2.6	9.0		0.2	32.2	7.8	0.1	0.2	0.9			98.68	16	1.0	9.0
Eccles et al., 2004	Alberta, Canada	27.5	1.3	2.8	8.2		0.2	29.5	12.0	0.1	0.3	1.0			99.28	17	1.0	8.2
Eccles et al., 2004	Alberta, Canada	40.8	0.5	5.9	5.5		0.1	19.6	7.2	0.1	1.5	0.5			99.13	18	2.1	5.5

Reference	Location	SiO2	TiO2	Al2O3	Fe2O3	FeO	MnO	MgO	CaO	Na2O	K2O	P2O5	CO2	H2O+	Total	LOI	C.I.	Fe_2O_3*
Eccles et al., 2004	Alberta, Canada	38.9	1.1	8.6	6.8		0.1	11.2	11.9	2.4	3.9	0.6			98.79	13	2.6	6.8
Eccles et al., 2004	Alberta, Canada	17.2	0.1	0.4	4.6		0.1	33.7	3.0	0.1	0.3	0.2			99.12	40	0.5	4.6
Eccles et al., 2004	Alberta, Canada	36.3	0.1	1.1	7.9		0.1	40.9	0.8	0.0	0.2	0.2			99.24	12	0.9	7.9
Eccles et al., 2004	Alberta, Canada	35.4	0.1	0.7	8.2		0.1	44.9	1.6	0.0	0.4	0.3			99.46	7.7	0.8	8.2
Eccles et al., 2004	Alberta, Canada	26.8	0.6	2.5	7.1		0.1	26.7	15.3	0.0	0.3	0.3			99.48	20	1.1	7.1
Eccles et al., 2004	Alberta, Canada	29.8	0.8	2.5	8.1		0.2	27.3	11.8	0.2	0.3	0.4			98.98	18	1.2	8.1
Eccles et al., 2004	Alberta, Canada	32.5	0.8	2.0	7.9		0.1	31.3	5.7	0.1	0.3	0.5			99.20	18	1.1	7.9
Eccles et al., 2004	Alberta, Canada	50.4	0.9	9.7	6.3		0.1	12.8	3.3	0.9	2.2	0.3			99.17	12	3.6	6.3
Eccles et al., 2004	Alberta, Canada	59.2	0.8	11.2	5.9		0.1	7.4	2.7	2.3	2.9	0.2			99.60	6.9	5.5	5.9
Eccles et al., 2004	Alberta, Canada	32.0	0.6	6.6	3.6		0.2	2.5	27.6	1.3	1.0	0.4			99.32	24	8.8	3.6
Eccles et al., 2004	Alberta, Canada	56.5	0.9	10.9	6.1		0.1	8.6	3.8	2.3	2.5	0.3			99.48	7.6	5.2	6.1
Eccles et al., 2004	Alberta, Canada	61.2	0.8	11.2	5.3		0.1	6.5	3.0	2.7	2.2	0.2			99.23	6.2	7.0	5.3
Eccles et al., 2004	Alberta, Canada	49.5	0.9	9.6	6.8		0.1	13.3	4.3	2.3	2.1	0.3			99.23	10	3.5	6.8
Eccles et al., 2004	Alberta, Canada	47.6	0.8	8.4	6.6		0.1	15.1	5.1	1.2	2.3	0.3			99.54	12	2.9	6.6
Eccles et al., 2004	Alberta, Canada	48.0	0.9	9.1	6.3		0.1	14.2	4.9	1.7	2.2	0.3			99.26	12	3.2	6.3
Eccles et al., 2004	Alberta, Canada	46.2	0.8	7.6	7.8		0.1	16.4	4.4	1.4	1.7	0.3			99.20	13	2.8	7.8
Eccles et al., 2004	Alberta, Canada	46.0	0.9	7.5	7.0		0.1	16.7	5.0	1.4	1.7	0.3			99.44	13	2.7	7.0
Eccles et al., 2004	Alberta, Canada	47.1	0.8	8.3	6.8		0.1	15.5	4.8	1.4	2.2	0.3			99.59	12	2.8	6.8
Eccles et al., 2004	Alberta, Canada	47.1	0.9	8.6	6.6		0.1	16.2	3.9	1.6	2.0	0.3			99.12	12	2.8	6.6
Eccles et al., 2004	Alberta, Canada	51.4	0.9	9.3	6.4		0.1	13.7	3.2	1.9	2.4	0.3			99.29	9.6	3.4	6.4
Eccles et al., 2004	Alberta, Canada	17.3	1.4	5.4	7.9		0.2	4.5	28.0	0.3	2.5	0.9			91.43	23	2.4	7.9
Eccles et al., 2004	Alberta, Canada	48.5	1.4	9.3	7.1		0.1	13.5	3.9	1.7	2.6	0.4			99.57	11	3.2	7.1
Eccles et al., 2004	Alberta, Canada	37.8	1.3	7.8	7.1		0.2	12.3	11.3	0.4	3.1	0.5			99.32	18	2.5	7.1
Eccles et al., 2004	Alberta, Canada		2.7	2.7	10.1		0.2	23.8	13.7	0.2	0.3	0.7			78.01	24	1.0	10.1
Eccles et al., 2004	Alberta, Canada	31.9	2.1	3.5	9.8		0.2	23.4	8.9	0.2	0.6	0.4			99.61	19	1.4	9.8
Eccles et al., 2004	Alberta, Canada	44.8	0.6	11.4	7.9		0.1	17.4	1.8	0.4	1.9	0.3			99.94	13	2.7	7.9
Eccles et al., 2004	Alberta, Canada	29.2	2.2	3.8	11.8		0.2	20.3	12.4	0.3	0.8	0.7			99.10	18	1.5	11.8
Eccles et al., 2004	Alberta, Canada	28.9	3.3	2.9	10.3		0.2	26.8	9.6	0.1	0.5	0.5			99.55	17	1.1	10.3
Eccles et al., 2004	Alberta, Canada	28.1	3.3	2.9	10.2		0.2	26.8	9.0	0.1	0.6	0.6			99.43	18	1.1	10.2
Eccles et al., 2004	Alberta, Canada	27.5	3.5	2.7	10.2		0.2	28.1	8.4	0.0	0.5	0.6			99.45	18	1.0	10.2
Eccles et al., 2004	Alberta, Canada	29.3	3.4	3.2	10.2		0.2	28.1	8.2	0.1	0.6	0.5			99.61	16	1.1	10.2
Eccles et al., 2004	Alberta, Canada	29.1	3.5	3.1	10.3		0.2	28.0	8.2	0.1	0.5	0.5			99.52	16	1.1	10.3
Eccles et al., 2004	Alberta, Canada	15.8	3.1	2.9	8.4		0.2	18.8	15.6	0.1	0.5	0.5			99.12	33	0.9	8.4

Reference	Location	SiO2	TiO2	Al2O3	Fe2O3	FeO	MnO	MgO	CaO	Na2O	K2O	P2O5	CO2	H2O+	Total	LOI	C.I.	$Fe_2O_3^*$
Eccles et al., 2004	Alberta, Canada	25.8	2.9	2.7	9.3		0.2	25.4	7.4	0.1	0.6	0.5			99.35	25	1.1	9.3
Eccles et al., 2004	Alberta, Canada	28.7	3.1	2.8	9.5		0.2	27.9	7.2	0.1	0.3	0.4			98.76	19	1.1	9.5
Eccles et al., 2004	Alberta, Canada	30.0	3.1	2.9	9.9		0.2	29.6	5.9	0.1	0.3	0.5			99.42	17	1.1	9.9
Eccles et al., 2004	Alberta, Canada	29.0	3.3	2.9	10.0		0.2	29.2	6.4	0.1	0.2	0.5			99.54	18	1.1	10.0
Eccles et al., 2004	Alberta, Canada	25.1	2.9	2.5	9.1		0.2	25.1	5.3	0.5	0.4	0.4			99.35	28	1.1	9.1
Eccles et al., 2004	Alberta, Canada	13.1	3.2	2.6	7.8		0.2	19.1	16.0	0.2	0.2	0.5			99.25	36	0.8	7.8
Eccles et al., 2004	Alberta, Canada	24.2	3.6	3.6	12.6		0.2	21.7	13.5	0.1	0.1	0.9			98.90	19	1.3	12.6
Eccles et al., 2004	Alberta, Canada	22.9	4.8	4.4	15.0		0.3	18.8	12.9	0.1	0.0	0.6			99.20	19	1.5	15.0
Eccles et al., 2004	Alberta, Canada	25.6	3.6	3.5	12.1		0.2	24.7	11.4	0.1	0.1	0.5			99.17	17	1.2	12.1
Eccles et al., 2004	Alberta, Canada	25.3	3.7	3.6	12.7		0.2	24.7	11.2	0.1	0.1	0.5			99.36	17	1.2	12.7
Eccles et al., 2004	Alberta, Canada	19.7	4.1	3.5	12.7		0.2	25.5	11.0	0.1	0.5	0.7			98.91	21	0.9	12.7
Eccles et al., 2004	Alberta, Canada	22.5	3.5	3.3	11.8		0.2	26.1	10.5	0.1	0.6	0.7			99.28	20	1.0	11.8
Eccles et al., 2004	Alberta, Canada	24.3	4.0	3.4	13.6		0.2	26.3	10.5	0.1	0.4	0.7			98.84	15	1.0	13.6
Eccles et al., 2004	Alberta, Canada	24.3	3.6	3.5	12.4		0.2	25.2	11.2	0.1	0.3	0.8			98.77	17	1.1	12.4
Eccles et al., 2004	Alberta, Canada	25.8	2.9	2.5	11.8		0.2	27.2	10.4	0.2	0.2	0.7			98.80	17	1.0	11.8
Eccles et al., 2004	Alberta, Canada	57.4	0.5	11.3	7.0		0.2	7.0	5.2	3.0	4.6	0.6			98.79	2	4.4	7.0
Eccles et al., 2004	Alberta, Canada	38.9	1.1	5.1	8.6		0.1	26.5	3.7	0.4	1.0	0.4			99.36	14	1.6	8.6
Eccles et al., 2004	Alberta, Canada	37.4	0.9	4.4	7.7		0.2	23.9	7.7	0.5	0.8	0.3			99.58	16	1.7	7.7
Eccles et al., 2004	Alberta, Canada	37.4	1.1	4.7	8.0		0.1	23.0	8.0	0.5	1.0	0.3			99.83	16	1.7	8.0
LeRoex et al.,2003	DuToitspan	30.5	0.9	0.8		8.6	0.2	33.4	8.3	0.2	0.2	1.5	4.7	10.0	99.23			9.6
LeRoex et al.,2003	DuToitspan	27.3	1.6	2.1		8.1	0.2	27.2	12.6	0.1	1.4	2.1	8.6	7.6	98.82			9.0
LeRoex et al.,2003	Bultfontein	21.1	2.4	2.0		9.5	0.2	22.9	19.9	0.1	0.1	4.1	7.3	9.4	99.04			10.5
LeRoex et al.,2003	Bultfontein	20.3	3.7	4.0		10.0	0.3	20.8	19.2	1.2	0.3	1.7	6.0	11.6	99.20			11.1
LeRoex et al.,2003	Bultfontein	27.7	0.7	0.7		7.9	0.2	26.4	11.2	0.3	0.3	1.1	12.1	10.4	98.84			8.8
LeRoex et al.,2003	Wesselton	30.9	2.2	2.5		9.2	0.2	31.7	8.9	0.4	1.5	1.6	4.3	6.7	99.88			10.2
LeRoex et al.,2003	Wesselton	32.7	2.0	2.3		8.3	0.2	33.5	7.2	0.0	1.4	0.9	2.8	7.7	99.00			9.2
LeRoex et al.,2003	Wesselton	29.3	2.3	2.1		8.8	0.2	32.0	10.0	0.2	0.7	1.1	4.3	9.1	99.87			9.8
LeRoex et al.,2003	Wesselton	32.2	1.9	2.1		8.3	0.2	33.3	9.0	0.2	1.1	1.1	4.9	5.0	99.23			9.2
LeRoex et al.,2003	DeBeers	32.8	1.9	2.4		8.1	0.2	31.2	9.7	0.4	1.7	1.5	3.5	6.4	99.73			9.0
LeRoex et al.,2003	DeBeers	32.7	1.7	2.4		8.1	0.2	30.5	8.2	0.4	0.6	1.6	3.7	8.3	98.22			9.0
LeRoex et al.,2003	DeBeers	35.8	1.6	1.0		8.1	0.1	33.5	4.9	0.2	1.3	0.4	2.8	10.0	99.60			9.0
LeRoex et al.,2003	DeBeers	32.7	1.9	2.3		8.3	0.2	32.3	8.4	0.4	1.8	2.1	2.9	6.9	100.07			9.2
LeRoex et al.,2003	DeBeers	30.6	0.9	1.4		7.9	0.2	34.3	10.7	0.0	0.5	1.6	9.8	2.7	100.37			8.7
LeRoex et al.,2003	DeBeers	30.2	2.0	1.9		8.1	0.2	31.8	10.0	0.0	0.7	1.3	9.1	4.6	99.85			9.0

Reference	Location	SiO2	TiO2	Al2O3	Fe2O3	FeO	MnO	MgO	CaO	Na2O	K2O	P2O5	CO2	H2O+	Total	LOI	C.I.	Fe_2O_3*
LeRoex et al.,2003	DeBeers	25.4	1.3	1.4		8.1	0.2	30.3	14.8	0.1	0.2	2.6	5.1	10.1	99.58			9.0
LeRoex et al.,2003	Big Hole - Kimb. Pipe	29.6	2.3	2.1		8.9	0.2	29.7	10.4	0.1	1.1	1.2	6.4	8.0	99.76			9.9
LeRoex et al.,2003	Big Hole - Kimb. Pipe	29.1	2.2	2.1		8.7	0.2	29.1	10.5	0.1	1.1	1.1	6.4	8.5	98.81			9.6
LeRoex et al.,2003	Big Hole - Kimb. Pipe	28.9	2.4	2.1		9.0	0.2	28.6	11.3	0.1	1.5	1.3	6.8	7.2	99.31			10.0
LeRoex et al.,2003	Big Hole - Kimb. Pipe	28.7	2.2	1.9		8.4	0.2	28.4	10.6	0.1	0.8	1.0	6.6	10.3	99.24			9.3
LeRoex et al.,2003	Big Hole - Kimb. Pipe	29.2	2.4	2.0		8.7	0.2	28.2	10.4	0.1	0.8	1.2	6.6	9.8	99.50			9.7
LeRoex et al.,2003	Wesselton Floors Sills	28.5	1.4	1.7		7.1	0.1	29.0	10.1	0.0	0.8	1.6	9.4	9.7	99.29			7.9
LeRoex et al.,2003	Wesselton Floors Sills	25.9	2.4	2.6		7.9	0.2	21.8	16.2	0.2	0.9	3.1	8.3	8.9	98.45			8.8
LeRoex et al.,2003	Wesselton Floors Sills	28.3	1.5	1.8		7.2	0.1	27.6	10.7	0.0	0.8	1.8	9.8	9.9	99.40			8.0
LeRoex et al.,2003	Wesselton Floors Sills	29.7	1.5	1.7		7.4	0.1	30.0	9.2	0.0	0.9	1.6	5.2	11.5	98.72			8.2
LeRoex et al.,2003	Wesselton Floors Sills	32.0	1.7	1.8		8.4	0.2	33.5	7.1	0.0	1.3	1.4	1.0	11.4	99.80			9.3
LeRoex et al.,2003	Wesselton Floors Sills	25.7	3.5	5.1		11.0	0.2	17.4	16.1	0.1	2.7	1.8	7.4	7.7	98.73			12.2
LeRoex et al.,2003	Wesselton Floors Sills	25.5	3.9	3.5		12.6	0.3	18.0	15.1	0.3	2.3	3.1	6.5	8.1	99.04			14.0

Appendix II. Database of global literature perovskite and their wt % compositions

Reference	Sample Number	Notes	Na2O	CaO	SrO	La2O3	Ce2O3	Pr2O3	Nd2O3	ThO2	TiO2	Al2O3	Fe2O3	Nb2O5	Ta2O5	Total
Eccles et al.,2004	ph01-02-03-1	Core	0.33	38.4	0.20	0.74	1.48	0.0	0.36	0.00	51.7	0.20	1.71	0.50	0.00	95.43
Eccles et al.,2004	ph01-02-03-10	Core	0.43	39.2	0.26	0.88	1.83	0.0	0.47	0.07	52.6	0.22	1.59	0.40	0.00	97.80
Eccles et al.,2004	ph01-02-03-1b	Core	0.56	37.2	0.20	0.91	2.02	0.0	0.54	0.05	51.4	0.17	1.64	0.52	0.00	95.02
Eccles et al.,2004	ph01-02-03-7	Core	0.33	39.2	0.28	1.14	2.06	0.0	0.51	0.08	52.5	0.44	1.56	0.31	0.00	98.23
Eccles et al.,2004	ph01-02-03-8	Core	0.44	39.2	0.24	0.90	1.99	0.0	0.52	0.15	52.4	0.23	1.49	0.45	0.00	97.88
Eccles et al.,2004	ph01-02-03-9	Core	0.80	36.4	0.23	1.27	3.47	0.0	1.14	1.32	51.6	0.37	1.66	0.24	0.00	98.40
Eccles et al.,2004	ph01-03-03-2	Core	0.33	38.8	0.24	1.15	2.16	0.0	0.58	0.01	52.5	0.30	1.61	0.36	0.00	97.93
Eccles et al.,2004	ph01-03-03-3	Core	0.36	39.0	0.22	1.11	2.39	0.0	0.65	0.07	51.8	0.39	1.74	0.39	0.00	97.92
Eccles et al.,2004	ph01-04-01-1	Core	1.39	33.4	0.23	1.77	4.76	0.0	1.62	1.62	51.1	0.17	1.44	0.30	0.00	97.61
Eccles et al.,2004	ph01-04-01-10	Core	1.28	33.6	0.24	1.83	4.75	0.0	1.59	1.40	50.2	0.16	1.69	0.38	0.00	96.90
Eccles et al.,2004	ph01-04-01-11	Core	1.21	33.6	0.23	1.84	4.73	0.0	1.63	1.39	51.1	0.14	1.50	0.36	0.00	97.58
Eccles et al.,2004	ph01-04-01-12	Core	1.21	33.6	0.23	1.84	4.76	0.0	1.61	1.58	50.0	0.19	2.06	0.38	0.00	97.31
Eccles et al.,2004	ph01-04-01-13	Core	1.48	33.4	0.29	1.87	4.84	0.0	1.57	1.42	50.5	0.14	1.50	1.33	0.00	98.16
Eccles et al.,2004	ph01-04-01-14	Core	1.36	33.3	0.26	1.89	4.82	0.0	1.62	1.50	50.6	0.14	1.34	0.36	0.00	97.09
Eccles et al.,2004	ph01-04-01-15	Core	1.28	33.6	0.23	1.82	4.79	0.0	1.62	1.31	50.4	0.17	1.49	0.36	0.00	96.96
Eccles et al.,2004	ph01-04-01-4	Core	1.29	33.6	0.23	1.71	4.61	0.0	1.56	1.45	51.1	0.14	1.55	0.33	0.00	97.38
Eccles et al.,2004	ph01-04-01-9	Core	1.39	33.1	0.24	1.90	5.02	0.0	1.66	1.65	50.5	0.16	1.55	0.36	0.00	97.39
Eccles et al.,2004	ph01-04-04-12	Core	1.27	33.1	0.25	1.79	4.70	0.0	1.60	1.75	50.0	0.17	1.98	0.33	0.00	96.73
Eccles et al.,2004	ph01-04-04-13	Core	0.76	36.9	0.25	1.51	3.25	0.0	0.85	0.09	51.3	0.21	1.71	0.55	0.00	97.18
Eccles et al.,2004	ph01-04-04-4	Core	1.31	33.6	0.24	1.79	4.70	0.0	1.50	1.49	50.2	0.18	1.81	0.39	0.00	97.00
Eccles et al.,2004	ph01-04-01-7	Dark	0.39	37.6	0.22	1.14	2.77	0.0	0.87	1.09	50.7	0.34	2.37	0.43	0.00	97.75
Eccles et al.,2004	ph01-05-03-2	Dark	0.43	39.1	0.23	1.17	2.05	0.0	0.49	0.05	52.0	0.29	1.76	0.42	0.00	97.80
Eccles et al.,2004	ph01-05-03-3	Dark	0.36	39.5	0.21	1.00	1.86	0.0	0.46	0.08	52.1	0.29	1.75	0.52	0.00	97.98
Eccles et al.,2004	ph01-02-03-7		0.44	38.2	0.26	1.31	2.42	0.0	0.67	0.13	51.6	0.40	1.75	0.36	0.00	97.27
Eccles et al.,2004	ph01-05-03-2	Light	0.60	38.2	0.25	1.13	1.88	0.0	0.54	0.00	50.4	0.22	2.25	0.88	0.00	96.13
Eccles et al.,2004	ph01-05-03-3	Light	0.39	38.6	0.25	1.16	2.45	0.0	0.71	0.00	51.9	0.42	1.82	0.53	0.00	98.00
Eccles et al.,2004	ph01-02-01-1	Rim	0.55	37.7	0.24	1.11	2.84	0.0	0.77	0.16	53.3	0.23	1.39	0.17	0.00	98.30
Eccles et al.,2004	ph01-02-01-3	Rim	0.70	37.1	0.23	1.24	2.98	0.0	0.89	0.26	52.5	0.22	1.55	0.27	0.00	97.81
Eccles et al.,2004	ph01-02-03-1	Rim	0.52	35.3	0.24	1.29	3.27	0.0	0.95	0.09	50.4	0.46	1.94	0.29	0.00	94.52
Eccles et al.,2004	ph01-02-03-10	Rim	0.49	37.4	0.29	1.49	3.35	0.0	0.99	0.07	51.4	0.52	2.02	0.32	0.00	98.14
Eccles et al.,2004	ph01-02-03-10	Rim	0.31	37.6	0.28	1.58	3.07	0.0	0.86	0.00	50.2	0.62	2.36	0.40	0.00	97.13
Eccles et al.,2004	ph01-02-03-1b	Rim	1.94	32.5	0.33	1.96	4.36	0.0	1.25	0.21	44.8	0.04	2.74	8.09	0.00	97.90

Reference	Sample Number	Notes	Na2O	CaO	SrO	La2O3	Ce2O3	Pr2O3	Nd2O3	ThO2	TiO2	Al2O3	Fe2O3	Nb2O5	Ta2O5	Total
Eccles et al.,2004	ph01-02-03-7	Rim	1.28	33.1	0.30	2.08	5.24	0.0	1.70	0.31	46.4	0.33	3.15	1.10	0.00	94.81
Eccles et al.,2004	ph01-02-03-8	Rim	0.49	36.5	0.25	1.44	3.40	0.0	0.95	0.08	50.7	0.46	2.03	0.41	0.00	96.42
Eccles et al.,2004	ph01-03-03-2	Rim	0.39	38.7	0.25	1.18	2.36	0.0	0.69	0.04	52.3	0.37	1.63	0.26	0.00	97.96
Eccles et al.,2004	ph01-04-01-1	Rim	0.45	36.4	0.23	1.32	3.58	0.0	1.28	1.37	49.6	0.64	2.50	0.27	0.00	97.41
Eccles et al.,2004	ph01-04-01-10	Rim	0.40	37.4	0.25	1.21	3.19	0.0	1.03	1.04	51.1	0.54	2.06	0.28	0.00	98.24
Eccles et al.,2004	ph01-04-01-11	Rim	0.48	37.1	0.22	1.14	2.84	0.0	1.02	1.40	50.6	0.45	2.26	0.29	0.00	97.63
Eccles et al.,2004	ph01-04-01-12	Rim	0.55	36.7	0.23	1.41	3.66	0.0	1.19	1.01	50.4	0.54	2.19	0.26	0.00	97.95
Eccles et al.,2004	ph01-04-01-13	Rim	0.37	32.8	0.16	1.08	2.85	0.0	1.03	0.96	49.0	0.31	2.05	0.31	0.00	90.69
Eccles et al.,2004	ph01-04-01-14	Rim	0.43	37.2	0.24	1.23	3.36	0.0	1.08	1.22	50.6	0.54	2.08	0.33	0.00	98.17
Eccles et al.,2004	ph01-04-01-15	Rim	0.42	37.5	0.24	1.20	2.98	0.0	1.00	0.98	51.0	0.54	2.05	0.25	0.00	97.95
Eccles et al.,2004	ph01-04-01-4	Rim	0.45	37.4	0.26	1.26	3.18	0.0	1.09	1.22	51.0	0.52	2.09	0.32	0.00	98.65
Eccles et al.,2004	ph01-04-01-9	Rim	0.44	36.9	0.24	1.29	3.38	0.0	1.19	1.19	50.4	0.57	2.25	0.34	0.00	97.99
Eccles et al.,2004	ph01-04-04-4	Rim	0.42	37.7	0.25	1.23	3.10	0.0	0.98	1.26	50.4	0.48	2.24	0.31	0.00	98.14
Eccles et al.,2004	ph01-05-03-2	Rim	0.54	37.9	0.26	1.36	2.56	0.0	0.67	0.06	51.2	0.28	1.97	0.53	0.00	97.12
Eccles et al.,2004	ph01-04-04-12	Rim	0.56	36.6	0.25	1.29	3.43	0.0	1.13	1.57	49.9	0.44	2.41	0.29	0.00	97.73
Eccles et al.,2004	ph01-04-04-13	Rim	0.59	37.5	0.26	1.43	3.37	0.0	0.99	0.15	52.6	0.34	1.54	0.14	0.00	98.78
Eccles et al.,2004	ph01-02-01-2		0.82	35.8	0.27	1.37	3.58	0.0	1.13	1.39	52.2	0.30	1.43	0.23	0.00	98.36
Eccles et al.,2004	ph01-02-03-4		0.37	38.0	0.22	1.03	2.13	0.0	0.49	0.04	51.7	0.34	1.70	0.37	0.00	96.30
Eccles et al.,2004	ph01-02-03-5		0.49	38.4	0.25	1.15	2.55	0.0	0.71	0.00	52.4	0.34	1.57	0.37	0.00	98.02
Eccles et al.,2004	ph01-03-03-1		0.76	36.6	0.21	1.21	3.28	0.0	1.11	1.31	52.0	0.30	1.39	0.14	0.00	98.16
Eccles et al.,2004	ph01-04-01-16		1.18	34.1	0.24	1.79	4.57	0.0	1.49	0.77	50.7	0.17	1.64	0.40	0.00	96.87
Eccles et al.,2004	ph01-04-01-17		1.21	33.9	0.25	1.85	4.69	0.0	1.59	1.28	50.5	0.17	1.63	0.29	0.00	97.17
Eccles et al.,2004	ph01-04-01-2		1.32	33.8	0.27	1.88	4.87	0.0	1.65	1.27	51.0	0.18	1.50	0.41	0.00	98.00
Eccles et al.,2004	ph01-04-01-3		1.29	33.4	0.24	1.79	4.79	0.0	1.59	1.58	50.8	0.16	1.54	0.33	0.00	97.39
Eccles et al.,2004	ph01-04-01-5		1.30	33.8	0.25	1.85	4.70	0.0	1.58	1.39	50.9	0.17	1.60	0.41	0.00	97.82
Eccles et al.,2004	ph01-04-01-6		1.38	33.7	0.26	1.72	4.80	0.0	1.57	1.40	51.1	0.15	1.40	0.41	0.00	97.71
Eccles et al.,2004	ph01-04-01-8		0.99	35.9	0.25	1.53	3.81	0.0	1.17	0.30	52.0	0.14	1.41	0.28	0.00	97.57
Eccles et al.,2004	ph01-04-04-1		0.95	36.1	0.23	1.56	3.75	0.0	1.23	0.33	51.8	0.15	1.46	0.33	0.00	97.70
Eccles et al.,2004	ph01-04-04-10		0.92	35.9	0.25	1.56	3.83	0.0	1.17	0.28	52.6	0.15	1.36	0.34	0.00	98.17
Eccles et al.,2004	ph01-04-04-11		1.16	33.9	0.27	1.79	4.69	0.0	1.58	1.30	50.4	0.19	2.04	0.38	0.00	97.48
Eccles et al.,2004	ph01-04-04-2		0.40	38.3	0.21	1.08	2.66	0.0	0.82	0.25	52.6	0.35	1.57	0.21	0.00	98.28
Eccles et al.,2004	ph01-04-04-3		1.27	33.3	0.22	1.83	4.87	0.0	1.64	1.38	50.4	0.19	1.65	0.39	0.00	96.94
Eccles et al.,2004	ph01-04-04-5		1.15	34.2	0.24	1.80	4.62	0.0	1.59	1.12	50.6	0.18	1.79	0.32	0.00	97.37

Reference	Sample Number	Notes	Na2O	CaO	SrO	La2O3	Ce2O3	Pr2O3	Nd2O3	ThO2	TiO2	Al2O3	Fe2O3	Nb2O5	Ta2O5	Total
Eccles et al.,2004	ph01-04-04-6		0.98	36.2	0.23	1.48	3.74	0.0	1.17	0.22	52.1	0.15	1.32	0.37	0.00	97.89
Eccles et al.,2004	ph01-04-04-7		0.94	36.2	0.25	1.54	3.73	0.0	1.19	0.26	52.0	0.17	1.33	0.28	0.00	97.79
Eccles et al.,2004	ph01-04-04-8		0.93	35.4	0.29	1.64	4.10	0.0	1.33	0.35	51.4	0.22	1.71	0.33	0.00	97.57
Eccles et al.,2004	ph01-04-04-9		1.08	34.8	0.23	1.74	4.52	0.0	1.50	1.15	50.6	0.16	2.00	0.27	0.00	97.93
Eccles et al.,2004	ph01-05-03-1		0.50	38.5	0.25	1.17	2.35	0.0	0.58	0.03	52.0	0.23	1.72	0.45	0.00	97.57
Ch & M, 2000	Matsoku	core	0.88	36.0	0.33	0.95	2.91	0.3	0.68	0.81	53.8		1.00	1.03	0.39	99.07
Ch & M, 2000	Matsoku	rim	0.42	39.0	0.34	0.38	0.89				55.3		1.31	0.75	0.46	98.85
Ch & M, 2000	Thaba Putsoa	core	0.60	38.7	0.27	0.02	1.23		0.13	0.36	57.3		0.86	0.46	0.45	100.38
Ch & M, 2000	Thaba Putsoa	rim	0.16	40.2	0.31		0.21				57.6		1.22	0.31	0.29	100.28
Ch & M, 2000	Wesselton,SA	core	0.82	34.8	0.24	2.24	4.42	0.5	1.35	1.04	53.0		2.28	0.71		101.33
Ch & M, 2000	Wesselton,SA	rim	0.68	35.7	0.46	1.41	2.86	0.7	1.39	0.10	52.8		1.76	0.92		98.75
Ch & M, 2000	Wesselton,SA	sill	0.40	37.7	0.27	0.79	2.39		0.59		54.8	0.36	1.53	0.83	0.23	99.92
Ch & M, 2000	Wesselton,SA	sill	0.12	38.9	0.37	0.79	1.46		0.22		55.6	0.29	1.39	0.70	0.31	100.10
Ch & M, 2000	Premier,SA		0.36	39.4	0.27					0.09	57.5		0.91	0.28		98.79
Ch & M, 2000	Premier,SA		0.63	39.2	0.18	0.19	0.93				57.5		0.82	0.60	0.49	100.68
Ch & M, 2000	Benfontein,SA	zoned	0.61	34.5	0.49	1.24	3.36		1.02	0.64	50.7		1.72	3.09	0.84	98.14
Ch & M, 2000	Benfontein,SA	zoned	0.49	35.5	0.20	1.58	3.80	0.4	1.39	0.43	52.3	0.38	1.69	1.64	0.36	100.20
Ch & M, 2000	Ondermatje,SA		0.36	38.9	0.17	0.72	1.50		0.24	0.13	55.8		0.97	0.15	0.33	99.20
Ch & M, 2000	Ondermatje,SA		0.30	38.9	0.36	0.41	1.01				55.8		1.18	0.58	0.20	98.75
Ch & M, 2000	Frank Smith,SA	core	0.96	34.6	0.32	1.61	3.93	0.2	0.50	0.45	53.6		1.32	0.99		98.39
Ch & M, 2000	Frank Smith,SA	rim	0.50	37.4	0.20	0.97	1.80	0.3	0.35		55.1		1.20	0.48		98.34
Ch & M, 2000	Yakutia,RS	int.	2.00	29.6	0.24	2.15	5.36	0.5	1.80	2.71	47.8	0.16	1.66	5.22	1.02	100.16
Ch & M, 2000	Yakutia,RS	int.	1.47	34.2	0.33	1.32	3.59	0.3	0.89	0.10	51.4	0.27	1.73	3.31		98.82
Ch & M, 2000	Yakutia,RS	int.	1.74	33.5	0.24	2.41	5.12		0.61	0.14	50.8	0.34	1.69	4.37		100.90
Ch & M, 2000	Yakutia,RS		0.42	38.6	0.28	0.50	1.64		0.33	0.16	56.8		1.07	0.35	0.06	100.21
Ch & M, 2000	Yakutia,RS		0.38	39.9	0.25	0.59	0.92				57.6		1.12	0.45	0.30	101.55
Ch & M, 2000	Yakutia,RS		0.35	35.1	0.37	1.98	3.85	0.9	1.55	0.85	52.7		1.81	0.65		100.12
Ch & M, 2000	XI-Yu,China		0.31	37.1	0.57	1.71	2.61	0.3	1.26		54.5		1.91	0.39		100.61
Ch & M, 2000	XI-Yu,China		0.40	34.2	0.39	2.72	4.82	0.8	1.35	0.77	52.5		2.00	0.62		100.55
Ch & M, 2000	XI-Yu,China		0.08	37.9	0.77	1.41	1.67	0.5	0.50		53.8		2.19	0.82		99.73
Ch & M, 2000	Wyoming	relict	0.43	36.0	0.31	1.09	2.37	0.6	0.77	0.17	53.4		1.89	0.86	0.20	98.19
Ch & M, 2000	Colorado		0.22	40.0	0.44	0.69	0.96				55.6	0.40	1.79	0.56	0.16	100.86
Ch & M, 2000	Colorado		0.44	38.3	0.29	0.82	2.02		0.16	0.24	56.6		1.12	0.50	0.24	99.41

Reference	Sample Number	Notes	Na2O	CaO	SrO	La2O3	Ce2O3	Pr2O3	Nd2O3	ThO2	TiO2	Al2O3	Fe2O3	Nb2O5	Ta2O5	Total
Ch & M, 2000	NW Alberta	rim	1.05	34.3	0.41	1.64	3.68	0.6	1.12	0.56	52.4		1.78	2.07	0.24	99.73
Ch & M, 2000	NW Alberta		0.84	36.0	0.20	1.22	3.25	0.4	0.95	0.44	53.6	0.34	1.45	0.97	0.37	99.99
Ch & M, 2000	NW Alberta		0.62	36.5	0.36	1.67	3.38	0.2	1.00	0.70	54.5	0.23	1.28	0.75	0.34	101.56
Ch & M, 2000	FalC		0.41	36.7	0.20	1.15	3.17	0.3	0.78		53.8	0.36	1.30	1.52	0.20	99.88
Ch & M, 2000	FalC		0.86	34.4	0.20	1.49	4.18		1.24	2.19	52.9	0.30	1.36	1.81	0.46	101.35
Ch & M, 2000	FalC		0.42	37.6	0.04	1.24	2.90		0.62	0.03	54.6	0.24	1.22	1.36	0.03	100.35
Ch & M, 2000	FalC		0.28	35.4	0.38	1.38	4.12	0.2	0.96	1.11	53.7	0.64	1.42	0.68	0.31	100.57
Ch & M, 2000	FalC		0.44	35.8	0.37	1.10	3.55	0.1	1.00	0.98	53.5	0.56	1.59	0.74	0.37	100.02
Ch & M, 2000	FalC		0.34	34.3	0.27	1.57	4.96	0.5	1.48	1.02	50.5	0.75	2.50	1.32	0.41	99.81
Ch & M, 2000	Lac deGras		0.48	34.6	0.26	1.84	4.84	0.3	0.99	0.46	49.2	0.60	4.18	1.67	0.50	99.88
Ch & M, 2000	Lac deGras		0.28	31.5	0.56	3.21	6.40	0.3	1.22	0.19	38.1	0.66	5.65	8.55	0.39	99.59
Ch & M, 2000	Lac deGras		1.07	30.3	0.63	2.15	6.14	0.4	1.94	2..93	43.8	0.35	5.24	3.65	1.05	100.10
Ch & M, 2000	Somerset Island		0.32	37.4	0.24	0.61	1.94		0.48	0.52	54.3	0.27	1.28	0.86	0.35	98.57
Ch & M, 2000	Somerset Island		0.53	36.4	0.30	0.74	2.77	0.3	0.59	0.70	54.5	0.17	1.24	0.84	0.24	99.27
Ch & M, 2000	Somerset Island	core	0.62	38.3	0.12	0.84	2.61		0.25	0.40	55.9	0.32	1.29	0.89		101.74
Ch & M, 2000	Somerset Island	rim	0.46	40.4	0.23		1.02				55.8	0.48	1.96	0.93	0.03	101.57
Ch & M, 2000	Somerset Island		0.62	37.4	0.26	1.39	2.29		0.31	0.33	54.6	0.40	1.27	0.86		99.93
Ch & M, 2000	Somerset Island	core	0.46	37.0	0.26	0.94	2.85		0.46	0.83	54.4		1.15	0.70	0.36	99.40
Ch & M, 2000	Somerset Island	rim	0.28	38.3	0.35	0.79	1.49		0.22		55.3		1.14	0.72	0.29	98.83
Ch & M, 2000	Somerset Island		0.28	37.2	0.30	0.96	2.62	0.3	0.50	0.52	54.7	0.37	1.29	0.67	0.25	99.93
Ch & M, 2000	Somerset Island		0.69	37.0	0.44	1.03	2.87		0.51	1.07	54.5	0.33	1.44	0.72		100.63
Ch & M, 2000	Somerset Island		0.25	37.3	0.38	1.38	2.62	0.4	0.74	0.11	54.1		1.61	0.82	0.25	99.99
Ch & M, 2000	Kirkland Lake	rxn rim	0.95	36.2	0.18	1.48	3.40	0.3	0.75		53.2	0.32	1.19	2.14		100.45
Ch & M, 2000	Kirkland Lake	core	1.60	31.5	0.40	1.63	5.60	0.3	1.84	1.84	50.8	0.19	1.43	2.39	0.27	99.99
Ch & M, 2000	Kirkland Lake	rim	0.89	37.0	0.24	1.16	2.65		0.31		51.7	0.27	0.31	2.62	3.51	100.72
Ch & M, 2000	Kirkland Lake	zoned	1.15	35.8	0.27	0.76	3.50	0.1	0.82	0.61	53.8	0.24	0.97	1.47	0.22	99.89
Ch & M, 2000	Kirkland Lake	zoned	0.93	34.3	0.18	1.09	4.30	0.4	1.34	1.20	52.0	0.34	1.21	1.88	0.08	99.60
Mitchell,1986	Benfontein sill		0.53	37.6		0.93	2.70	0.2	0.98		52.4		1.71	0.55		97.59
Mitchell,1986	Benfontein sill		0.33	35.7	0.23	1.04	3.05	0.3	1.26		52.1	0.51	1.94	1.33		97.88
Mitchell,1986	Wesselton		0.67	35.5	0.19	0.88	2.83	0.3	1.29		53.9	0.28	1.18	0.80		97.89
Mitchell,1986	Premier		0.36	39.5	0.08	0.32	0.80	0.1	0.30		55.8	0.17	1.04	0.90		99.39
Mitchell,1986	Liqhobong		0.79	36.5		0.67	2.41	0.1	1.14		54.3		1.38			97.30
Mitchell,1986	Bellsbank		1.54	27.4		3.70	7.90	1.0	1.75		50.0		1.80	2.18		97.56

Reference	Sample Number	Notes	Na_2O	CaO	SrO	La_2O_3	Ce_2O_3	Pr_2O_3	Nd_2O_3	ThO_2	TiO_2	Al_2O_3	Fe_2O_3	Nb_2O_5	Ta_2O_5	Total
Mitchell,1986	Green Mountain		1.88	30.0		1.98	5.88	0.8	1.64		43.0		2.87	11.50		99.59
Mitchell,1986	Turmannosti		0.32	38.4	0.26	0.12	0.26	0.1	0.13		55.2	1.12	1.82	0.24		98.93
Mitchell, 1878	Somerset Island												1.60			
M & F, 1973	Somerset Island												1.71			
Cl & M, 1975	Somerset Island	rim		37.1							55.4	0.42	1.90	0.89		
Cl & M, 1975	Somerset Island			36.5							54.3	0.38	2.24	0.77		

Ch & M, 2000=Chakhmouradian and Mitchell, 2000
Cl & M, 1975=Clarke and Mitchell, 1975
M & F, 1973=Mitchell and Fritz, 1973

Appendix III. Experimental Phases (wt%) with STDEV (1σ) and Mass Balance (modal)

Label	T(°C)	ΔNNO	Na2O	MgO	Al2O3	SiO2	P2O5	K2O	CaO	TiO2	MnO	FeO*	SrO	Nb2O5	La2O3	Ce2O3	Total	MB
DT301WC-AVG-L	1300	4.1	0.02	12.64	5.68	28.69	4.01	0.02	34.17	6.60	0.30	6.62					98.75	
DT301WC-AVG-PV	1300	4.1	0.02	0.51	0.81	1.39	0.22	0.01	40.55	52.60	0.07	2.82					98.99	
DT301WC-STDEV-L	1300	4.1	0.02	0.13	0.16	0.32	0.10	0.02	1.05	0.29	0.04	0.39						
DT301WC-STDEV-PV	1300	4.1	0.00	0.31	0.18	0.61	0.12	0.00	0.40	0.93	0.04	0.25						
DT305WC-AVG-L	1332	-2.0	0.01	14.27	0.36	34.60	0.10	0.01	29.37	11.21	0.03	9.07					99.03	0.76
DT305WC-AVG-OLV	1332	-2.0	0.01	48.25	0.00	41.00		0.01	4.29	0.17	0.02	6.12					99.88	0.23
DT305WC-STDEV-L	1332	-2.0	0.01	0.31	0.01	0.28	0.04	0.01	0.16	0.13	0.01	0.23						
DT305WC-STDEV-OLV	1332	-2.0	0.01	0.15	0.00	0.14		0.01	0.11	0.02	0.02	0.15						
DT306WC-AVG-L	1332	-0.4	0.01	12.34	0.38	33.61	0.11	0.01	28.81	11.66	0.03	12.04					99.00	0.74
DT306WC-AVG-OLV	1332	-0.4	0.01	48.59	0.00	41.00		0.01	4.34	0.18	0.00	6.07					100.20	0.25
DT306WC-STDEV-L	1332	-0.4	0.01	1.79	0.04	0.60	0.03	0.01	0.16	1.17	0.02	0.32						
DT306WC-STDEV-OLV	1332	-0.4	0.00	0.40	0.00	0.22		0.00	0.29	0.02	0.00	0.20						
DT312WC-AVG-L	1275	-2.1	0.02	10.02	0.69	33.54	0.20	0.01	27.21	12.46	0.01	14.81					98.97	0.52
DT312WC-AVG-Me(Ak)	1275	-2.1	0.01	12.63	0.12	43.02		0.01	40.38	0.21	0.02	2.91					99.31	0.12
DT312WC-AVG-OLV	1275	-2.1	0.01	44.94	0.01	40.28		0.01	3.98	0.21	0.01	10.39					99.85	0.31
DT312WC-AVG-PV	1275	-2.1	0.01	0.10	0.05	0.09	0.02	0.01	40.91	58.18	0.02	1.12					100.52	0.03
DT312WC-STDEV-L	1275	-2.1	0.01	1.15	0.05	0.71	0.04	0.01	0.42	0.92	0.01	0.18						
DT312WC-STDEV-Me(Ak)	1275	-2.1	0.01	0.08	0.01	0.09		0.01	0.18	0.04	0.02	0.08						
DT312WC-STDEV-OLV	1275	-2.1	0.01	0.38	0.01	0.13		0.01	0.23	0.04	0.01	0.08						
DT312WC-STDEV-PV	1275	-2.1	0.01	0.03	0.03	0.05	0.03	0.01	0.25	0.28	0.02	0.24						
DT313WC-AVG-L	1296	-2.1	0.02	11.85	0.57	35.06	0.16	0.01	28.10	12.19	0.01	11.33					99.29	0.74
DT313WC-AVG-Me(Ak)	1296	-2.1	0.01	12.95	0.13	43.10		0.00	40.55	0.22	0.02	2.38					99.38	-0.01
DT313WC-AVG-OLV	1296	-2.1	0.01	46.50	0.01	40.44		0.01	4.00	0.22	0.01	8.81					100.01	0.26
DT313WC-AVG-PV	1296	-2.1	0.01	0.14	0.05	0.14	0.04	0.00	40.91	58.09	0.02	1.03					100.43	0.00
DT313WC-STDEV-L	1296	-2.1	0.00	0.42	0.01	0.16	0.05	0.01	0.36	0.17	0.01	0.37						
DT313WC-STDEV-Me(Ak)	1296	-2.1	0.02	0.12	0.02	0.26		0.00	0.14	0.02	0.04	0.12						
DT313WC-STDEV-OLV	1296	-2.1	0.01	0.38	0.00	0.12		0.01	0.19	0.09	0.01	0.32						
DT313WC-STDEV-PV	1296	-2.1	0.01	0.06	0.01	0.23	0.04	0.01	0.28	0.31	0.02	0.13						

Label	T(°C)	ΔNNO	Na2O	MgO	Al2O3	SiO2	P2O5	K2O	CaO	TiO2	MnO	FeO*	SrO	Nb2O5	La2O3	Ce2O3	Total	MB
DT316WC-AVG-L	1276	-0.7	0.01	10.72	0.59	32.19	0.20	0.01	25.77	11.92	0.01	16.75					98.17	0.51
DT316WC-AVG-Me(Ak)	1276	-0.7	0.02	13.03	0.13	43.08		0.02	39.96	0.21	0.00	2.69					99.14	0.15
DT316WC-AVG-OLV	1276	-0.7	0.01	46.88	0.00	40.30		0.01	3.68	0.17	0.01	9.49					100.55	0.29
DT316WC-AVG-PV	1276	-0.7	0.02	0.08	0.06	0.02	0.06	0.01	40.28	56.98	0.02	1.50					99.03	0.04
DT316WC-STDEV-L	1276	-0.7	0.01	0.70	0.04	1.75	0.07	0.01	1.36	1.79	0.02	1.53						
DT316WC-STDEV-Me(Ak)	1276	-0.7	0.01	0.10	0.02	0.12		0.01	0.16	0.02	0.01	0.06						
DT316WC-STDEV-OLV	1276	-0.7	0.01	0.62	0.00	0.17		0.01	0.34	0.03	0.01	0.32						
DT316WC-STDEV-PV	1276	-0.7	0.01	0.01	0.01	0.01	0.01	0.01	0.22	0.22	0.03	0.02						
DT317WC-AVG-L	1276	-0.1	0.01	11.71	0.45	32.82	0.14	0.00	27.58	11.32	0.01	15.00					99.04	0.62
DT317WC-AVG-Me(Ak)	1276	-0.1	0.01	12.91	0.09	43.22		0.00	40.29	0.20	0.00	2.24					98.98	-0.02
DT317WC-AVG-Mo	1276	-0.1	0.01	25.54	0.02	37.39		0.01	29.23	0.25	0.00	7.27					99.73	0.15
DT317WC-AVG-OLV	1276	-0.1	0.00	47.68	0.01	40.83		0.01	3.68	0.19	0.01	7.63					100.04	0.22
DT317WC-AVG-PV	1276	-0.1	0.01	0.08	0.03	0.04	0.03	0.01	41.06	57.69	0.01	1.61					100.57	0.01
DT317WC-STDEV-L	1276	-0.1	0.01	0.34	0.01	0.29	0.04	0.00	0.25	0.27	0.02	0.16						
DT317WC-STDEV-Me(Ak)	1276	-0.1	0.01	0.18	0.02	0.09		0.00	0.10	0.07	0.00	0.00						
DT317WC-STDEV-Mo	1276	-0.1	0.00	0.14	0.02	0.17		0.02	0.42	0.04	0.00	0.29						
DT317WC-STDEV-OLV	1276	-0.1	0.01	0.47	0.01	0.15		0.01	0.43	0.04	0.01	0.29						
DT317WC-STDEV-PV	1276	-0.1	0.00	0.01	0.02	0.02	0.03	0.01	0.28	0.34	0.01	0.27						
DT321WC-AVG-L	1344	-1.9	0.03	14.48	0.34	34.98	0.23	0.01	29.42	10.96	0.02	8.25					98.71	0.76
DT321WC-AVG-OLV	1344	-1.9	0.00	49.26	0.01	41.11		0.01	4.29	0.20	0.00	5.38					100.27	0.22
DT321WC-STDEV-L	1344	-1.9	0.01	0.52	0.01	0.34	0.02	0.01	0.12	0.21	0.02	0.15						
DT321WC-STDEV-OLV	1344	-1.9	0.01	0.22	0.01	0.23		0.01	0.20	0.01	0.00	0.24						
DT328WC-AVG-L	1305	-0.1	0.01	13.34	0.35	33.07	0.12	0.01	28.60	11.12	0.00	12.49					99.10	0.77
DT328WC-AVG-Mo	1305	-0.1	0.01	26.54	0.01	37.75		0.01	29.33	0.26	0.03	5.62					99.54	-0.03
DT328WC-AVG-OLV	1305	-0.1	0.00	48.64	0.01	40.82		0.01	4.16	0.17	0.01	6.37					100.19	0.24
DT328WC-STDEV-L	1305	-0.1	0.01	0.13	0.02	0.15	0.03	0.01	0.13	0.04	0.01	0.20						
DT328WC-STDEV-Mo	1305	-0.1	0.01	0.24	0.00	0.08		0.01	0.18	0.03	0.03	0.21						
DT328WC-STDEV-OLV	1305	-0.1	0.00	0.46	0.01	0.20		0.01	0.31	0.02	0.01	0.11						

Label	T(°C)	ΔNNO	Na2O	MgO	Al2O3	SiO2	P2O5	K2O	CaO	TiO2	MnO	FeO*	SrO	Nb2O5	La2O3	Ce2O3	Total	MB
DT331WC-AVG-L	1357	-2.0	0.00	12.49	0.39	35.14	0.11	0.00	28.84	12.15	0.02	9.60					98.75	0.71
DT331WC-AVG-Mo	1357	-2.0	0.00	24.57	0.02	36.48		0.01	29.55	1.50	0.01	7.30					99.44	0.04
DT331WC-AVG-OLV	1357	-2.0	0.01	49.23	0.01	40.92		0.01	4.06	0.22	0.01	5.73					100.19	0.23
DT331WC-STDEV-L	1357	-2.0	0.00	2.67	0.07	0.52	0.04	0.00	0.47	1.67	0.02	0.54						
DT331WC-STDEV-Mo	1357	-2.0	0.00	0.65	0.02	0.79		0.01	0.60	1.24	0.01	0.79						
DT331WC-STDEV-OLV	1357	-2.0	0.01	0.44	0.00	0.20		0.00	0.08	0.03	0.01	0.22						
DT336WC-AVG-L	1248	-0.2	0.02	8.50	0.66	30.61	0.20	0.02	25.33	11.97	0.01	21.05					98.37	0.36
DT336WC-AVG-Me(Ak)	1248	-0.2	0.02	12.81	0.14	42.96		0.02	40.11	0.20	0.01	3.05					99.32	0.23
DT336WC-AVG-OLV	1248	-0.2	0.00	45.88	0.01	40.15		0.01	3.49	0.16	0.01	10.77					100.47	0.33
DT336WC-AVG-PV	1248	-0.2	0.01	0.08	0.02	0.13	0.01	0.00	40.11	56.76	0.01	1.76					98.90	0.06
DT336WC-STDEV-L	1248	-0.2	0.02	1.25	0.07	0.58	0.06	0.01	0.96	1.30	0.02	0.76						
DT336WC-STDEV-Me(Ak)	1248	-0.2	0.01	0.11	0.01	0.16		0.02	0.10	0.03	0.02	0.05						
DT336WC-STDEV-OLV	1248	-0.2	0.01	0.33	0.01	0.12		0.01	0.19	0.02	0.01	0.20						
DT336WC-STDEV-PV	1248	-0.2	0.01	0.04	0.01	0.16	0.01	0.01	0.25	0.26	0.02	0.11						
DT339WC-AVG-L	1253	-0.7	0.02	9.21	0.65	31.85	0.21	0.03	25.47	11.98	0.02	18.96					98.39	0.38
DT339WC-AVG-Me(Ak)	1253	-0.7	0.02	15.50	0.12	41.50		0.01	37.16	0.21	0.00	4.78					99.30	0.18
DT339WC-AVG-Mo	1253	-0.7	0.03	24.13	0.00	36.86		0.00	28.66	0.22	0.00	9.27					99.18	0.08
DT339WC-AVG-OLV	1253	-0.7	0.00	45.53	0.01	40.09		0.01	3.64	0.17	0.01	10.94					100.40	0.28
DT339WC-AVG-PV	1253	-0.7	0.01	0.09	0.04	0.14	0.03	0.00	40.26	56.96	0.01	1.48					99.03	0.06
DT339WC-STDEV-L	1253	-0.7	0.01	1.21	0.07	0.37	0.07	0.01	0.74	0.85	0.02	1.07						
DT339WC-STDEV-Mo	1253	-0.7																
DT339WC-STDEV-Me(Ak)	1253	-0.7	0.02	5.52	0.07	2.98		0.01	5.66	0.03	0.00	3.17						
DT339WC-STDEV-OLV	1253	-0.7	0.00	0.26	0.01	0.28		0.01	0.14	0.03	0.01	0.31						
DT339WC-STDEV-PV	1253	-0.7	0.01	0.04	0.02	0.15	0.03	0.01	0.41	0.26	0.02	0.08						

Label	T(°C)	ΔNNO	Na2O	MgO	Al2O3	SiO2	P2O5	K2O	CaO	TiO2	MnO	FeO*	SrO	Nb2O5	La2O3	Ce2O3	Total	MB
DT342WC-AVG-L	1252	-0.8	0.03	9.46	0.64	32.05	0.26	0.03	25.62	11.40	0.02	18.86					98.36	0.39
DT342WC-AVG-Me(Ak)	1252	-0.8	0.04	12.92	0.12	42.99		0.03	40.16	0.20	0.02	3.05					99.52	0.14
DT342WC-AVG-Mo	1252	-0.8	0.00	23.86	0.00	37.00		0.01	28.90	0.24	0.00	9.48					99.50	0.11
DT342WC-AVG-OLV	1252	-0.8	0.02	45.22	0.01	40.14		0.01	3.75	0.14	0.00	10.87					100.15	0.29
DT342WC-AVG-PV	1252	-0.8	0.01	0.13	0.04	0.12	0.02	0.01	40.12	56.76	0.01	1.47					98.69	0.06
DT342WC-STDEV-L	1252	-0.8	0.01	0.90	0.03	0.42	0.05	0.01	0.57	0.77	0.03	0.59						
DT342WC-STDEV-Me(Ak)	1252	-0.8	0.02	0.09	0.01	0.06		0.01	0.06	0.02	0.03	0.07						
DT342WC-STDEV-Mo	1252	-0.8	0.00	0.09	0.00	0.06		0.01	0.31	0.02	0.00	0.16						
DT342WC-STDEV-OLV	1252	-0.8	0.01	0.19	0.01	0.17		0.01	0.19	0.02	0.00	0.10						
DT342WC-STDEV-PV	1252	-0.8	0.01	0.14	0.02	0.10	0.03	0.01	0.34	0.32	0.01	0.27						
DT343WC-AVG-L	1253	-0.7	0.03	10.36	0.66	31.90	0.26	0.02	25.35	11.28	0.00	18.29					98.14	0.42
DT343WC-AVG-Me(Ak)	1253	-0.7	0.03	12.88	0.11	43.03		0.02	39.96	0.19	0.00	3.00					99.23	0.19
DT343WC-AVG-OLV	1253	-0.7	0.01	44.61	0.01	40.13		0.01	3.92	0.16	0.00	11.15					100.00	0.32
DT343WC-AVG-PV	1253	-0.7	0.01	0.07	0.05	0.09	0.04	0.01	40.32	56.96	0.00	1.34					98.90	0.06
DT343WC-STDEV-L	1253	-0.7	0.01	0.37	0.04	0.13	0.05	0.01	1.55	0.15	0.00	1.44						
DT343WC-STDEV-Me(Ak)	1253	-0.7	0.01	0.17	0.05	0.18		0.00	0.39	0.03	0.01	0.04						
DT343WC-STDEV-OLV	1253	-0.7	0.00	0.40	0.01	0.21		0.01	0.40	0.02	0.01	0.08						
DT343WC-STDEV-PV	1253	-0.7	0.01	0.02	0.01	0.08	0.03	0.01	0.33	0.21	0.00	0.14						
DT346WC-AVG-L	1248	-2.1	0.04	9.22	0.75	32.53	0.22	0.02	25.25	11.85	0.01	18.72					98.59	0.37
DT346WC-AVG-Me(Ak)	1248	-2.1	0.02	12.51	0.13	42.98		0.02	40.02	0.16	0.01	3.65					99.50	0.22
DT346WC-AVG-OLV	1248	-2.1	0.00	44.69	0.01	40.13		0.01	3.40	0.20	0.00	11.94					100.39	0.33
DT346WC-AVG-PV	1248	-2.1	0.02	0.08	0.06	0.13	0.03	0.01	40.24	57.23	0.00	1.14					98.93	0.07
DT346WC-STDEV-L	1248	-2.1	0.01	1.08	0.05	0.25	0.05	0.01	0.69	0.84	0.01	0.63						
DT346WC-STDEV-Me(Ak)	1248	-2.1	0.01	0.07	0.04	0.08		0.02	0.08	0.02	0.02	0.11						
DT346WC-STDEV-OLV	1248	-2.1	0.01	1.29	0.01	0.32		0.01	0.51	0.05	0.01	1.05						
DT346WC-STDEV-PV	1248	-2.1	0.02	0.02	0.01	0.10	0.02	0.01	0.18	0.26	0.01	0.12						

Label	T(°C)	ΔNNO	Na2O	MgO	Al2O3	SiO2	P2O5	K2O	CaO	TiO2	MnO	FeO*	SrO	Nb2O5	La2O3	Ce2O3	Total	MB
DT347WC-AVG-L	1253	-3.2	0.01	9.73	0.75	32.81	0.23	0.00	25.56	11.77	0.01	17.44					98.32	0.34
DT347WC-AVG-Me(Ak)	1253	-3.2	0.03	12.42	0.17	42.88		0.02	39.80	0.19	0.02	3.52					99.04	0.12
DT347WC-AVG-Mo	1253	-3.2	0.00	23.02	0.00	36.96		0.00	28.29	0.19	0.00	11.00					99.47	0.18
DT347WC-AVG-OLV	1253	-3.2	0.01	43.09	0.01	39.86		0.00	3.99	0.20	0.01	12.92					100.10	0.29
DT347WC-AVG-PV	1253	-3.2	0.01	0.08	0.07	0.05	0.02	0.00	40.65	57.39	0.00	0.90					99.18	0.07
DT347WC-STDEV-L	1253	-3.2	0.01	1.14	0.07	0.89	0.05	0.01	0.60	1.09	0.02	0.86						
DT347WC-STDEV-Me(Ak)	1253	-3.2	0.02	0.10	0.02	0.07		0.01	0.21	0.01	0.01	0.10						
DT347WC-STDEV-Mo	1253	-3.2																
DT347WC-STDEV-OLV	1253	-3.2	0.02	0.37	0.01	0.15		0.01	0.14	0.03	0.01	0.19						
DT347WC-STDEV-PV	1253	-3.2	0.01	0.01	0.02	0.02	0.02	0.00	0.22	0.35	0.01	0.09						
DT350WC-AVG-L	1256	-4.1	0.02	7.71	0.94	33.04	0.35	0.01	25.37	13.27	0.01	17.69					98.42	0.32
DT350WC-AVG-Me(Ak)	1256	-4.1	0.03	12.41	0.15	42.82		0.01	39.74	0.19	0.00	3.73					99.08	0.24
DT350WC-AVG-OLV	1256	-4.1	0.01	42.90	0.01	39.50		0.00	4.01	0.22	0.01	13.54					100.20	0.36
DT350WC-AVG-PV	1256	-4.1	0.01	0.08	0.09	0.09	0.05	0.01	40.39	57.89	0.01	0.83					99.46	0.07
DT350WC-STDEV-L	1256	-4.1	0.02	1.33	0.11	0.60	0.04	0.01	0.84	1.40	0.01	1.01						
DT350WC-STDEV-Me(Ak)	1256	-4.1	0.01	0.05	0.03	0.09		0.01	0.27	0.03	0.01	0.08						
DT350WC-STDEV-OLV	1256	-4.1	0.01	0.43	0.01	0.20		0.01	0.46	0.04	0.02	0.44						
DT350WC-STDEV-PV	1256	-4.1	0.02	0.02	0.01	0.11	0.03	0.01	0.33	0.18	0.02	0.08						
DT351WC-AVG-L	1256	-3.5	0.01	8.35	0.82	32.99	0.22	0.01	25.41	12.93	0.01	17.63					98.39	0.32
DT351WC-AVG-Me(Ak)	1256	-3.5	0.01	12.64	0.13	42.99		0.00	40.06	0.15	0.02	3.61					99.63	0.11
DT351WC-AVG-Mo	1256	-3.5	0.00	22.77	0.00	36.50		0.01	29.01	0.56	0.00	10.80					99.65	0.21
DT351WC-AVG-OLV	1256	-3.5	0.00	43.98	0.02	39.58		0.00	3.82	0.20	0.00	12.84					100.46	0.28
DT351WC-AVG-PV	1256	-3.5	0.01	0.09	0.06	0.13	0.03	0.00	40.50	57.30	0.01	0.98					99.11	0.06
DT351WC-STDEV-L	1256	-3.5	0.01	1.27	0.08	0.34	0.07	0.01	0.84	1.14	0.02	0.90						
DT351WC-STDEV-Me(Ak)	1256	-3.5	0.01	0.08	0.02	0.14		0.00	0.11	0.03	0.03	0.04						
DT351WC-STDEV-Mo	1256	-3.5	0.00	0.30	0.00	0.14		0.01	0.59	0.39	0.00	0.58						
DT351WC-STDEV-OLV	1256	-3.5	0.00	0.65	0.01	0.21		0.00	0.16	0.02	0.01	0.39						
DT351WC-STDEV-PV	1256	-3.5	0.01	0.02	0.02	0.09	0.03	0.00	0.40	0.50	0.02	0.31						

Label	T(°C)	ΔNNO	Na2O	MgO	Al2O3	SiO2	P2O5	K2O	CaO	TiO2	MnO	FeO*	SrO	Nb2O5	La2O3	Ce2O3	Total	MB
DT353WC-AVG-L	1252	-1.5	0.02	9.20	0.72	31.76	0.25	0.02	25.71	12.14	0.01	18.54					98.36	0.36
DT353WC-AVG-Me(Ak)	1252	-1.5	0.02	12.67	0.16	42.73		0.01	39.97	0.16	0.01	3.37					99.11	0.16
DT353WC-AVG-Mo	1252	-1.5	0.03	23.25	0.00	36.85		0.00	28.34	0.24	0.03	10.58					99.31	0.11
DT353WC-AVG-OLV	1252	-1.5	0.01	45.02	0.01	39.76		0.01	3.33	0.19	0.02	11.87					100.21	0.30
DT353WC-AVG-PV	1252	-1.5	0.02	0.07	0.05	0.16	0.03	0.01	40.26	56.71	0.01	1.42					98.73	0.06
DT353WC-STDEV-L	1252	-1.5	0.02	1.17	0.11	0.95	0.07	0.01	0.79	1.72	0.01	0.62						
DT353WC-STDEV-Me(Ak)	1252	-1.5	0.02	0.12	0.03	0.26		0.01	0.35	0.01	0.02	0.07						
DT353WC-STDEV-Mo	1252	-1.5																
DT353WC-STDEV-OLV	1252	-1.5	0.01	1.13	0.01	0.08		0.01	0.57	0.04	0.01	0.61						
DT353WC-STDEV-PV	1252	-1.5	0.01	0.02	0.01	0.11	0.03	0.01	0.25	0.49	0.01	0.27						
DT382-WC-AVG-L	1253	-2.9	0.01	7.92	0.98	32.30	0.29	0.01	24.77	12.51	0.01	19.70					98.50	
DT382-WC-AVG-Mo	1253	-2.9	0.01	12.21	0.12	43.00		0.01	39.93	0.18	0.00	4.08					99.54	
DT382-WC-AVG-OLV	1253	-2.9	0.00	42.72	0.01	39.49		0.01	3.61	0.17	0.01	13.95					99.97	
DT382-WC-AVG-PV	1253	-2.9	0.01	0.11	0.07	0.36	0.04	0.01	40.62	57.46	0.01	1.21					99.89	
DT382WC-STDEV-L	1253	-2.9	0.00	1.23	0.14	0.43	0.06	0.01	0.75	1.10	0.01	0.90						
DT382WC-STDEV-Mo	1253	-2.9	0.01	0.09	0.03	0.26		0.01	0.16	0.04	0.00	0.11						
DT382WC-STDEV-OLV	1253	-2.9	0.00	1.02	0.01	0.44		0.01	0.24	0.04	0.01	1.04						
DT382WC-STDEV-PV	1253	-2.9	0.01	0.14	0.01	0.60	0.04	0.01	0.29	0.74	0.02	0.33						
DT384-WC-AVG-L	1256	-1.6	0.01	8.04	0.85	31.30	0.18	0.01	25.02	13.11	0.01	19.54					98.07	
DT384-WC-AVG-Mo	1256	-1.6	0.01	12.50	0.13	43.15		0.01	40.03	0.16	0.01	3.64					99.65	
DT384-WC-AVG-OLV	1256	-1.6	0.00	43.78	0.01	39.65		0.00	3.54	0.17	0.02	13.05					100.22	
DT384-WC-AVG-PV	1256	-1.6	0.00	0.08	0.06	0.12	0.03	0.00	40.68	57.72	0.00	1.18					99.86	
DT384WC-STDEV-L	1256	-1.6	0.01	1.46	0.12	1.14	0.04	0.01	0.56	1.83	0.01	0.87						
DT384WC-STDEV-Mo	1256	-1.6	0.01	0.10	0.04	0.13		0.01	0.17	0.03	0.02	0.09						
DT384WC-STDEV-OLV	1256	-1.6	0.00	0.69	0.01	0.25		0.00	0.29	0.03	0.02	0.55						
DT384WC-STDEV-PV	1256	-1.6	0.01	0.02	0.01	0.13	0.03	0.00	0.21	0.31	0.00	0.08						

Label	T(°C)	ΔNNO	Na2O	MgO	Al2O3	SiO2	P2O5	K2O	CaO	TiO2	MnO	FeO*	SrO	Nb2O5	La2O3	Ce2O3	Total	MB
DT389-WC-AVG-L	1256	-3.5	0.01	7.33	1.02	32.55	0.25	0.01	24.88	13.10	0.01	19.30					98.45	
DT389-WC-AVG-Mo	1256	-3.5	0.01	14.42	0.12	41.46		0.00	37.40	0.19	0.01	5.94					99.54	
DT389-WC-AVG-OLV	1256	-3.5	0.00	42.28	0.01	39.34		0.00	3.85	0.18	0.01	14.55					100.23	
DT389-WC-AVG-PV	1256	-3.5	0.01	0.07	0.08	0.15	0.03	0.00	40.61	57.65	0.01	1.08					99.69	
DT389WC-STDEV-L	1256	-3.5	0.01	1.00	0.11	0.29	0.04	0.01	0.88	1.02	0.01	0.81						
DT389WC-STDEV-Mo	1256	-3.5	0.01	4.37	0.07	2.88		0.00	5.13	0.06	0.01	3.61						
DT389WC-STDEV-OLV	1256	-3.5	0.00	0.29	0.01	0.17		0.00	0.15	0.02	0.01	0.24						
DT389WC-STDEV-PV	1256	-3.5	0.01	0.02	0.02	0.31	0.03	0.00	0.27	0.36	0.01	0.25						
WCglass-AVG			0.03	21.28	0.25	34.19	0.31	0.01	22.18	7.83	0.02	12.03					98.12	
WCglass-STDEV			0.01	0.13	0.01	0.14	0.05	0.01	0.22	0.09	0.02	0.10						
DT384WC2-AVG-L	1256	-1.6	0.02	9.47	1.44	32.58	0.14	0.02	25.53	11.20	0.01	18.14				0.03	98.57	
DT384WC2-AVG-Me(Ak)	1256	-1.6	0.02	12.51	0.25	42.87		0.01	40.11	0.16	0.01	3.53					99.48	
DT384WC2-AVG-OLV	1256	-1.6	0.01	43.95	0.02	39.66		0.00	3.69	0.19	0.02	12.84					100.38	
DT384WC2-AVG-PV	1256	-1.6	0.01	0.10	0.12	0.20	0.03	0.00	40.44	57.23	0.01	1.26				0.33	99.74	
DT384WC2-STDEV-L	1256	-1.6	0.01	0.14	0.04	0.23	0.04	0.01	0.87	0.18	0.01	0.87				0.02		
DT384WC2-STDEV-PV	1256	-1.6	0.01	0.10	0.02	0.39	0.03	0.01	0.29	0.51	0.01	0.21				0.05		
DT389WC2-AVG-L	1256	-3.5	0.01	8.05	1.69	32.80	0.14	0.01	25.71	12.23	0.01	17.70				0.01	98.35	
DT389WC2-AVG-Me(Ak)	1256	-3.5	0.01	12.42	0.21	42.92		0.00	40.08	0.18	0.02	3.77					99.60	
DT389WC2-AVG-OLV	1256	-3.5	0.00	42.96	0.02	39.88		0.01	3.77	0.18	0.01	13.55					100.38	
DT389WC2-AVG-PV	1256	-3.5	0.01	0.08	0.13	0.06	0.03	0.00	40.36	57.65	0.01	0.95				0.32	99.59	
DT389WC2-STDEV-L	1256	-3.5	0.01	0.99	0.19	0.29	0.03	0.01	0.36	1.09	0.02	0.38				0.01		
DT389WC2-STDEV-PV	1256	-3.5	0.01	0.02	0.02	0.06	0.02	0.01	0.14	0.31	0.02	0.15				0.05		

Label	T(°C)	ΔNNO	Na2O	MgO	Al2O3	SiO2	P2O5	K2O	CaO	TiO2	MnO	FeO*	SrO	Nb2O5	La2O3	Ce2O3	Total	MB
DT444WC3-AVG-L	1180	-2.0	0.01	6.74	0.35	32.63	0.16	0.01	22.79	12.22	0.01	24.20					99.13	0.70
DT444WC3-AVG-Me(Ak)	1180	-2.0	0.02	10.68	0.09	43.22	0.00	0.01	39.77	0.18	0.00	6.46					100.44	0.16
DT444WC3-AVG-OLV	1180	-2.0	0.01	34.82	0.01	38.17	0.00	0.01	3.29	0.21	0.01	24.61					101.14	0.06
DT444WC3-AVG-PV	1180	-2.0	0.01	0.04	0.03	0.05	0.03	0.01	40.69	57.16	0.01	1.12					99.13	0.06
DT444WC3-STDEV-L	1180	-2.0	0.01	0.08	0.02	0.20	0.05	0.01	0.16	0.14	0.02	0.13						
DT444WC3-STDEV-Me(Ak)	1180	-2.0	0.01	0.09	0.02	0.25	0.00	0.01	0.10	0.04	0.01	0.08						
DT444WC3-STDEV-OLV	1180	-2.0	0.01	0.22	0.01	0.20	0.00	0.01	0.11	0.03	0.01	0.21						
DT444WC3-STDEV-PV	1180	-2.0	0.01	0.01	0.01	0.02	0.02	0.01	0.24	0.36	0.01	0.09						
DT451WC3-AVG-L	1130	-2.1	0.03	4.23	0.76	30.45	3.45	0.06	24.02	9.20	0.01	26.31					98.53	0.01
DT451WC3-AVG-Me(Ak)	1130	-2.1	0.02	9.35	0.10	42.04	0.00	0.03	38.87	0.20	0.01	8.72					99.34	0.37
DT451WC3-AVG-PV	1130	-2.1	0.01	0.05	0.04	0.13	0.05	0.01	40.37	56.65	0.00	1.30					98.43	0.08
DT451WC3-AVG-Px	1130	-2.1	0.01	13.72	0.16	51.09	0.00	0.01	24.05	2.66	0.02	8.26					99.98	0.31
DT451WC3-AVG-Ulv	1130	-2.1	0.02	5.11	0.49	0.25	0.03	0.01	0.88	28.48	0.01	62.58					97.86	0.22
DT451WC3-STDEV-L	1130	-2.1	0.02	0.41	0.03	0.62	0.47	0.03	0.63	0.35	0.02	0.91						
DT451WC3-STDEV-Me(Ak)	1130	-2.1	0.01	0.09	0.03	0.20	0.00	0.01	0.20	0.03	0.01	0.20						
DT451WC3-STDEV-PV	1130	-2.1	0.01	0.04	0.02	0.21	0.05	0.01	0.24	0.36	0.01	0.19						
DT451WC3-STDEV-Px	1130	-2.1	0.01	0.31	0.06	0.44	0.00	0.01	0.22	0.37	0.02	0.54						
DT451WC3-STDEV-Ulv	1130	-2.1	0.02	0.04	0.02	0.57	0.02	0.01	0.65	0.52	0.02	0.88						
DT460WC3-AVG-L	1130	-2.7	0.02	3.89	0.77	30.48	4.40	0.21	23.67	8.90	0.01	25.93					98.28	0.02
DT460WC3-AVG-Me(Ak)	1130	-2.7	0.03	9.12	0.21	41.97	0.00	0.06	38.81	0.20	0.01	8.79					99.22	0.32
DT460WC3-AVG-Mo(kct)	1130	-2.7	0.01	16.01	0.01	34.95	0.00	0.00	22.43	0.34	0.02	25.98					99.75	0.07
DT460WC3-AVG-PV	1130	-2.7	0.02	0.04	0.03	0.07	0.05	0.01	40.34	57.40	0.01	1.04					99.01	0.09
DT460WC3-AVG-Px	1130	-2.7	0.01	12.94	0.24	50.85	0.00	0.01	24.00	2.80	0.01	9.19					100.05	0.30
DT460WC3-AVG-Ulv	1130	-2.7	0.01	4.72	0.49	0.07	0.02	0.01	0.47	28.49	0.01	63.62					97.89	0.19
DT460WC3-STDEV-L	1130	-2.7	0.01	0.33	0.10	0.60	0.76	0.06	0.95	0.83	0.02	1.65						
DT460WC3-STDEV-Me(Ak)	1130	-2.7	0.02	0.11	0.06	0.34	0.00	0.02	0.23	0.03	0.01	0.17						
DT460WC3-STDEV-Mo(kct)	1130	-2.7	0.01	6.51	0.01	0.85	0.00	0.01	10.34	0.04	0.02	3.52						
DT460WC3-STDEV-PV	1130	-2.7	0.01	0.02	0.01	0.02	0.03	0.01	0.19	0.37	0.01	0.07						
DT460WC3-STDEV-Px	1130	-2.7	0.01	0.47	0.12	0.54	0.00	0.01	0.16	0.26	0.01	0.63						
DT460WC3-STDEV-Ulv	1130	-2.7	0.01	0.13	0.04	0.01	0.02	0.01	0.16	0.32	0.01	0.55						

Label	T(°C)	ΔNNO	Na2O	MgO	Al2O3	SiO2	P2O5	K2O	CaO	TiO2	MnO	FeO*	SrO	Nb2O5	La2O3	Ce2O3	Total	MB
DT463WC3-AVG-L	1130	-3.6	0.02	7.24	0.67	32.59	0.55	0.04	23.20	6.38	0.02	28.01					98.72	-0.56
DT463WC3-AVG-Me(Ak)	1130	-3.6	0.05	8.13	0.18	41.33	0.00	0.03	38.30	0.24	0.01	10.54					98.81	0.70
DT463WC3-AVG-PV	1130	-3.6	0.01	0.04	0.04	0.09	0.05	0.01	40.56	56.51	0.02	1.21					98.07	0.03
DT463WC3-AVG-Px	1130	-3.6	0.01	12.98	0.26	49.93	0.00	0.01	24.04	2.94	0.00	9.29					99.47	0.41
DT463WC3-AVG-Ulv	1130	-3.6	0.01	3.99	0.64	0.06	0.03	0.01	0.51	31.52	0.01	62.49					99.26	0.39
DT463WC3-STDEV-L	1130	-3.6	0.02	4.35	0.58	2.61	0.48	0.04	2.54	4.82	0.02	2.43						
DT463WC3-STDEV-Me(Ak)	1130	-3.6	0.02	0.20	0.04	0.72	0.00	0.01	0.84	0.11	0.01	0.09						
DT463WC3-STDEV-PV	1130	-3.6	0.01	0.02	0.02	0.08	0.01	0.01	0.11	0.52	0.01	0.15						
DT463WC3-STDEV-Px	1130	-3.6	0.01	0.40	0.16	0.61	0.00	0.01	0.22	0.43	0.01	0.66						
DT463WC3-STDEV-Ulv	1130	-3.6	0.01	0.05	0.02	0.02	0.03	0.01	0.09	0.20	0.01	0.13						
DT468WC3-AVG-L	1130	-4.8	0.03	3.65	1.18	30.59	0.57	0.04	21.22	11.05	0.00	29.37					97.71	0.14
DT468WC3-AVG-Mo(kct)	1130	-4.8	0.01	11.39	0.01	33.40	0.00	0.00	25.54	0.32	0.01	28.05					98.73	0.38
DT468WC3-AVG-PV	1130	-4.8	0.02	0.04	0.04	0.05	0.04	0.01	40.37	56.97	0.01	1.12					98.50	0.14
DT468WC3-AVG-Px	1130	-4.8	0.02	13.11	0.16	49.99	0.00	0.01	23.91	2.57	0.01	9.09					98.86	0.29
DT468WC3-AVG-Ulv	1130	-4.8	0.01	4.19	0.58	0.06	0.02	0.01	0.60	33.91	0.01	59.79					99.20	0.04
DT468WC3-STDEV-L	1130	-4.8	0.02	0.28	0.09	0.38	0.05	0.02	0.27	0.73	0.00	0.62						
DT468WC3-STDEV-Mo(kct)	1130	-4.8	0.01	0.40	0.01	0.21	0.00	0.00	0.41	0.04	0.01	0.46						
DT468WC3-STDEV-PV	1130	-4.8	0.02	0.02	0.02	0.01	0.04	0.01	0.29	0.37	0.01	0.05						
DT468WC3-STDEV-Px	1130	-4.8	0.01	0.44	0.09	0.38	0.00	0.01	0.18	0.16	0.02	0.70						
DT468WC3-STDEV-Ulv	1130	-4.8	0.01	0.03	0.02	0.03	0.03	0.01	0.47	0.37	0.02	0.64						
WC3glass-AVG			0.03	8.84	0.22	31.51	0.09	0.03	25.40	11.91	0.02	20.02					98.06	
WC3glass-STDEV			0.01	0.05	0.01	0.16	0.04	0.01	0.15	0.11	0.02	0.08						

Label	T(°C)	ΔNNO	Na2O	MgO	Al2O3	SiO2	P2O5	K2O	CaO	TiO2	MnO	FeO*	SrO	Nb2O5	La2O3	Ce2O3	Total	MB
DT460WC4-AVG-L	1130	-2.7	0.02	4.46	0.80	30.77	3.35	0.05	23.67	8.24	0.01	26.26	0.07	0.35	0.27	0.19	98.52	0.06
DT460WC4-AVG-Me(Ak)	1130	-2.7	0.04	9.64	0.20	40.92	0.00	0.02	36.35	0.22	0.01	12.41	0.06	0.00	0.03	0.01	99.92	0.32
DT460WC4-AVG-Mo(kct)	1130	-2.7	0.01	15.59	0.01	35.28	0.00	0.01	22.66	0.31	0.02	26.64	0.00	0.00	0.00	0.02	100.55	0.03
DT460WC4-AVG-PV	1130	-2.7	0.01	0.07	0.05	0.17	0.04	0.00	39.62	56.77	0.02	1.11	0.09	0.35	0.47	0.48	99.25	0.11
DT460WC4-AVG-Px	1130	-2.7	0.01	13.58	0.19	51.63	0.00	0.01	24.21	2.61	0.02	8.48	0.00	0.00	0.02	0.01	100.78	0.30
DT460WC4-AVG-Ulv	1130	-2.7	0.02	4.88	0.51	0.07	0.03	0.01	0.57	28.02	0.01	64.14	0.00	0.02	0.02	0.02	98.33	0.16
DT460WC4-STDEV-L	1130	-2.7	0.02	0.23	0.08	0.53	0.19	0.02	0.66	0.52	0.01	0.68	0.03	0.04	0.05	0.08		
DT460WC4-STDEV-Me(Ak)	1130	-2.7	0.02	1.39	0.11	3.28	0.00	0.02	4.94	0.08	0.01	7.24	0.03	0.00	0.02	0.01		
DT460WC4-STDEV-Mo(kct)	1130	-2.7	0.01	6.01	0.01	0.77	0.00	0.01	10.32	0.04	0.02	4.03	0.00	0.00	0.00	0.04		
DT460WC4-STDEV-PV	1130	-2.7	0.01	0.03	0.02	0.21	0.03	0.01	0.22	0.34	0.02	0.09	0.02	0.05	0.06	0.08		
DT460WC4-STDEV-Px	1130	-2.7	0.01	0.57	0.08	0.29	0.00	0.01	0.17	0.25	0.02	1.02	0.00	0.01	0.03	0.02		
DT460WC4-STDEV-Ulv	1130	-2.7	0.02	0.12	0.02	0.02	0.03	0.01	0.11	0.14	0.01	0.21	0.00	0.02	0.02	0.03		
DT463WC4-AVG-L	1130	-3.6	0.02	3.99	0.91	31.45	0.85	0.02	21.31	10.32	0.01	29.54	0.14	0.09	0.06	0.04	98.74	0.21
DT463WC4-AVG-Me(Ak)	1130	-3.6	0.04	8.50	0.08	42.01	0.00	0.02	38.19	0.27	0.00	10.32	0.23	0.00	0.01	0.03	99.70	-0.11
DT463WC4-AVG-Mo(kct)	1130	-3.6	0.02	11.73	0.02	35.17	0.00	0.01	27.08	0.32	0.01	25.64	0.00	0.00	0.02	0.02	100.04	0.47
DT463WC4-AVG-PV	1130	-3.6	0.01	0.04	0.06	0.04	0.06	0.01	39.62	56.25	0.01	1.37	0.17	0.38	0.43	0.46	98.90	0.16
DT463WC4-AVG-Px	1130	-3.6	0.02	13.20	0.18	51.58	0.00	0.00	24.14	2.63	0.02	8.97	0.00	0.01	0.02	0.02	100.79	0.26
DT463WC4-AVG-Ulv	1130	-3.6	0.02	4.31	0.49	0.08	0.02	0.01	0.67	31.10	0.01	61.58	0.00	0.00	0.01	0.01	98.31	0.00
DT463WC4-STDEV-L	1130	-3.6	0.01	0.22	0.04	0.15	0.06	0.01	0.28	0.22	0.01	0.48	0.02	0.01	0.04	0.03		
DT463WC4-STDEV-Me(Ak)	1130	-3.6	0.01	0.08	0.01	0.48	0.00	0.01	0.42	0.03	0.00	0.39	0.08	0.00	0.02	0.04		
DT463WC4-STDEV-Mo(kct)	1130	-3.6	0.01	1.05	0.02	1.86	0.00	0.01	3.59	0.06	0.01	5.16	0.00	0.00	0.03	0.02		
DT463WC4-STDEV-PV	1130	-3.6	0.01	0.01	0.02	0.03	0.05	0.01	0.25	0.41	0.02	0.13	0.06	0.06	0.05	0.08		
DT463WC4-STDEV-Px	1130	-3.6	0.01	0.54	0.10	0.38	0.00	0.01	0.29	0.28	0.02	0.65	0.00	0.01	0.02	0.02		
DT463WC4-STDEV-Ulv	1130	-3.6	0.01	0.07	0.03	0.02	0.03	0.01	0.18	0.32	0.01	0.45	0.00	0.00	0.02	0.02		

Label	T(°C)	ΔNNO	Na2O	MgO	Al2O3	SiO2	P2O5	K2O	CaO	TiO2	MnO	FeO*	SrO	Nb2O5	La2O3	Ce2O3	Total	MB
DT468WC4-AVG-L	1130	-4.8	0.02	4.19	1.05	31.51	1.03	0.01	21.30	10.19	0.01	28.85	0.17	0.10	0.08	0.04	98.54	0.21
DT468WC4-AVG-Me(Ak)	1130	-4.8	0.03	8.61	0.09	42.17	0.00	0.02	38.47	0.30	0.01	10.05	0.08	0.00	0.02	0.02	99.89	-0.06
DT468WC4-AVG-Mo(kct)	1130	-4.8	0.01	11.83	0.01	34.32	0.00	0.01	25.59	0.36	0.01	27.90	0.00	0.00	0.03	0.01	100.07	0.42
DT468WC4-AVG-PV	1130	-4.8	0.02	0.05	0.07	0.03	0.04	0.01	39.69	56.39	0.01	1.13	0.17	0.42	0.38	0.41	98.82	0.16
DT468WC4-AVG-Px	1130	-4.8	0.02	13.45	0.14	51.56	0.00	0.01	24.08	2.70	0.00	8.61	0.00	0.01	0.01	0.02	100.62	0.26
DT468WC4-STDEV-L	1130	-4.8	0.01	0.18	0.04	0.16	0.06	0.01	0.25	0.21	0.01	0.32	0.01	0.02	0.04	0.04		
DT468WC4-STDEV-Me(Ak)	1130	-4.8	0.01	0.09	0.02	0.22	0.00	0.01	0.14	0.13	0.01	0.17	0.07	0.00	0.02	0.03		
DT468WC4-STDEV-Mo(kct)	1130	-4.8	0.01	0.46	0.02	0.14	0.00	0.01	0.36	0.16	0.01	0.38	0.00	0.00	0.05	0.01		
DT468WC4-STDEV-PV	1130	-4.8	0.01	0.01	0.04	0.02	0.02	0.01	0.21	0.35	0.02	0.16	0.09	0.06	0.05	0.06		
DT468WC4-STDEV-Px	1130	-4.8	0.01	0.55	0.04	0.38	0.00	0.01	0.22	0.26	0.01	0.79	0.00	0.01	0.02	0.03		
WC4glass-AVG			0.02	8.78	0.21	31.67	0.19	0.04	25.37	11.98	0.01	19.57	0.00	0.08	0.08	0.08	98.07	
WC4glass-STDEV			0.02	0.08	0.01	0.07	0.04	0.01	0.18	0.11	0.02	0.14	0.00	0.02	0.05	0.04		
DT336WD2-AVG-L	1248	0.0	0.06	11.27	9.34	32.69	0.11	0.57	25.00	8.34	0.32	10.39					98.10	0.76
DT336WD2-AVG-OLV	1248	0.0	0.01	50.94	0.19	41.43		0.01	2.71	0.20	0.30	5.02					100.81	0.17
DT336WD2-AVG-Sp	1248	0.0	0.01	22.97	46.31	4.93		0.07	2.95	3.73	0.21	17.41					98.59	0.00
DT336WD2-STDEV-L	1248	0.0	0.01	0.15	0.10	0.13	0.04	0.02	0.23	0.06	0.03	0.19						
DT336WD2-STDEV-OLV	1248	0.0	0.01	1.17	0.08	0.40		0.01	0.19	0.03	0.04	1.32						
DT336WD2-STDEV-Sp	1248	0.0	0.01	2.53	7.20	5.93		0.08	3.37	0.78	0.04	1.88						
DT339WD2-AVG-L	1253	-0.7	0.06	10.80	0.69	40.06	0.20	0.13	25.94	4.82	0.01	15.00					97.70	0.39
DT339WD2-AVG-Me	1253	-0.7	0.06	12.67	0.13	42.91		0.03	39.76	0.08	0.01	3.40					99.05	0.17
DT339WD2-AVG-Mo	1253	-0.7	0.03	17.30	0.11	53.43		0.01	24.57	1.03	0.01	3.01					99.50	0.00
DT339WD2-AVG-OLV	1253	-0.7	0.01	45.32	0.01	39.94		0.00	2.40	0.06	0.00	11.86					99.61	0.19
DT339WD2-STDEV-L	1253	-0.7	0.02	0.71	0.04	0.48	0.07	0.03	0.78	0.29	0.01	0.44						
DT339WD2-STDEV-Me	1253	-0.7	0.02	0.08	0.03	0.15		0.02	0.22	0.03	0.01	0.06						
DT339WD2-STDEV-Mo	1253	-0.7	0.01	0.14	0.01	0.16		0.01	0.28	0.09	0.01	0.13						
DT339WD2-STDEV-OLV	1253	-0.7	0.01	0.17	0.01	0.16		0.01	0.11	0.02	0.01	0.20						

Label	T(°C)	ΔNNO	Na2O	MgO	Al2O3	SiO2	P2O5	K2O	CaO	TiO2	MnO	FeO*	SrO	Nb2O5	La2O3	Ce2O3	Total	MB
DT342WD2-AVG-L	1252	-0.7	0.04	11.34	9.68	32.27	0.09	0.06	25.38	8.32	0.30	10.20					97.67	0.76
DT342WD2-AVG-OLV	1252	-0.7	0.01	49.71	0.13	40.71		0.00	2.48	0.18	0.29	6.60					100.11	0.18
DT342WD2-STDEV-L	1252	-0.7	0.00	0.27	0.12	0.33	0.05	0.02	0.33	0.06	0.04	0.12						
DT342WD2-STDEV-OLV	1252	-0.7	0.01	0.54	0.02	0.27		0.00	0.13	0.03	0.02	0.40						
DT343WD2-AVG-OLV	1253	-0.7	0.01	49.73	0.13	40.61		0.02	2.49	0.18	0.28	6.66					100.10	1.00
DT343WD2-STDEV-OLV	1253	-0.7	0.01	0.15	0.03	0.12		0.01	0.08	0.02	0.04	0.22						
DT346WD2-AVG-L	1248	-2.2	0.03	10.32	10.00	32.34	0.07	0.14	26.02	8.57	0.32	10.61					98.41	0.74
DT346WD2-AVG-OLV	1248	-2.2	0.01	50.11	0.16	41.04		0.01	2.77	0.19	0.28	5.80					100.37	0.20
DT346WD2-AVG-Sp	1248	-2.2	0.03	17.41	38.93	16.33		0.08	12.50	5.14	0.23	9.96					100.59	-0.01
DT346WD2-STDEV-L	1248	-2.2	0.01	0.97	0.29	0.15	0.03	0.01	0.43	0.26	0.02	0.11						
DT346WD2-STDEV-OLV	1248	-2.2	0.00	1.19	0.07	0.26		0.01	0.32	0.06	0.03	1.19						
DT346WD2-STDEV-Sp	1248	-2.2	0.02	4.30	11.93	7.51		0.03	6.24	1.77	0.04	0.22						
DT350WD2-AVG-L	1256	-4.0	0.03	10.48	10.30	32.96	0.11	0.02	26.59	8.77	0.32	8.77					98.36	0.71
DT350WD2-AVG-OLV	1256	-4.0	0.01	48.87	0.13	40.30		0.01	2.72	0.19	0.30	7.37					99.89	0.20
DT350WD2-STDEV-L	1256	-4.0	0.01	1.35	0.42	0.17	0.04	0.02	0.62	0.35	0.05	0.12						
DT350WD2-STDEV-OLV	1256	-4.0	0.01	0.51	0.01	0.22		0.01	0.18	0.02	0.02	0.61						
DT353WD2-AVG-Sp	1252	-1.5	0.00	23.72	57.54	1.44		0.01	1.10	2.69	0.18	12.47					99.16	1.00
DT353WD2-STDEV-Sp	1252	-1.5	0.00	0.41	2.18	0.92		0.03	0.67	0.54	0.02	1.72						
DT376WD2-AVG-L	1180	-2.3	0.08	7.94	11.18	34.44	0.15	1.24	24.26	7.28	0.36	11.53					98.47	0.53
DT376WD2-AVG-Mo	1180	-2.3	0.12	10.98	4.25	41.06		0.44	39.38	0.17	0.09	3.07					99.55	0.10
DT376WD2-AVG-OLV	1180	-2.3	0.01	44.25	0.11	39.59		0.01	2.87	0.22	0.47	12.61					100.14	0.26
DT376WD2-AVG-PV	1180	-2.3	0.02	0.10	0.54	0.30	0.04	0.04	40.59	57.29	0.04	0.94					99.90	0.04
DT376WD2-STDEV-L	1180	-2.3	0.01	0.26	0.08	0.28	0.03	0.04	0.18	0.07	0.04	0.14						
DT376WD2-STDEV-Mo	1180	-2.3	0.02	0.10	0.19	0.28		0.04	0.25	0.03	0.03	0.07						
DT376WD2-STDEV-OLV	1180	-2.3	0.01	0.52	0.07	0.23		0.01	0.14	0.08	0.02	0.41						
DT376WD2-STDEV-PV	1180	-2.3	0.02	0.09	0.13	0.47	0.02	0.02	0.22	0.67	0.03	0.12						

Label	T(°C)	ΔNNO	Na2O	MgO	Al2O3	SiO2	P2O5	K2O	CaO	TiO2	MnO	FeO*	SrO	Nb2O5	La2O3	Ce2O3	Total	MB
DT387WD2-AVG-L	1180	-2.0	0.06	8.15	10.83	33.93	0.13	1.01	24.44	7.41	0.36	11.58					97.89	0.57
DT387WD2-AVG-Mo	1180	-2.0	0.13	11.03	4.16	40.86		0.36	39.54	0.43	0.10	2.96					99.55	0.08
DT387WD2-AVG-OLV	1180	-2.0	0.02	45.66	0.21	39.87		0.01	3.07	0.31	0.43	10.63					100.19	0.25
DT387WD2-AVG-PV	1180	-2.0	0.01	0.24	0.70	0.92	0.03	0.06	40.18	56.34	0.05	1.11					99.64	0.03
DT387WD2-STDEV-L	1180	-2.0	0.01	0.40	0.10	0.70	0.05	0.09	0.37	0.15	0.04	0.34						
DT387WD2-STDEV-Mo	1180	-2.0	0.02	0.15	0.23	0.52		0.04	0.15	0.46	0.02	0.13						
DT387WD2-STDEV-OLV	1180	-2.0	0.03	1.79	0.17	0.26		0.01	0.38	0.13	0.06	2.45						
DT387WD2-STDEV-PV	1180	-2.0	0.01	0.28	0.39	1.33	0.03	0.04	0.62	1.81	0.03	0.35						
WD2glass-AVG			0.12	17.75	7.57	32.74	0.08	2.69	19.95	6.57	0.32	10.18					97.96	
WD2glass-STDEV			0.02	0.10	0.05	0.12	0.04	0.04	0.17	0.06	0.03	0.12						
DT451WD3-AVG-L	1130	-2.1	0.06	4.61	8.79	32.47	0.77	0.47	23.79	6.62	0.76	19.63					97.96	0.33
DT451WD3-AVG-Me(geh)	1130	-2.1	0.02	11.63	19.44	20.86	0.03	0.01	13.89	12.88	0.34	20.01					99.12	0.06
DT451WD3-AVG-Me(mel)	1130	-2.1	0.18	8.51	4.33	40.54	0.00	0.31	38.51	0.15	0.23	6.65					99.40	0.09
DT451WD3-AVG-PV	1130	-2.1	0.01	0.03	0.44	0.12	0.02	0.02	40.39	55.96	0.06	1.21					98.26	0.01
DT451WD3-AVG-Px	1130	-2.1	0.01	9.77	13.48	38.51	0.00	0.01	24.16	6.97	0.15	6.13					99.18	0.48
DT451WD3-STDEV-L	1130	-2.1	0.02	0.05	0.09	0.28	0.04	0.05	0.18	0.07	0.04	0.26						
DT451WD3-STDEV-Me(geh)	1130	-2.1	0.02	0.92	0.42	0.32	0.04	0.01	0.18	0.25	0.05	1.76						
DT451WD3-STDEV-Me(mel)	1130	-2.1	0.02	0.15	0.32	0.25	0.00	0.03	0.23	0.02	0.03	0.11						
DT451WD3-STDEV-PV	1130	-2.1	0.01	0.01	0.03	0.07	0.03	0.02	0.05	0.55	0.03	0.49						
DT451WD3-STDEV-Px	1130	-2.1	0.01	0.78	1.39	1.62	0.00	0.01	0.16	0.75	0.04	0.76						

Label	T(°C)	ΔNNO	Na2O	MgO	Al2O3	SiO2	P2O5	K2O	CaO	TiO2	MnO	FeO*	SrO	Nb2O5	La2O3	Ce2O3	Total	MB
DT460WD3-AVG-L	1130	-2.7	0.07	4.43	8.99	32.75	0.65	0.65	23.51	6.61	0.66	19.86					98.17	0.34
DT460WD3-AVG-Me(geh)	1130	-2.7	0.03	11.36	18.42	21.00	0.02	0.01	13.76	13.41	0.31	21.12					99.42	0.05
DT460WD3-AVG-Me(mel)	1130	-2.7	0.20	8.36	5.29	39.25	0.00	0.40	35.93	1.43	0.26	7.80					98.91	0.13
DT460WD3-AVG-PV	1130	-2.7	0.02	0.04	0.51	0.06	0.04	0.01	40.68	56.73	0.04	0.67					98.78	0.02
DT460WD3-AVG-Px	1130	-2.7	0.01	10.20	12.37	39.64	0.00	0.01	24.19	7.33	0.15	5.56					99.46	0.43
DT460WD3-AVG-Ulv	1130	-2.7	0.01	21.53	65.27	0.09	0.02	0.01	0.25	1.12	0.20	11.21					99.69	0.01
DT460WD3-STDEV-L	1130	-2.7	0.01	0.07	0.08	0.24	0.06	0.04	0.14	0.10	0.04	0.26						
DT460WD3-STDEV-Me(geh)	1130	-2.7	0.01	0.25	0.43	0.36	0.01	0.00	0.15	0.15	0.04	0.47						
DT460WD3-STDEV-Me(mel)	1130	-2.7	0.08	2.20	2.03	3.34	0.00	0.15	6.37	2.74	0.20	6.18						
DT460WD3-STDEV-PV	1130	-2.7	0.02	0.01	0.08	0.02	0.04	0.01	0.24	0.32	0.02	0.22						
DT460WD3-STDEV-Px	1130	-2.7	0.01	0.99	2.22	2.89	0.00	0.01	0.16	2.04	0.04	1.12						
DT460WD3-STDEV-Ulv	1130	-2.7	0.01	0.57	0.58	0.01	0.02	0.01	0.07	0.15	0.05	0.52						
DT463WD3-AVG-L	1130	-3.6	0.07	4.59	9.01	31.48	0.65	0.64	23.11	6.44	0.68	20.08					96.74	0.39
DT463WD3-AVG-Me(mel)	1130	-3.6	0.17	8.60	4.11	39.18	0.00	0.29	38.28	0.13	0.20	6.28					97.24	0.02
DT463WD3-AVG-PV	1130	-3.6	0.02	0.03	0.42	0.05	0.05	0.01	40.70	56.41	0.05	0.76					98.23	0.02
DT463WD3-AVG-Px	1130	-3.6	0.02	10.21	11.73	39.62	0.00	0.01	23.96	6.25	0.15	5.84					97.78	0.53
DT463WD3-STDEV-L	1130	-3.6	0.02	0.06	0.06	0.24	0.05	0.05	0.19	0.08	0.05	0.15						
DT463WD3-STDEV-Me(mel)	1130	-3.6	0.02	0.17	0.38	0.53	0.00	0.03	0.21	0.02	0.02	0.30						
DT463WD3-STDEV-PV	1130	-3.6	0.02	0.01	0.03	0.03	0.03	0.01	0.31	0.22	0.03	0.09						
DT463WD3-STDEV-Px	1130	-3.6	0.01	0.87	1.95	2.34	0.00	0.01	0.18	1.21	0.04	0.63						
DT468WD3-AVG-L	1130	-4.8	0.04	4.85	9.51	31.91	0.70	0.18	23.91	6.54	0.66	19.61					97.90	0.43
DT468WD3-AVG-Me(mel)	1130	-4.8	0.17	9.32	4.87	39.77	0.00	0.24	39.11	0.13	0.13	4.89					98.62	0.05
DT468WD3-AVG-PV	1130	-4.8	0.02	0.05	0.56	0.06	0.03	0.02	40.85	56.67	0.02	0.54					98.69	0.03
DT468WD3-AVG-Px	1130	-4.8	0.02	10.73	11.22	40.70	0.00	0.01	24.09	5.90	0.15	5.25					98.07	0.45
DT468WD3-AVG-Ulv	1130	-4.8	0.01	21.26	65.44	0.29	0.03	0.01	0.44	1.01	0.21	10.97					99.66	0.02
DT468WD3-STDEV-L	1130	-4.8	0.02	0.10	0.25	0.22	0.25	0.21	0.29	0.12	0.04	0.61						
DT468WD3-STDEV-Me(mel)	1130	-4.8	0.05	0.43	0.40	0.55	0.00	0.06	0.19	0.02	0.03	0.80						
DT468WD3-STDEV-PV	1130	-4.8	0.01	0.01	0.06	0.02	0.03	0.01	0.15	0.35	0.02	0.13						
DT468WD3-STDEV-Px	1130	-4.8	0.02	0.65	0.63	0.85	0.00	0.01	0.19	0.25	0.02	0.64						
DT468WD3-STDEV-Ulv	1130	-4.8	0.01	0.71	1.16	0.46	0.03	0.01	0.32	0.11	0.03	0.69						

Label	T(°C)	ΔNNO	Na2O	MgO	Al2O3	SiO2	P2O5	K2O	CaO	TiO2	MnO	FeO*	SrO	Nb2O5	La2O3	Ce2O3	Total	MB
WD3glass-AVG			0.12	7.98	11.03	34.26	0.26	0.88	24.35	7.26	0.30	11.46					97.91	
WD3glass-STDEV			0.02	0.08	0.11	0.20	0.05	0.04	0.11	0.09	0.04	0.12						
DT312JC-AVG-L	1275	-2.1	0.01	13.64	0.66	41.98	0.21	0.01	25.91	4.57	0.00	12.24					99.23	0.61
DT312JC-AVG-Me(Ak)	1248	-2.1	0.01	12.84	0.13	43.45		0.01	39.80	0.07	0.00	3.06					99.37	0.13
DT312JC-AVG-Mo	1248	-2.1	0.01	17.77	0.06	54.21		0.01	24.80	0.86	0.01	2.52					100.24	0.26
DT312JC-AVG-OLV	1248	-2.1	0.01	46.35	0.01	40.69		0.00	2.45	0.06	0.01	11.06					100.65	0.19
DT312JC-STDEV-L	1248	-2.1	0.01	2.46	0.04	0.16	0.05	0.01	1.53	0.24	0.00	0.15						
DT312JC-STDEV-Me(Ak)	1248	-2.1	0.01	0.01	0.03	0.07		0.01	0.30	0.02	0.00	0.05						
DT312JC-STDEV-Mo	1248	-2.1	0.01	0.05	0.01	0.24		0.01	0.13	0.05	0.01	0.08						
DT312JC-STDEV-OLV	1248	-2.1	0.01	0.30	0.01	0.05		0.01	0.17	0.04	0.01	0.20						
DT313JC-AVG-L	1296	-1.9	0.01	13.90	0.56	43.82	0.15	0.01	26.65	3.79	0.02	10.18					99.10	0.83
DT313JC-AVG-Me(Ak)	1252	-1.9	0.01	13.10	0.12	43.50		0.01	40.11	0.06	0.01	2.46					99.38	0.10
DT313JC-AVG-Mo	1252	-1.9	0.01	18.06	0.05	54.42		0.01	24.59	0.91	0.01	2.09					100.16	0.24
DT313JC-AVG-OLV	1253	-1.9	0.01	48.55	0.01	40.91		0.01	2.26	0.03	0.02	8.72					100.51	0.17
DT313JC-STDEV-L	1252	-1.9	0.01	0.09	0.01	0.26	0.05	0.01	0.53	0.07	0.02	0.32						
DT313JC-STDEV-Me(Ak)	1252	-1.9	0.01	0.03	0.02	0.11		0.01	0.19	0.03	0.01	0.09						
DT313JC-STDEV-Mo	1252	-1.9	0.01	0.25	0.02	0.25		0.01	0.13	0.12	0.01	0.10						
DT313JC-STDEV-OLV	1253	-1.9	0.01	0.28	0.01	0.17		0.01	0.14	0.02	0.02	0.21						
DT316JC-AVG-L	1276	-0.9	0.03	11.61	0.77	40.46	0.26	0.01	27.01	5.22	0.00	13.08					98.45	0.53
DT316JC-AVG-Me(Ak)	1185	-0.9	0.03	12.70	0.14	42.96		0.00	39.30	0.07	0.01	3.08					98.30	0.23
DT316JC-AVG-Mo	1185	-0.9	0.01	18.74	0.12	51.83		0.01	24.72	1.01	0.01	3.44					99.90	0.40
DT316JC-AVG-OLV	1253	-0.9	0.01	46.26	0.01	40.48		0.01	2.36	0.05	0.00	11.27					100.46	0.29
DT316JC-STDEV-L	1248	-0.9	0.01	0.64	0.03	0.45	0.04	0.01	0.61	0.14	0.00	0.56						
DT316JC-STDEV-Me(Ak)	1185	-0.9	0.01	0.28	0.04	0.34		0.01	0.38	0.02	0.01	0.10						
DT316JC-STDEV-Mo	1185	-0.9	0.01	3.33	0.03	4.64		0.01	0.53	0.43	0.01	1.20						
DT316JC-STDEV-OLV	1253	-0.9	0.01	0.15	0.01	0.35		0.01	0.04	0.03	0.01	0.16						

Label	T(°C)	ΔNNO	Na2O	MgO	Al2O3	SiO2	P2O5	K2O	CaO	TiO2	MnO	FeO*	SrO	Nb2O5	La2O3	Ce2O3	Total	MB
DT317JC-AVG-L	1276	-0.2	0.01	12.91	0.58	41.81	0.16	0.01	26.27	3.97	0.01	12.77					98.51	0.63
DT317JC-AVG-Mo	1296	-0.2	0.01	17.66	0.07	54.16		0.00	24.59	0.89	0.01	2.55					99.95	0.04
DT317JC-AVG-OLV	1296	-0.2	0.01	45.87	0.06	40.23		0.01	3.98	0.35	0.01	10.00					100.52	0.15
DT317JC-STDEV-L	1296	-0.2	0.01	0.12	0.01	0.22	0.03	0.01	0.06	0.04	0.01	0.14						
DT317JC-STDEV-Mo	1296	-0.2	0.01	0.26	0.02	0.46		0.00	0.26	0.08	0.01	0.05						
DT317JC-STDEV-OLV	1296	-0.2	0.01	5.26	0.11	0.14		0.01	3.83	0.69	0.02	0.55						
DT323JC-AVG-L	1229	-2.0	0.02	9.56	1.12	38.07	0.34	0.01	23.38	7.75	0.02	18.23					98.50	0.28
DT323JC-AVG-Me(Ak)	1253	-2.0	0.03	12.14	0.21	42.74		0.01	39.38	0.13	0.01	4.21					98.84	0.11
DT323JC-AVG-Mo	1253	-2.0	0.00	16.67	0.21	52.11		0.02	24.45	1.88	0.02	4.08					99.43	0.25
DT323JC-STDEV-L	1253	-2.0	0.01	0.61	0.04	0.51	0.07	0.01	1.16	0.44	0.02	1.24						
DT323JC-STDEV-Me(Ak)	1253	-2.0	0.01	0.21	0.11	0.25		0.01	0.52	0.05	0.01	0.18						
DT323JC-STDEV-Mo	1253	-2.0	0.00	0.02	0.07	0.09		0.02	0.06	0.20	0.03	0.16						
DT328JC-AVG-L	1305	-0.3	0.01	15.17	0.37	44.87	0.11	0.02	26.34	2.54	0.02	9.41					98.86	0.87
DT328JC-AVG-OLV	1276	-0.3	0.01	50.61	0.00	41.09		0.01	1.84	0.02	0.01	7.03					100.62	0.16
DT328JC-STDEV-L	1276	-0.3	0.01	0.62	0.01	0.14	0.05	0.01	0.45	0.06	0.02	0.11						
DT328JC-STDEV-OLV	1276	-0.3	0.01	0.23	0.00	0.17		0.01	0.09	0.01	0.01	0.13						
DT330JC-AVG-L	1185	-0.4	0.04	7.90	1.37	32.03	0.80	0.05	23.26	12.14	0.01	21.44					99.03	0.15
DT330JC-AVG-Me(Ak)	1296	-0.4	0.04	11.88	0.15	42.78		0.01	39.40	0.13	0.00	4.72					99.12	-0.01
DT330JC-AVG-Mo	1276	-0.4	0.01	16.38	0.29	52.08		0.01	24.66	2.19	0.00	4.39					100.03	0.28
DT330JC-AVG-OLV	1276	-0.4	0.01	41.25	0.01	39.06		0.01	2.56	0.10	0.00	17.02					100.02	0.15
DT330JC-STDEV-L	1276	-0.4	0.03	5.80	0.31	1.19	0.13	0.02	2.73	2.40	0.01	0.64						
DT330JC-STDEV-Me(Ak)	1296	-0.4	0.02	0.11	0.02	0.10		0.01	0.28	0.05	0.00	0.18						
DT330JC-STDEV-Mo	1276	-0.4	0.01	0.18	0.01	0.15		0.01	0.12	0.07	0.00	0.14						
DT330JC-STDEV-OLV	1276	-0.4	0.02	0.13	0.01	0.10		0.01	0.14	0.02	0.00	0.27						

Label	T(°C)	ΔNNO	Na2O	MgO	Al2O3	SiO2	P2O5	K2O	CaO	TiO2	MnO	FeO*	SrO	Nb2O5	La2O3	Ce2O3	Total	MB
DT336JC-AVG-L	1248	0.0	0.03	10.01	0.71	39.25	0.21	0.17	26.09	5.16	0.00	16.68					98.32	0.38
DT336JC-AVG-Me(Ak)	1275	0.0	0.02	12.97	0.11	43.01		0.04	39.21	0.12	0.01	3.72					99.20	0.06
DT336JC-AVG-Mo	1275	0.0	0.00	17.37	0.12	53.66		0.00	24.72	1.05	0.01	3.19					100.12	0.18
DT336JC-AVG-OLV	1275	0.0	0.00	45.54	0.01	40.19		0.01	2.32	0.06	0.01	12.19					100.34	0.15
DT336JC-STDEV-L	1275	0.0	0.01	1.13	0.05	0.53	0.03	0.01	0.74	0.30	0.01	0.29						
DT336JC-STDEV-Me(Ak)	1275	0.0	0.01	0.08	0.02	0.16		0.01	0.41	0.12	0.02	0.32						
DT336JC-STDEV-Mo	1275	0.0	0.00	0.12	0.01	0.24		0.00	0.10	0.01	0.03	0.13						
DT336JC-STDEV-OLV	1275	0.0	0.01	0.22	0.01	0.13		0.01	0.02	0.02	0.02	0.09						
DT339JC-AVG-L	1253	-0.7	0.03	11.57	9.63	32.54	0.06	0.23	25.29	8.34	0.32	10.36					98.38	0.99
DT339JC-AVG-OLV	1305	-0.7	0.00	50.12	0.13	41.29		0.00	2.70	0.17	0.29	6.14					100.85	0.12
DT339JC-AVG-Sp	1248	-0.7	0.01	22.09	48.28	6.35		0.05	4.53	4.02	0.20	14.26					99.78	-0.18
DT339JC-STDEV-L	1305	-0.7	0.02	0.18	0.10	0.25	0.04	0.01	0.17	0.09	0.03	0.30						
DT339JC-STDEV-OLV	1305	-0.7	0.00	0.72	0.03	0.26		0.00	0.11	0.02	0.04	0.70						
DT339JC-STDEV-Sp	1248	-0.7	0.01	1.99	7.08	6.19		0.04	4.21	0.85	0.03	1.96						
DT342JC-AVG-L	1252	-0.7	0.02	11.61	0.64	41.15	0.17	0.06	26.13	4.52	0.01	14.27					98.59	0.48
DT342JC-AVG-Me(Ak)	1229	-0.7	0.02	12.81	0.12	43.15		0.03	39.81	0.07	0.01	3.32					99.34	-0.03
DT342JC-AVG-Mo	1229	-0.7	0.01	17.47	0.11	53.81		0.00	24.75	0.93	0.01	2.89					99.98	0.68
DT342JC-AVG-OLV	1248	-0.7	0.00	46.01	0.00	40.32		0.00	2.48	0.05	0.00	11.56					100.43	0.18
DT342JC-STDEV-L	1185	-0.7	0.01	0.21	0.02	0.32	0.06	0.01	0.29	0.05	0.02	0.22						
DT342JC-STDEV-Me(Ak)	1229	-0.7	0.01	0.08	0.04	0.19		0.01	0.22	0.03	0.01	0.08						
DT342JC-STDEV-Mo	1229	-0.7	0.01	0.08	0.03	0.21		0.00	0.13	0.10	0.01	0.24						
DT342JC-STDEV-OLV	1248	-0.7	0.00	0.42	0.01	0.25		0.01	0.30	0.02	0.01	0.20						
DT343JC-AVG-L	1253	-0.7	0.01	11.71	0.73	40.46	0.13	0.01	25.67	5.01	0.01	14.48					98.21	0.47
DT343JC-AVG-Me(Ak)	1276	-0.7	0.01	12.77	0.12	43.15		0.01	39.86	0.09	0.01	3.28					99.30	0.03
DT343JC-AVG-Mo	1276	-0.7	0.00	17.34	0.10	53.79		0.00	24.74	1.07	0.00	2.98					100.02	0.22
DT343JC-AVG-OLV	1185	-0.7	0.00	46.01	0.01	40.21		0.00	2.35	0.05	0.00	11.76					100.39	0.21
DT343JC-STDEV-L	1229	-0.7	0.01	0.21	0.03	0.34	0.05	0.01	0.67	0.15	0.02	0.61						
DT343JC-STDEV-Me(Ak)	1276	-0.7	0.01	0.07	0.03	0.16		0.01	0.19	0.03	0.01	0.07						
DT343JC-STDEV-Mo	1276	-0.7	0.00	0.13	0.02	0.27		0.01	0.09	0.08	0.00	0.07						
DT343JC-STDEV-OLV	1185	-0.7	0.01	0.11	0.01	0.10		0.00	0.05	0.03	0.01	0.07						

Label	T(°C)	ΔNNO	Na2O	MgO	Al2O3	SiO2	P2O5	K2O	CaO	TiO2	MnO	FeO*	SrO	Nb2O5	La2O3	Ce2O3	Total	MB
DT346JC-AVG-L	1248	-2.2	0.04	10.72	0.70	40.70	0.23	0.09	26.30	4.80	0.01	14.89					98.47	0.42
DT346JC-AVG-Me(Ak)	1253	-2.2	0.03	12.68	0.10	43.29		0.02	39.42	0.08	0.01	3.66					99.30	0.13
DT346JC-AVG-Mo	1253	-2.2	0.01	17.32	0.08	53.72		0.00	24.71	1.03	0.01	3.16					100.05	0.24
DT346JC-AVG-OLV	1253	-2.2	0.01	44.91	0.01	39.95		0.01	2.36	0.07	0.00	12.84					100.14	0.19
DT346JC-STDEV-L	1253	-2.2	0.01	0.78	0.03	0.81	0.03	0.02	0.71	0.17	0.02	0.98						
DT346JC-STDEV-Me(Ak)	1253	-2.2	0.02	0.24	0.02	0.34		0.01	0.59	0.05	0.01	0.11						
DT346JC-STDEV-Mo	1253	-2.2	0.01	0.19	0.02	0.24		0.01	0.08	0.04	0.01	0.19						
DT346JC-STDEV-OLV	1253	-2.2	0.01	0.32	0.01	0.23		0.01	0.08	0.02	0.00	0.14						
DT347JC-AVG-L	1253	-3.4	0.04	10.66	0.73	40.88	0.19	0.11	26.11	5.06	0.01	14.45					98.23	0.43
DT347JC-AVG-Me(Ak)	1256	-3.4	0.02	12.48	0.11	42.99		0.02	39.56	0.07	0.01	3.79					99.04	0.12
DT347JC-AVG-Mo	1256	-3.4	0.00	17.44	0.10	53.77		0.00	24.53	1.04	0.00	3.24					100.13	0.25
DT347JC-AVG-OLV	1256	-3.4	0.01	45.25	0.01	40.14		0.00	2.22	0.06	0.01	12.68					100.38	0.14
DT347JC-STDEV-L	1256	-3.4	0.02	1.12	0.03	0.45	0.04	0.01	0.37	0.22	0.02	0.56						
DT347JC-STDEV-Me(Ak)	1256	-3.4	0.01	0.07	0.04	0.14		0.02	0.22	0.02	0.01	0.06						
DT347JC-STDEV-Mo	1256	-3.4	0.00	0.31	0.04	0.69		0.00	0.29	0.07	0.00	0.58						
DT347JC-STDEV-OLV	1256	-3.4	0.01	1.01	0.01	0.32		0.00	0.20	0.02	0.01	0.99						
DT350JC-AVG-L	1256	-4.0	0.02	14.41	0.69	40.73	0.21	0.03	24.04	4.54	0.01	14.23					98.90	0.48
DT350JC-AVG-Me(Ak)	1252	-4.0	0.02	12.53	0.10	43.20		0.00	39.55	0.11	0.01	3.66					99.18	0.13
DT350JC-AVG-Mo	1252	-4.0	0.00	17.36	0.08	53.88		0.00	24.64	1.10	0.03	3.05					100.13	0.27
DT350JC-AVG-OLV	1252	-4.0	0.00	44.13	0.02	40.21		0.00	2.70	0.14	0.01	12.93					100.14	0.18
DT350JC-STDEV-L	1252	-4.0	0.01	10.64	0.24	0.78	0.08	0.02	7.62	1.59	0.02	0.85						
DT350JC-STDEV-Me(Ak)	1252	-4.0	0.01	0.06	0.03	0.13		0.01	0.22	0.10	0.01	0.15						
DT350JC-STDEV-Mo	1252	-4.0	0.00	0.06	0.04	0.23		0.01	0.24	0.10	0.02	0.18						
DT350JC-STDEV-OLV	1252	-4.0	0.00	0.80	0.02	0.17		0.00	0.44	0.13	0.01	0.19						

Label	T(°C)	ΔNNO	Na2O	MgO	Al2O3	SiO2	P2O5	K2O	CaO	TiO2	MnO	FeO*	SrO	Nb2O5	La2O3	Ce2O3	Total	MB
DT351JC-AVG-L	1256	-3.6	0.01	11.75	0.74	41.10	0.20	0.03	25.90	4.99	0.01	13.81					98.54	0.46
DT351JC-AVG-Me(Ak)	1256	-3.6	0.02	12.61	0.10	43.04		0.01	39.47	0.12	0.01	3.76					99.15	0.12
DT351JC-AVG-Mo	1256	-3.6	0.00	17.40	0.10	53.65		0.00	24.61	1.10	0.00	3.30					100.16	0.12
DT351JC-AVG-OLV	1256	-3.6	0.00	33.90	0.03	45.30		0.00	11.33	0.49	0.01	9.08					100.14	0.30
DT351JC-STDEV-L	1256	-3.6	0.01	0.14	0.03	0.42	0.06	0.01	0.15	0.08	0.02	0.27						
DT351JC-STDEV-Me(Ak)	1256	-3.6	0.01	0.17	0.02	0.17		0.01	0.30	0.09	0.02	0.15						
DT351JC-STDEV-Mo	1256	-3.6	0.01	0.27	0.04	0.12		0.00	0.25	0.07	0.00	0.26						
DT351JC-STDEV-OLV	1256	-3.6	0.00	14.85	0.04	7.64		0.00	12.15	0.62	0.01	5.53						
DT353JC-AVG-L	1252	-1.5	0.04	11.34	0.72	40.42	0.21	0.09	25.62	4.99	0.01	14.92					98.36	0.42
DT353JC-AVG-Me(Ak)	1248	-1.5	0.04	12.56	0.15	43.03		0.03	39.61	0.08	0.00	3.64					99.13	0.13
DT353JC-AVG-Mo	1248	-1.5	0.00	17.37	0.11	53.30		0.00	24.68	1.12	0.01	3.31					99.90	0.30
DT353JC-AVG-OLV	1252	-1.5	0.00	45.10	0.01	40.03		0.00	2.36	0.07	0.00	12.94					100.52	0.17
DT353JC-STDEV-L	1253	-1.5	0.01	0.23	0.01	0.14	0.04	0.01	0.29	0.08	0.01	0.19						
DT353JC-STDEV-Me(Ak)	1248	-1.5	0.02	0.15	0.02	0.16		0.02	0.25	0.02	0.01	0.07						
DT353JC-STDEV-Mo	1248	-1.5	0.00	0.21	0.03	0.26		0.00	0.22	0.06	0.01	0.29						
DT353JC-STDEV-OLV	1252	-1.5	0.01	0.27	0.01	0.24		0.01	0.09	0.04	0.00	0.26						
JCglass-AVG			0.06	19.03	0.32	44.01	0.23	0.02	22.86	2.19	0.02	10.00					98.72	
JCglass-STDEV			0.01	0.12	0.01	0.18	0.04	0.01	0.10	0.03	0.02	0.13						
DT451JC2-AVG-L	1130	-2.1	0.02	3.52	0.81	31.68	0.87	0.02	22.60	10.19	0.01	28.69					98.42	0.18
DT451JC2-AVG-Me(Ak)	1130	-2.1	0.03	8.01	0.18	41.86	0.00	0.01	38.53	0.19	0.01	10.73					99.56	0.17
DT451JC2-AVG-PV	1130	-2.1	0.01	0.03	0.04	0.04	0.03	0.01	40.51	56.93	0.01	1.19					98.56	0.02
DT451JC2-AVG-Px	1130	-2.1	0.01	14.47	0.12	51.31	0.00	0.00	24.33	2.57	0.01	7.02					99.84	0.49
DT451JC2-AVG-Ulv	1130	-2.1	0.01	3.71	0.42	0.07	0.04	0.00	0.39	28.62	0.02	64.94					98.21	0.12
DT451JC2-STDEV-L	1130	-2.1	0.02	0.18	0.02	0.25	0.06	0.01	0.53	0.24	0.01	0.72						
DT451JC2-STDEV-Me(Ak)	1130	-2.1	0.02	0.09	0.06	0.24	0.00	0.01	0.26	0.16	0.02	0.30						
DT451JC2-STDEV-PV	1130	-2.1	0.01	0.01	0.02	0.01	0.03	0.01	0.23	0.39	0.01	0.06						
DT451JC2-STDEV-Px	1130	-2.1	0.01	0.83	0.02	0.35	0.00	0.00	0.14	0.22	0.01	1.28						
DT451JC2-STDEV-Ulv	1130	-2.1	0.01	0.23	0.04	0.01	0.04	0.01	0.12	0.25	0.02	0.66						

Label	T(°C)	ΔNNO	Na2O	MgO	Al2O3	SiO2	P2O5	K2O	CaO	TiO2	MnO	FeO*	SrO	Nb2O5	La2O3	Ce2O3	Total	MB
DT460JC2-AVG-L	1130	-2.7	0.03	2.81	0.90	31.89	1.45	0.07	24.20	9.74	0.01	27.21					98.31	0.10
DT460JC2-AVG-Me(Ak)	1130	-2.7	0.05	7.84	0.23	41.45	0.00	0.04	38.58	0.16	0.02	10.90					99.28	0.20
DT460JC2-AVG-PV	1130	-2.7	0.01	0.04	0.04	0.05	0.05	0.01	40.34	57.68	0.01	0.92					99.14	0.02
DT460JC2-AVG-Px	1130	-2.7	0.01	13.92	0.16	51.50	0.00	0.00	24.34	2.51	0.01	7.86					100.32	0.52
DT460JC2-AVG-Ulv	1130	-2.7	0.03	3.44	0.51	0.06	0.03	0.01	0.43	28.95	0.02	64.74					98.22	0.15
DT460JC2-STDEV-L	1130	-2.7	0.01	0.37	0.05	0.52	0.14	0.02	1.20	0.55	0.02	1.59						
DT460JC2-STDEV-Me(Ak)	1130	-2.7	0.02	0.07	0.06	0.31	0.00	0.02	0.25	0.03	0.02	0.18						
DT460JC2-STDEV-PV	1130	-2.7	0.01	0.01	0.01	0.03	0.03	0.01	0.24	0.27	0.02	0.14						
DT460JC2-STDEV-Px	1130	-2.7	0.01	1.05	0.07	0.58	0.00	0.00	0.19	0.29	0.02	1.55						
DT460JC2-STDEV-Ulv	1130	-2.7	0.02	0.07	0.02	0.02	0.04	0.01	0.09	1.97	0.02	2.14						
DT463JC2-AVG-L	1130	-3.6	0.03	3.52	0.85	30.80	0.63	0.02	22.01	10.17	0.01	30.07					98.12	0.18
DT463JC2-AVG-Me(Ak)	1130	-3.6	0.04	8.20	0.15	41.28	0.00	0.02	38.50	0.12	0.01	10.30					98.62	0.18
DT463JC2-AVG-PV	1130	-3.6	0.02	0.04	0.04	0.06	0.02	0.00	40.63	56.74	0.02	1.15					98.27	0.01
DT463JC2-AVG-Px	1130	-3.6	0.01	14.04	0.12	50.87	0.00	0.01	24.20	2.43	0.01	7.48					99.16	0.50
DT463JC2-AVG-Ulv	1130	-3.6	0.01	3.78	0.43	0.06	0.03	0.01	0.34	31.48	0.01	62.79					98.93	0.12
DT463JC2-STDEV-L	1130	-3.6	0.01	0.12	0.02	0.23	0.05	0.01	0.22	0.14	0.02	0.34						
DT463JC2-STDEV-Me(Ak)	1130	-3.6	0.01	0.21	0.04	0.54	0.00	0.02	0.27	0.03	0.01	0.27						
DT463JC2-STDEV-PV	1130	-3.6	0.02	0.01	0.01	0.02	0.02	0.01	0.32	0.32	0.02	0.10						
DT463JC2-STDEV-Px	1130	-3.6	0.01	0.96	0.05	0.80	0.00	0.01	0.27	0.15	0.01	1.37						
DT463JC2-STDEV-Ulv	1130	-3.6	0.02	0.07	0.01	0.02	0.03	0.01	0.09	0.24	0.01	0.27						
DT468JC2-AVG-L	1130	-4.8	0.02	3.45	0.79	30.99	0.47	0.01	22.13	10.56	0.01	29.95					98.38	0.26
DT468JC2-AVG-Mo(kct)	1130	-4.8	0.02	10.04	0.03	35.55	0.00	0.01	30.20	0.24	0.01	22.63					98.74	0.16
DT468JC2-AVG-PV	1130	-4.8	0.02	0.03	0.04	0.03	0.02	0.01	40.61	56.84	0.01	1.15					98.77	0.03
DT468JC2-AVG-Px	1130	-4.8	0.01	14.19	0.12	51.01	0.00	0.00	24.37	2.52	0.00	7.43					99.65	0.48
DT468JC2-AVG-Ulv	1130	-4.8	0.03	4.42	0.39	1.49	0.03	0.02	1.89	31.44	0.01	58.73					98.45	0.06
DT468JC2-STDEV-L	1130	-4.8	0.01	0.52	0.05	0.55	0.05	0.01	0.52	0.39	0.02	0.70						
DT468JC2-STDEV-Mo(kct)	1130	-4.8	0.01	1.06	0.05	4.08	0.00	0.01	5.86	0.15	0.01	9.16						
DT468JC2-STDEV-PV	1130	-4.8	0.02	0.01	0.01	0.01	0.03	0.00	0.28	0.26	0.01	0.14						
DT468JC2-STDEV-Px	1130	-4.8	0.01	1.04	0.04	0.65	0.00	0.01	0.18	0.13	0.00	1.40						
DT468JC2-STDEV-Ulv	1130	-4.8	0.04	0.74	0.07	3.47	0.04	0.02	2.78	3.52	0.02	3.00						

Label	T(°C)	ΔNNO	Na2O	MgO	Al2O3	SiO2	P2O5	K2O	CaO	TiO2	MnO	FeO*	SrO	Nb2O5	La2O3	Ce2O3	Total	MB
JC2glass-AVG			0.02	9.55	0.27	38.18	0.13	0.06	23.52	7.69	0.01	18.61					98.03	
JC2glass-STDEV			0.01	0.09	0.02	0.32	0.04	0.02	0.16	0.09	0.01	0.10						
DT312JD-AVG-L	1275	-2.1	0.04	13.49	6.10	42.40	1.62	0.06	25.03	2.50	0.37	7.61					99.21	0.85
DT312JD-AVG-OLV	1275	-2.1	0.01	49.89	0.06	41.23		0.01	1.67	0.04	0.34	7.46					100.71	0.14
DT312JD-STDEV-L	1275	-2.1	0.01	0.06	0.04	0.13	0.06	0.01	0.23	0.06	0.04	0.04						
DT312JD-STDEV-OLV	1275	-2.1	0.01	0.53	0.04	0.19		0.02	0.14	0.02	0.03	0.28						
DT313JD-AVG-L	1296	-1.9	0.00	14.31	6.11	43.22	1.59	0.01	25.19	2.52	0.35	6.13					99.43	0.84
DT313JD-AVG-OLV	1296	-1.9	0.01	51.25	0.03	41.38		0.01	1.56	0.02	0.36	6.29					100.90	0.12
DT313JD-STDEV-L	1296	-1.9	0.00	0.08	0.04	0.27	0.05	0.01	0.22	0.04	0.04	0.08						
DT313JD-STDEV-OLV	1296	-1.9	0.01	0.55	0.02	0.23		0.01	0.07	0.01	0.04	0.49						
DT316JD-AVG-L	1276	-0.9	0.09	13.10	6.06	42.14	1.56	0.08	25.41	2.54	0.37	7.86					99.22	0.84
DT316JD-AVG-OLV	1276	-0.9	0.01	48.81	0.22	40.92		0.01	2.21	0.12	0.33	7.01					99.65	0.15
DT316JD-STDEV-L	1276	-0.9	0.01	0.18	0.06	0.18	0.07	0.01	0.14	0.07	0.01	0.07						
DT316JD-STDEV-OLV	1276	-0.9	0.01	1.76	0.40	0.52		0.01	1.28	0.22	0.03	0.19						
DT317JD-AVG-L	1276	-0.2	0.12	13.12	6.10	41.81	1.50	0.16	24.87	2.48	0.37	8.15					98.66	0.86
DT317JD-AVG-OLV	1276	-0.2	0.01	50.64	0.03	40.99		0.00	1.64	0.03	0.34	6.92					100.61	0.14
DT317JD-STDEV-L	1276	-0.2	0.01	0.06	0.07	0.21	0.06	0.02	0.30	0.04	0.04	0.11						
DT317JD-STDEV-OLV	1276	-0.2	0.01	0.47	0.01	0.18		0.00	0.06	0.02	0.03	0.17						
DT323JD-AVG-L	1229	-2.0	0.17	11.82	6.35	41.38	1.86	0.33	25.60	2.52	0.35	8.54					98.91	0.84
DT323JD-AVG-OLV	1229	-2.0	0.01	49.23	0.07	40.27		0.02	1.85	0.05	0.39	8.39					100.29	0.17
DT323JD-STDEV-L	1229	-2.0	0.01	0.14	0.08	0.31	0.06	0.02	0.30	0.03	0.03	0.12						
DT323JD-STDEV-OLV	1229	-2.0	0.01	0.91	0.05	0.46		0.01	0.09	0.01	0.05	0.92						
DT328JD-AVG-L	1305	-0.3	0.03	14.76	5.87	42.26	1.31	0.02	24.20	2.39	0.35	7.38					98.57	0.88
DT328JD-AVG-OLV	1305	-0.3	0.01	51.19	0.06	41.38		0.01	1.52	0.03	0.33	5.83					100.36	0.10
DT328JD-STDEV-L	1305	-0.3	0.01	0.20	0.06	0.16	0.06	0.01	0.17	0.06	0.06	0.08						
DT328JD-STDEV-OLV	1305	-0.3	0.01	0.45	0.05	0.09		0.01	0.18	0.02	0.02	0.24						

Label	T(°C)	ΔNNO	Na2O	MgO	Al2O3	SiO2	P2O5	K2O	CaO	TiO2	MnO	FeO*	SrO	Nb2O5	La2O3	Ce2O3	Total	MB
DT330JD-AVG-L	1185	-0.4	0.37	9.89	7.69	37.98	2.53	0.73	25.75	3.16	0.42	10.08					98.59	0.67
DT330JD-AVG-Mo	1185	-0.4	0.18	15.08	3.09	47.72		0.10	28.45	1.16	0.12	3.65					99.54	0.15
DT330JD-AVG-OLV	1185	-0.4	0.02	46.75	0.09	40.35		0.02	1.99	0.06	0.46	10.23					99.98	0.21
DT330JD-STDEV-L	1185	-0.4	0.03	0.09	0.11	0.19	0.14	0.01	0.13	0.04	0.04	0.12						
DT330JD-STDEV-Mo	1185	-0.4	0.23	1.84	0.92	3.42		0.08	6.49	0.76	0.03	0.68						
DT330JD-STDEV-OLV	1185	-0.4	0.02	46.75	0.09	40.35		0.02	1.99	0.06	0.46	10.23						
JDglass-AVG			0.09	18.15	5.08	41.48	0.65	0.02	21.35	2.12	0.35	9.39					98.68	
JDglass-STDEV			0.02	0.09	0.05	0.17	0.08	0.01	0.12	0.06	0.04	0.07						
DT503-WC5(.5)-AVG-L	1240	-3.0	0.01	9.49	0.19	33.36		0.01	25.38	10.88	0.01	19.80		0.13			99.26	
DT503-WC5(.5)-AVG-Pv	1240	-3.0	0.01	0.08	0.00	0.02		0.01	39.62	56.53	0.02	1.11		0.42			97.81	
DT503-WC5(.5)-STDEV-L	1240	-3.0	0.01	0.07	0.02	0.17		0.01	0.28	0.18	0.02	0.11		0.02				
DT503-WC5(.5)-STDEV-Pv	1240	-3.0	0.01	0.02	0.00	0.01		0.01	0.26	0.35	0.03	0.09		0.04				
DT503-WC5(2)-AVG-L	1240	-3.0	0.01	6.31	1.03	31.01		0.01	23.70	13.28	0.02	22.87		1.46			99.73	
DT503-WC5(2)-AVG-Pv	1240	-3.0	0.01	0.15	0.00	0.04		0.00	39.98	53.88	0.01	1.70		3.24			99.04	
DT503-WC5(2)-STDEV-L	1240	-3.0	0.01	1.39	0.13	2.28		0.01	2.12	2.15	0.02	2.95		0.26				
DT503-WC5(2)-STDEV-Pv	1240	-3.0	0.01	0.01	0.00	0.01		0.01	0.24	0.42	0.01	0.11		0.23				
DT503-WC5(5)-AVG-L	1240	-3.0	0.01	7.44	0.77	31.36		0.01	24.80	11.88	0.00	19.92		3.35			99.54	
DT503-WC5(5)-AVG-Pv	1240	-3.0	0.01	0.35	0.00	0.53		0.01	39.09	49.60	0.01	3.20		6.42			99.23	
DT503-WC5(5)-STDEV-L	1240	-3.0	0.01	0.98	0.08	1.18		0.01	1.72	1.37	0.01	1.96		0.56				
DT503-WC5(5)-STDEV-Pv	1240	-3.0	0.01	0.31	0.01	1.40		0.01	0.73	1.90	0.02	0.88		0.53				
DT504-WC5(2)-AVG-L	1240	-1.5	0.01	8.16	0.74	31.33		0.00	24.92	10.98	0.01	22.05		1.03			99.25	
DT504-WC5(2)-AVG-Pv	1240	-1.5	0.01	0.24	0.00	0.70		0.01	39.54	52.54	0.01	2.70		3.27			99.03	
DT504-WC5(2)-STDEV-L	1240	-1.5	0.01	1.04	0.07	0.54		0.00	0.25	1.08	0.01	0.49		0.11				
DT504-WC5(2)-STDEV-Pv	1240	-1.5	0.01	0.36	0.01	1.67		0.01	0.84	2.33	0.02	1.12		0.18				

Label	T(°C)	ΔNNO	Na2O	MgO	Al2O3	SiO2	P2O5	K2O	CaO	TiO2	MnO	FeO*	SrO	Nb2O5	La2O3	Ce2O3	Total	MB
DT504-WC5(5)-AVG-L	1240	-1.5	0.01	8.21	0.69	30.99		0.01	24.54	10.31	0.01	21.58		2.72			99.07	
DT504-WC5(5)-AVG-Pv	1240	-1.5	0.01	0.22	0.00	0.07		0.01	39.07	48.87	0.01	3.49		7.27			99.01	
DT504-WC5(5)-STDEV-L	1240	-1.5	0.01	1.06	0.11	0.52		0.01	0.86	0.76	0.01	1.15		0.24				
DT504-WC5(5)-STDEV-Pv	1240	-1.5	0.01	0.04	0.00	0.07		0.01	0.27	0.80	0.02	0.45		0.49				
DT507-WC5(2)-AVG-L	1240	-1.0	0.01	5.17	0.97	30.35		0.01	24.07	13.42	0.01	25.10		1.23			100.33	
DT507-WC5(2)-AVG-Pv	1240	-1.0	0	0.10	0.00	0.11		0.00	39.88	52.80	0.01	2.63		3.45			98.99	
DT507-WC5(2)-STDEV-L	1240	-1.0	0.01	1.06	0.12	0.78		0.01	0.52	1.45	0.02	0.70		0.14				
DT507-WC5(2)-STDEV-Pv	1240	-1.0	0.01	0.03	0.00	0.11		0.00	0.17	0.31	0.01	0.15		0.10				
DT507-WC5(5)-AVG-L	1240	-1.0	0.01	6.17	0.70	30.48		0.00	24.73	11.82	0.01	23.08		2.88			99.88	
DT507-WC5(5)-AVG-Pv	1240	-1.0	0.01	0.18	0.00	0.04		0.00	39.62	49.11	0.00	3.78		6.70			99.44	
DT507-WC5(5)-STDEV-L	1240	-1.0	0.01	0.61	0.04	0.54		0.00	0.76	0.72	0.01	0.82		0.18				
DT507-WC5(5)-STDEV-Pv	1240	-1.0	0.01	0.02	0.00	0.01		0.01	0.16	0.61	0.00	0.34		0.22				
DT510-WC5(2)-AVG-Pv	1240	3.5	0.02	0.09	0.00	0.05		0.00	40.05	51.92	0.02	3.36		4.15			99.66	
DT511-WC5(2)-AVG-Pv	1230	0.6	0.02	0.15	0.00	0.18		0.01	39.82	52.70	0.01	2.77		3.76			99.41	
DT511-WC5(5)-AVG-Pv	1240	3.5	0.02	0.14	0.00	0.03		0.01	39.56	48.78	0.01	4.22		7.35			100.12	
DT510-WC5(5)-AVG-Pv	1230	0.6	0.01	0.21	0.00	0.35		0.00	39.28	46.77	0.01	5.08		7.83			99.53	

* Total Fe is expressed as FeO for all phases except Pv (expressed as Fe_2O_3)

Appendix IV. Experimental Perovskite (wt%)

Sample		T(°C)	ΔNNO	SiO2	Al2O3	CaO	MgO	Na2O	K2O	Fe2O3*	MnO	TiO2	P2O5	Nb2O5	Ce2O3	SrO	La2O3	Total
DT301	WC	1300	4.1	0.71	0.87	40.75	0.26	0.01	0.01	2.62	0.04	53.52	0.14					98.93
DT312	WC	1275	-2.1	0.09	0.05	40.91	0.10	0.01	0.01	1.24	0.02	58.18	0.02					100.52
DT313	WC	1295	-2.1	0.14	0.05	40.91	0.14	0.01	0.00	1.15	0.02	58.09	0.04					100.43
DT316	WC	1275	-0.7	0.02	0.06	40.28	0.08	0.02	0.01	1.66	0.02	56.98	0.06					99.03
DT317	WC	1275	-0.1	0.04	0.03	41.06	0.08	0.01	0.01	1.79	0.01	57.69	0.03					100.57
DT336	WC	1250	-0.2	0.13	0.02	40.11	0.08	0.01	0.00	1.96	0.01	56.76	0.01					98.90
DT339	WC	1255	-0.7	0.14	0.04	40.26	0.09	0.01	0.00	1.64	0.01	56.96	0.03					99.03
DT342	WC	1255	-0.8	0.12	0.04	40.12	0.13	0.01	0.01	1.63	0.01	56.76	0.02					98.69
DT343	WC	1255	-0.7	0.09	0.05	40.32	0.07	0.01	0.01	1.49	0.00	56.96	0.04					98.90
DT346	WC	1250	-2.1	0.13	0.06	40.24	0.08	0.02	0.01	1.26	0.00	57.23	0.03					98.93
DT347	WC	1255	-3.2	0.05	0.07	40.65	0.08	0.01	0.00	1.01	0.00	57.39	0.02					99.18
DT350	WC	1255	-4.1	0.09	0.09	40.39	0.08	0.01	0.01	0.93	0.01	57.89	0.05					99.46
DT351	WC	1255	-3.5	0.13	0.06	40.50	0.09	0.01	0.00	1.09	0.01	57.30	0.03					99.11
DT353	WC	1250	-1.5	0.16	0.05	40.26	0.07	0.02	0.01	1.58	0.01	56.71	0.03					98.73
DT382	WC	1255	-2.9	0.36	0.07	40.62	0.11	0.01	0.01	1.34	0.01	57.46	0.04					99.99
DT384	WC	1255	-1.6	0.12	0.06	40.68	0.08	0.00	0.00	1.31	0.00	57.72	0.03					99.96
DT389	WC	1255	-3.5	0.15	0.08	40.61	0.07	0.01	0.00	1.19	0.01	57.65	0.03					99.78
DT384	WC2	1255	-1.6	0.20	0.12	40.44	0.10	0.01	0.00	1.40	0.01	57.23	0.03		0.33			99.89
DT389	WC2	1255	-3.5	0.06	0.13	40.36	0.08	0.01	0.00	1.06	0.01	57.65	0.03		0.32			99.70
DT444	WC3	1180	-2.0	0.05	0.03	40.69	0.04	0.01	0.01	1.25	0.01	57.16	0.03					99.13
DT451	WC3	1130	-2.1	0.13	0.04	40.37	0.05	0.01	0.01	1.45	0.00	56.65	0.05					98.43
DT460	WC3	1130	-2.7	0.07	0.03	40.34	0.04	0.02	0.01	1.15	0.01	57.40	0.05					99.01
DT463	WC3	1130	-3.6	0.09	0.04	40.56	0.04	0.01	0.01	1.34	0.02	56.51	0.05					98.07
DT468	WC3	1130	-4.8	0.05	0.04	40.37	0.04	0.02	0.01	1.24	0.01	56.97	0.04					98.50
DT460	WC4	1130	-2.7	0.17	0.05	39.62	0.07	0.01	0.00	1.23	0.02	56.77	0.04	0.35	0.48	0.09	0.47	99.34
DT503	WC4	1240	-3.0	0.02	0.00	39.62	0.08	0.01	0.01	1.11	0.02	56.53		0.42				97.81
DT463	WC4	1130	-3.6	0.04	0.06	39.62	0.04	0.01	0.01	1.52	0.01	56.25	0.06	0.38	0.46	0.17	0.43	98.90
DT468	WC4	1130	-4.8	0.03	0.07	39.69	0.05	0.02	0.01	1.25	0.01	56.39	0.04	0.42	0.41	0.17	0.38	98.82
DT451	WD3	1130	-2.1	0.12	0.44	40.39	0.03	0.01	0.02	1.34	0.06	55.96	0.02					97.04
DT460	WD3	1130	-2.7	0.06	0.51	40.68	0.04	0.02	0.01	0.74	0.04	56.73	0.04					98.07
DT463	WD3	1130	-3.6	0.05	0.42	40.70	0.03	0.02	0.01	0.84	0.05	56.41	0.05					98.23
DT468	WD3	1130	-4.8	0.06	0.56	40.85	0.05	0.02	0.02	0.59	0.02	56.67	0.03					98.69

Sample		T(°C)	ΔNNO	SiO2	Al2O3	CaO	MgO	Na2O	K2O	Fe2O3*	MnO	TiO2	P2O5	Nb2O5	Ce2O3	SrO	La2O3	Total
DT451	JC2	1130	-2.1	0.04	0.04	40.51	0.03	0.01	0.01	1.32	0.01	56.93	0.03					98.56
DT460	JC2	1130	-2.7	0.05	0.04	40.34	0.04	0.01	0.01	1.02	0.01	57.68	0.05					99.14
DT463	JC2	1130	-3.6	0.06	0.04	40.63	0.04	0.02	0.00	1.28	0.02	56.74	0.02					98.27
DT468	JC2	1130	-4.8	0.03	0.04	40.61	0.03	0.02	0.01	1.28	0.01	56.84	0.02					98.77
DT510	WC5(2)	1240	3.5	0.05	0.00	40.05	0.09	0.02	0.00	3.36	0.02	51.92		4.15				99.66
DT511	WC5(2)	1230	0.6	0.18	0.00	39.82	0.15	0.02	0.01	2.77	0.01	52.70		3.76				99.41
DT507	WC5(2)	1240	-1.0	0.11	0.00	39.88	0.10	0.00	0.00	2.63	0.01	52.80		3.45				98.99
DT504	WC5(2)	1240	-1.6	0.18	0.00	39.80	0.13	0.01	0.01	2.36	0.02	53.25		3.30				99.04
DT503	WC5(2)	1240	-3.0	0.04	0.00	39.98	0.15	0.01	0.00	1.70	0.01	53.88		3.24				99.01
DT511	WC5(5)	1240	3.5	0.03	0.00	39.56	0.14	0.02	0.01	4.22	0.01	48.78		7.35				100.12
DT510	WC5(5)	1230	0.6	0.35	0.00	39.28	0.21	0.01	0.00	5.08	0.01	46.77		7.83				99.53
DT504	WC5(5)	1240	-1.0	0.07	0.00	39.06	0.23	0.01	0.00	3.35	0.01	49.03		7.23				99.00
DT507	WC5(5)	1240	-1.6	0.04	0.00	39.62	0.18	0.01	0.00	3.78	0.00	49.11		6.70				99.44
DT503	WC5(5)	1240	-3.0	0.09	0.00	39.32	0.26	0.01	0.01	2.85	0.02	50.44		6.28				99.27

Appendix V. Experimental Perovskite (cations)

Sample		T(°C)	ΔNNO	Si4+	Al3+	Ca2+	Mg2+	Na+	K+	Fe3+	Mn2+	Ti4+	P5+	Nb5+	Ce3+	Sr2+	La3+	Total
DT301	WC	1300	4.1	0.0163	0.0234	1.00	0.0090	0.0006	0.0003	0.0452	0.0007	0.92	0.0027	0.0000	0.0000	0.0000	0.0000	2.02
DT312	WC	1275	-2.1	0.0021	0.0014	0.99	0.0034	0.0004	0.0002	0.0211	0.0005	0.99	0.0004	0.0000	0.0000	0.0000	0.0000	2.00
DT313	WC	1295	-2.1	0.0032	0.0012	0.99	0.0045	0.0003	0.0001	0.0194	0.0004	0.98	0.0008	0.0000	0.0000	0.0000	0.0000	2.00
DT316	WC	1275	-0.7	0.0006	0.0015	0.99	0.0028	0.0008	0.0002	0.0286	0.0004	0.98	0.0011	0.0000	0.0000	0.0000	0.0000	2.00
DT317	WC	1275	-0.1	0.0009	0.0008	0.99	0.0026	0.0003	0.0002	0.0304	0.0002	0.98	0.0007	0.0000	0.0000	0.0000	0.0000	2.00
DT336	WC	1250	-0.2	0.0030	0.0006	0.98	0.0028	0.0003	0.0001	0.0337	0.0002	0.98	0.0002	0.0000	0.0000	0.0000	0.0000	2.00
DT339	WC	1255	-0.7	0.0031	0.0011	0.99	0.0032	0.0003	0.0001	0.0282	0.0003	0.98	0.0006	0.0000	0.0000	0.0000	0.0000	2.00
DT342	WC	1255	-0.8	0.0028	0.0011	0.99	0.0044	0.0006	0.0002	0.0281	0.0002	0.98	0.0004	0.0000	0.0000	0.0000	0.0000	2.00
DT343	WC	1255	-0.7	0.0022	0.0013	0.99	0.0025	0.0007	0.0003	0.0257	0.0000	0.98	0.0007	0.0000	0.0000	0.0000	0.0000	2.00
DT346	WC	1250	-2.1	0.0029	0.0015	0.99	0.0028	0.0009	0.0003	0.0217	0.0001	0.98	0.0005	0.0000	0.0000	0.0000	0.0000	2.00
DT347	WC	1255	-3.2	0.0011	0.0018	0.99	0.0029	0.0004	0.0000	0.0173	0.0000	0.99	0.0005	0.0000	0.0000	0.0000	0.0000	2.00
DT350	WC	1255	-4.1	0.0021	0.0023	0.98	0.0029	0.0007	0.0003	0.0158	0.0003	0.99	0.0010	0.0000	0.0000	0.0000	0.0000	2.00
DT351	WC	1255	-3.5	0.0029	0.0015	0.99	0.0032	0.0003	0.0000	0.0188	0.0003	0.98	0.0006	0.0000	0.0000	0.0000	0.0000	2.00
DT353	WC	1250	-1.5	0.0037	0.0013	0.99	0.0025	0.0008	0.0003	0.0272	0.0001	0.98	0.0006	0.0000	0.0000	0.0000	0.0000	2.00
DT382	WC	1255	-2.9	0.0082	0.0020	0.98	0.0036	0.0004	0.0002	0.0228	0.0003	0.98	0.0008	0.0000	0.0000	0.0000	0.0000	2.00
DT384	WC	1255	-1.6	0.0027	0.0015	0.99	0.0026	0.0002	0.0001	0.0223	0.0000	0.98	0.0006	0.0000	0.0000	0.0000	0.0000	2.00
DT389	WC	1255	-3.5	0.0033	0.0021	0.99	0.0025	0.0004	0.0001	0.0204	0.0002	0.98	0.0006	0.0000	0.0000	0.0000	0.0000	2.00
DT384	WC2	1255	-1.6	0.0046	0.0032	0.98	0.0034	0.0006	0.0001	0.0240	0.0002	0.98	0.0006	0.0000	0.0027	0.0000	0.0000	2.00
DT389	WC2	1255	-3.5	0.0014	0.0034	0.98	0.0027	0.0002	0.0001	0.0181	0.0002	0.99	0.0005	0.0000	0.0026	0.0000	0.0000	2.00
DT444	WC3	1180	-2.0	0.0011	0.0007	1.00	0.0012	0.0003	0.0002	0.0214	0.0002	0.98	0.0005	0.0000	0.0000	0.0000	0.0000	2.00
DT451	WC3	1130	-2.1	0.0030	0.0009	0.99	0.0018	0.0003	0.0003	0.0250	0.0001	0.98	0.0009	0.0000	0.0000	0.0000	0.0000	2.00
DT460	WC3	1130	-2.7	0.0017	0.0007	0.99	0.0014	0.0008	0.0002	0.0198	0.0002	0.99	0.0010	0.0000	0.0000	0.0000	0.0000	2.00
DT463	WC3	1130	-3.6	0.0021	0.0011	1.00	0.0014	0.0003	0.0003	0.0232	0.0003	0.98	0.0010	0.0000	0.0000	0.0000	0.0000	2.01
DT468	WC3	1130	-4.8	0.0011	0.0010	0.99	0.0013	0.0007	0.0002	0.0214	0.0002	0.98	0.0008	0.0000	0.0000	0.0000	0.0000	2.00
DT460	WC4	1130	-2.7	0.0039	0.0014	0.97	0.0022	0.0005	0.0001	0.0213	0.0003	0.98	0.0007	0.0036	0.0041	0.0012	0.0040	2.00
DT503	WC4	1240	-3.0	0.0004	0.0000	0.98	0.0029	0.0005	0.0002	0.0194	0.0003	0.99	0.0000	0.0044	0.0000	0.0000	0.0000	2.00
DT463	WC4	1130	-3.6	0.0009	0.0016	0.98	0.0015	0.0005	0.0002	0.0263	0.0002	0.98	0.0011	0.0040	0.0039	0.0023	0.0036	2.00
DT468	WC4	1130	-4.8	0.0006	0.0019	0.98	0.0017	0.0008	0.0002	0.0217	0.0003	0.98	0.0009	0.0044	0.0034	0.0023	0.0032	2.00
DT451	WD3	1130	-2.1	0.0029	0.0120	1.00	0.0011	0.0003	0.0005	0.0233	0.0012	0.97	0.0004	0.0000	0.0000	0.0000	0.0000	2.01
DT460	WD3	1130	-2.7	0.0014	0.0137	1.00	0.0013	0.0008	0.0003	0.0128	0.0007	0.98	0.0008	0.0000	0.0000	0.0000	0.0000	2.01
DT463	WD3	1130	-3.6	0.0012	0.0114	1.00	0.0011	0.0007	0.0004	0.0146	0.0010	0.98	0.0009	0.0000	0.0000	0.0000	0.0000	2.01
DT468	WD3	1130	-4.8	0.0013	0.0152	1.00	0.0016	0.0007	0.0006	0.0102	0.0005	0.98	0.0005	0.0000	0.0000	0.0000	0.0000	2.01

Sample		T(°C)	ΔNNO	Si4+	Al3+	Ca2+	Mg2+	Na+	K+	Fe3+	Mn2+	Ti4+	P5+	Nb5+	Ce3+	Sr2+	La3+	Total
DT451	JC2	1130	-2.1	0.0008	0.0010	1.00	0.0010	0.0005	0.0002	0.0228	0.0002	0.98	0.0006	0.0000	0.0000	0.0000	0.0000	2.00
DT460	JC2	1130	-2.7	0.0012	0.0011	0.99	0.0013	0.0003	0.0003	0.0176	0.0003	0.99	0.0009	0.0000	0.0000	0.0000	0.0000	2.00
DT463	JC2	1130	-3.6	0.0014	0.0012	1.00	0.0012	0.0010	0.0001	0.0220	0.0003	0.98	0.0005	0.0000	0.0000	0.0000	0.0000	2.01
DT468	JC2	1130	-4.8	0.0007	0.0012	1.00	0.0010	0.0010	0.0003	0.0221	0.0002	0.98	0.0005	0.0000	0.0000	0.0000	0.0000	2.01
DT510	WC5(2)	1240	3.5	0.0012	0.0000	0.99	0.0031	0.0009	0.0001	0.0585	0.0003	0.90	0.0000	0.0434	0.0000	0.0000	0.0000	2.00
DT511	WC5(2)	1230	0.6	0.0041	0.0000	0.98	0.0053	0.0008	0.0002	0.0481	0.0001	0.92	0.0000	0.0393	0.0000	0.0000	0.0000	2.00
DT507	WC5(2)	1240	-1.0	0.0025	0.0000	0.99	0.0034	0.0002	0.0001	0.0459	0.0002	0.92	0.0000	0.0362	0.0000	0.0000	0.0000	2.00
DT504	WC5(2)	1240	-1.6	0.0041	0.0000	0.99	0.0045	0.0003	0.0002	0.0410	0.0003	0.93	0.0000	0.0344	0.0000	0.0000	0.0000	2.00
DT503	WC5(2)	1240	-3.0	0.0009	0.0000	0.99	0.0052	0.0004	0.0001	0.0296	0.0001	0.94	0.0000	0.0339	0.0000	0.0000	0.0000	2.00
DT511	WC5(5)	1240	3.5	0.0006	0.0000	0.98	0.0048	0.0007	0.0002	0.0738	0.0003	0.85	0.0000	0.0772	0.0000	0.0000	0.0000	1.99
DT510	WC5(5)	1230	0.6	0.0081	0.0000	0.99	0.0072	0.0006	0.0001	0.0896	0.0001	0.82	0.0000	0.0829	0.0000	0.0000	0.0000	2.00
DT504	WC5(5)	1240	-1.0	0.0016	0.0000	0.98	0.0082	0.0003	0.0001	0.0591	0.0002	0.86	0.0000	0.0765	0.0000	0.0000	0.0000	1.99
DT507	WC5(5)	1240	-1.6	0.0009	0.0000	0.99	0.0062	0.0002	0.0001	0.0663	0.0000	0.86	0.0000	0.0707	0.0000	0.0000	0.0000	2.00
DT503	WC5(5)	1240	-3.0	0.0021	0.0000	0.98	0.0091	0.0005	0.0002	0.0498	0.0003	0.88	0.0000	0.0661	0.0000	0.0000	0.0000	1.99